Semiclassical quantization of integrable and chaotic billiard systems by harmonic inversion

Von der Fakultät für Physik der Universität Stuttgart
zur Erlangung der Würde einer Doktorin der
Naturwissenschaften (Dr. rer. nat.) genehmigte Abhandlung

Vorgelegt von

Kirsten Weibert

aus Heide

Hauptberichter:	Prof. Dr. G. Wunner
Mitberichter:	Prof. Dr. R. Friedrich
Tag der mündlichen Prüfung:	26. März 2001

Institut für Theoretische Physik I
Universität Stuttgart

2001

Contents

Chapter 1

Introduction

A question of fundamental interest for systems with both regular and chaotic dynamics is how quantum mechanical eigenvalues can be obtained by quantization of classical orbits. The EBK torus quantization method of Einstein, Brillouin, and Keller [1, 2, 3] is restricted to integrable systems, i. e., the method cannot be generalized to systems with a chaotic or mixed regular-chaotic dynamics [1]. Furthermore, EBK quantization requires the knowledge of all the constants of motion, which are not normally given in explicit form, and therefore its practical application based on the direct or indirect numerical construction of the constants of motion turns out to be a formidable task [4]. As an alternative, EBK quantization was recast as a sum over all periodic orbits of a given topology on respective tori by Berry and Tabor [5, 6]. In contrast to the EBK method, *periodic orbit theory* can be applied to systems with a more general classical dynamics: Gutzwiller's trace formula [7, 8, 9] for chaotic systems and the corresponding Berry-Tabor formula for regular systems [5, 6] provide the semiclassical approximation to the density of states as a sum over the periodic orbits of the underlying classical system. However, a fundamental problem of these periodic orbit sums is that they usually do not converge, or if they do, the convergence is extremely slow. During recent years, various techniques have been developed to overcome this problem. Most of them are especially designed for chaotic systems [10, 11, 12, 13] and cannot be applied to systems with regular or mixed regular-chaotic dynamics, or they depend on special properties of the system such as the existence of a symbolic dynamics. Applications of these methods are therefore restricted to a relatively small number of physical systems. It would be desirable to have a method at hand which is universal in the sense that it is applicable for all systems and all types of classical dynamics.

Recently, a method for periodic orbit quantization based on harmonic inversion of a semiclassical signal has been developed [14, 15, 16], which does not require any special properties of the system and therefore possesses the desired universality. The harmonic inversion procedure allows the extraction of semiclassical eigenvalues or resonances from the periodic orbit sum including a finite set of orbits up to a maximum action. The method does not depend on whether the system is bound or open and should also be capable of handling, e. g., systems with strong pruning. In addition to periodic orbit quantization, the method can be used, vice versa, for the high resolution analysis of quantum spectra in terms of the periodic orbit contributions to the trace formula. Due to the close analogy of Gutzwiller's trace formula for chaotic systems with the Berry-Tabor formula for integrable systems, the general procedures are the same for both types of underlying dynamics. The

semiclassical quantization of integrable and chaotic systems on an equal footing will be the basis for applications to systems with even more general, i.e., mixed regular-chaotic dynamics [17].

In the present work, the universality of the harmonic inversion method is demonstrated by application of the general procedures to two billiard systems with completely different properties – the circle billiard as a representative of integrable and bound systems, and the three-disk scattering system at different disk separations as an example of a chaotic system. As an especially challenging system for periodic orbit quantization, the closed three-disk system will be considered. This system does not fulfill the requirements of other semiclassical methods as it exhibits strong pruning. Up to now, no other semiclassical method has been able to reproduce more than the lowest eigenvalues of this system.

In addition to the evaluation of the periodic orbit sum and the high resolution analysis of quantum spectra, the harmonic inversion technique is generalized in this work in two directions: Firstly, the periodic orbit quantization is extended to include higher order $\hbar$ corrections in the periodic orbit sum. Secondly, the method is generalized to the construction and analysis of cross-correlated periodic orbit sums, which allows a significant reduction of the required number of orbits for semiclassical quantization and thus an improvement of the efficiency of the method.

In Chapter 2 a brief review of the periodic orbit theory for integrable and chaotic systems is given. The formulae are generalized, firstly, to describe the density of states weighted with the diagonal matrix elements of one or more given operators [18, 19], and, secondly, to include higher order $\hbar$ corrections in the semiclassical trace formulae [20, 21]. The chapter also reviews some of the methods for the evaluation of the periodic orbit sum which have been developed in recent years.

The high precision analysis of quantum spectra and the method for the analytic continuation of non-convergent periodic orbit sums applied in this work are based on the *harmonic inversion* of time signals. In Chapter 3, the technical tools and the general procedures for the different applications of the harmonic inversion method discussed in this work are developed. Section 3.1 provides a brief introduction to harmonic inversion by filter-diagonalization [22, 23, 24] and the analysis of band-limited signals by decimated signal diagonalization [25]. In addition, an extension of the harmonic inversion method to cross-correlation functions [22, 26, 27] is discussed, which will be used to extract semiclassical eigenvalues and matrix elements from cross-correlated periodic orbit sums with a significantly reduced set of periodic orbits.

Harmonic inversion circumvents the uncertainty principle of the conventional Fourier transform and is thus able to provide a high resolution analysis of quantum spectra in terms of periodic orbit contributions [16, 28], as will be discussed in Section 3.2. This procedure allows a test of the validity of the Berry-Tabor and the Gutzwiller formula and their generalization to spectra weighted with diagonal matrix elements discussed in Section 2.2. Furthermore, harmonic inversion will be applied to determine higher order $\hbar$ contributions to the periodic orbit sum. The Gutzwiller and the Berry-Tabor formula are only the leading order contributions of an expansion of the density of states in terms of $\hbar$ and therefore only yield semiclassical approximations to the eigenvalues. By analyzing the difference spectrum between exact and semiclassical eigenvalues, first order $\hbar$ corrections to the periodic orbit sum can be determined, as will be demonstrated in Section 3.2.2. The results can be used as a test for the analytic expressions for the $\hbar$ expansion of the periodic orbit sum given in Section 2.3.

In Section 3.3, the general procedures for periodic orbit quantization by harmonic inversion are developed. First, it is shown how in general the problem of extracting semiclassical eigenvalues from periodic orbit sums can be reformulated as a harmonic inversion problem: A semiclassical signal is constructed from the periodic orbit sum, the analysis of which yields the semiclassical eigenvalues or resonances of the system. In Section 3.3.2 it is demonstrated how the accuracy of the semiclassical eigenvalues can be improved with the help of higher order $\hbar$ corrections to the periodic orbit sum. Section 3.3.3 addresses the question of how to improve the efficiency of the semiclassical quantization method, i. e., how to extract the same number of eigenvalues with a reduced set of periodic orbits, which is important especially when the orbits must be searched numerically. This improvement is achieved by constructing cross-correlated periodic orbit sums, which are then simultaneously harmonically inverted with the generalized filter-diagonalization or decimated signal diagonalization method of Sections 3.1.2 and 3.1.3.

In Chapter 4, the general procedures developed in Chapter 3 are applied to the circle billiard in order to demonstrate the applicability of the method for integrable systems. Since the periodic orbits as well as the exact quantum and EBK eigenvalues of the circle billiard can easily be obtained, the harmonic inversion results can directly be compared with the theoretical values, which provides a test for the accuracy of the method.

In Chapter 5, the same procedures are applied to the three-disk scatterer, which serves as a prototype of a chaotic system. The three-disk system will be considered at different disk separations – in the open case as well as in the limiting case of touching disks. For the closed three-disk system, it will be demonstrated that the harmonic inversion method is not affected by the property of strong pruning, and accurate semiclassical eigenvalues of this system can be obtained. For comparison, an alternative method for periodic orbit quantization based on a Padé approximation to the periodic orbit sum [29] is also tested for the closed three-disk system.

Because of their high topicality, part of the results presented in this work have been published in advance. The corresponding references are Refs. [30, 31, 32].

Chapter 2

Periodic orbit theory for integrable and chaotic systems

2.1 Periodic orbit theory versus EBK quantization

Historically, semiclassical quantization conditions were for a long time only known for integrable systems. The Bohr-Sommerfeld quantization conditions, which played a very important rôle in the early days of quantum mechanics, were extended and corrected by Einstein, Brillouin and Keller [1, 2, 3], resulting in the well-established EBK torus quantization scheme for the semiclassical quantization of integrable systems.

Integrable systems are characterized by the property that their dynamics can be expressed in action-angle variables. The action variables, which are defined as action integrals along certain "irreducible" closed paths,

$$I_j = \frac{1}{2\pi} \oint_{C_j} \mathbf{p}_j \, d\mathbf{q}_j \; , \tag{2.1}$$

are constants of motion. In the $2n$-dimensional phase space, the motion of an integrable system is restricted to n-dimensional tori, which are given by the values of the action variables.

In the EBK theory, the energy eigenvalues of the system are directly associated with certain classical tori. These tori are defined by the EBK quantization conditions, which select special sets from all possible values of the action variables of the system,

$$I_j = \left(m_j + \frac{\alpha_j}{4} \right) \hbar, \qquad j = 1, \ldots, n \; , \tag{2.2}$$

where m_j are arbitrary positive integer numbers, and the Maslov indices α_j depend on certain geometrical properties of the trajectories. Each set of numbers m_j corresponds to a quantum mechanical eigenstate of the system. The tori selected by the EBK conditions are usually not rational, i. e., the orbits on these tori are usually not periodic.

For many physical systems the application of the EBK quantization scheme is a non-trivial task. Especially for non-separable or near-integrable systems the irreducible paths are difficult to find. Most importantly, as already discussed by Einstein [1], the torus quantization scheme cannot be extended to chaotic systems as it is based on the existence of invariant tori. For chaotic systems, a completely different approach is needed.

A semiclassical theory for chaotic systems was developed by Gutzwiller [7, 8, 9] in the 1960's. The Gutzwiller trace formula connects the density of states to the periodic orbits of the corresponding classical system, which for chaotic systems lie isolated in phase space. A detailed derivation of the Gutzwiller trace formula can be found in many references, see e. g. [33]. In the following, the main ideas will be sketched. The derivation of Gutzwiller's trace formula is based on the path integral representation of the time domain propagator $K(q, q', t)$ of the Schrödinger equation,

$$K(q, q', t) = \int \mathcal{D}q'' \, e^{\frac{i}{\hbar} S(q, q', t; q'')} \, , \tag{2.3}$$

where $\int \mathcal{D}q''$ is the functional integral measure for all paths connecting the points q and q' in time t, and $S(q, q', t; q'')$ is the classical action between q and q' calculated along the path q''. The semiclassical density of states can be expressed in terms of the trace of the energy domain Green's function $G^+(E)$, which is the Fourier transform of the time domain propagator,

$$\rho(E) = -\frac{1}{\pi} \operatorname{Im} \int dq \, G^+(q, q, E) \, , \tag{2.4}$$

with

$$G^+(q, q', E) = \frac{1}{i\hbar} \int_0^\infty dt \, K(q, q', t) \, e^{iEt/\hbar} \, . \tag{2.5}$$

The integrals are evaluated via stationary phase approximation. The path integral for the trace (2.4) involves all paths connecting the point q with itself. From all possible paths, the condition of stationary phase singles out the classical periodic orbits. The resulting semiclassical density of states consists of a smooth background and an oscillating part,

$$\rho(E) = \rho_0(E) + \rho^{\mathrm{osc}}(E) \, , \tag{2.6}$$

where the term $\rho_0(E)$ results from "zero length contributions", i. e., trajectories going directly from q to q' with their length tending to zero in the limit $q \to q'$. For n-dimensional systems, $\rho_0(E)$ is given by the Weyl term

$$\rho_0(E) = \frac{1}{(2\pi\hbar)^n} \int dp^n dq^n \, \delta(E - H(\mathbf{p}, \mathbf{q})) \, , \tag{2.7}$$

where H is the classical Hamiltonian. The oscillating part consists of contributions from all classical periodic orbits and is given by

$$\rho^{\mathrm{osc}}(E) = \frac{1}{\pi\hbar} \sum_{\mathrm{po}} \frac{T_{\mathrm{po}}}{r |\det(M_{\mathrm{po}} - \mathbf{1})|^{1/2}} \cos\left(\frac{S_{\mathrm{po}}}{\hbar} - \mu_{\mathrm{po}} \frac{\pi}{2}\right) \, . \tag{2.8}$$

The sum runs over all periodic orbits (po) of the system, including multiple traversals. Here, T and S are the period and the action of the orbit, M and μ are the monodromy matrix and the Maslov index, and the repetition number r counts the traversals of the underlying primitive orbit, where "primitive" means that there is no sub-period. The Gutzwiller formula (2.8) for the density of states of chaotic systems and the EBK quantization condition for integrable systems possess a completely different structure. While in EBK theory the quantum states are directly related to certain classical tori, there is no such direct connection between quantum states and periodic orbits for chaotic systems.

For integrable systems, a semiclassical formula analogous to the Gutzwiller trace formula was derived by Berry and Tabor [5, 6]. Their derivation starts from the EBK quantization condition for the energy, $E_{\mathbf{m}} = H(\mathbf{I_m})$, where H is the classical Hamiltonian and $\mathbf{I_m} = (\mathbf{m} + \boldsymbol{\alpha}/4)\hbar$ is the set of quantized action variables. The density of states $\rho(E) = \sum_{\mathbf{m}} \delta(E - E_{\mathbf{m}})$ is transformed into a series of integrals over the action variables using the Poisson sum formula. These integrals are evaluated in a special set of coordinates using the stationary phase approximation (for details see Ref. [5]). Like the Gutzwiller formula, the Berry-Tabor formula gives the density of states as the sum of a smooth background and oscillating contributions from periodic orbits,

$$\rho(E) = \rho_0(E) + \rho^{\mathrm{osc}}(E) , \tag{2.9}$$

where $\rho_0(E)$ is again given by Eq. (2.7). While in chaotic systems the periodic orbits are isolated, the periodic orbits of integrable systems are all those orbits lying on rational tori – i. e., tori on which the frequencies of the motion are commensurable – and thus are non-isolated. The Berry-Tabor formula gives the oscillating part of the density of states in terms of the rational tori,

$$\rho^{\mathrm{osc}}(E) = \frac{2}{\hbar^{\frac{1}{2}(n+1)}} \sum_{\mathbf{M}} \frac{\cos(S_{\mathbf{M}}/\hbar - \frac{1}{2}\pi\boldsymbol{\alpha} \cdot \mathbf{M} + \frac{1}{4}\pi\beta_{\mathbf{M}})}{|\mathbf{M}|^{\frac{1}{2}(n-1)} \, |\boldsymbol{\omega}_{\mathbf{M}}| \, |K(\mathbf{I_M})|^{\frac{1}{2}}} . \tag{2.10}$$

The sum runs over all rational tori at given energy E, characterized by the frequency ratios given by the ray of integer numbers $\mathbf{M}$. The sum includes cases where the M_i are not relatively prime, $\mathbf{M} = r\boldsymbol{\mu}$, which corresponds to multiple traversals of the primitive periodic orbits on the torus characterized by $\boldsymbol{\mu}$. Here, n is the dimension of the system, $\mathbf{I_M}$ and $\boldsymbol{\omega}_{\mathbf{M}}$ are the values of the action variables and the frequencies on the torus, $S_{\mathbf{M}}$ is the action of the periodic orbits on the torus, and K is the scalar curvature of the energy contour. The components of $\boldsymbol{\alpha}$ are the Maslov indices of the irreducible paths on which the action variables are defined, and the phase β is obtained from the second derivative matrix of the action variables in terms of the coordinates.

The Berry-Tabor formula is the analogue of the Gutzwiller formula for integrable systems and possesses the same structure. In contrast to the EBK torus quantization, there is no direct relation between the eigenvalues of the system and the tori which enter the Berry-Tabor formula. In fact, as was demonstrated by Reimann et al. [34], the Berry-Tabor formula can be derived from the same expressions (2.3) to (2.5) for the time domain propagator and the trace of the Green's function which were the starting point for the derivation of the Gutzwiller formula. The difference to the case of chaotic systems is how the integrals are evaluated. While for chaotic systems the periodic orbits are isolated and all integrals perpendicular to the orbit can be evaluated by stationary phase approximation, the evaluation of the trace (2.4) for integrable systems involves the integration over rational tori. This can explicitly be carried out in action-angle variables, finally leading to Eq. (2.10).

Both the EBK torus quantization and the Berry-Tabor formula are semiclassical theories delivering lowest order $\hbar$ approximations to the exact quantum eigenvalues. In general, the results of the two approaches can only be expected to be the same in lowest order of $\hbar$ but not necessarily beyond. (Although Berry and Tabor's derivation of Eq. (2.10) starts from the EBK quantization condition, higher order terms in $\hbar$ are lost in the calculations, as was discussed in Ref. [34].) However, it was shown in Ref. [34] that

for the circle billiard, which will be discussed in Chapter 4, the two approaches are in fact equivalent and should yield exactly the same results beyond the lowest order of $\hbar$.

For the periodic orbit quantization of the circle billiard, I will use a simplified version of Eq. (2.10) for the special case $n = 2$, i.e., for two-dimensional regular systems, which was derived by Ullmo et al. [35]:

$$\rho^{\text{osc}}(E) = \frac{1}{\pi \hbar^{3/2}} \sum_{\mathbf{M}} \frac{T_{\mathbf{M}}}{M_2^{3/2} |g_E''|^{1/2}} \cos\left(\frac{S_{\mathbf{M}}}{\hbar} - \eta_{\mathbf{M}} \frac{\pi}{2} - \frac{\pi}{4}\right) . \tag{2.11}$$

The sum extends over all rational tori at energy E, characterized by the frequency ratio given by the integer numbers $\mathbf{M} = (M_1, M_2)$, including multiple traversals (i.e., cases where M_1, M_2 are not relatively prime). Here, $T_{\mathbf{M}}$ is the traversal time, and g_E is the function describing the energy surface, $H(I_1, I_2 = g_E(I_1)) = E$, where I_1 and I_2 are the action variables. The Maslov index $\eta_{\mathbf{M}}$ is obtained from the Maslov indices α_1, α_2 of the paths on which the action variables are defined,

$$\eta_{\mathbf{M}} = (M_1 \alpha_1 + M_2 \alpha_2) - \Theta(g_E'') , \tag{2.12}$$

where Θ is the Heaviside step function.

For general systems, the semiclassical density of states can be expressed in terms of the semiclassical response function $g(E)$,

$$\rho(E) = -\frac{1}{\pi} \text{Im} \, g(E) . \tag{2.13}$$

The exact quantum response function is given by the trace of the Green's function $G^+(E)$,

$$g_{\text{qm}}(E) = \text{Tr} \, G^+(E) = \sum_n \frac{1}{E - E_n + i0} . \tag{2.14}$$

For bound systems, the poles E_n of the Green's function are real and equal to the energy eigenvalues of the system. For open systems, the Green's function possesses complex poles or resonances. [In the case of degenerate eigenvalues, the corresponding terms have to be multiplied by the degeneracy factors. In this chapter, I will assume, for simplicity, that all multiplicities are equal to 1.] For both chaotic and regular systems the semiclassical approximation to the response function is of the form

$$g(E) = g_0(E) + \sum_{\text{po}} \mathcal{A}_{\text{po}} e^{\frac{i}{\hbar} S_{\text{po}}} , \tag{2.15}$$

where the amplitudes are given by the Gutzwiller or the Berry-Tabor formula, respectively.

In the following I will always consider scaling systems, i.e., physical systems which possess a scaling parameter w such that the form of the periodic orbits is independent of w and the action scales like

$$\frac{1}{\hbar} S_{\text{po}} = w s_{\text{po}} , \tag{2.16}$$

with the scaled action s_{po} being independent of w. In billiard systems, the wave number k is such a quantity. For scaling systems, it is quite natural to quantize the scaling

parameter w rather than the energy E. One can therefore introduce a density depending on the scaling parameter:

$$\rho(w) = -\frac{1}{\pi} \operatorname{Im} g(w) = -\frac{1}{\pi} \operatorname{Im} \sum_n \frac{1}{w - w_n + i0} \ . \tag{2.17}$$

The semiclassical approximation to the scaled response function $g(w)$ resulting from the Gutzwiller or the Berry-Tabor formula is of the form

$$g(w) = g_0(w) + \sum_{\mathrm{po}} \tilde{\mathcal{A}}_{\mathrm{po}} e^{iws_{\mathrm{po}}} \ . \tag{2.18}$$

In practical applications both the Gutzwiller formula (2.8) and the Berry-Tabor formula (2.10) suffer from the fact that the periodic orbit sums usually do not converge. Depending on the system in question, this problem may be overcome, e. g., by convolution of the periodic orbit sum with a suitable averaging function, as was done in Ref. [34]. But even then the convergence will usually be slow, and a large number of orbits has to be included to obtain the semiclassical eigenvalues. In Section 3.3, it will be demonstrated how the convergence problem can be circumvented by the harmonic inversion method and the eigenvalues or resonances can be calculated from a relatively small set of periodic orbits.

2.2 Semiclassical matrix elements

The semiclassical trace formula for both regular and chaotic systems can be extended to include diagonal matrix elements. The calculation of individual semiclassical matrix elements is an objective in its own right. Furthermore, the extended trace formulae allow the construction of cross-correlated periodic orbit signals and thus a significant reduction of the number of orbits required for periodic orbit quantization, as will be demonstrated in Section 3.3.3. Here, I will briefly recapitulate the basic ideas and equations.

Both Gutzwiller's and Berry and Tabor's formula give the semiclassical response function as a sum over contributions from periodic orbits, see (2.15). The quantum mechanical response function is the trace over the Green's function $G^+(E)$, see (2.14). As a generalization of (2.14), one can consider the quantum mechanical response function weighted with the diagonal matrix elements of some operator $\hat{A}$, i. e.,

$$g_{A,\mathrm{qm}}(E) = \sum_n \frac{\langle n|\hat{A}|n\rangle}{E - E_n + i0} = \operatorname{Tr}\left(G^+(E)\hat{A}\right) \ . \tag{2.19}$$

As was derived by Wilkinson [36, 37] and Eckhardt et al. [38] for chaotic systems and by Mehlig [39] for integrable systems, the semiclassical approximation to Eq. (2.19) is obtained by weighting the contributions of the periodic orbits in (2.15) with the average $\bar{A}_p$ of the corresponding classical quantity $A(\mathbf{q}, \mathbf{p})$ over the periodic orbits:

$$g_A(E) = g_{A,0}(E) + \sum_{\mathrm{po}} \mathcal{A}_{\mathrm{po}} \bar{A}_p e^{\frac{i}{\hbar} S_{\mathrm{po}}} \ . \tag{2.20}$$

For chaotic systems, the average is taken over one period T_p of the isolated periodic orbit [36, 37, 38]:

$$\bar{A}_p = \frac{1}{T_p} \int_0^{T_p} A(\mathbf{q}(t), \mathbf{p}(t)) \ dt \ . \tag{2.21}$$

For an N-dimensional integrable system, the quantity A has to be expressed in action-angle variables $(\mathbf{I}, \boldsymbol{\theta})$ and averaged over the rational torus [39]:

$$\bar{A}_p = \frac{1}{(2\pi)^N} \int A(\mathbf{I}, \boldsymbol{\theta}) d^N\theta . \qquad (2.22)$$

Eq. (2.19) can even be further generalized by introducing a second operator $\hat{B}$ and considering the quantity

$$g_{AB,\mathrm{qm}}(E) = \sum_n \frac{\langle n|\hat{A}|n\rangle\langle n|\hat{B}|n\rangle}{E - E_n + i0} . \qquad (2.23)$$

If either $\hat{A}$ or $\hat{B}$ commutes with the Hamiltonian, Eq. (2.23) can be written as a trace formula and a calculation similar to that in Ref. [38] yields the semiclassical approximation

$$g_{AB}(E) = g_{AB,0}(E) + \sum_{\mathrm{po}} \mathcal{A}_{\mathrm{po}} \bar{A}_p \bar{B}_p e^{\frac{i}{\hbar}S_{\mathrm{po}}} . \qquad (2.24)$$

Note that for general operators $\hat{A}$ and $\hat{B}$, Eq. (2.23) cannot be written as a trace any more. However, strong numerical evidence was provided by Main and Wunner [18] (for both regular and chaotic systems) that Eq. (2.24) is correct *in general*, i.e., even if neither operator $\hat{A}$ nor $\hat{B}$ commutes with the Hamiltonian. For chaotic systems, a mathematical proof of Eq. (2.24) was given by Hortikar and Srednicki [19]. An analogous rigorous derivation for integrable systems is, to my knowledge, still lacking.

In Refs. [18, 19], the relations (2.23) and (2.24) were generalized to products of diagonal matrix elements of more than two operators. As a further extension, one can also introduce functions of diagonal matrix elements in the response function:

$$g_{f(A),\mathrm{qm}}(E) = \sum_n \frac{f(\langle n|\hat{A}|n\rangle)}{E - E_n + i0} . \qquad (2.25)$$

By a Taylor expansion of the (sufficiently smooth) function f, and using the results of Refs. [18, 19] for multiple products of matrix elements, one obtains the semiclassical approximation

$$g_{f(A)}(E) = g_{f(A),0}(E) + \sum_{\mathrm{po}} \mathcal{A}_{\mathrm{po}} f(\bar{A}_p) e^{\frac{i}{\hbar}S_{\mathrm{po}}} . \qquad (2.26)$$

The extended trace formulae in combination with an extension of the harmonic inversion procedure to cross-correlated signals will be used to significantly reduce the number of orbits which have to be included in the periodic orbit sum.

The diagonal matrix elements obtained from the extended trace formulae are semiclassical approximations to the exact quantum matrix elements. For the circle billiard, these values can be compared with those given by EBK theory. According to EBK theory, the diagonal matrix element of an operator $\hat{A}$ with respect to an eigenstate $|n\rangle$ is obtained by averaging the corresponding classical quantity $A(\mathbf{I}, \boldsymbol{\theta})$ over the quantized torus related to this eigenstate:

$$\langle n|\hat{A}|n\rangle = \frac{1}{(2\pi)^N} \int A(\mathbf{I}_n, \boldsymbol{\theta}_n) d^N\theta_n . \qquad (2.27)$$

Note the difference to Eq. (2.22), where the average is taken over the rational tori.

2.3 Higher order $\hbar$ corrections

The Berry-Tabor formula for integrable systems and Gutzwiller's trace formula for chaotic systems are only the leading order terms of an expansion of the density of states in terms of $\hbar$. In billiard systems, the scaling parameter w of the classical action (cf. Eq. (2.16)) is proportional to $\hbar^{-1}$ and thus plays the rôle of an inverse effective Planck constant,

$$w = \hbar_{\text{eff}}^{-1} \ . \tag{2.28}$$

The $\hbar$ expansion of the response function can therefore be written as a power series in terms of w^{-1}:

$$g^{\text{osc}}(w) = \sum_{n=0}^{\infty} g_n(w) = \sum_{n=0}^{\infty} \frac{1}{w^n} \sum_{\text{po}} \mathcal{A}_{\text{po}}^{(n)} e^{i s_{\text{po}} w}. \tag{2.29}$$

The zeroth order amplitudes $\mathcal{A}_{\text{po}}^{(0)}$ are those of the Berry-Tabor or Gutzwiller formula, respectively, whereas for $n > 0$, the amplitudes $\mathcal{A}_{\text{po}}^{(n)}$ give the nth order corrections $g_n(w)$ to the response function. Two different methods for the calculation of higher order $\hbar$ correction terms in chaotic systems have been derived, one by Gaspard and Alonso [40, 41], and the other by Vattay and Rosenqvist [20, 21, 42]. The latter method has been specialized to two-dimensional chaotic billiards in Ref. [42]. I will adopt the method of Vattay and Rosenqvist to compute the first order $\hbar$ corrections to the semiclassical eigenvalues of the open three-disk scatterer and the circle billiard. However, it is important to note that the method cannot be applied to integrable systems in a straightforward manner and additional assumptions will be necessary to derive an expression for the first order $\hbar$ corrections for the circle billiard. A general theory for the calculation of higher order $\hbar$ corrections to the Berry-Tabor formula (2.10) for integrable systems is, to the best of my knowledge, still lacking.

Vattay and Rosenqvist give a quantum generalization of the Gutzwiller formula which is of the form

$$g^{\text{osc}}(E) = \frac{1}{i\hbar} \sum_p \sum_l \left(T_p(E) - i\hbar \frac{d \ln R_p^l(E)}{dE} \right) \sum_{r=1}^{\infty} (R_p^l(E))^r e^{\frac{i}{\hbar} r S_p(E)}. \tag{2.30}$$

The first sum runs over all primitive periodic orbits; T_p and S_p are the traversal time and the action of the periodic orbit, respectively. The sum over r corresponds to multiple traversals of the primitive orbit. The quantities R_p^l are associated with the local eigenspectra determined by the local Schrödinger equation in the neighbourhood of the periodic orbits. Details are given in Appendix A.1. An expansion of the quantities R_p^l in terms of $\hbar$,

$$R^l(E) \;=\; \exp \left\{ \sum_{m=0}^{\infty} \left(\frac{i\hbar}{2} \right)^m C_l^{(m)} \right\} \tag{2.31}$$

$$\approx\; \exp(C_l^{(0)}) \left(1 + \frac{i\hbar}{2} C_l^{(1)} + \dots \right) , \tag{2.32}$$

yields the $\hbar$ expansion of the generalized trace formula (2.30). For two-dimensional hyperbolic systems, the zeroth order terms are given by

$$\exp(C_l^{(0)}) = \frac{e^{i\mu_p \pi/2}}{|\lambda_p|^{1/2} \lambda_p^l} , \tag{2.33}$$

14

where μ_p and λ_p are the Maslov index and the expanding stability eigenvalue (i. e., the stability eigenvalue with an absolute value larger than one) of the orbit, respectively. By summation over l, the Gutzwiller trace formula is regained as zeroth order approximation to Eq. (2.30). If the zeroth order terms do not depend on the energy, as is the case for billiard systems, the first order correction (cf. Eq. (2.29)) to the Gutzwiller formula is given by

$$ g_1(E) = \frac{1}{i\hbar} \sum_p \sum_l T_p(E) \sum_{r=1}^{\infty} \exp(rC_l^{(0)}) \, \frac{i\hbar}{2} \, rC_l^{(1)} e^{\frac{i}{\hbar} r S_p(E)}. \qquad (2.34) $$

An explicit recipe for the calculation of the correction terms $C_l^{(1)}$ for two-dimensional chaotic billiards is given in Ref. [42]. I summarize the basic formulae in Appendix A.1. The correction terms must in general be calculated numerically. A numerical code which determines the first order corrections for two-dimensional chaotic billiards can also be found in Ref. [42]. I will use that code to obtain the correction terms $C_l^{(1)}$ for the three-disk system.

As mentioned before, the method outlined above cannot directly be applied to integrable systems, as its derivation is valid only for isolated periodic orbits. A general theory for $\hbar$ corrections to the Berry-Tabor formula does not yet exist. Nevertheless, for the circle billiard I have succeeded in obtaining an explicit expression for the first order $\hbar$ corrections to the Berry-Tabor formula by introducing certain additional assumptions resulting from the symmetry of the system. The calculations are very lengthy and therefore deferred to Appendix A.2. However, this derivation cannot be applied to general integrable systems. It will be an interesting task for the future to develop a *general* theory for the higher order $\hbar$ corrections to the Berry-Tabor formula.

2.4 High resolution methods for the evaluation of Gutzwiller's trace formula

As already stated, the semiclassical trace formulae relating the quantum spectrum of a system to the periodic orbits of the corresponding classical system suffer from the fact that they usually diverge in the region where the eigenvalues or resonances of the system are located. In recent years, a number of different techniques have been developed to overcome this problem. In this section, I will briefly summarize some of the methods which have proven very efficient for different classes of chaotic systems. However, all the methods developed so far depend on special properties of the system, such as ergodicity, and are therefore not universal.

A method which has proven very successful for a number of chaotic systems is the cycle expansion method developed by Cvitanović and Eckhardt [10]. The problem of extracting eigenvalues or resonances from the Gutzwiller trace formula can be reformulated as finding the zeros of zeta functions. Cycle expansion provides a way to analytically continue the different zeta functions into the region of physical interest. For the open three-disk system, which has served as a prototype model for the cycle expansion method, semiclassical resonances have been obtained by cycle expansion of several different zeta functions. Since I will compare my results for the three-disk system obtained by harmonic inversion with data from cycle expansion, I now briefly review the different zeta functions and the basic ideas of the cycle expansion method.

The semiclassical density of states given by the Gutzwiller formula can directly be reexpressed in terms of the Gutzwiller-Voros zeta function [9, 43]. For hyperbolic systems with two degrees of freedom, the denominator of Eq. (2.8) can be written in terms of the expanding stability eigenvalue λ. Writing out explicitly the sum over multiple traversals of the primitive orbits, one can rewrite Eq. (2.8) as

$$
\rho^{\mathrm{osc}}(E) = \mathrm{Re}\frac{1}{\pi\hbar}\sum_p\sum_{r=1}^{\infty}T_p\frac{\exp[ir(\frac{S_p}{\hbar}-\mu_{\mathrm{po}}\frac{\pi}{2})]}{|\lambda_p|^{r/2}(1-\frac{1}{\lambda_p^r})} \tag{2.35}
$$

$$
= \mathrm{Re}\frac{1}{\pi\hbar}\sum_p\sum_{r=1}^{\infty}\sum_{j=0}^{\infty}T_p\left(\frac{\exp[i(\frac{S_p}{\hbar}-\mu_{\mathrm{po}}\frac{\pi}{2})]}{|\lambda_p|^{1/2}\lambda_p^j}\right)^r \tag{2.36}
$$

$$
= \mathrm{Re}\frac{1}{\pi\hbar}\sum_p\sum_{j=0}^{\infty}T_p\frac{t_p^{(j)}}{1-t_p^{(j)}}\,, \tag{2.37}
$$

where the first sum now runs over all *primitive* periodic orbits, respectively, and

$$
t_p^{(j)} = \frac{\exp[i(\frac{S_p}{\hbar}-\mu_{\mathrm{po}}\frac{\pi}{2})]}{|\lambda_p|^{1/2}\lambda_p^j}\,. \tag{2.38}
$$

From $\frac{\partial S_p}{\partial E}=T_p$ it follows that

$$
\rho^{\mathrm{osc}}(E) = -\frac{1}{\pi}\mathrm{Im}\sum_p\sum_{j=0}^{\infty}\frac{\partial}{\partial E}\ln(1-t_p^{(j)}) \tag{2.39}
$$

$$
= -\frac{1}{\pi}\mathrm{Im}\left(\frac{\partial}{\partial E}\ln Z_{\mathrm{GV}}(E)\right) \tag{2.40}
$$

with

$$
Z_{\mathrm{GV}}(E) = \prod_{j=0}^{\infty}\prod_p(1-t_p^{(j)}) = \prod_{j=0}^{\infty}\zeta_j^{-1}\,. \tag{2.41}
$$

The quantity $Z_{\mathrm{GV}}(E)$ is the Gutzwiller-Voros zeta function. Formally, the zeros of this function are the semiclassical approximations to the resonances or energy eigenvalues of the system. The quantities

$$
\zeta_j^{-1} = \prod_p(1-t_p^{(j)}) \tag{2.42}
$$

are called dynamical zeta functions. The leading resonances of the spectrum (i.e., the resonances closest to the real axis) can be obtained as zeros of the dynamical zeta function ζ_0^{-1} or Ruelle zeta function, which is the $j=0$ approximation to Eq. (2.41).

The Gutzwiller-Voros zeta function and the dynamical zeta functions are no entire functions since they possess poles in the lower half of the complex plane, as was demonstrated by Eckhardt and Russberg [44]. An entire zeta function, the so-called quasiclassical zeta function, was introduced by Cvitanović and Vattay [45]. In two dimensions, this zeta function reads

$$
Z_{\mathrm{CV}}(E) = \prod_p\prod_{j=0}^{\infty}\prod_{l=0}^{\infty}\left(1-\frac{t_p^{(j)}}{\lambda_p^{2l}}\right)^{j+1}\,. \tag{2.43}
$$

16

In the quasiclassical zeta function, the poles of the Gutzwiller-Voros zeta function have been removed by multiplication with regularization terms. The spectrum of the quasiclassical zeta function contains the semiclassical Gutzwiller spectrum (i. e., the semiclassical resonances are again zeros of this zeta function), but also additional spurious zeros which result from the regularization terms and do not correspond to physical resonances.

Although the resonances or eigenvalues of the system are formally given by the zeros of the zeta functions, the zeta functions – like the Gutzwiller trace formula – usually do not converge in the regions where the resonances or eigenvalues are located (on and below the real axis). In order to obtain the physical resonances, the zeta functions have to be analytically continued into the region of physical interest. For systems with a complete symbolic dynamics, this can be achieved by the cycle expansion method. The basic idea is to expand and regroup the terms in the infinite product over periodic orbits in such a way that contributions from long orbits are shadowed by those of short orbits. For the rearrangement of the product, a bookkeeping variable z is introduced, and the weights $t_p^{(j)}$ in the zeta functions are replaced with $z^{n_p} t_p^{(j)}$, where n_p is the length of the symbolic code or cycle length of the periodic orbit. (For $z = 1$, the original zeta function is regained.) Then, the infinite product over the periodic orbit contributions is carried out formally, and the terms are grouped by orders of z. The resulting expansion of the zeta function (with z set to 1 in the end) is of the form

$$\zeta^{-1} = 1 - \sum_f t_f - \sum_n c_n \, , \tag{2.44}$$

where t_f are contributions from a few fundamental periodic orbits and c_n are the higher curvature corrections, containing all orbits of symbol length n and all combinations of shorter orbits with combined symbol length n, respectively. E. g., in the case of a binary symbolic dynamics, as it exists in the symmetry reduced three-disk system, the cycle expansion of the dynamical zeta function ζ_0^{-1} reads

$$
\begin{aligned}
\zeta_0^{-1} = \quad & 1 - t_0 - t_1 \\
& -[(t_{01} - t_0 t_1)] \\
& -[(t_{001} - t_0 t_{01}) + (t_{011} - t_{01} t_1)] \\
& -[(t_{0001} - t_0 t_{001}) + (t_{0111} - t_{011} t_1) + (t_{0011} - t_{001} t_1 - t_0 t_{011} + t_0 t_{01} t_1)] \\
& - \ldots \, ,
\end{aligned}
\tag{2.45}
$$

where the upper index (0) has been omitted at the weight factors t_p (cf. Eq. (2.42)).

While the zeta functions in their original form have the same radius of convergence as the underlying trace formulae, the cycle expanded zeta functions typically converge much better. The actual radius of convergence depends on the analyticity properties of the zeta functions. For the Gutzwiller-Voros and the dynamical zeta function, the radius of convergence is still finite, i. e., only resonances near the real axis can be obtained. The radius of convergence is given by the poles of the dynamical zeta function. On the other hand, the quasiclassical zeta function (2.43) is entire, and its cycle expansion should converge in the whole lower half of the complex plane. A disadvantage of the quasiclassical zeta function is that it contains spurious zeros which do not correspond to physical resonances.

The cycle expansion can be expected to converge fast with respect to the curvature order n if the approximation $t_{ab} \approx t_a t_b$ for any two symbol sequences a and b is well

satisfied. The convergence sensitively depends on whether or not the symbolic code is complete. In the case of pruning, i.e., if periodic orbits are missing, some contributions will remain uncompensated in every order of the cycle expansion. In general, the cycle expansion works best for open systems. It requires the system to be completely hyperbolic and to possess a complete symbolic dynamics.

For bound hyperbolic systems several different methods for the extraction of eigenvalues from Gutzwiller's trace formula were developed. One is the "Riemann-Siegel lookalike" formula by Berry and Keating [12, 46]. The method is based on a pseudo-orbit expansion of the spectral determinant resulting from the Gutzwiller formula and a resummation of the divergent tail of this series, which is performed in analogy with the Riemann-Siegel formula for the zeros of the Riemann zeta function. The semiclassical eigenvalues are then obtained as zeros of a finite sum over periodic orbits and pseudo-orbits (i.e., linear combinations of primitive periodic orbits and their repetitions).

Sieber and Steiner [47, 48, 49] replaced the Gutzwiller formula with a generalized trace formula relating the traces of suitable spectral functions (i.e., functions of the quantum Hamiltonian $\hat{H}$) to the periodic orbits of the corresponding classical system. For properly chosen spectral functions, the resulting periodic orbit sum is absolutely convergent. Explicit examples used for periodic orbit quantization are the Gaussian smoothed density of states and the trace of the heat kernel, $\mathrm{Tr}\, e^{-\hat{H}t/\hbar}$.

Bogomolny [50, 51] derived a quantization condition for bound chaotic systems from a quantum version of the classical Poincaré map. The basic idea of this method is to transform the Schrödinger equation into a quantum map $\psi' = T\psi$, where the transition operator T is built from classical periodic orbits corresponding to a classical Poincaré map. The semiclassical eigenvalues are then obtained as zeros of the determinant $\det(1 - T)$.

As explained above, although the methods discussed in this section have proven very efficient for specific classes of physical systems, they all suffer from the disadvantage of non-universality. In the following chapter, harmonic inversion will be introduced as a universal tool for periodic orbits quantization, which, in contrast to other methods, is applicable to a wide range of physical systems.

Chapter 3

Harmonic inversion techniques for semiclassical quantization

3.1 Harmonic inversion of time signals

The extraction of eigenvalues from the periodic orbit sum as well as the analysis of quantum spectra in terms of periodic orbit contributions can be reformulated as harmonic inversion problems, based on formulae which have been introduced in Chapter 2. Before discussing these applications in Sections 3.2 and 3.3, I briefly recapitulate the basic ideas and the technical tools of harmonic inversion by filter-diagonalization and the analysis of band-limited signals by decimated signal diagonalization. In addition, I review a generalization of the method to the harmonic inversion of cross-correlated signals, which will allow a significant reduction of the signal length required for periodic orbit quantization.

3.1.1 Harmonic inversion by filter-diagonalization

The harmonic inversion problem can be formulated as a nonlinear fit of a signal $C(t)$ to the form

$$C(t) = \sum_k d_k e^{-i\omega_k t} , \tag{3.1}$$

where d_k and ω_k are, in general, complex variational parameters. Other than, e. g., in a simple Fourier transformation of the signal, there is no restriction as to the closeness of the frequencies ω_k. Solving (3.1) will therefore yield a high resolution analysis of the signal $C(t)$. The signal length required for resolving the frequencies ω_k by harmonic inversion can be estimated to be

$$t_{\max} \approx 4\pi\bar{\rho}(\omega), \tag{3.2}$$

where $\bar{\rho}(\omega)$ is the mean density of frequencies in the range of interest.

In the applications that are considered here, namely, periodic orbit quantization and the analysis of quantum spectra by harmonic inversion, the signal will usually contain an infinite number of frequencies. A method which has proven very useful for solving the harmonic inversion problem in a finite frequency window is the filter-diagonalization procedure, which was developed by Wall and Neuhauser [22] and significantly improved by Mandelshtam and Taylor [23, 24]. This procedure allows the computation of the frequencies ω_k in any small interval $[\omega_{\min}, \omega_{\max}]$ given. The idea is to consider the signal

$C(t)$ on an equidistant grid

$$c_n = C(n\tau) ; \quad n = 0, 1, 2, \ldots \tag{3.3}$$

and to associate c_n with an autocorrelation function of a suitable fictitious dynamical system, described by a complex symmetric effective Hamiltonian H_{eff}:

$$c_n = \left(\Phi_0 | e^{-in\tau H_{\text{eff}}} \Phi_0\right) . \tag{3.4}$$

Here, the brackets denote a complex symmetric inner product $(a|b) = (b|a)$, i.e., no complex conjugation of either a or b. The harmonic inversion problem can then be reformulated as solving the eigenvalue problem for the effective Hamiltonian H_{eff}. The frequencies ω_k are the eigenvalues of the Hamiltonian

$$H_{\text{eff}} |\Upsilon_k) = \omega_k |\Upsilon_k) , \tag{3.5}$$

and the amplitudes are obtained from the eigenvectors Υ_k:

$$d_k = (\Phi_0 | \Upsilon_k)^2 . \tag{3.6}$$

The filter-diagonalization method solves this eigenvalue problem in a small set of basis vectors Ψ_j. The Hamiltonian and the initial state Φ_0 do not have to be known explicitly but are given implicitly by the quantities c_n. In detail, the procedure works as follows:

A small set of values φ_j in the frequency interval of interest is chosen. The set must be larger than the number of frequencies in this interval. The values φ_j are used to construct the small Fourier-type basis

$$\Psi_j = \sum_{n=0}^{M} e^{in(\varphi_j - \tau H_{\text{eff}})} \Phi_0 . \tag{3.7}$$

The matrix elements of the evolution operator at a given time $p\tau$ in this basis can be expressed in terms of the quantities c_n:

$$U_{jj'}^{(p)} \equiv \left(\Psi_j | e^{-ip\tau H_{\text{eff}}} \Psi_{j'}\right) = \sum_{n=0}^{M} \sum_{n'=0}^{M} e^{i(n\varphi_j + n'\varphi_{j'})} c_{n+n'+p} . \tag{3.8}$$

The frequencies ω_k are then obtained by solving the generalized eigenvalue problem

$$\mathbf{U}^{(p)} \mathbf{B}_k = e^{-ip\tau\omega_k} \mathbf{U}^{(0)} \mathbf{B}_k . \tag{3.9}$$

The amplitudes d_k can be calculated from the (normalized) eigenvectors and are given by

$$d_k = \left(\sum_j B_{jk} \sum_{n=0}^{M} c_n e^{in\varphi_j}\right)^2 . \tag{3.10}$$

The values of ω_k and d_k obtained by the above procedure should be independent of p. This condition can be used to identify non-converged frequencies by comparing the results for different values of p. The difference between the frequency values obtained for different p can be used as a simple error estimate.

3.1.2 Extension to cross-correlated signals

An important extension of the filter-diagonalization method for harmonic inversion is the generalization to cross-correlation functions, which was developed by Wall and Neuhauser [22], Narevicius et al. [26] and Mandelshtam [27]. The idea is not to consider a single signal $C(t)$ as given in Eq. (3.1) but a set of cross-correlated signals

$$C_{\alpha\alpha'}(t) = \sum_k d_{\alpha\alpha',k} e^{-i\omega_k t} \; ; \quad \alpha, \alpha' = 1, \ldots, N \qquad (3.11)$$

with the restriction

$$d_{\alpha\alpha',k} = b_{\alpha,k} b_{\alpha',k} \; . \qquad (3.12)$$

This set of signals considered on an equidistant grid

$$c_{n\alpha\alpha'} = C_{\alpha\alpha'}(n\tau) \; ; \quad n = 0, 1, 2, \ldots \qquad (3.13)$$

is now associated with a time cross-correlation function between an initial state Φ_α and a final state $\Phi_{\alpha'}$:

$$c_{n\alpha\alpha'} = \left(\Phi_{\alpha'} | e^{-in\tau H_{\text{eff}}} \Phi_\alpha \right) \; . \qquad (3.14)$$

Again, the frequencies ω_k are obtained as the eigenvalues of the effective Hamiltonian H_{eff}. The amplitudes are now given by the relation

$$b_{\alpha,k} = (\Phi_\alpha | \Upsilon_k) \; . \qquad (3.15)$$

In a manner similar to the procedure described in Section 3.1.1, this eigenvalue problem is solved using a small set of basis vectors $\Psi_{j\alpha}$ to obtain the frequencies in a given interval $[\omega_{\min}, \omega_{\max}]$.

The advantage of the above procedure becomes evident if one considers the information content of the set of signals. Due to the restriction (3.12), the $N \times N$ set of signals $C_{\alpha\alpha'}(t)$ may contain N independent signals, which are known to possess the same frequencies ω_k. This means that, at constant signal length, the matrix may contain N times as much information about the frequencies as a single signal, provided that the whole set is inverted simultaneously. On the other hand, the information content is proportional to the signal length. Hence the signal length required to resolve the frequencies in a given interval is reduced by a factor of N. This statement clearly holds only approximately and for small matrix dimensions N. In any case, however, a significant reduction of the required signal length can be achieved.

3.1.3 Decimated signal diagonalization of band-limited signals

In the harmonic inversion scheme using filter-diagonalization, the filtering procedure selecting a small frequency window is directly intertwined with the harmonic inversion procedure itself. In order to attain a deeper understanding of the periodic orbit quantization method, it would be desirable to separate the technical step of filtering from the extraction of frequencies and amplitudes. Main et al. [25] demonstrated how this can be achieved by first constructing a band-limited decimated signal from the original signal, which can then be harmonically inverted by a number of different numerical techniques without further filtering.

The band-limited signal can be constructed from the original one by Fourier transformation. The time signal is first transformed to the frequency domain. The transformed signal is then multiplied by a frequency filter function, typically a rectangular window or a Gaussian function, localized around a central frequency ω_0. The resulting signal is shifted by $-\omega_0$ and then transformed back to the time domain by inverse Fourier transformation. [The special form of the signal in the periodic orbit quantization allows an even simpler procedure, namely analytic filtering, as will be discussed in Section 3.3.] If the bandwidth of the resulting filtered signal is M times smaller than that of the original signal, the sampling rate, i.e., the time between signal samplings, may now be chosen M times larger in order to supply the same information for signal processing. The number of signal points can therefore be reduced by a factor of M ("decimation" of the signal).

In Ref. [25], three different methods were introduced for the harmonic inversion of the band-limited decimated signal: decimated linear predictor, decimated Padé approximant and decimated signal diagonalization. I will use the latter method for the periodic orbit quantization of the three-disk system. The decimated signal diagonalization uses the same formalism as the filter-diagonalization method discussed in the previous sections (see Eqs. (3.3) to (3.6)). Instead of the Fourier-type basis (3.7), the eigenvalue problem is now solved in terms of the primitive basis

$$\Phi_n = e^{-in\tau H_{\text{eff}}} \Phi_0 \ , \qquad n = 0, 1, \ldots, K - 1 \ , \tag{3.16}$$

where K must be equal to or larger than the number of frequencies in the band-limited signal. The matrix elements of the evolution operator at a given time $p\tau$ are then simply given by

$$U_{jj'}^{(p)} = c_{j+j'+p} \ . \tag{3.17}$$

This implies that $2K+p$ signal points are needed. The frequencies ω_k are again determined by solving the eigenvalue problem

$$\mathbf{U}^{(p)}\mathbf{B}_k = e^{-ip\tau\omega_k}\mathbf{U}^{(0)}\mathbf{B}_k \ , \tag{3.18}$$

and the amplitudes d_k are given in terms of the (normalized) eigenvectors,

$$d_k = \left(\sum_n B_{nk} c_n \right)^2 \ . \tag{3.19}$$

By analogy with the procedure described in Section 3.1.2, the method can be generalized to cross-correlation functions in order to reduce the signal length which is required to resolve the frequencies.

Besides the separation of filtering and the extraction of frequencies, an advantage of the above method as concerns semiclassical quantization by harmonic inversion is that only a small number of signal points has to be considered. As will be demonstrated in Section 3.3.1, the extraction of eigenvalues from the periodic orbit sum can be reformulated as an analysis of a semiclassical signal which consists of a sum over unevenly spaced δ-functions. If the filter-diagonalization method is to be applied, the signal must be smoothed by convolution with a Gaussian function. To avoid an overly strong damping of the amplitudes, the width of the Gaussian functions must not be chosen too large. A proper sampling of the signal therefore requires a small step width, which results in a large

number of data points. This may lead to rounding errors and, as a consequence, to a loss in accuracy in the numerical results. By contrast, the number of signal points required for the analysis of a band-limited signal by decimated signal diagonalization is usually much smaller. As has been demonstrated in Ref. [25], the harmonic inversion of band-limited decimated signals may indeed yield more accurate results than the filter-diagonalization method.

3.2 High resolution analysis of quantum spectra by harmonic inversion

Harmonic inversion is a powerful tool for the high resolution analysis of quantum mechanical or experimental spectra in terms of classical periodic orbit contributions. As was demonstrated by Main et al. [28, 16], the method allows one, e.g., to resolve clusters of orbits or to discover hidden ghost orbit contributions in the spectra, which would not be resolved by conventional Fourier analysis. In this section, I discuss the general procedures for the analysis of quantum spectra by harmonic inversion. The procedures can be used to test the validity of the Berry-Tabor or the Gutzwiller formula and their extensions to semiclassical matrix elements discussed in Section 2.2. As a generalization, the method will be extended to the determination of higher order $\hbar$ corrections to the trace formulae, which provides a test for the correction terms to the periodic orbit sums discussed in Section 2.3. The general procedures developed in this section will be applied to the circle billiard in Section 4.2 and to the open three-disk system in Section 5.2.

3.2.1 Leading order periodic orbit contributions to the density of states

In the following, I describe how the leading order $\hbar$ contributions from the classical periodic orbits can be extracted from the quantum spectrum by harmonic inversion. This procedure, which was developed by Main et al. [28], is universal in the sense that it can be applied to both regular and chaotic systems and does not depend on whether the system is bound or open.

The starting point is the semiclassical density of states given by the Berry-Tabor or the Gutzwiller formula. As explained in Section 2.1, I consider scaling systems where the density of states depends on the scaling parameter w, i.e., $\rho(w) = -(1/\pi) \operatorname{Im} g(w)$ with $g(w)$ the semiclassical response function. Both the Berry-Tabor and the Gutzwiller formula give the oscillating part of the response function in the form

$$g^{\mathrm{osc}}(w) = \sum_{\mathrm{po}} \mathcal{A}_{\mathrm{po}} e^{iws_{\mathrm{po}}} , \qquad (3.20)$$

where the sum runs over all rational tori (regular systems) or all periodic orbits (chaotic systems) of the underlying classical system, respectively. In (3.20), s_{po} is the scaled action of the periodic orbit. The form of the amplitude $\mathcal{A}_{\mathrm{po}}$ depends on whether the system is chaotic or regular and also contains phase information.

The exact quantum mechanical density of states is given by

$$\rho_{\mathrm{qm}}(w) = -\frac{1}{\pi} \operatorname{Im} \sum_{k} \frac{m_k}{w - w_k + i0} , \qquad (3.21)$$

where the w_k are the exact quantum eigenvalues or resonances of the scaling parameter, and the m_k are their multiplicities. As was proposed in Ref. [28], the analysis of the quantum spectrum in terms of periodic orbit contributions can now be reformulated as adjusting the exact quantum mechanical density of states (3.21) to the semiclassical form

$$
\begin{aligned}
\rho^{\mathrm{osc}}(w) &= -\frac{1}{\pi} \, \mathrm{Im} \, g^{\mathrm{osc}}(w) \\
&= -\frac{1}{2\pi i} \, \sum_{\mathrm{po}} \left(\mathcal{A}_{\mathrm{po}} e^{iws_{\mathrm{po}}} - \mathcal{A}^*_{\mathrm{po}} e^{-iws_{\mathrm{po}}} \right) \; .
\end{aligned}
\tag{3.22}
$$

If the amplitudes $\mathcal{A}_{\mathrm{po}}$ do not depend on w, the semiclassical density of states is of the form (3.1) [here, with w playing the rôle of t and s_{po} playing the rôle of ω_k]. That means, the problem of extracting the periodic contributions from the quantum spectrum has been reformulated as a harmonic inversion problem. In the fitting procedure, the non-oscillating, smooth part of the density of states is ignored. This part does not fulfill the ansatz (3.1) of the harmonic inversion method and therefore acts as a kind of noise, which will be separated from the oscillating part of the "signal" by the harmonic inversion procedure.

For open systems without bound states, i. e., only complex values w_k, the expression (3.21) remains finite for real w and can directly be analyzed by harmonic inversion using the filter-diagonalization method. If the system possesses real eigenvalues w_k (bound states), the density of states is regularized by the convolution of both expressions (3.21) and (3.22) with a Gaussian function,

$$
C_\sigma(w) = \frac{1}{\sqrt{2\pi}\sigma} \int_{-\infty}^{\infty} \rho(w') e^{-(w-w')^2/2\sigma^2} \, dw' \; .
\tag{3.23}
$$

In the calculations for the circle billiard, the convolution width will usually be taken to be about three times the step width τ in the signal (3.3). Typical values are $\tau = \Delta w = 0.002$ and $\sigma = 0.006$. The resulting quantum mechanical signal is

$$
C_{\mathrm{qm},\sigma}(w) = \frac{1}{\sqrt{2\pi}\sigma} \sum_k m_k e^{-(w-w_k)^2/2\sigma^2} \; ,
\tag{3.24}
$$

and the corresponding semiclassical quantity reads

$$
C_\sigma(w) = -\frac{1}{2\pi i} \, \sum_{\mathrm{po}} \left(\mathcal{A}_{\mathrm{po}} e^{iws_{\mathrm{po}}} - \mathcal{A}^*_{\mathrm{po}} e^{-iws_{\mathrm{po}}} \right) e^{-\frac{1}{2}\sigma^2 s_{\mathrm{po}}^2} \; .
\tag{3.25}
$$

The above procedure still works if the amplitudes in (3.20) are not independent of w but possess a dependence of the form

$$
A_{\mathrm{po}} = w^\alpha a_{\mathrm{po}},
\tag{3.26}
$$

which is, for example, the case for regular billiards. This dependence can be eliminated by replacing the semiclassical response function $g(w)$ with the quantity

$$
g'(w) = w^{-\alpha} g(w) = w^{-\alpha} g_0(w) + \sum_{\mathrm{po}} a_{\mathrm{po}} e^{iws_{\mathrm{po}}} \; .
\tag{3.27}
$$

When introducing the corresponding quantum mechanical response function

$$g'_{\text{qm}}(w) = \sum_k \frac{m_k w_k^{-\alpha}}{w - w_k + i0} \tag{3.28}$$

the procedure can be carried out for $\rho'(w) = (-1/\pi)\text{Im}\, g'(w)$ as described above.

As an alternative to the convolution with a Gaussian function and the application of the filter-diagonalization method, a band-limited signal could be constructed from (3.22) by the procedure outlined in Section 3.1.3, which can then be analyzed with the decimated signal diagonalization method.

In addition to considering the pure density of states, the relations of Section 2.2 can be used to calculate the averages of classical quantities over the periodic orbits from the quantum diagonal matrix elements of the corresponding operators. If one starts from the extended quantum response function (2.19), including diagonal matrix elements of some operator $\hat{A}$, the analysis of the signal should again yield the actions s_{po} as frequencies but with the amplitudes weighted with the classical averages $\bar{A}_p$ of the corresponding classical quantities. In the same way, one can also use the extended response function (2.23), which includes diagonal matrix elements of two different operators.

3.2.2 Higher order $\hbar$ corrections to the trace formula

An interesting application of the method described in the previous section is the determination of higher order $\hbar$ contributions to the periodic orbit sum. The higher orders can be obtained by analysis of the difference spectrum between the exact quantum and semiclassical eigenvalues, as I will demonstrate below. The general procedure has been developed in collaboration with Main and has been published in advance in Ref. [32].

As explained in Section 2.3, the Berry-Tabor formula for integrable systems as well as the Gutzwiller formula for chaotic systems correspond to the leading order terms of an expansion of the response function in terms of $\hbar$, which for scaling systems can be put in the form (cf. (2.29))

$$g^{\text{osc}}(w) = \sum_{n=0}^{\infty} g_n(w) = \sum_{n=0}^{\infty} \frac{1}{w^n} \sum_{\text{po}} \mathcal{A}_{\text{po}}^{(n)} e^{is_{\text{po}}w} \,. \tag{3.29}$$

In Eq. (3.29), the amplitudes $\mathcal{A}_{\text{po}}^{(0)}$ are those of the Berry-Tabor or Gutzwiller formula, and for $n > 0$, the amplitudes $\mathcal{A}_{\text{po}}^{(n)}$ (including also phase information) give the nth order $\hbar$ corrections to the response function.

Provided that the amplitudes $\mathcal{A}_{\text{po}}^{(n)}$ in (3.29) do not depend on w, only the zeroth order term fulfills the ansatz (3.1) for the harmonic inversion procedure with constant amplitudes and frequencies. In systems like regular billiards, where the amplitudes possess a w dependence of the form $\mathcal{A}_{\text{po}}^{(n)} = w^\alpha a_{\text{po}}^{(n)}$, the same argumentation holds if one considers $g'(w) = w^{-\alpha} g(w)$ instead of $g(w)$ (cf. Section 3.2.1). For this reason, the higher order $\hbar$ terms cannot be obtained by a direct analysis of the quantum spectrum. The direct analysis will only yield the lowest order amplitudes, with the higher order corrections acting as a kind of weak noise.

Nevertheless, the higher order terms can still be extracted from the spectrum by harmonic inversion. Assume that the exact eigenvalues w_k and their $(n-1)^{\text{st}}$ order

approximations $w_{k,n-1}$ are given. One can then calculate the difference between the exact quantum mechanical and the $(n-1)^{\text{st}}$ order response function

$$g^{\text{qm}}(w) - \sum_{j=0}^{n-1} g_j(w) = \sum_{j=n}^{\infty} g_j(w) = \sum_{j=n}^{\infty} \frac{1}{w^j} \sum_{\text{po}} \mathcal{A}_{\text{po}}^{(j)} e^{is_{\text{po}}w}. \tag{3.30}$$

The leading order terms in (3.30) are $\sim w^{-n}$, i.e., multiplication with w^n yields

$$w^n \left[g^{\text{qm}}(w) - \sum_{j=0}^{n-1} g_j(w) \right] = \sum_{\text{po}} \mathcal{A}_{\text{po}}^{(n)} e^{is_{\text{po}}w} + \mathcal{O}\left(\frac{1}{w}\right). \tag{3.31}$$

In (3.31) the functional form (3.1) has been restored. The harmonic inversion of the function (3.31) will now provide the periods s_{po} and the nth order amplitudes $\mathcal{A}_{\text{po}}^{(n)}$ of the $\hbar$ expansion (3.29).

In practice, the procedure outlined in Section 3.2.1 will be used to construct a smooth signal, i.e., the densities of states $\rho(w) = -(1/\pi)\operatorname{Im} g(w)$ rather than the response functions $g(w)$ are considered, and for bound systems the signal is smoothed by convolution with a Gaussian function. The signal is then analyzed with the help of the filter-diagonalization method. As an alternative, one can again construct a band-limited signal and use the decimated signal diagonalization method as discussed in Section 3.1.3.

3.3 Periodic orbit quantization by harmonic inversion

I shall now turn to the problem of extracting eigenvalues from the periodic orbit sum. As discussed in Chapter 2, a fundamental problem of the Gutzwiller and the Berry-Tabor formula is that the periodic orbit sums usually do not converge. In this section, I will describe how the semiclassical eigenvalues or resonances can be obtained from a finite set of periodic orbits by harmonic inversion of a semiclassical signal. As a generalization, the method will be extended to include higher order $\hbar$ corrections in the periodic orbit sums. Furthermore, I will demonstrate how the signal length required for periodic orbit quantization can be reduced by the construction of cross-correlated periodic orbit signals. The general procedures developed in this section can be applied to both chaotic and integrable systems and do not depend on whether the system is bound or open. The methods will be applied to the circle billiard and the three-disk scatterer in Sections 4.3 and 5.3, respectively.

3.3.1 Semiclassical density of states

In the following, I describe the general procedure for the calculation of semiclassical eigenvalues or resonances from the periodic orbit sum by harmonic inversion, which was developed by Main et al. [14, 15]. As previously, I consider scaling systems and start from the response function

$$g(w) = g_0(w) + \sum_{\text{po}} \mathcal{A}_{\text{po}} e^{iws_{\text{po}}}, \tag{3.32}$$

depending on the scaling parameter w. The amplitudes $\mathcal{A}_{\mathrm{po}}$ are those of the Berry-Tabor or the Gutzwiller formula for regular and chaotic systems, respectively. The periodic orbit sum in (3.32) usually does not converge, or, at least, the convergence will be very slow. In practice, especially for chaotic systems, only the orbits with small scaled actions will be known. Nevertheless, the eigenvalues of the scaling parameter can still be extracted from the periodic orbit sum. The central idea is to adjust Eq. (3.32), with the sum including periodic orbits up to a finite action s_{max}, to the functional form of the corresponding quantum mechanical response function

$$g_{\mathrm{qm}}(w) = \sum_k \frac{m_k}{w - w_k + i0} \ . \tag{3.33}$$

This fitting problem cannot be solved directly, but can be reformulated as a harmonic inversion problem, as was demonstrated in Ref. [14, 15]. The first step of the reformulation is a Fourier transformation of the response functions with respect to w:

$$C(s) = \frac{1}{2\pi} \int_{-\infty}^{\infty} g(w) e^{-isw} dw \ . \tag{3.34}$$

In the semiclassical response function, only the oscillating part of $g(w)$ is considered. The smooth part, which does not possess a suitable form for the harmonic inversion method, would only give a contribution to the signal for very small s. Assuming that the amplitudes in (3.32) do not depend on w, the result of the Fourier transformation is

$$C(s) = \sum_{\mathrm{po}} \mathcal{A}_{\mathrm{po}} \delta(s - s_{\mathrm{po}}) \ , \tag{3.35}$$

$$C_{\mathrm{qm}}(s) = -i \sum_k m_k e^{-isw_k}. \tag{3.36}$$

As in Section 3.2.1, the δ-functions can be regularized by convoluting the signals (3.35) and (3.36) with a Gaussian function with width σ, resulting in

$$C_\sigma(s) = \frac{1}{\sqrt{2\pi}\sigma} \sum_{\mathrm{po}} \mathcal{A}_{\mathrm{po}} e^{-(s-s_{\mathrm{po}})^2/2\sigma^2} \ , \tag{3.37}$$

$$C_{\mathrm{qm},\sigma}(s) = -i \sum_k m_k e^{-\frac{1}{2}\sigma^2 w_k^2} e^{-isw_k} \ . \tag{3.38}$$

As already mentioned in Section 3.2.1, typical values of the convolution width are $\sigma = 0.006$ for signals with step width $\Delta s = 0.002$. The eigenvalues of the scaling parameter are obtained by adjusting the signal $C_\sigma(s)$ to (3.38), which is of the functional form (3.1). For the circle billiard, I will use the filter-diagonalization method (cf. Section 3.1.1) to calculate the frequencies in a given frequency window. The frequencies w_k obtained by harmonic inversion of the signal (3.37) are the eigenvalues or resonances of the scaling parameter w; from the amplitudes d_k, the multiplicities m_k can be calculated. According to Eq. (3.2), the signal length s_{max} required to resolve the eigenvalues is approximately given by $s_{\mathrm{max}} \approx 4\pi\bar{\rho}(w)$, where $\bar{\rho}(w)$ is the mean density of states. I.e., the eigenvalues can be calculated from a finite set of periodic orbits including all orbits up to the scaled action s_{max}.

As an alternative to the filter-diagonalization method, one can construct a band-limited signal and apply the decimated signal diagonalization method introduced in Section 3.1.3. The special form of the periodic orbit sum even allows one to simplify the filtering procedure outlined in Section 3.1.3: As was proposed by Main et al. [25], an analytical filter can directly be built into the semiclassical signal by multiplying the response function $g(w)$ by a window function $f(w)$ before carrying out the Fourier transformation in Eq. (3.34). I choose a rectangular filter, i.e., $f(w) = 1$ for $w \in [w_0 - \Delta w, w_0 + \Delta w]$ and $f(w) = 0$ outside the window. The band-limited signal is then given by

$$
C(s) \;=\; \frac{1}{2\pi} \int_{w_0-\Delta w}^{w_0+\Delta w} g^{\mathrm{osc}}(w) e^{-is(w-w_0)} dw \tag{3.39}
$$

$$
=\; \sum_{\mathrm{po}} \mathcal{A}_{\mathrm{po}} \frac{\sin[\Delta w(s - s_{\mathrm{po}})]}{\pi(s - s_{\mathrm{po}})} \, e^{is_{\mathrm{po}}w_0} \;. \tag{3.40}
$$

The introduction of w_0 in the exponential function in Eq. (3.39) causes a shift of the frequency window by $-w_0$. In contrast to the semiclassical signal (3.35), the band-limited signal (3.40) is already a smooth function, i.e., no additional smoothing is necessary. The same filter is now applied to the quantum response function, resulting in the quantum signal

$$
C_{\mathrm{qm}}(s) = -i \sum_k m_k \, e^{-is(w_k - w_0)} \quad ; \qquad |\mathrm{Re}\, w_k - w_0| < \Delta w \;. \tag{3.41}
$$

The filtered quantum signal is of the same form as the quantum signal (3.36), but the sum now contains only frequencies in the chosen window. Additionally, the frequencies are shifted by $-w_0$. The harmonic inversion of the semiclassical signal (3.40) by decimated signal diagonalization yields the eigenvalues or resonances in the chosen window together with their multiplicities.

Like the general procedure for analyzing quantum spectra (see Section 3.2.1), both procedures outlined above even work if the amplitudes in (3.32) are not independent of w but possess a dependence of the form

$$
\mathcal{A}_{\mathrm{po}} = w^\alpha a_{\mathrm{po}} \;. \tag{3.42}
$$

One can again eliminate this dependence by replacing $g(w)$ with the quantity

$$
g'(w) = w^{-\alpha} g(w) \;. \tag{3.43}
$$

The semiclassical signal is then of the same form as (3.37) or (3.40), respectively, but with the amplitudes $\mathcal{A}_{\mathrm{po}}$ replaced with a_{po}. The corresponding quantum signal is given by (3.38) or (3.41), respectively, with the amplitudes m_k replaced with $m_k w_k^{-\alpha}$.

In addition to the determination of semiclassical eigenvalues or resonances and their multiplicities, the procedures can be extended to the calculation of semiclassical diagonal matrix elements with the help of the extended response functions discussed in Section 2.2. Instead of the semiclassical response function (3.32), the semiclassical signal is constructed from the extended response function weighted with the averages of some classical quantity (cf. Eq. (2.20)). The amplitudes obtained by harmonic inversion then yield the diagonal semiclassical matrix elements of the corresponding quantum operator.

3.3.2 Higher order $\hbar$ corrections

The eigenvalues obtained by harmonic inversion of the periodic orbit sums are not the exact quantum mechanical eigenvalues but semiclassical approximations for the reason that the Berry-Tabor and the Gutzwiller formula are only the leading order terms of an $\hbar$ expansion of the density of states (see Sections 2.3 and 3.2.2). I will now demonstrate how to obtain corrections to the semiclassical eigenvalues from the $\hbar$ expansion (2.29) of the periodic orbit sum

$$g^{\mathrm{osc}}(w) = \sum_{n=0}^{\infty} g_n(w) = \sum_{n=0}^{\infty} \frac{1}{w^n} \sum_{\mathrm{po}} \mathcal{A}_{\mathrm{po}}^{(n)} e^{is_{\mathrm{po}}w} \, , \tag{3.44}$$

with the scaling parameter w playing the rôle of an effective inverse Planck constant $\hbar_{\mathrm{eff}}^{-1}$. The general procedure outlined in this section has been developed in collaboration with Main and has been published in advance in Refs. [30, 32].

For simplicity, I will assume in the following that the amplitudes $\mathcal{A}_{\mathrm{po}}^{(n)}$ in (3.44) do not depend on w. Again, in systems where the amplitudes possess a w dependence of the form $\mathcal{A}_{\mathrm{po}}^{(n)} = w^\alpha a_{\mathrm{po}}^{(n)}$, the same line of arguments holds if one considers $g'(w) = w^{-\alpha}g(w)$ instead of $g(w)$ (cf. Section 3.3.1).

For periodic orbit quantization the zeroth order contributions $\mathcal{A}_{\mathrm{po}}^{(0)}$, corresponding to the Gutzwiller or Berry-Tabor formula, are usually considered only. As demonstrated in Section 3.3.1 (see Eqs. (3.35) and (3.36)), the Fourier transform of the principal periodic orbit sum

$$C_0(s) = \sum_{\mathrm{po}} \mathcal{A}_{\mathrm{po}}^{(0)} \delta(s - s_{\mathrm{po}})$$

is adjusted by application of the harmonic inversion technique to the functional form of the exact quantum expression

$$C_{\mathrm{qm}}(s) = -i \sum_{k} m_k e^{-iw_k s} \, ,$$

with $\{w_k, m_k\}$ the eigenvalues and multiplicities.

For $n \geq 1$, the asymptotic expansion (3.44) of the semiclassical response function suffers from the singularities at $w = 0$. It is therefore not appropriate to harmonically invert the Fourier transform of (3.44) as a whole, although the Fourier transform formally exists. This means that the method of periodic orbit quantization by harmonic inversion cannot, in a straightforward way, be extended to the $\hbar$ expansion of the periodic orbit sum. Instead, the correction terms to the semiclassical eigenvalues will be calculated separately, order by order.

Let us assume that the $(n-1)^{\mathrm{st}}$ order approximations $w_{k,n-1}$ to the semiclassical eigenvalues have already been obtained and the $w_{k,n}$ are to be calculated. The difference between the two subsequent approximations to the quantum mechanical response function reads

$$
\begin{aligned}
g_n(w) &= \sum_{k} \left(\frac{m_k}{w - w_{k,n} + i0} - \frac{m_k}{w - w_{k,n-1} + i0} \right) \\
&\approx \sum_{k} \frac{m_k \Delta w_{k,n}}{(w - \bar{w}_{k,n} + i0)^2} \, ,
\end{aligned}
\tag{3.45}
$$

with $\bar{w}_{k,n} = \frac{1}{2}(w_{k,n} + w_{k,n-1})$ and $\Delta w_{k,n} = w_{k,n} - w_{k,n-1}$. Integration of (3.45) and multiplication by w^n yields

$$\mathcal{G}_n(w) = w^n \int g_n(w)dw = \sum_k \frac{-m_k w^n \Delta w_{k,n}}{w - \bar{w}_{k,n} + i0} \, , \qquad (3.46)$$

which has the functional form of a quantum mechanical response function but with residues proportional to the nth order corrections $\Delta w_{k,n}$ to the semiclassical eigenvalues. The semiclassical approximation to (3.46) is obtained from the term $g_n(w)$ in the periodic orbit sum (3.44) by integration and multiplication by w^n, i.e.,

$$\begin{aligned}
\mathcal{G}_n(w) &= w^n \int g_n(w)dw \\
&= -i \sum_{\text{po}} \frac{1}{s_{\text{po}}} \mathcal{A}_{\text{po}}^{(n)} e^{iws_{\text{po}}} + \mathcal{O}\left(\frac{1}{w}\right) \, .
\end{aligned} \qquad (3.47)$$

One can now Fourier transform both (3.46) and (3.47), and obtains ($n \geq 1$)

$$\begin{aligned}
C_n(s) &\equiv \frac{1}{2\pi} \int_{-\infty}^{+\infty} \mathcal{G}_n(w) e^{-iws} dw && (3.48) \\
&= i \sum_k m_k (\bar{w}_k)^n \Delta w_{k,n} e^{-i\bar{w}_k s} && (3.49) \\
&\overset{\text{h.i.}}{=} -i \sum_{\text{po}} \frac{1}{s_{\text{po}}} \mathcal{A}_{\text{po}}^{(n)} \delta(s - s_{\text{po}}) \, . && (3.50)
\end{aligned}$$

Equations (3.49) and (3.50) imply that the $\hbar$ expansion of the semiclassical eigenvalues can be obtained, order by order, by adjusting the periodic orbit signal (3.50) to the functional form of (3.49) by harmonic inversion (h.i.). [In practice, one can again convolute both expressions with a Gaussian function in order to regularize the δ-functions in (3.50), or one can construct a band-limited signal by carrying out the Fourier transformation in (3.48) over a finite frequency window, cf. Section 3.3.1.] The frequencies $\bar{w}_k$ of the periodic orbit signal (3.50) are the semiclassical eigenvalues or resonances, averaged over different orders of $\hbar$. Note that the accuracy of these values does not necessarily increase with increasing order n. I indicate this in (3.49) by omitting the index n at the eigenvalues $\bar{w}_k$. My numerical calculations for the circle billiard and the open three-disk system show that, in practice, the frequencies $\bar{w}_k$ one obtains from the first order $\hbar$ terms are approximately equal to the zeroth order $\hbar$ eigenvalues rather than the exact average between zeroth and first order eigenvalues. The corrections $\Delta w_{k,n}$ to the eigenvalues are not obtained from the frequencies, but from the amplitudes, $m_k (\bar{w}_k)^n \Delta w_{k,n}$, of the periodic orbit signal.

3.3.3 Reduction of the required signal length via harmonic inversion of cross-correlated periodic orbit sums

As described in the previous sections, the harmonic inversion method is able to extract quantum mechanical eigenvalues or resonances from the semiclassical periodic orbit sum including periodic orbits up to a *finite* action s_{max}. This means that in practice, although the periodic orbit sum does not converge, the eigenvalues can be obtained from a *finite*

set of periodic orbits. The required signal length for harmonic inversion depends on the mean density of states, i. e., $s_{\max} \approx 4\pi\bar{\rho}(w)$ (cf. (3.2)). Depending on the mean density of states, the action $s_{\max}$ up to which the periodic orbits have to be known may therefore be large. Due to the rapid proliferation of the number of periodic orbits with growing action, the efficiency and practicability of the procedure depends sensitively on the signal length required. This is the case especially when the periodic orbits have to be found numerically.

The quantization method can be improved with the help of cross-correlated periodic orbit sums. The extended response functions weighted with products of diagonal matrix elements discussed in Section 2.2, in combination with the method for harmonic inversion of cross-correlation functions presented in Section 3.1.2, can be used to significantly reduce the signal length required for the periodic orbit quantization. The general procedure outlined in the following has been developed in collaboration with Main and Mandelshtam and has been published in advance in Refs. [31, 32].

The basic idea is to construct a set of signals where each individual signal contains the same frequencies (i. e., semiclassical eigenvalues), and the amplitudes are correlated by obeying the restriction (3.12). This can be achieved using the generalized periodic orbit sum (2.24) introduced in Section 2.2:

A set of operators $\hat{A}_\alpha$, $\alpha = 1, \ldots, N$ is chosen. From the corresponding classical quantities, the general semiclassical response functions

$$g_{\alpha\alpha'}^{\mathrm{osc}}(w) = \sum_{\mathrm{po}} \mathcal{A}_{\mathrm{po}} \bar{A}_{\alpha,p} \bar{A}_{\alpha',p} e^{is_{\mathrm{po}}w} \tag{3.51}$$

are constructed, where the means $\bar{A}_{\alpha,p}$ are defined by (2.21) or (2.22) for chaotic or integrable systems, respectively. Following the procedure described in Section 3.3.1, the response functions are Fourier transformed to obtain the semiclassical signals

$$C_{\alpha\alpha'}(s) = \sum_{\mathrm{po}} \mathcal{A}_{\mathrm{po}} \bar{A}_{\alpha,p} \bar{A}_{\alpha',p} \delta(s - s_{\mathrm{po}}) \,. \tag{3.52}$$

According to Eqs. (2.23) and (3.36), the corresponding quantum mechanical signals are given by

$$C_{\mathrm{qm},\alpha\alpha'}(s) = -i \sum_k m_k \langle k|\hat{A}_\alpha|k\rangle \langle k|\hat{A}_{\alpha'}|k\rangle e^{-isw_k} \,, \tag{3.53}$$

where the amplitudes satisfy the condition (3.12). As in Section 3.3.1, the semiclassical eigenvalues w_k are obtained by adjusting the set of periodic orbit signals (3.52) to the functional form of the cross-correlated quantum signal (3.53), with the important difference that now the extension of the harmonic inversion technique to cross-correlation functions (see Section 3.1.2) is applied. In practice, one can again either convolute the signal with a Gaussian function and apply the filter-diagonalization method, or one constructs a band-limited signal which is then analyzed by decimated signal diagonalization.

The cross-correlation technique is particularly helpful for chaotic systems, where the periodic orbits must be found numerically and where the number of periodic orbits grows exponentially with their action. However, for regular systems the number of orbits which have to be included can also be reduced significantly, as will be demonstrated for the circle billiard in Section 4.3.4.

Chapter 4

Application to an integrable system: The circle billiard

While most high precision methods for the extraction of eigenvalues from the periodic orbit sum depend on specific properties of the system, such as ergodicity and the existence of a complete symbolic code, the harmonic inversion method for periodic orbit quantization does not require any special properties of the system. The general procedures can be applied to both chaotic and integrable systems and do not depend on whether the system is bound or open. To demonstrate the universality of the method, the general techniques developed in Chapter 3 will be applied to the circle billiard as an example of an integrable and closed system. The system has been chosen for the reason that its periodic orbits and exact quantum eigenvalues can easily be obtained.

4.1 Periodic orbits and quantum eigenvalues

I start by summarizing the basic properties of the circle billiard which are relevant for periodic orbit quantization and calculating an explicit expression for the density of states resulting from the Berry-Tabor formula.

The circle billiard problem in two dimensions is separable in polar coordinates. The semiclassical expressions for both EBK torus quantization and the Berry-Tabor formula for the density of states are based on the action-angle variables associated with the angular φ-motion and the radial r-motion. The action variables are given by

$$
\begin{aligned}
I_\varphi &= \frac{1}{2\pi} \oint p_\varphi \, d\varphi = L \qquad\qquad\qquad (4.1)\\
I_r &= \frac{1}{2\pi} \oint p_r \, dr \\
&= \frac{1}{\pi}\left(\sqrt{2MER^2 - L^2} - |L|\arccos\frac{|L|}{\sqrt{2MER}} \right), \qquad (4.2)
\end{aligned}
$$

where E and L are the energy and the angular momentum, respectively, and R is the radius of the billiard. The frequencies of the classical motion on the two-dimensional tori can be found to be

$$
\omega_\varphi = \frac{\partial E}{\partial I_\varphi} = \frac{2E}{\sqrt{2MER^2 - L^2}}\arccos\frac{|L|}{\sqrt{2MER}} \qquad (4.3)
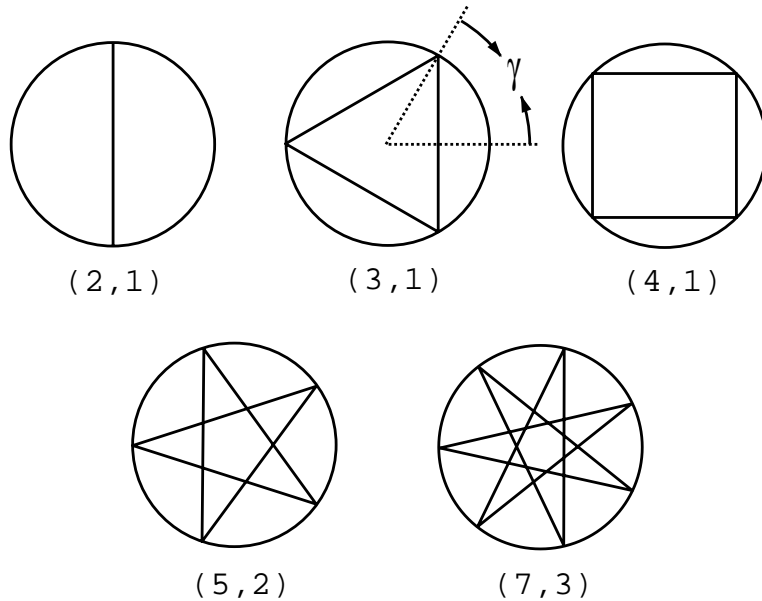$$

Figure 4.1: *Some examples of periodic orbits of the circle billiard. The orbits are labelled by the numbers (M_r, M_φ), which correspond to the number of sides of the polygons and the number of turns around the center. The angle γ is given by $\gamma = \pi M_\varphi / M_r$.*

$$\omega_r = \frac{\partial E}{\partial I_r} = \frac{2\pi E}{\sqrt{2MER^2 - L^2}} \ . \tag{4.4}$$

The Berry-Tabor formula includes all tori with a rational frequency ratio, i.e., tori on which the orbits are periodic. In the case of the circle billiard, the rational tori are given by the condition

$$\frac{\omega_\varphi}{\omega_r} = \frac{M_\varphi}{M_r} \ , \tag{4.5}$$

with positive integers M_r, M_φ and

$$M_r \geq 2M_\varphi \ . \tag{4.6}$$

The periodic orbits of the circle billiard have the form of regular polygons. The numbers M_r and M_φ can be shown to be identical to the number of sides of the corresponding polygon and its number of turns around the center of the circle, respectively (see, e.g., Ref. [52]). A few examples are shown in Figure 4.1. A pair of numbers (M_r, M_φ) which are not relatively prime corresponds to multiple traversals of a primitive periodic orbit.

The classical action of the periodic orbits is given by

$$
\begin{aligned}
S_{\mathbf{M}} &= 2\pi M_\varphi I_\varphi^{(\mathbf{M})} + 2\pi M_r I_r^{(\mathbf{M})} \\
&= \sqrt{2MER}\, 2M_r \sin\left(\frac{M_\varphi}{M_r}\pi\right) \ .
\end{aligned}
\tag{4.7}
$$

As in all billiard systems, the action scales like

$$S/\hbar = ws \ , \tag{4.8}$$

here with the scaling parameter

$$w \equiv \sqrt{2ME}\, R/\hbar = kR \tag{4.9}$$

and the scaled action

$$s \equiv 2M_r \sin\left(\frac{M_\varphi}{M_r}\pi\right) . \tag{4.10}$$

The form of the corresponding classical trajectory is independent of w. For the circle billiard with unit radius $R = 1$, the scaling parameter w is identical to the wave number k, and the scaled action is the length of the orbit.

For the semiclassical density of states, I start from the special version of the Berry-Tabor formula for two-dimensional systems, Eq. (2.11). Using the relation

$$\rho(w) = \frac{dE}{dw}\,\rho(E) \tag{4.11}$$

valid for billiard systems, I introduce the density of states depending on the scaling parameter w. Evaluating the different expressions in (2.11) for the circle billiard then finally leads to

$$\rho^{\mathrm{osc}}(w) = -\frac{1}{\pi}\mathrm{Im}\, g^{\mathrm{osc}}(w) , \tag{4.12}$$

with

$$g^{\mathrm{osc}}(w) = \sqrt{\frac{\pi}{2}}\sqrt{w}\sum_{\mathbf{M}} m_{\mathbf{M}}\frac{s_{\mathbf{M}}^{3/2}}{M_r^2}e^{i(ws_{\mathbf{M}}-\frac{3}{2}M_r\pi-\frac{\pi}{4})} , \tag{4.13}$$

where the relations $\alpha_\varphi = 0$ and $\alpha_r = 3$ for the Maslov indices have been used. The sum runs over all pairs of positive integers $\mathbf{M} = (M_r, M_\varphi)$ with $M_r \geq 2M_\varphi$. The degeneracy factor

$$m_{\mathbf{M}} = \begin{cases} 1 ; & M_r = 2M_\varphi \\ 2 ; & M_r > 2M_\varphi \end{cases} , \tag{4.14}$$

accounts for the fact that all trajectories with $M_r \neq 2M_\varphi$ can be traversed in two opposite directions.

Due to the rapid increase of the number of periodic orbits with growing action, the sum (4.13) does not converge. In the case of the circle billiard, the problem is even more complicated by the fact that there exist accumulation points of periodic orbits at scaled actions of multiples of 2π (see Fig. 4.2), which means that it is even impossible to include all periodic orbits up to a given finite action. In Ref. [34] the convergence problem of the sum (4.13) was solved by averaging with a Gaussian function. The semiclassical eigenvalues of the circle billiard were calculated from the periodic orbit sum by including a very large number of periodic orbits. My aim is to demonstrate that by using the harmonic inversion scheme, one can obtain eigenvalues of $w = kR$ from a relatively small set of periodic orbits. I will return to this problem in Section 3.3.

For the high resolution analysis of the quantum spectrum and for comparisons with the results from periodic orbit quantization by harmonic inversion, the exact quantum eigenvalues of the circle billiard are needed. I therefore briefly review the quantum mechanical expressions and the EBK quantization condition for this system. The exact quantum mechanical energy eigenvalues of the circle billiard with radius R are given by the condition

$$J_m(kR) = 0 , \quad m \in \mathbb{Z} , \quad E = \frac{\hbar^2 k^2}{2M} , \tag{4.15}$$

where J_m are the Bessel functions of integer order. Here, M denotes the mass of the particle, E is the energy, and $k = \sqrt{2ME}/\hbar$ is the wave number. The corresponding wave
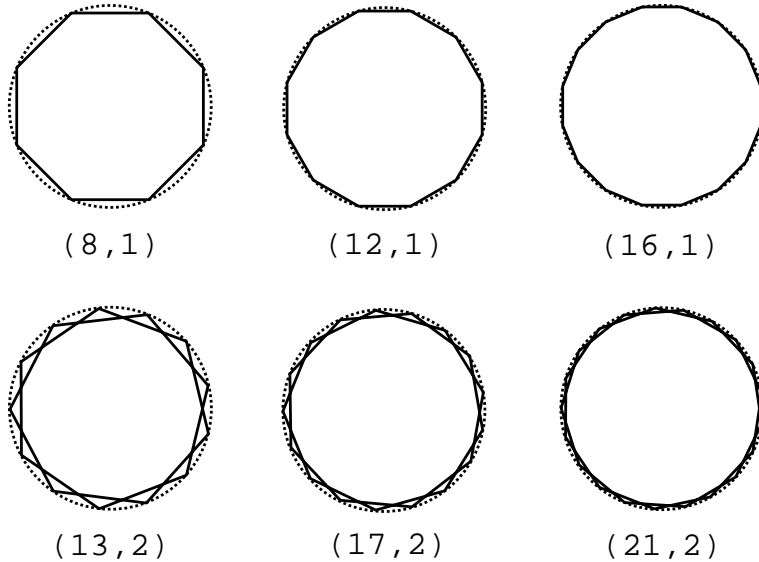
Figure 4.2: *Behaviour of the periodic orbits of the circle billiard (labelled by (M_r, M_φ)) for large M_r. As $M_r \to \infty$ at constant M_φ, the orbit converges to the boundary of the circle, with M_φ giving the number of revolutions around the center. The length of each single side of the orbit tends to zero, while the total length of the orbit $2M_r \sin(\pi M_\varphi/M_r)R$ converges to $2\pi M_\varphi R$ (R: radius of the billiard). The circle billiard therefore possesses accumulation points of orbits at scaled actions of multiples of 2π.*

functions are given by

$$\psi(r, \varphi) = J_m(kr)e^{im\varphi} . \tag{4.16}$$

As $J_{-m}(x) = (-1)^m J_m(x)$, all energy eigenvalues belonging to nonzero angular momentum quantum numbers $(m \neq 0)$ are twofold degenerate. In the following the exact quantum mechanical results for the circle billiard are used as a benchmark for the development and application of semiclassical quantization methods for integrable systems.

The EBK eigenvalues are obtained by quantization of the action variables

$$I_\varphi = \left(m + \frac{\alpha_\varphi}{4}\right)\hbar , \quad m \in \mathbb{Z} \tag{4.17}$$

$$I_r = \left(n + \frac{\alpha_r}{4}\right)\hbar , \quad n = 0, 1, 2, \ldots \tag{4.18}$$

with $\alpha_\varphi = 0$ and $\alpha_r = 3$ for the circle billiard. This yields the EBK quantization condition

$$\sqrt{(kR)^2 - m^2} - |m| \arccos\frac{|m|}{kR} = \left(n + \frac{3}{4}\right)\pi , \tag{4.19}$$

where $L = m\hbar$ are the angular momentum eigenvalues.

4.2 High resolution analysis of the quantum spectrum

In this section, the harmonic inversion procedures for the analysis of quantum spectra developed in Section 3.2 are applied to the circle billiard. The analysis of the exact

quantum spectrum in terms of periodic orbit contributions will provide a test for the validity of the Berry-Tabor formula as the leading order $\hbar$ contribution to the density of states. The quantum spectrum will also be weighted with diagonal matrix elements of different operators in order to verify the validity of the extended trace formulae discussed in Section 2.2. By the analysis of the difference spectrum between exact quantum and EBK eigenvalues, the first order $\hbar$ corrections to the trace formula can be determined. The results will be compared with the analytic expressions for the circle billiard found in Appendix A.2.

4.2.1 Leading order periodic orbit contributions to the density of states

For the circle billiard, the oscillating part $g^{\mathrm{osc}}(w)$ of the semiclassical response function is given by Eq. (4.13). If one eliminates the dependence of the amplitudes on w by defining

$$\rho'(w) = \frac{1}{\sqrt{w}}\rho(w) , \tag{4.20}$$

the resulting expression for the density of states

$$\rho'(w) = \frac{1}{\sqrt{8\pi}} \sum_{\mathbf{M}} m_{\mathbf{M}} \frac{s_{\mathbf{M}}^{3/2}}{M_r^2} \left(e^{i(\frac{3}{2}M_r\pi - \frac{\pi}{4})} e^{-iws_{\mathbf{M}}} + e^{-i(\frac{3}{2}M_r\pi - \frac{\pi}{4})} e^{iws_{\mathbf{M}}} \right) \tag{4.21}$$

is of the form (3.1), with $S_{\mathbf{M}}$ playing the rôle of ω_k. The quantum mechanical quantity corresponding to (4.20) is

$$\rho'_{\mathrm{qm}}(w) = \sum_{k} \frac{m_k}{\sqrt{w_k}} \delta(w - w_k) . \tag{4.22}$$

In addition to analyzing the pure quantum spectrum of the circle billiard, I also consider spectra weighted with diagonal matrix elements of different operators (cf. Section 2.2). The three different operators used are

- the absolute value of the angular momentum L, as an example of a constant of motion,

- the distance r from the center, as an example of a quantity which is no constant of motion,

- the variance of the radius $\langle r^2 \rangle - \langle r \rangle^2$, as an example using the relation (2.24) for products of operators.

The classical angular momentum L is proportional to w, which means that when constructing the signal for L, $g(w)$ now has to be multiplied by $w^{-3/2}$ instead of $w^{-1/2}$ (cf. Eq. (3.27)).

I calculated the scaled actions and classical amplitudes of the periodic orbits in the interval $s_{\mathbf{M}} \in [15, 23]$ with the help of the filter-diagonalization method. The signal was constructed from the exact zeros of the Bessel functions, up to a value of $w_{\max} = 500$. The accuracy of the results is improved if one cuts off the lower part of the signal, using
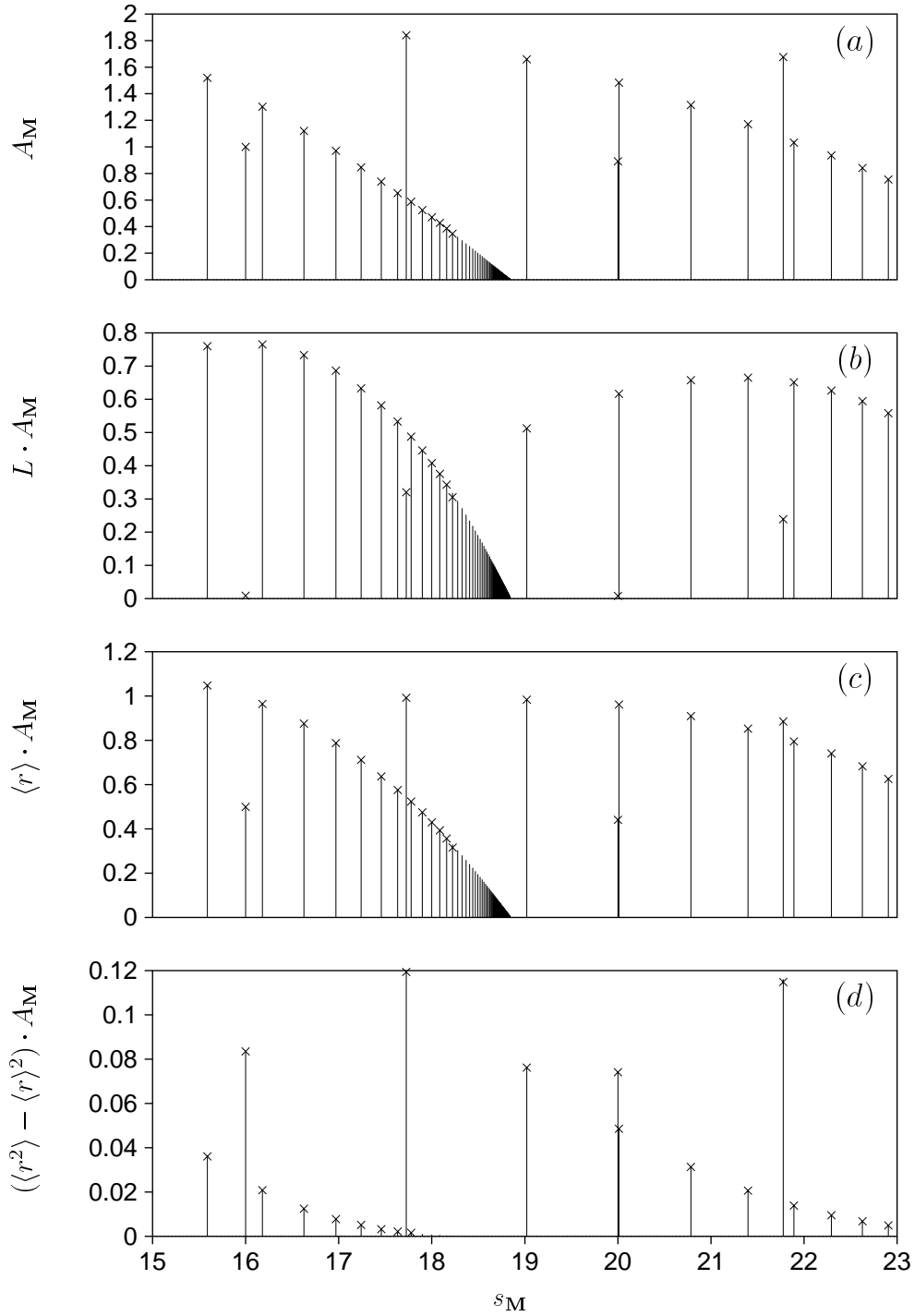
Figure 4.3: *Periodic orbit contributions to the trace formula calculated from the quantum spectrum of the circle billiard, including different operators. The quantities plotted are the classical amplitudes $A_{\mathbf{M}} = m_{\mathbf{M}} s_{\mathbf{M}}^{3/2}/M_r^2$ times the classical averages of the operators indicated, versus the scaled actions of the orbits. Crosses: values obtained from the quantum spectrum by harmonic inversion. Solid lines: values obtained from classical calculations. L: angular momentum in units of $\hbar w$ (w: scaling parameter), r: distance from the center in units of the radius R of the billiard.*

only zeros larger than $w_{\min} = 300$. A possible explanation for this is that the low zeros are in a sense "too much quantum" for the semiclassical periodic orbit sum.

Figure 4.3 shows the results of the calculation. The positions of the solid lines are the scaled actions of the classical periodic orbits, their heights are the classical amplitudes $m_{\mathbf{M}} s_{\mathbf{M}}^{3/2}/M_r^2$ times the respective averaged classical quantity. The crosses are the results obtained by harmonic inversion of the signal constructed from the zeros of the Bessel functions. There is an excellent agreement between the spectra, illustrating the validity of the Berry-Tabor formula and its extension to semiclassical matrix elements discussed in Section 2.2. The interval examined contains an accumulation point of orbits ($s = 6\pi$). Here, only those orbits were resolved which were still sufficiently isolated.

Although the Berry-Tabor formula only gives a semiclassical approximation to the density of states and the calculations in this section started from the exact quantum mechanical density, the results for the periodic orbit contributions are exact and do not show any deviations due to the error of the semiclassical approximation. The reason for this lies in the form of the $\hbar$ expansion of the density of states, as was discussed in Section 3.2.2: The higher order $\hbar$ contributions to the exact density of states do not satisfy the ansatz of the harmonic inversion procedure. Therefore the zeroth order contributions $\mathcal{A}_{\text{po}}^{(0)}$ are the best fit for the amplitudes. The higher oder terms have similar properties as a weak noise and are separated from the "true" signal by the harmonic inversion procedure.

4.2.2 First order $\hbar$ corrections

For the circle billiard, the exact quantum eigenvalues are given by the condition (4.15), while the zeroth order $\hbar$ eigenvalues are equal to the EBK eigenvalues given by (4.19) (cf. Section 2.1). From the difference between the exact and the semiclassical density of states, the amplitudes $\mathcal{A}_{\text{po}}^{(1)}$ of the first order correction to the trace formula can be calculated with the help of the procedure developed in Section 3.2.2.

I analyzed the difference spectrum between the exact and the EBK eigenvalues of the circle billiard in the range $100 < w < 500$. Figure 4.4 shows a small part of this difference spectrum. The results of the harmonic inversion of the spectrum are presented in Figure 4.5. The crosses mark the values

$$ f(\gamma) \equiv \frac{2}{\sqrt{\pi M_r}} \frac{1}{\sqrt{w}} |\mathcal{A}_{\text{po}}^{(1)}| \, , \tag{4.23} $$

with $\gamma = \pi M_\varphi / M_r$, which were obtained for the periodic orbits by harmonic inversion of the difference spectrum. The crosses are labelled by the numbers (M_r, M_φ) of the orbits. The solid line in Fig. 4.5 is the theoretical curve

$$ f(\gamma) = \frac{5 - 2\sin^2\gamma}{3\sin^{3/2}\gamma} \, , \tag{4.24} $$

which results from the analytical expression (A.38) for the first order amplitudes discussed in Appendix A.2. The results obtained by harmonic inversion are in excellent agreement with the theoretical curve, which clearly illustrates the validity of Eq. (A.38).
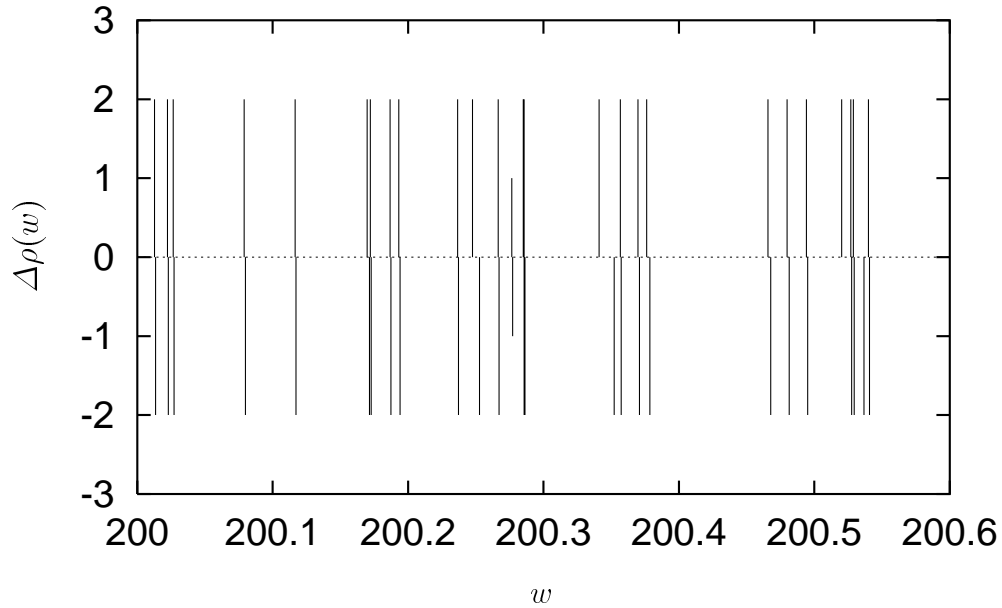
Figure 4.4: *Part of the difference spectrum* $\Delta\rho(w) = \rho_{\mathrm{qm}}(w) - \rho_{\mathrm{EBK}}(w)$ *between the exact quantum mechanical and the semiclassical density of states. The absolute values of the peak heights mark the multiplicities of the states.*
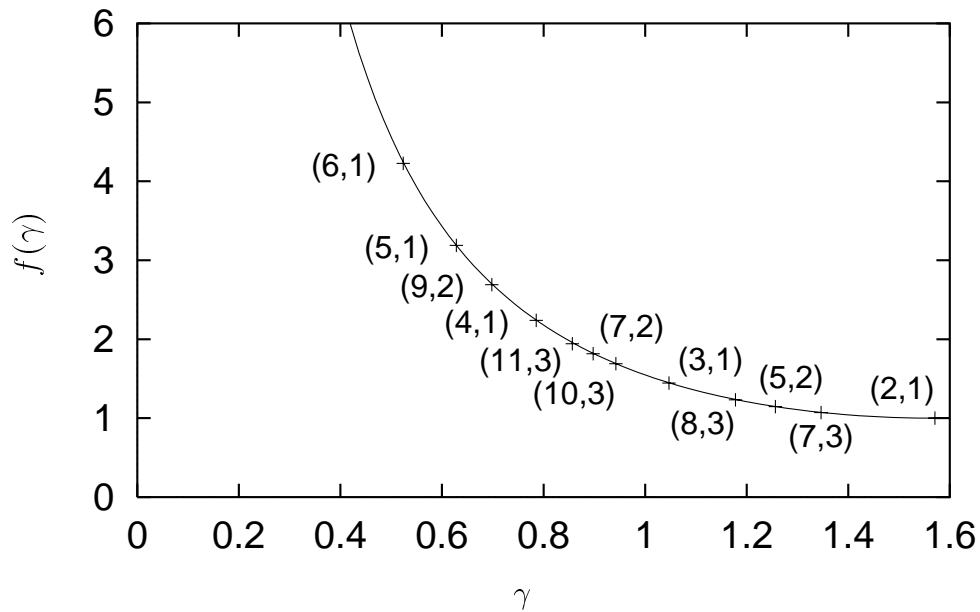

Figure 4.5: *First order $\hbar$ corrections to the Berry-Tabor formula for the circle billiard. Crosses: amplitudes $(2/\sqrt{\pi M_r w})\,|\mathcal{A}_{\mathrm{po}}^{(1)}|$ obtained by harmonic inversion. The orbits are labelled by the numbers (M_r, M_φ). Solid line: theoretical curve $f(\gamma) = (5 - 2\sin^2\gamma)/(3\sin^{3/2}\gamma)$, where $\gamma = \pi M_\varphi/M_r$.*

39

4.3 Periodic orbit quantization of the circle billiard by harmonic inversion

In this section, I turn to the semiclassical quantization of the circle billiard by harmonic inversion. The techniques developed in Section 3.3 are applied to the circle billiard in order to extract the eigenvalues and semiclassical matrix elements from the periodic orbit sum. In addition to the semiclassical eigenvalues, the first order $\hbar$ corrections to the eigenvalues will be determined. Finally, it is demonstrated how the resolution of the harmonic inversion results can be improved by the construction and analysis of cross-correlated periodic orbit sums. The efficiency of the method will be discussed for various sets of operators and various sizes of the cross-correlation matrix.

4.3.1 Calculation of the lowest eigenvalues

The semiclassical response function of the circle billiard is given by Eq. (4.13). The amplitudes in (4.13) are proportional to $w^{1/2}$. As described in Section 3.3.1, one can eliminate this dependence on w by introducing the quantity

$$g'(w) = w^{-1/2} g(w) \ . \tag{4.25}$$

Following the procedure outlined in Section 3.3.1, I construct a Gaussian smoothed semiclassical signal, which is analyzed with the filter-diagonalization method. The semiclassical and the corresponding exact quantum signal (cf. Eqs. (3.37) and (3.38)) for the circle billiard read:

$$C_\sigma(s) = \frac{e^{-i\frac{\pi}{4}}}{2\sigma} \sum_{\mathbf{M}} m_{\mathbf{M}} \frac{s_{\mathbf{M}}^{3/2}}{M_r^2} e^{-i\frac{3}{2}M_r\pi} e^{-(s-s_{\mathbf{M}})^2/2\sigma^2} \ , \tag{4.26}$$

$$C_{\mathrm{qm},\sigma}(s) = -i \sum_k \frac{m_k}{\sqrt{w_k}} e^{-\frac{1}{2}\sigma^2 w_k^2} e^{-isw_k} \ . \tag{4.27}$$

Eq. (4.27) possesses the functional form (3.1) with

$$d_k = -i \frac{m_k}{\sqrt{w_k}} e^{-\frac{1}{2}\sigma^2 w_k^2} \ . \tag{4.28}$$

Applying the harmonic inversion method to the signal (4.26) should yield the eigenvalues of w as frequencies, with the amplitudes given by Eq. (4.28).

I calculated the eigenvalues of the scaling parameter $w = kR$ for the lowest states of the circle billiard from a signal of length $s_{\max} = 150$. For the construction of the signal, I chose a minimum length for the sides of the periodic orbits as cut-off criterion at the accumulation points (cf. Fig. 4.2). It could be observed that the results were nearly independent of the choice of this parameter, as long as the minimum length was not chosen too large.

Table 4.1 presents the semiclassical eigenvalues w_{hi} and multiplicities m_{hi} obtained by harmonic inversion of the periodic orbit signal (4.26). For comparison, the exact quantum mechanical and the EBK results are also given in Table 4.1. The eigenvalues obtained by harmonic inversion clearly reproduce the EBK eigenvalues to within an accuracy of 10^{-4} or better. The deviation of the harmonic inversion results w_{hi} from the EBK eigenvalues is significantly smaller than the error of the semiclassical approximation.

Table 4.1: *Lowest eigenvalues w_k and multiplicities m_k of the scaling parameter $w = kR$ of the circle billiard. w_{ex} and m_{ex}: exact quantum values. w_{EBK}: EBK eigenvalues. w_{hi} and m_{hi}: values obtained by harmonic inversion of a signal of length $s_{\text{max}} = 150$. The numbers n and m are the radial and angular momentum quantum numbers. The nearly degenerate eigenvalues at $w \approx 11.0$ and $w \approx 13.3$ were not resolved.*

n	m	w_{ex}	w_{EBK}	m_{ex}	w_{hi}	m_{hi}
0	0	2.404826	2.356194	1	2.356204	1.0005
0	1	3.831706	3.794440	2	3.794444	1.9983
0	2	5.135622	5.100386	2	5.100391	1.9996
1	0	5.520078	5.497787	1	5.497785	0.9988
0	3	6.380162	6.345186	2	6.345191	2.0000
1	1	7.015587	6.997002	2	6.997006	2.0001
0	4	7.588342	7.553060	2	7.553065	1.9992
1	2	8.417244	8.400144	2	8.400149	1.9998
2	0	8.653728	8.639380	1	8.639404	0.9987
0	5	8.771484	8.735670	2	8.735677	2.0013
1	3	9.761023	9.744628	2	9.744632	1.9999
0	6	9.936110	9.899671	2	9.899675	1.9999
2	1	10.173468	10.160928	2	10.160932	2.0000
1	4	11.064709	11.048664	2	11.048968	4.0012
0	7	11.086370	11.049268	2		
2	2	11.619841	11.608251	2	11.608256	2.0006
3	0	11.791534	11.780972	1	11.780978	1.0001
0	8	12.225092	12.187316	2	12.187319	1.9993
1	5	12.338604	12.322723	2	12.322724	2.0000
2	3	13.015201	13.004166	2	13.004168	1.9997
3	1	13.323692	13.314197	2	13.315045	4.0287
0	9	13.354300	13.315852	2		
1	6	13.589290	13.573465	2	13.573465	2.0000
2	4	14.372537	14.361846	2	14.361849	1.9994
0	10	14.475501	14.436391	2	14.436395	2.0006
3	2	14.795952	14.787105	2	14.787076	1.9909
1	7	14.821269	14.805435	2	14.805453	2.0066
4	0	14.930918	14.922565	1	14.922569	1.0001

Note that for calculating the eigenvalues of the circle billiard by a direct evaluation of the periodic orbit sum, a huge number of periodic orbit terms is required, e.g., orbits with maximum length $s_{\mathrm{max}} = 30\,000$ were included in Ref. [34]. I obtained similar results using only orbits up to length $s_{\mathrm{max}} = 150$. This demonstrates the high efficiency of the harmonic inversion method in extracting eigenvalues from the periodic orbit sum. The efficiency can even be further increased with the help of the cross-correlation technique (cf. Section 3.3.3), as will be demonstrated for the circle billiard in Section 4.3.4.

In Table 4.1 the exact multiplicities m_{ex} of eigenvalues and the multiplicities m_{hi} obtained by harmonic inversion also agree to very good precision. The deviations are one or two orders of magnitude larger than those of the frequencies, which reflects the fact that, with the harmonic inversion method using filter-diagonalization, the amplitudes usually converge more slowly than the frequencies.

In the frequency interval shown, there are two cases of nearly degenerate frequencies which have not been resolved by harmonic inversion of the periodic orbit signal with $s_{\mathrm{max}} = 150$. The harmonic inversion yielded only one frequency, which is the average of the two nearly degenerate ones, with the amplitudes of the two added ($m_{\mathrm{hi}} \approx 4$). These nearly degenerate states can be resolved when the signal length is increased to about $s_{\mathrm{max}} = 500$ or with the help of cross-correlated periodic orbit sums (see Section 4.3.4).

4.3.2 Semiclassical matrix elements

Using the extended periodic orbit sums discussed in Section 2.2, one can now also calculate semiclassical diagonal matrix elements for the circle billiard. Following the procedure described in Section 3.3.1, a semiclassical signal can be constructed from the extended response function weighted with the averages of some classical quantity, the analysis of which should again yield the eigenvalues w_k as frequencies but with the amplitudes weighted with the diagonal matrix elements of the corresponding operator. As examples, I used the same operators as in Section 4.2.1 to calculate the diagonal matrix elements $\langle L \rangle$, $\langle r \rangle$, and the variance of the radius, $\langle r^2 \rangle - \langle r \rangle^2$.

Figure 4.6 shows the results in the range $25 \leq w \leq 30$. For comparison, Fig. 4.6a presents the spectrum for the identity operator. The positions of the solid lines are the EBK eigenvalues, their heights are the semiclassical matrix elements obtained from EBK theory times the multiplicities. The crosses are the results of the harmonic inversion of a signal of length $s_{\mathrm{max}} = 300$. The diagrams show an excellent agreement between the results obtained by harmonic inversion and those from EBK torus quantization. This is even the case for the variance of r, which is a very small quantity.

For the states shown in Fig. 4.6, I have also compared the semiclassical with the exact quantum mechanical matrix elements. The agreement is also excellent. The deviations between the semiclassical and quantum matrix elements turn out to be typically of the order of $\sim 10^{-3}$, which reflects the error of the semiclassical approximation.

4.3.3 Higher order $\hbar$ corrections

I will now apply the technique of Section 3.3.2 to the circle billiard in order to calculate the first order corrections to the semiclassical eigenvalues obtained in Section 4.3.1. According
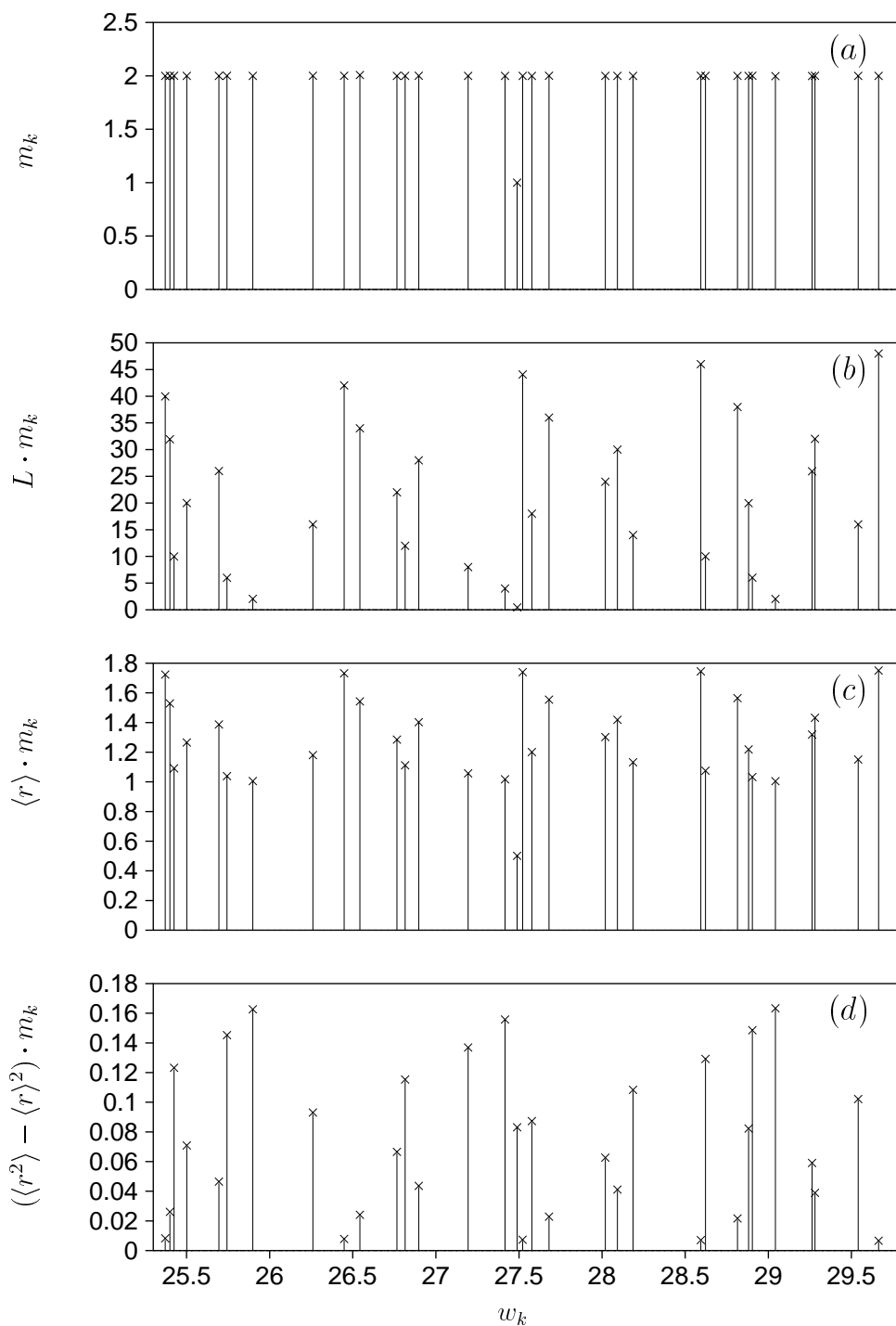
Figure 4.6: *Circle billiard: Results of the harmonic inversion of a semiclassical signal of length $s_{\max} = 300$ constructed from the periodic orbit sum including different operators. The quantities plotted are the diagonal matrix elements of the operators indicated times the multiplicities m_k, versus the eigenvalues w_k of the scaling parameter. Crosses: results of the harmonic inversion procedure. Solid lines: semiclassical matrix elements obtained from EBK theory and EBK eigenvalues. L: angular momentum in units of $\hbar$, r: distance from the center in units of the radius R of the billiard.*
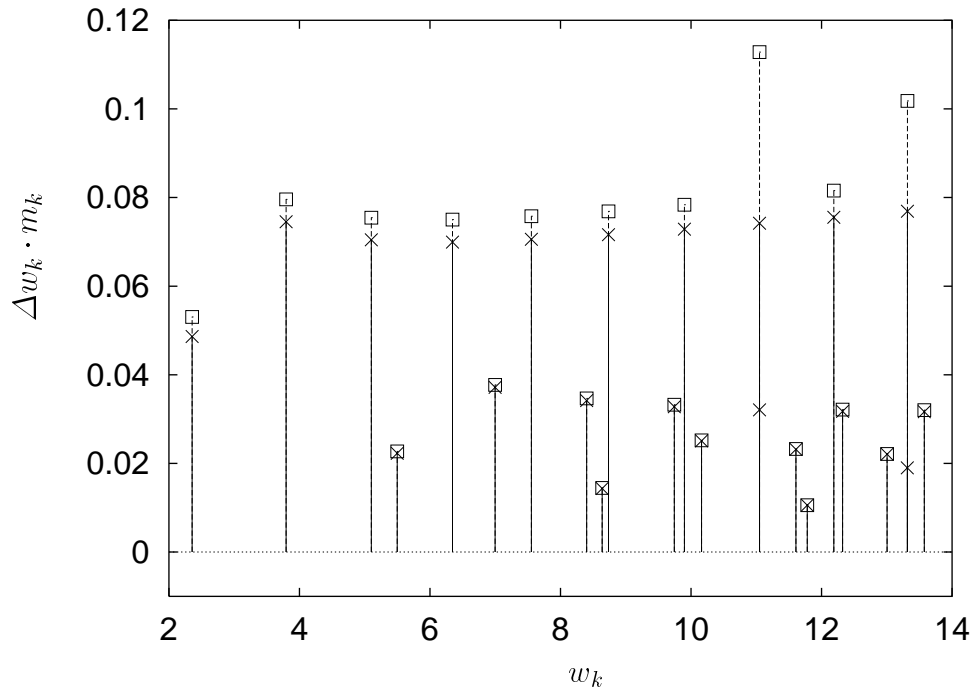
43

Figure 4.7: *Correction terms to the semiclassical eigenvalues of the circle billiard. Squares: corrections $\Delta w_{k,1} = w_{k,1} - w_{k,0}$ between first and zeroth order approximations (times multiplicities) obtained by harmonic inversion. Crosses: differences $w_{\text{ex}} - w_{\text{EBK}}$ between exact quantum and EBK eigenvalues (times multiplicities).*
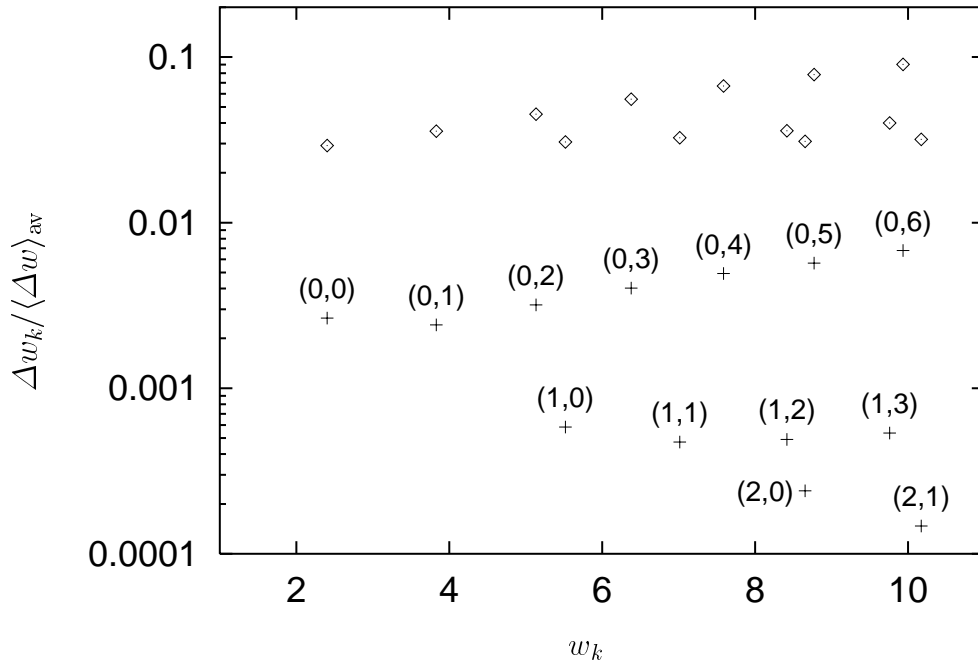

Figure 4.8: *Semiclassical errors $|w_{k,0} - w_{\text{ex}}|$ (diamonds) and $|w_{k,1} - w_{\text{ex}}|$ (crosses) of zeroth and first order approximations to the eigenvalues obtained by harmonic inversion, in units of the average level spacing $\langle \Delta w \rangle_{\text{av}} \approx 4/w$. The states are labelled by the quantum numbers (n, m).*

44

to Section 4.1, the zeroth order amplitudes of the circle billiard are given by (cf. Eq. (4.13))

$$\frac{1}{\sqrt{w}}\mathcal{A}_{\mathrm{po}}^{(0)} = \sqrt{\frac{\pi}{2}}m_{\mathbf{M}}\frac{s_{\mathbf{M}}^{3/2}}{M_r^2}e^{-i(\frac{3}{2}M_r\pi+\frac{\pi}{4})} \ , \tag{4.29}$$

with $s_{\mathbf{M}}$ and $m_{\mathbf{M}}$ the action and multiplicity of the orbit, respectively. The expression for the first order amplitudes derived in Appendix A.2 (cf. Eq. (A.38)) reads

$$\frac{1}{\sqrt{w}}\mathcal{A}_{\mathrm{po}}^{(1)} = \sqrt{\pi M_r}\,\frac{2\sin^2\gamma - 5}{6\sin^{3/2}\gamma}\,e^{-i(\frac{3}{2}M_r\pi-\frac{\pi}{4})} \ , \tag{4.30}$$

with $\gamma \equiv \pi M_\varphi/M_r$.

Using these expressions, I have calculated the first order corrections $\Delta w_{k,1}$ to the lowest eigenvalues of the circle billiard. A periodic orbit signal of length $s_{\max} = 200$ was constructed, which was analyzed with the help of the filter-diagonalization method. Part of the resulting spectrum is presented in Figure 4.7. The peak heights (squares) are the corrections $\Delta w_{k,1} = w_{k,1} - w_{k,0}$ times the multiplicities obtained by harmonic inversion. For comparison, the differences between the exact and the EBK eigenvalues at the positions of the EBK eigenvalues are also plotted (crosses in Fig. 4.7). Both spectra are in excellent agreement. Only the nearly degenerate states at $w \approx 11.0$ and $w \approx 13.3$ were again not resolved; in these cases, the harmonic inversion again yielded a mean frequency with the amplitudes of the two unresolved frequencies added. The remaining small deviations of the peak heights arise from second or higher order corrections to the eigenvalues.

An appropriate measure for the accuracy of semiclassical eigenvalues is the deviation from the exact quantum eigenvalues in units of the average level spacings, $\langle\Delta w\rangle_{\mathrm{av}} = 1/\bar{\rho}(w)$. Figure 4.8 presents the semiclassical error in units of the average level spacings $\langle\Delta w\rangle_{\mathrm{av}} \approx 4/w$ for the zeroth order (diamonds) and first order (crosses) approximations to the eigenvalues. In zeroth order approximation the semiclassical error for the low lying states is about 3 to 10 percent of the mean level spacing. This error is reduced in the first order approximation by at least one order of magnitude for the "least semiclassical" states with radial quantum number $n = 0$. The accuracy of states with $n \geq 1$ is improved by two or more orders of magnitude.

4.3.4 Reduction of the required signal length via harmonic inversion of cross-correlated periodic orbit sums

In this section, the cross-correlation technique developed in Section 3.3.3 is applied to the circle billiard in order to demonstrate how the efficiency of the harmonic inversion method is improved by this procedure.

For the circle billiard, the mean density of states – with all multiplicities taken as one – is given by $\bar{\rho}(w) \approx w/4$. According to (3.2), the signal length required for a single signal to resolve the frequencies in a given interval around w is therefore approximately

$$s_{\max} \approx 4\pi\bar{\rho}(w) \approx \pi w \approx 2S_H \ , \tag{4.31}$$

where $S_H = 2\pi\bar{\rho}$ is the Heisenberg period (which is action instead of time for scaling systems). By using an $N \times N$ set of cross-correlated signals, it should be possible to

Table 4.2: *Nearly degenerate eigenvalues of the circle billiard, obtained by harmonic inversion of a 2×2 cross-correlated signal of length $s_{\max} = 150$. The meanings of the quantities are the same as in Table 4.1. The nearly degenerate eigenvalues are now resolved, which for a single signal would have required a signal length of $s_{\max} \approx 500$.*

n	m	w_{ex}	w_{EBK}	m_{ex}	w_{hi}	m_{hi}
1	4	11.064709	11.048664	2	11.048664	2.0665
0	7	11.086370	11.049268	2	11.049295	1.9315
3	1	13.323692	13.314197	2	13.314205	1.9987
0	9	13.354300	13.315852	2	13.315839	2.0016

Table 4.3: *Maximum frequencies $w_{\max}$ up to which the spectrum could be resolved with an $N \times N$ cross-correlated signal. The b_α are the classical quantities or functions of classical quantities used to build the signal (see text); r: distance from center, L: angular momentum in units of $\hbar w$.*

N	$w_{\max}$	b_α
1	45	1
2	65	1, $\langle r \rangle$
3	90	1, $\langle r \rangle$, L^2
4	120	1, $\langle r \rangle$, L^2, $e^{-(\langle r \rangle - 0.7)^2/3}$
5	130	1, $\langle r \rangle$, L^2, $1/\langle r \rangle^2$, $e^{-(L-1)^2/10}$

extract about the same number of semiclassical eigenvalues from a reduced signal length $s_{\max} \ll 2S_H$, or, vice versa, if the signal length is held constant, the resolution and therefore the number of converged eigenvalues should significantly increase.

To demonstrate the power of the cross-correlation technique, I first analyze a 2×2 cross-correlated periodic orbit signal of the circle billiard with $\hat{A}_1 = \mathbf{1}$ the identity operator and $\hat{A}_2 = r$. For comparison with the results in Section 4.3.1, the same signal length $s_{\max} = 150$ is chosen. By contrast with the eigenvalues in Table 4.1 obtained from the one-dimensional signal the nearly degenerate states around $w \approx 11.0$ and $w \approx 13.3$ are now resolved as can be seen in Table 4.2. Note that a signal length $s_{\max} \approx 500$ is required to resolve these states without application of the cross-correlation technique.

As in all other calculations using cross-correlated signals, the results were improved by not making a sharp cut at the accumulation points but by damping the amplitudes of the orbits near these points. With the same cut-off criterion at the accumulation points, the total number of orbits in the signal with $s_{\max} = 150$ was about 10 times smaller than in the signal with $s_{\max} = 500$. This means, the required number of orbits could be reduced by one order of magnitude. For chaotic systems, where the number of orbits grows more rapidly (exponentially) with the maximum action, the improvement in the required number of orbits may even be better.

I now investigate the number of eigenvalues which do converge for fixed signal length,
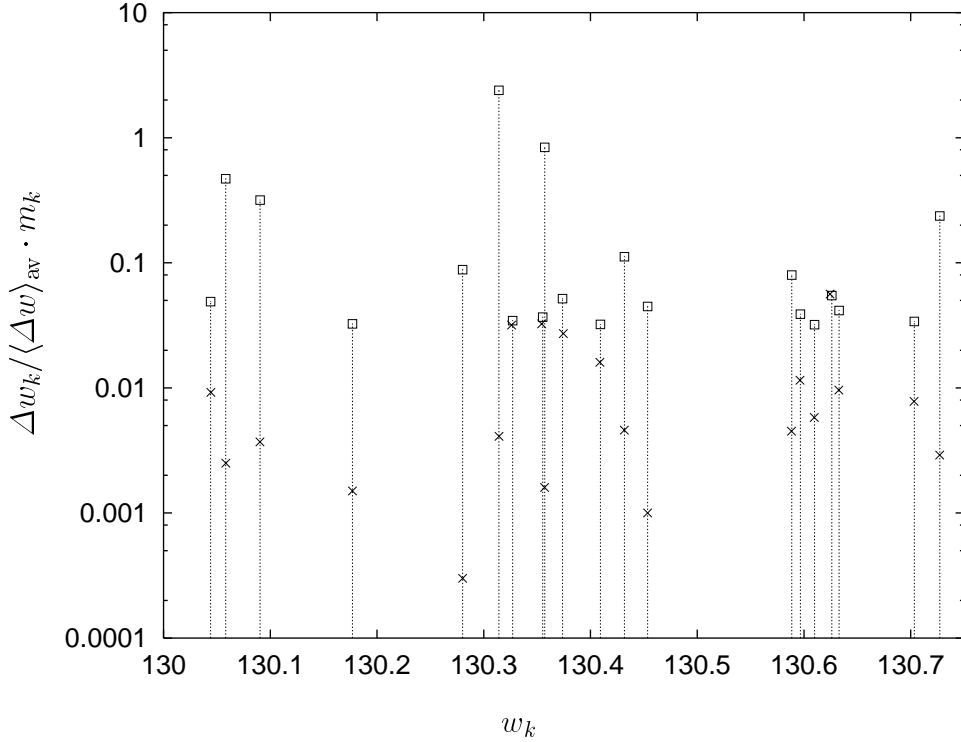
Figure 4.9: *Eigenvalues of the circle billiard (abscissa) in the dense part of the spectrum obtained from a 5×5 cross-correlated signal of length $s_{\max} = 150 = 0.735 S_H$ with S_H the Heisenberg period. With a single signal the required signal length would be $s_{\max} \approx 2 S_H$. Squares and sticks: EBK eigenvalues. Crosses: results of harmonic inversion. The peak heights give the semiclassical error $|w_{\mathrm{EBK}} - w_{\mathrm{ex}}|$ (squares) and the difference between harmonic inversion results and EBK eigenvalues $|w_{\mathrm{hi}} - w_{\mathrm{EBK}}|$ (crosses) in units of the mean level spacing $\langle \Delta w \rangle_{\mathrm{av}} \approx 4/w$. The error of the harmonic inversion procedure is about one order of magnitude smaller than the semiclassical error.*

but different sets of operators and dimensions of the cross-correlation matrix. Generally, the highest eigenvalue $w_{\max}$ which can be resolved increases significantly when the cross-correlation technique is applied. However, the detailed results depend on the operators chosen. Furthermore, with increasing dimension of the matrix, the range in which the transition from resolved to unresolved eigenvalues takes place becomes broader, and the amplitudes in this region become less well converged. Rough estimates of $w_{\max}$ for various sets of operators and fixed signal length $s_{\max} = 150$ are given in Table 4.3. For some of the signals, the extension of the trace formula to functions of matrix elements, Eqs. (2.25) and (2.26), was used. The improvement achieved by increasing the dimension of the matrix by one is most distinct for very small N; for $N \geq 5$, the improvement is found to be only small. This suggests that, at given signal length and frequency range, the matrix dimension should not be chosen too large, i.e., there exists an optimal matrix dimension, which at constant signal length becomes larger with increasing eigenvalues w.

With a 5×5 signal of length $s_{\max} = 150$, eigenvalues up to the region $w \approx 130$ can be resolved. The results are presented in Figure 4.9. There are two points which should be emphasized: The first point is that, even in this dense part of the spectrum, the error of the method is still by about one order of magnitude smaller than the semiclassical error, which is illustrated in Fig. 4.9 by the peak heights. The squares and crosses mark the

47

semiclassical error $|w_{\mathrm{EBK}} - w_{\mathrm{ex}}|$ and the numerical error $|w_{\mathrm{hi}} - w_{\mathrm{EBK}}|$ of the harmonic inversion procedure in units of the mean level spacing $\langle \Delta w \rangle_{\mathrm{av}} \approx 4/w$. The second point concerns the signal length compared to the Heisenberg action $S_H = 2\pi\bar{\rho}$. For $w = 130$, one obtains $S_H \approx 204.2$. A one-dimensional signal would have required a signal length $s_{\max} \approx 2S_H$. With the cross-correlation technique, I have calculated the eigenvalues from a signal of length $s_{\max} = 150 \approx 0.735 S_H$. This is about the same signal length as required by the semiclassical quantization method of Berry and Keating [12, 13], which, however, only works for ergodic systems.

In summary, the results demonstrate that by analyzing cross-correlated signals instead of a single signal, the required signal length can indeed be significantly reduced. Clearly, the signal length cannot be made arbitrarily small, and the method is restricted to small dimensions of the cross-correlation matrix. However, the number of orbits which have to be included can be very much reduced. Another advantage of the method is that not only the frequencies and the multiplicities but also the diagonal matrix elements of the chosen operators are obtained by one single calculation.

4.3.5   Including higher order $\hbar$ corrections

In the cases discussed so far, the cross-correlated signal was constructed by including different operators and making use of Eq. (2.24). By this procedure, it was possible to obtain the semiclassical eigenvalues from a signal of reduced length or improve the resolution of the spectrum at constant signal length, while simultaneously obtaining the diagonal matrix elements of the operators. For the circle billiard, one can now even go one step further and include higher $\hbar$ corrections in the signal. The first order correction term (A.38), which in Section 4.3.3 was harmonically inverted as a single signal, is now included as part of a cross-correlated signal. This procedure combines all the techniques discussed in the previous sections.

Formally, the frequencies in the zeroth and first order $\hbar$ parts of the cross-correlated signal are not exactly the same [see the denominators in Eqs. (3.33) and (3.46)], however, as already mentioned in Section 3.3.2, the values obtained numerically for the frequencies $\bar{w}_k$ in (3.49) are equal to the lowest order $\hbar$ eigenvalues rather than the exact average of the zeroth and first order eigenvalues. In practice, the cross-correlated signal is therefore in fact of the form (3.11). One can now, on the one hand, improve the resolution of the spectrum, and, on the other hand, obtain semiclassical matrix elements and the first order corrections to the eigenvalues with the same high resolution by one single harmonic inversion of a cross-correlated signal.

As an example, I built a 3×3 signal from the first order correction term given by (4.30) and the operators $\hat{A}_1 = \mathbf{1}$ (identity) and $\hat{A}_2 = r$. Again, the signal length was chosen to be $s_{\max} = 150$. By harmonic inversion of the cross-correlated signal, the semiclassical eigenvalues, their first order order corrections, and the semiclassical matrix elements of the operator r are simultaneously obtained. The results for the zeroth order approximations $w_{k,0}$ to the eigenvalues and the first order approximations $w_{k,1} = w_{k,0} + \Delta w_{k,1}$ are presented in Table 4.4. For comparison the exact and the EBK eigenvalues are also given. As with the results presented in Table 4.2, the nearly degenerate states have been resolved in the zeroth order approximation, which for a single signal would have required a signal length of $s_{\max} \approx 500$. Moreover, in contrast to the results of Section 4.3.3, it was now also possible to resolve the first order approximations to the nearly degenerate states.

Table 4.4: Zeroth ($w_{k,0}$) and first ($w_{k,1}$) order semiclassical approximations to the eigenvalues of the circle billiard, obtained simultaneously by harmonic inversion of a 3×3 cross-correlated signal of length $s_{\max} = 150$. The nearly degenerate eigenvalues at $w \approx 11.0$ and $w \approx 13.3$ (marked by vertical lines) are well resolved.

n	m	w_{EBK}	$w_{k,0}$	$w_{k,1}$	w_{ex}
0	0	2.356194	2.356230	2.409288	2.404826
0	1	3.794440	3.794440	3.834267	3.831706
0	2	5.100386	5.100382	5.138118	5.135622
1	0	5.497787	5.497816	5.520550	5.520078
0	3	6.345186	6.345182	6.382709	6.380162
1	1	6.997002	6.997006	7.015881	7.015587
0	4	7.553060	7.553055	7.590990	7.588342
1	2	8.400144	8.400145	8.417503	8.417244
2	0	8.639380	8.639394	8.653878	8.653728
0	5	8.735670	8.735672	8.774213	8.771484
1	3	9.744628	9.744627	9.761274	9.761023
0	6	9.899671	9.899660	9.938954	9.936110
2	1	10.160928	10.160949	10.173568	10.173468
1	4	11.048664	11.048635	11.063791	11.064709
0	7	11.049268	11.049228	11.087943	11.086370
2	2	11.608251	11.608254	11.619919	11.619841
3	0	11.780972	11.780993	11.791599	11.791534
0	8	12.187316	12.187302	12.228037	12.225092
1	5	12.322723	12.322721	12.338847	12.338604
2	3	13.004166	13.004167	13.015272	13.015201
3	1	13.314197	13.314192	13.323418	13.323692
0	9	13.315852	13.315782	13.356645	13.354300
1	6	13.573465	13.573464	13.589544	13.589290
2	4	14.361846	14.361846	14.372606	14.372537
0	10	14.436391	14.436375	14.478531	14.475501
3	2	14.787105	14.787091	14.795970	14.795952
1	7	14.805435	14.805457	14.821595	14.821269
4	0	14.922565	14.922572	14.930938	14.930918
0	11	15.550089	15.550084	15.593060	15.589848
2	5	15.689703	15.689701	15.700239	15.700174
1	8	16.021889	16.021888	16.038034	16.037774
3	3	16.215041	16.215047	16.223499	16.223466
4	1	16.462981	16.462982	16.470648	16.470630
0	12	16.657857	16.657846	16.701442	16.698250
2	6	16.993489	16.993486	17.003884	17.003820
1	9	17.225257	17.225252	17.241482	17.241220
3	4	17.607830	17.607831	17.615994	17.615966
0	13	17.760424	17.760386	17.804708	17.801435
4	2	17.952638	17.952662	17.959859	17.959819
5	0	18.064158	18.064201	18.071125	18.071064

Chapter 5

Application to a chaotic system: The open and closed three-disk scattering system

In the previous chapter, the harmonic inversion techniques developed in Chapter 3 have been successfully applied to an integrable and bound system. For the example of the circle billiard, harmonic inversion has proven to be a powerful method for the high precision analysis of quantum spectra as well as for the extraction of eigenvalues from the periodic orbit sum. To demonstrate the universality of the harmonic inversion method, the same techniques will now be applied to the three-disk scatterer as an example of a system with a completely chaotic dynamics.

The system considered here consists of three equally spaced hard disks of unit radius. The existence or nonexistence of periodic orbits and the behaviour of the periodic orbit parameters in the three-disk system sensitively depend on the distance d between the centers of the disks. The case of large disk separations, especially $d = 6$, has served as a model for periodic orbit quantization of chaotic systems in many investigations during recent years. In particular, the system has served as a prototype model for periodic orbit quantization by cycle expansion techniques [10, 44, 53, 54]. For large disk separations, the assumptions of the cycle expansion, namely that the contributions from long orbits are shadowed by those of short orbits, is ideally fulfilled. This is not true for small disk separations. As the disks approach each other, the convergence of the cycle expansion becomes slower and slower until it finally breaks down. On the other hand, periodic orbit quantization by harmonic inversion does not depend on properties like the shadowing of orbits and should therefore also work well for small disk separations. I will apply the harmonic inversion techniques to the case of the large disk separation $d = 6$ as well as to the small separation $d = 2.5$, where the convergence of the cycle expansion is already slow. As an especially challenging system, I will also consider the limiting case of touching disks, $d = 2$. This system does not fulfill the requirements of the cycle expansion and other semiclassical methods at all as it exhibits strong pruning (see following sections). To the best of my knowledge, no other semiclassical method has succeeded in calculating more than the very lowest eigenvalues of the closed three-disk system so far.

## 5.1 Periodic orbits and quantum eigenvalues

I start by summarizing the basic properties of the three-disk system relevant for periodic orbit quantization. Furthermore, the behaviour of the periodic orbits and the distribution of the orbit parameters at different disk separations are investigated, and the resulting strategies for the numerical search for periodic orbits are discussed.

5.1.1 Symbolic code and symmetry reduction

The periodic orbits of the three-disk system can be labelled by a ternary symbolic code, which is complete for sufficiently separated disks. The classical dynamics of the three-disk system has been studied, among others, by Gaspard and Rice [55]. If the disks are labelled by the numbers 1, 2, 3, each periodic orbit is characterized by a sequence of these numbers, indicating the disks the particle collides with during one period of the orbit (see Fig. 5.1a). For sufficiently separated disks, there is a one-to-one correspondence between the symbolic code and the periodic orbits of the system: For every sequence there exists one unique periodic orbit (with the restriction that consecutive repetitions of the same symbol are forbidden and circular shifts of a sequence describe the same orbit). As was shown by Hansen [56], at disk separation $d = 2.04821419$ pruning sets in, i. e., part of the orbits become nonphysical as they run through one of the disks, and the symbolic code is no longer complete. The number of pruned orbits rapidly becomes larger and larger if the disks continue to approach each other. In the limiting case of touching disks, $d = 2$, the system exhibits strong pruning. Examples of pruned orbits will be discussed in Section 5.1.3.

In my calculations, I will make use of the symmetry reduction introduced by Cvitanović and Eckhardt in Ref. [10]: The three-disk system is invariant under the symmetry operations of the group C_{3v}, i. e., reflections at three symmetry lines and rotations by $2\pi/3$ and $4\pi/3$. The periodic orbits fall into three classes of distinct symmetry: orbits invariant under reflections at one of the symmetry lines (multiplicity 3), orbits invariant under rotations by $2\pi/3$ and $4\pi/3$ (multiplicity 2), and orbits with no symmetry (multiplicity 6). Accordingly, the periodic orbits appear in multiplets of 2, 3 or 6 orbits which emerge from each other by application of the symmetry operations. The quantum states are grouped in the three irreducible subspaces A_1, A_2, and E, where the states of the A_1 (A_2) subspace are symmetric (antisymmetric) under reflection at the symmetry lines, respectively, and the states of the E subspace are invariant under rotations by $2\pi/3$ and $4\pi/3$.

Following Refs. [10, 53], one can map the system into a fundamental domain, which consists of a one sixth slice of the full system with the symmetry axes acting as straight mirror walls (see Fig. 5.1). The periodic orbits of the full system can completely be described in terms of the periodic orbits in the fundamental domain. The multiplets of symmetry-related periodic orbits in the full domain map into the same symmetry reduced periodic orbit when folded into the fundamental domain. Each periodic orbit in the fundamental domain therefore corresponds to a multiplet of periodic orbits in the full domain, which can be pieced together from the segments of the symmetry reduced orbit. The symmetry reduced periodic orbits can be labelled by a binary code, where the symbol '0' represents backscattering (or change between clockwise and anti-clockwise scattering) and the symbol '1' stands for scattering to the third disk in the original full domain picture. For orbits with one of the distinct symmetries, the segments of the orbits which
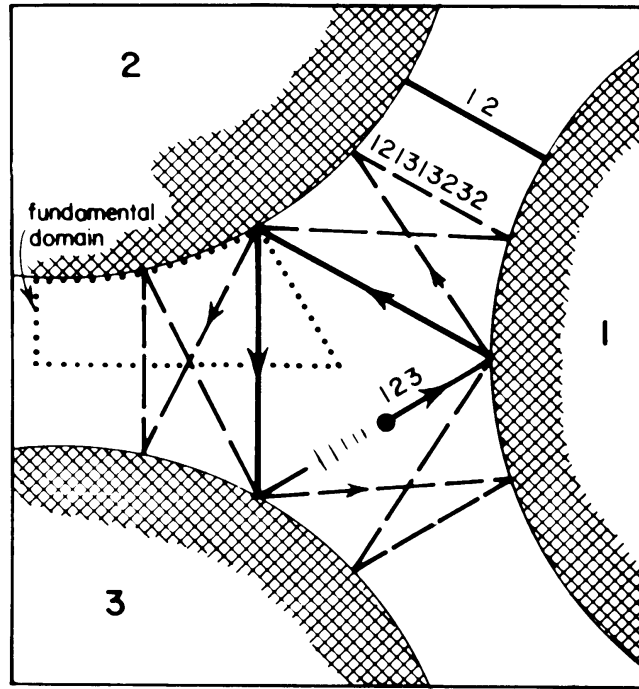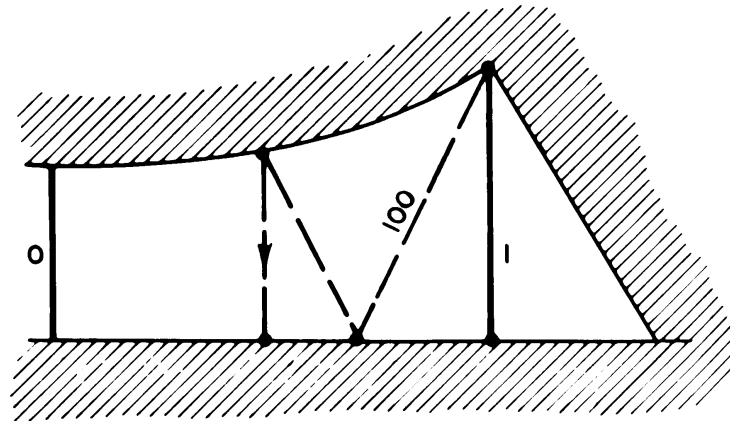
Figure 5.1: *The scattering geometry of the three-disk system. (a) The three disks with the 12, 123, and 121313232 cycles indicated. (b) The fundamental domain, i.e., a wedge consisting of a section of a disk, two segments of symmetry axes acting as straight mirror walls, and an escape gap. The above cycles restricted to the fundamental domain are now the 0, 1, and 100 cycle. The figures have been reproduced from Ref. [10].*

are related by symmetry map into the same sequence in the fundamental domain. The symmetry reduced orbit therefore has a shorter period: If m is the multiplicity of the set of full domain orbits, the corresponding symmetry reduced orbit has a period equal to $m/6$ times the full domain period. E. g., the shortest full domain orbit 12 maps onto the 0 orbit and the 123 orbit maps onto the 1 orbit (see Fig. 5.1).

5.1.2 Semiclassical density of states

The quantum resonances of the three different subspaces A_1, A_2 and E can be obtained separately from the periodic orbits in the fundamental domain by the introduction of appropriate weight factors for the orbits in Gutzwiller's trace formula, as was shown by Cvitanović and Eckhardt [57] (see table 5.1). I concentrate on the A_1 subspace, for which each orbit has a weight factor equal to 1. The semiclassical density of states in the A_1 subspace is then given by equation (2.8), where the sum now runs over all symmetry reduced periodic orbits.

Table 5.1: *Weight factors of the symmetry reduced periodic orbits in the Gutzwiller formula for the three different quantum subspaces A_1, A_2 and E (taken from Ref. [57]). The weight factors depend on the multiplicity of the corresponding full domain orbit, i. e., on its symmetry properties.*

multiplicity	A_1	A_2	E
2	1	1	-1
3	1	-1	0
6	1	1	2

As for the circle billiard, a scaling parameter w can be introduced such that the shape of the orbit does not depend on w and the action scales like

$$S/\hbar = ws. \tag{5.1}$$

For the three-disk system with unit disk radius, the scaling parameter is equal to the wave number k,

$$w = k = \sqrt{2mE}/\hbar, \tag{5.2}$$

where E and m are the energy and the mass of the particle, respectively, and the scaled action s is equal to the length of the orbit. As for the circle billiard, I consider the density of states as a function of the scaling parameter,

$$\rho(w) = \frac{dE}{dw}\, \rho(E)\,. \tag{5.3}$$

The denominator of the Gutzwiller formula can be expressed in terms of the stability eigenvalues of the orbit, i. e., eigenvalues of the monodromy matrix M. As was demonstrated in Ref. [53], the symmetry reduced periodic orbits are hyperbolic for even number of symbols '1' and inverse hyperbolic for odd number of symbols '1' in the code. The stability eigenvalues λ_1, λ_2 are related by $\lambda_1 = 1/\lambda_2$. The Maslov index entering the Gutzwiller formula increases by 2 for each reflection on a disk and is therefore equal to

twice the length of the symbolic code (in the following called "symbol length"). If λ denotes the expanding stability eigenvalue (i.e., the eigenvalue with an absolute value larger than one), the semiclassical density of states of the A_1 subspace resulting from Eq. (2.8) is then given by

$$\rho^{\mathrm{osc}}(w) = -\frac{1}{\pi} \operatorname{Im} g^{\mathrm{osc}}(w) , \tag{5.4}$$

with

$$g^{\mathrm{osc}}(w) = -i \sum_{\mathrm{po}} (-1)^{l_s} \frac{s_{\mathrm{po}}}{r|(\lambda_{\mathrm{po}} - 1)(\frac{1}{\lambda_{\mathrm{po}}} - 1)|^{1/2}} \, e^{iws_{\mathrm{po}}} , \tag{5.5}$$

where l_s is the symbol length. The sum runs over all symmetry reduced periodic orbits including multiple traversals. Here, r denotes the repetition number with respect to the corresponding primitive orbit.

In practice, only the primitive periodic orbits have to be determined. The parameters of the rth repetition of the primitive orbit (here characterized by index 0) are then given by $l_s = r l_{s0}$, $s = r s_0$ and $\lambda = \lambda_0^r$.

5.1.3 Numerical search for periodic orbits

For extracting the quantum resonances of the system from Eq. (5.5) by harmonic inversion, all periodic orbits up to a maximum scaled action have to be included. The parameters of the periodic orbits – scaled action and stability eigenvalues – have to be determined numerically. I calculate the primitive periodic orbits using the symbolic code as input. For simplicity, the calculations are carried out in the full domain, and the results are then translated back into the symmetry reduced system. The disks are "connected" according to the code, starting with arbitrary reflection points on the disks as initial condition. The reflection points are then varied such that the total length (i.e., the action) of the orbit reaches a minimum. All orbit parameters can then be calculated from the reflection points. The scaled action is given by the length of the (symmetry reduced) orbit, and the stability eigenvalue λ can be determined by an algorithm proposed by Bogomolny [58]. Details are given in Appendix B. In addition to action and stability, one can also determine averages of different classical quantities (distance from the center of the system, angular momentum, etc.), which are needed for the cross-correlation technique (see Section 3.3.3).

For disk separations smaller than the pruning limit $d = 2.04821419$, it has to be checked whether or not the orbits are physical, i.e., if they stay completely outside the disks. In my numerical calculations, I found two different classes of pruned orbits. An example of the first class is given in Figure 5.2: As the disks approach each other, a section of the orbit connecting two of the disks gets inside the third disk. The pruned orbit still corresponds to a unique minimum of the total length when the reflection points on the disks are varied for given symbolic code. This is not the case for the second class, an example of which is shown in Figure 5.3: In this case, as the disks come closer, the reflection angle at one specific reflection point approaches π. As the value π is reached, the minimum of the action with respect to this specific reflection point splits into two equal minima and one local maximum. Accordingly, the orbit splits into three unphysical orbits with the same symbolic code. In one case, the orbit is now reflected on the inside of the disk (see Fig. 5.3c), which corresponds to a reflection angle larger than π. This orbit does not correspond to a minimum of the total length but to a saddle point. In the other two cases, Figs. 5.3d and 5.3e, the reflection point moves along the disk in such a way
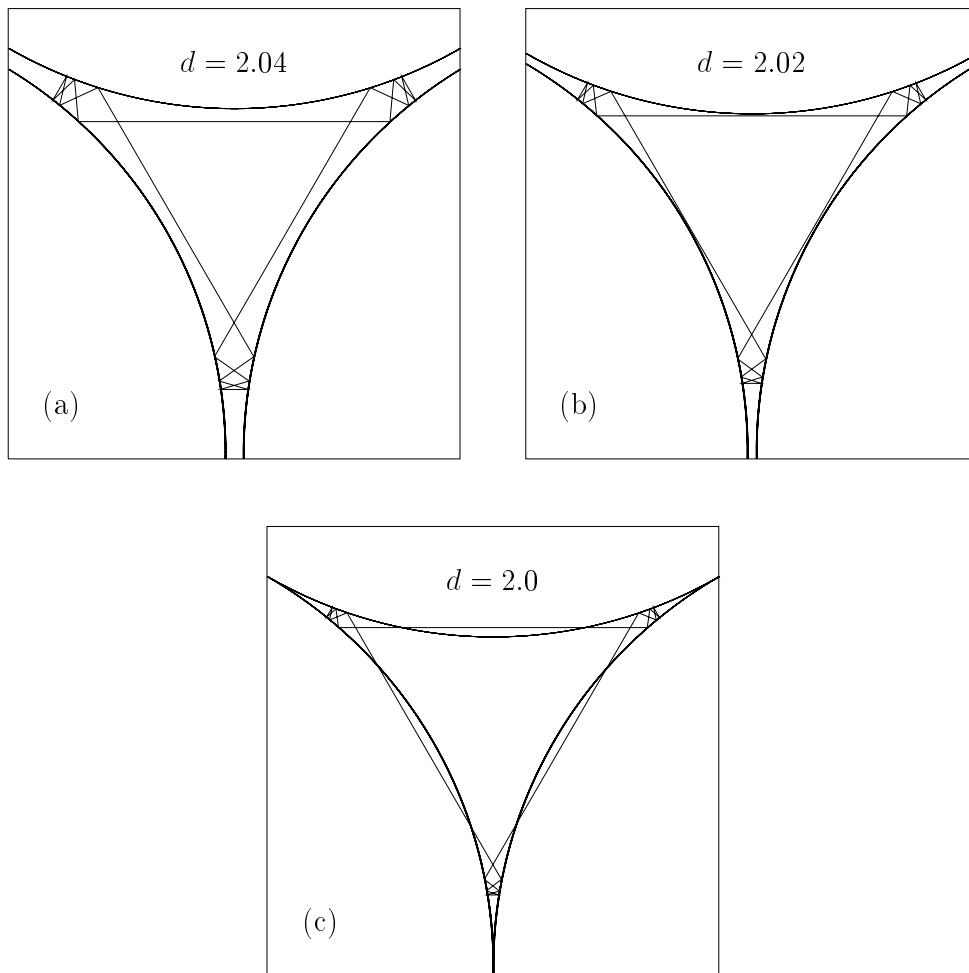
54

Figure 5.2: *An example of the first class of pruned orbits (see text), plotted in full domain representation. The symmetry reduced code of the orbit is 000011. The orbit is shown at three different disk separations d, indicated at the top of each diagram. At $d = 2.04$ and $d = 2.02$, the orbit is still physical. At $d = 2.0$ it has become unphysical as is penetrates the disks.*
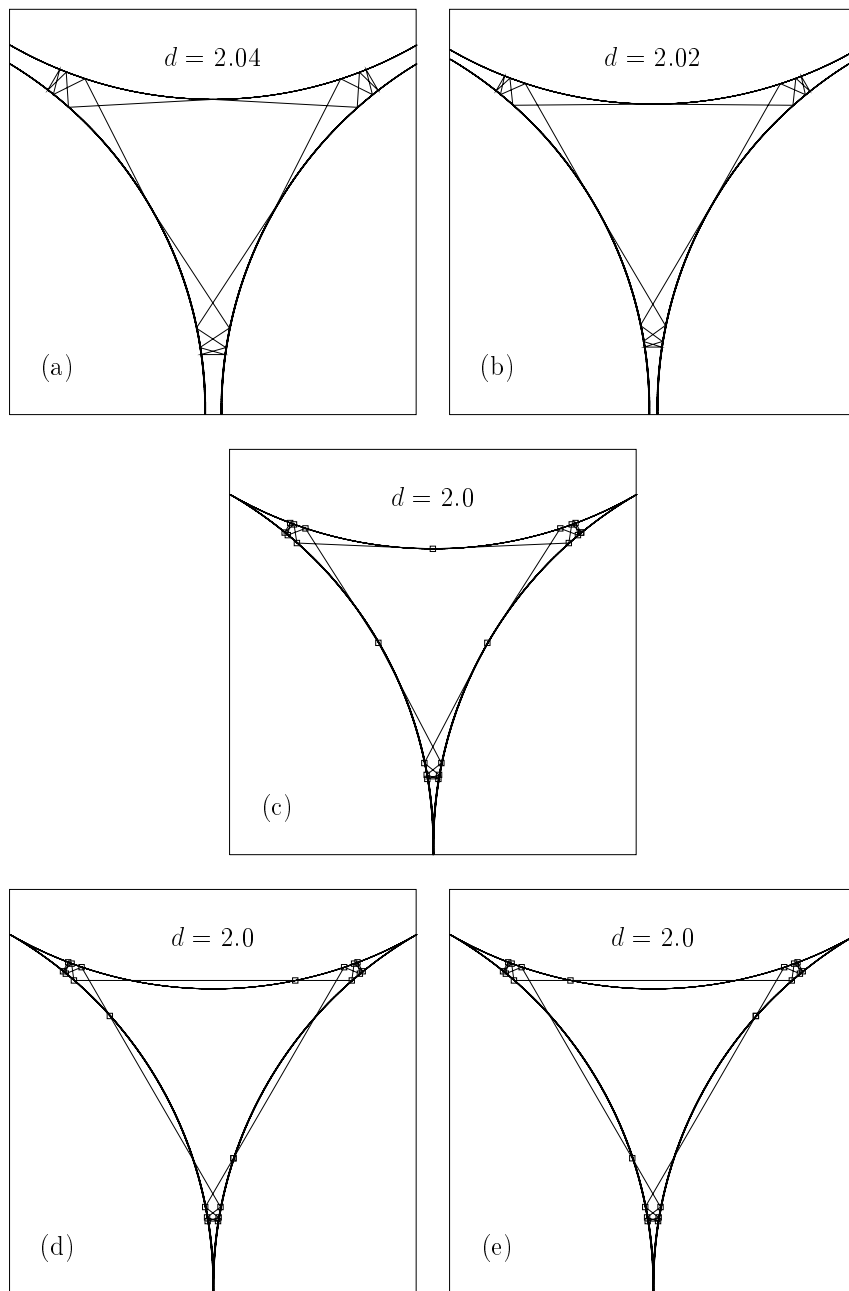
Figure 5.3: *An example of the second class of pruned orbits (see text), plotted in full domain representation. The symmetry reduced code of the orbit is 0000001. The orbit is still physical at disk separations $d = 2.04$ and $d = 2.02$. At $d = 2.0$ it has split into three unphysical orbits. The squares indicate the "reflection points".*

that the reflection law is no longer fulfilled but the orbit just passes the "reflection point" in a straight line and penetrates into the disk. These two cases correspond to two equally deep minima of the total length. The two orbits have the same shape but only differ concerning as to which penetration point is considered as "reflection point", indicated by the squares in Figs. 5.3d and 5.3e. In fact, the shape of the orbit is equal to that of a pruned orbit with a (symmetry reduced) symbol length that is shorter by 1 and which belongs to the first class of pruned orbits as defined above. (In this orbit the reflection point in question is simply missing, i.e., none of the penetration points is considered as reflection point.)

In order to determine whether or not an orbit is physical, one has to check for both cases of pruning discussed above. Pruned orbits of the first class are excluded by the condition that for each section of the orbit (connecting two of the disks) its minimum distance from the center of the third disk must be larger than the disk radius. The second class of pruning is accounted for by the condition that at each reflection point the angle of incidence as well as the reflection angle must be smaller than π.

For periodic orbit quantization by harmonic inversion, all (physical) primitive periodic orbits up to a maximum scaled action have to be found. However, the distance between the disks strongly influences the existence or nonexistence of periodic orbits and the distribution of the orbit parameters. Figures 5.4 to 5.6 show the orbit parameters of the shortest primitive periodic orbits found for the disk separations $d = 6$, $d = 2.5$ and $d = 2$. For $d = 6$, the action and stability of the orbits are mainly determined by the symbol length, and the number of orbits up to a given action is relatively small. However, this picture changes completely when the disks approach each other: As all orbits become shorter, the total number of orbits up to a given action increases rapidly. The parameters of the orbits are no longer simply determined by the symbol length, but their behaviour becomes much more complicated.

For $d = 2$, the orbits can be grouped in "channels" with the same "tail" (end figures) but growing number of leading '0's in the code. (A sequence of n leading '0's in the code will in the following be denoted by 0^n). These orbits have the same basic shape but run deeper and deeper into the corner formed by two touching disks, bouncing back and forth between the two disks (see Figs. 5.7 to 5.9). Fig. 5.6 shows the distribution of orbit parameters, which now exhibits a completely different structure than for the large disk separation $d = 6$. In Fig. 5.6b, only orbits with up to 25 consecutive '0's in the code were included. Some channels have been marked by different symbols. Note that the 0 orbit, bouncing back and forth between two disks, does not exist in the closed three-disk system.

In each channel, the action of the orbits grows very slowly with increasing symbol length, while the expanding stability eigenvalue increases relatively fast (in fact exponentially) with every additional collision. As by adding a leading '0' to the symbolic code the action does not change considerably, there is a huge number of orbits with a very long symbol length but a relatively small action. In fact, most channels break off because of pruning. E.g., the $0^n 1$ series, labelled (A) in Fig. 5.6b, breaks off after six orbits, and the $0^n 11$ series, marked (B), already breaks off after three orbits (see Fig. 5.7). My analysis strongly suggests that there exist only two infinite channels: The $0^n 101$ and the $0^n 111$ series, dubbed (C) in Fig. 5.6b (the channels are only shown up to 25 leading '0's in the code). The shapes and actions of these orbits converge very slowly towards the shape and action of the limiting orbit which starts exactly in the touching point of two disks
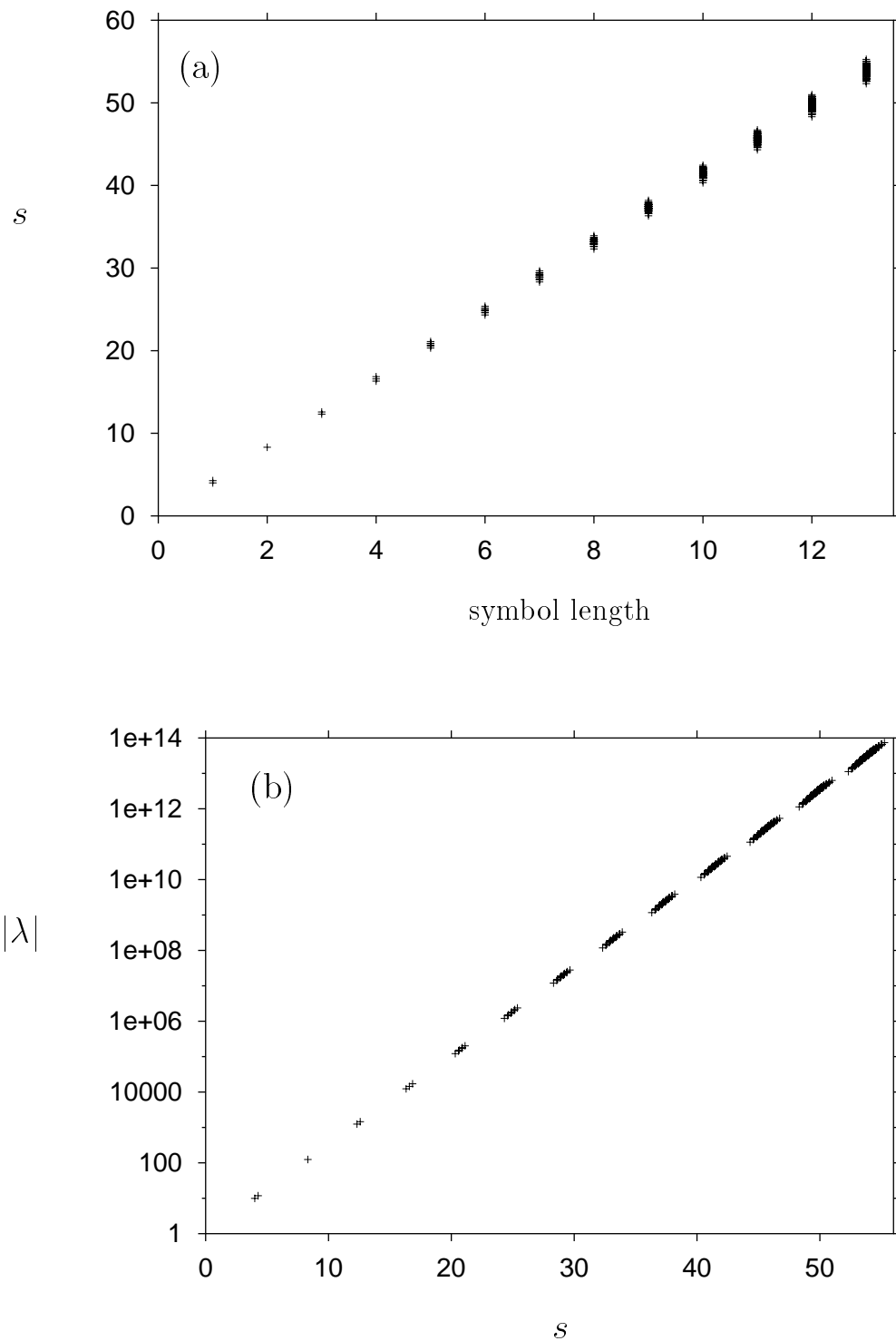
Figure 5.4: *Distribution of periodic orbit parameters of the symmetry reduced three-disk scatterer with disk separation $d = 6$ (only primitive orbits included): (a) scaled action versus symbol length, (b) absolute value of the expanding stability eigenvalue λ versus scaled action. The set of primitive periodic orbits included is complete.*
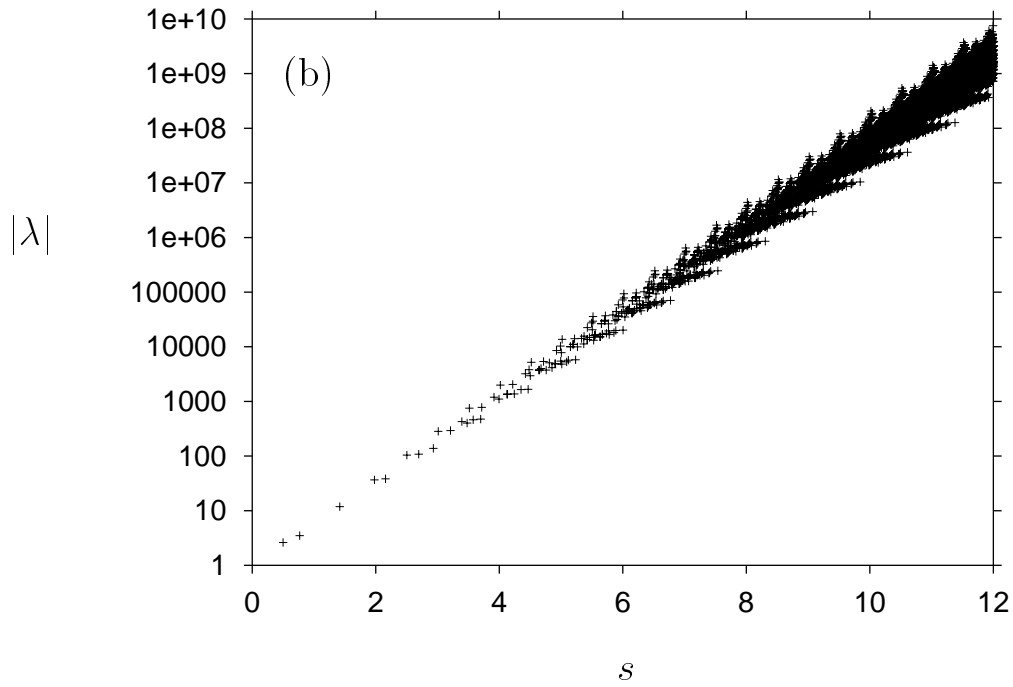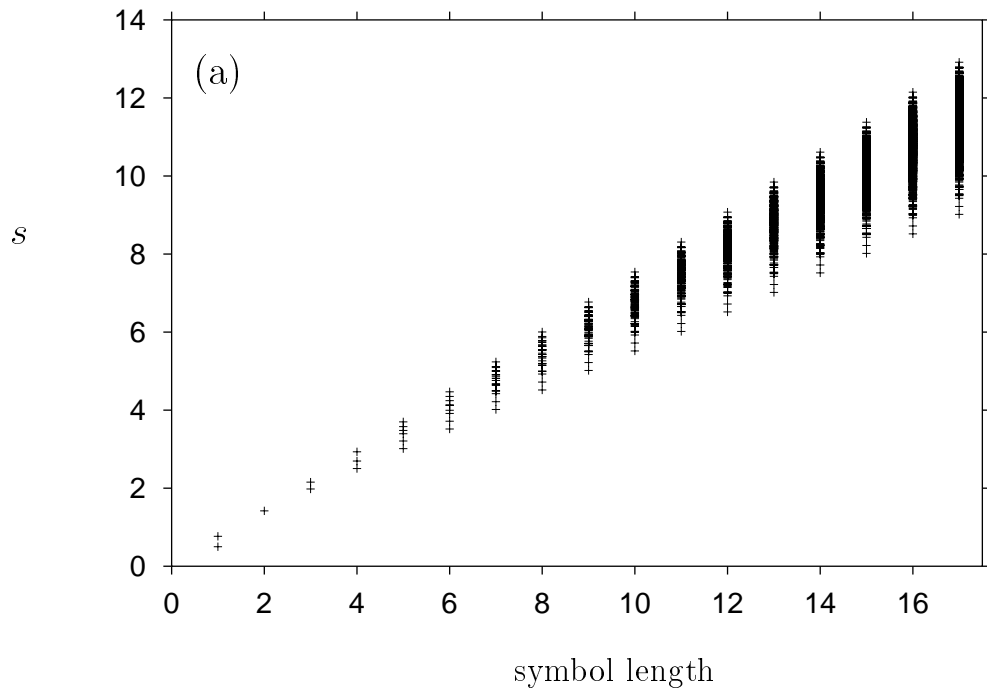
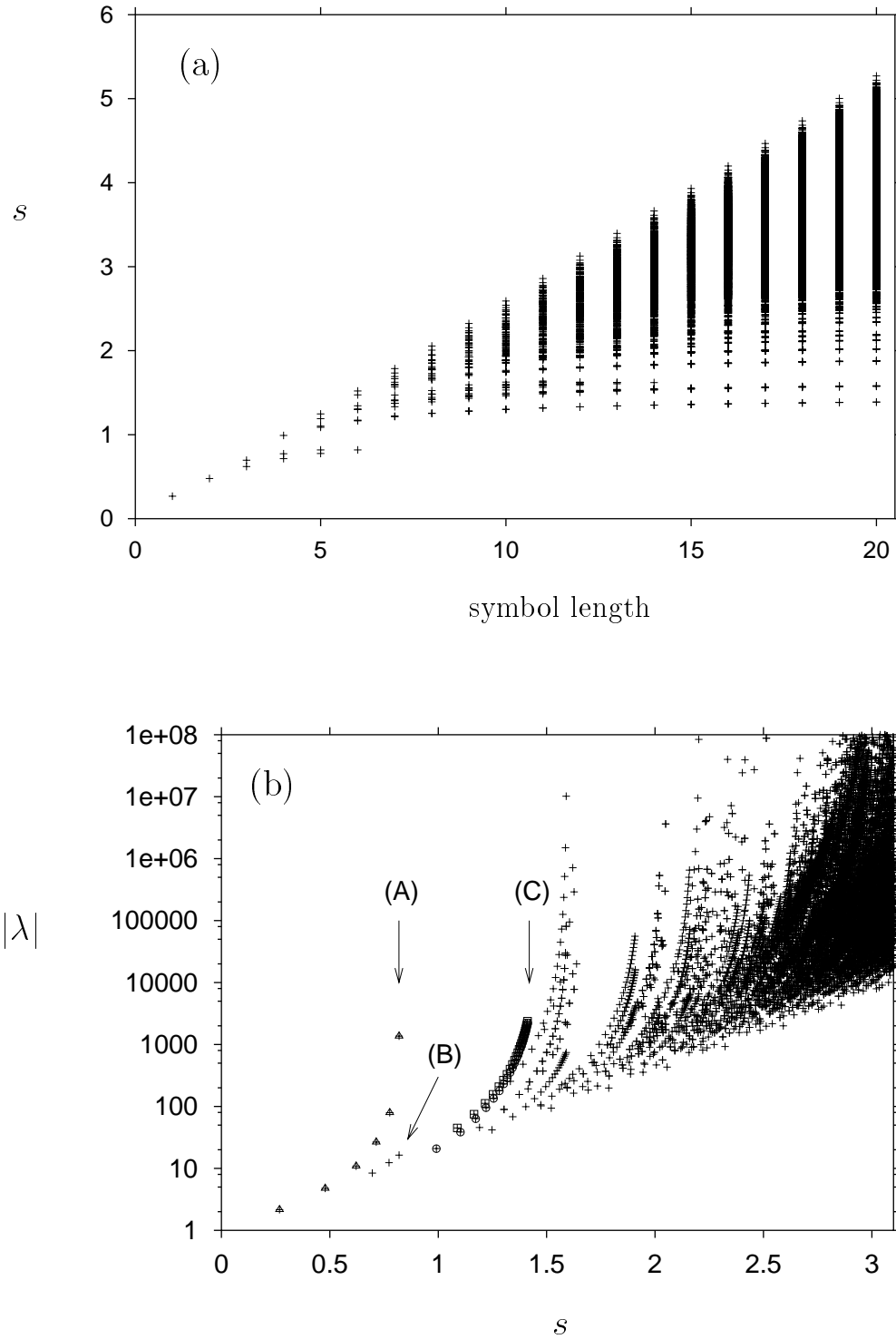Figure 5.5: *As Fig. 5.4, but for disk separation $d = 2.5$.*

Figure 5.6: *As Fig. 5.4, but for the case of touching disks, $d = 2$. The set of orbits shown in (b) is not complete. As cut-off criteria, I used a maximum value of 10^8 for the absolute value of the stability eigenvalue and a maximum value of 25 for the number of consecutive symbols '0' in the symbolic code. A number of channels break off because of pruning before these limits are reached. The channels marked by special symbols are (A) $0^n 1$, (B) $0^n 11$, and (C) $0^n 101$ (squares) and $0^n 111$ (circles).*
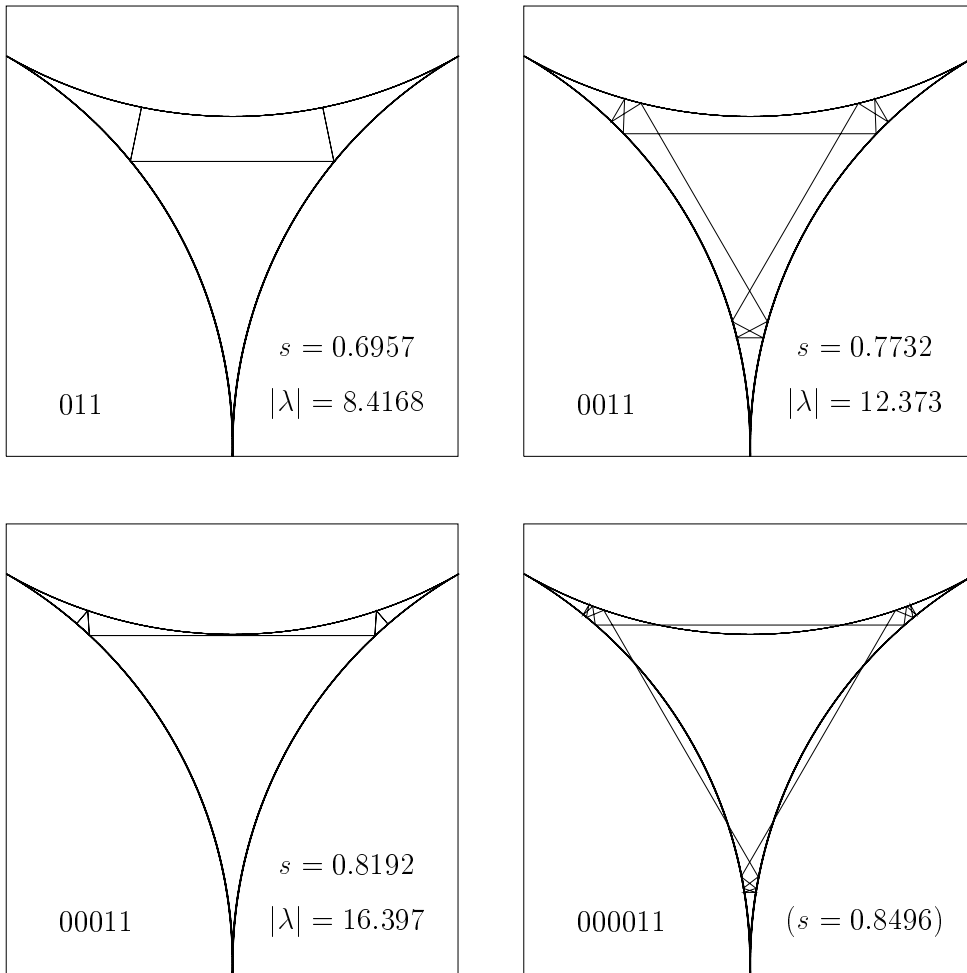
Figure 5.7: *Orbits of the 0^n11 channel (marked (B) in Fig. 5.6b) as an example of a channel that breaks off because of pruning. For simplicity, the full domain counterparts of the symmetry reduced orbits are shown, which in this case are alternately symmetric under reflections and under rotations. For each orbit, the symmetry reduced code as well as the scaled action and the expanding stability eigenvalue are given. The fourth orbit of the channel is already pruned.*

and is directly reflected back by the opposite disk (cf. Figs. 5.8 and 5.9). Although all other channels break off because of pruning, the number of orbits in a channel up to a given action often becomes very large (or, in the two cases mentioned, even infinite). The search for the relevant periodic orbits up to a given action therefore becomes a nontrivial task.

The behaviour of the periodic orbit parameters at different disk separations requires different strategies for the search for periodic orbits in order to keep the search effective. For $d = 6$, the actions of the orbits with different symbol lengths lie in clearly separated intervals (at least in the range examined, see Fig. 5.4a). Finding all orbits up to a given action therefore corresponds to calculating all orbits up to a certain maximum symbol length. I therefore start by generating a complete list of code strings up to a maximum symbol length. This is most easily done by – for each symbol length – running through all binary numbers with a fixed number of digits equal to the symbol length. From these
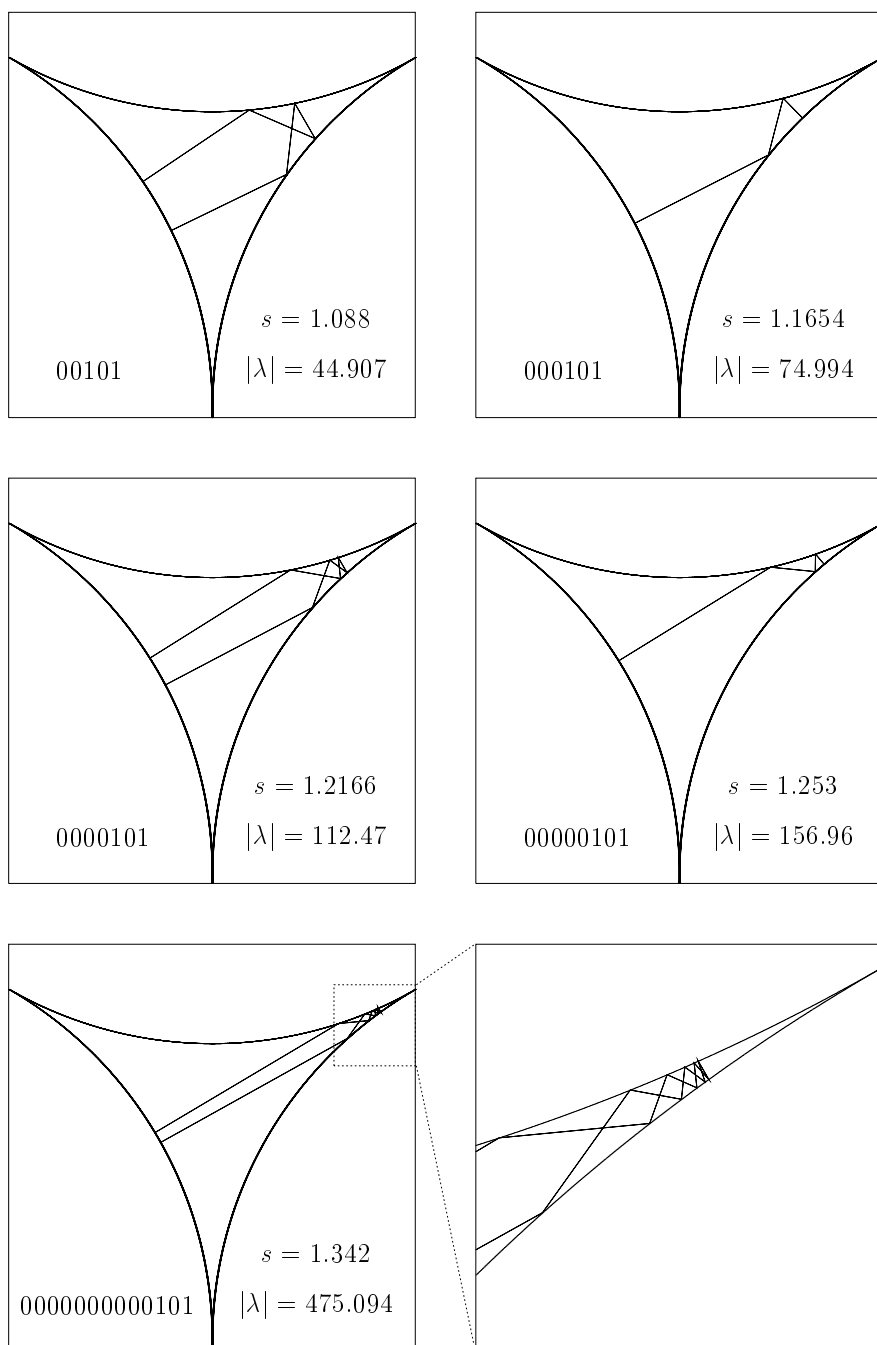
Figure 5.8: *Examples of orbits of the 0^n101 channel (dubbed (C) in Fig. 5.6b) in full domain representation. With growing number of leading '0's, the orbits run deeper and deeper into the corners between the disks. For the longest orbit, a magnification of the corner region is given. The series converges towards the limiting orbit that starts exactly in the point where the disks touch and is then directly reflected back from the opposite disk.*
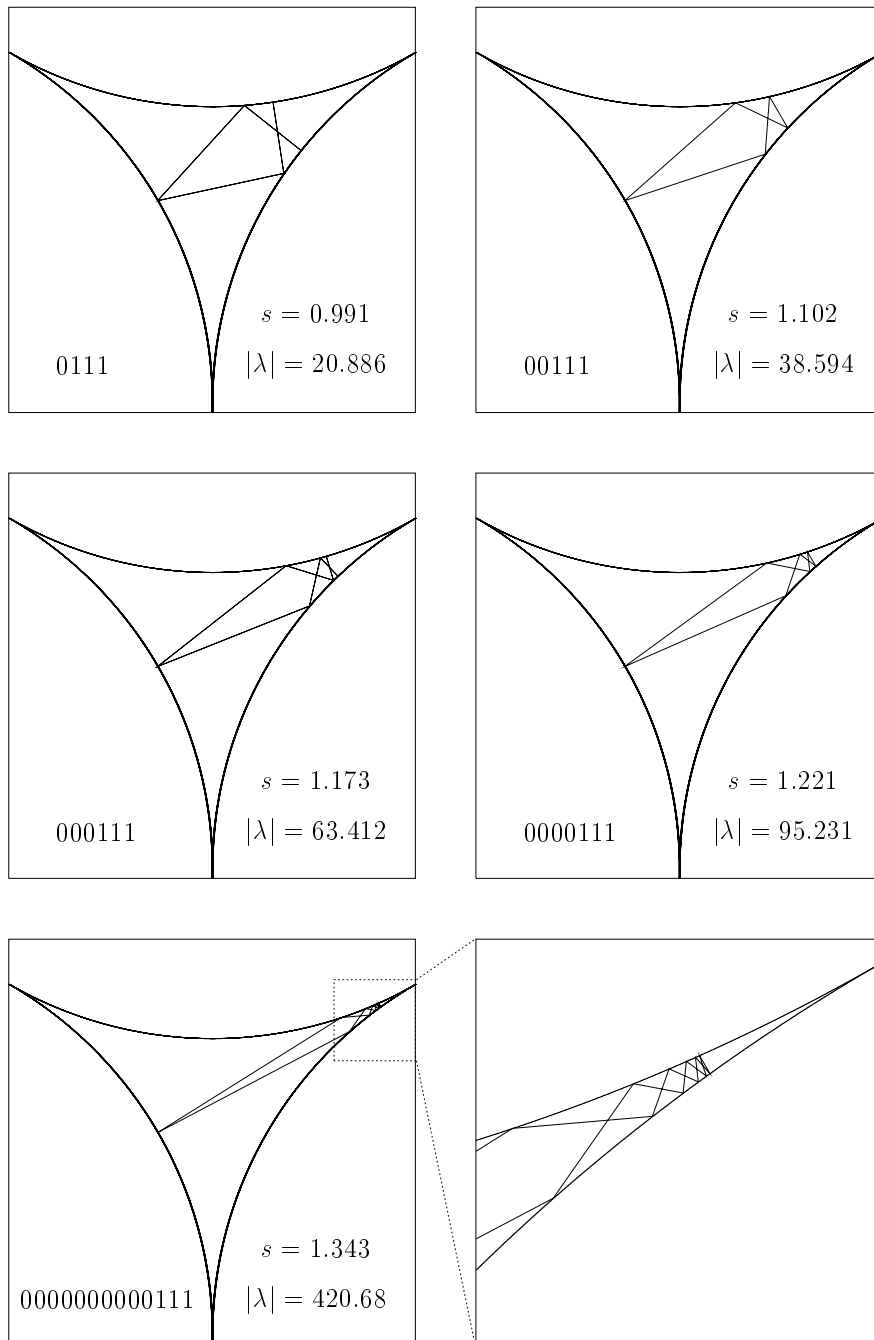
Figure 5.9: *As Fig. 5.8, but for the $0^n 111$ channel. This series converges towards the same limiting orbit as the $0^n 101$ series.*

binary numbers all those are excluded which possess a sub-period (e. g. 0101), and it has to be taken into account that, as the orbits are periodic, strings which can be transformed into each other by a circular shift describe the same orbit (e. g. 0111 and 1011). The symbolic code is then used as an input to obtain a complete set of primitive periodic orbits up to the maximum action corresponding to the maximum symbol length chosen.

The above procedure still works effectively enough for $d = 2.5$. However, the action intervals covered by orbits with the same symbol length begin to overlap (see Fig. 5.5a). Thus, if one calculates all orbits up to a symbol length l_s, the set will only be complete up to an action which corresponds to the shortest orbit with symbol length $l_s + 1$. Many of the calculated orbits will be longer than this limit and are therefore superfluous, which makes the search less effective.

For the closed three-disk system, the overlapping of the action intervals for different symbol lengths is so strong (see Fig. 5.6a) that a completely different procedure must be applied. Instead of the symbol length, the most relevant quantity determining the action is now the number of symbols '1' in the code. Although a large portion of the orbits is pruned, the number of physical periodic orbits up to a given maximum action is huge as compared to the larger disk separations discussed above. It is therefore impossible to include all periodic orbits, and further restrictions have to be introduced in order to single out the most relevant orbits. As the amplitude in the Gutzwiller formula strongly depends on the stability parameter, a reasonable cut-off criterion is the stability of the orbit. On the other hand, since in each channel the absolute value of the expanding stability eigenvalue grows exponentially fast, the main contributions of each channel to the periodic orbit sum come from the orbits with small symbol lengths. As a second criterion, I therefore restrict the number of consecutive symbols '0' in the symbolic code, thus selecting the most relevant orbits of each channel.

The orbits are calculated channel by channel. The calculation starts from the shortest orbit with a given number of symbols '1' in the code. Then symbols '0' are inserted between the '1's in all possible combinations up to a maximum number of successive '0's. To each such "tail", more and more leading '0's are added and the corresponding orbits are caculated. With every leading '0', the action and the absolute value of the expanding stability eigenvalue become larger. The calculation of the channel is broken off if one of the following conditions is fulfilled:

- The action exceeds the maximum action s_{max}.

- The absolute value of the stability eigenvalue exceeds the given value λ_{max}.

- The maximum number of consecutive symbols '0' is reached.

- The orbits become pruned.

5.1.4 Quantum resonances

For the open three-disk system, exact quantum resonances of the A_1 subspace for different disk separations have been calculated by Wirzba [54, 59, 60] using stationary scattering theory. The open three-disk scatterer does not possess any bound states, i. e., all resonances are complex and located below the real axis. Figures 5.10 and 5.11 show the exact quantum resonances (marked by symbols '+') for disk separation $d = 6$ in the region

Figure 5.10: *Three-disk system with $d = 6$ (A_1 subspace): Exact quantum resonances $(+)$ and semiclassical results $(\times)$ from a 12th order cycle expansion of (a) the Gutzwiller-Voros zeta function and (b) the dynamical zeta function (cf. Section 2.4). The figures have been reproduced from Ref. [54].*
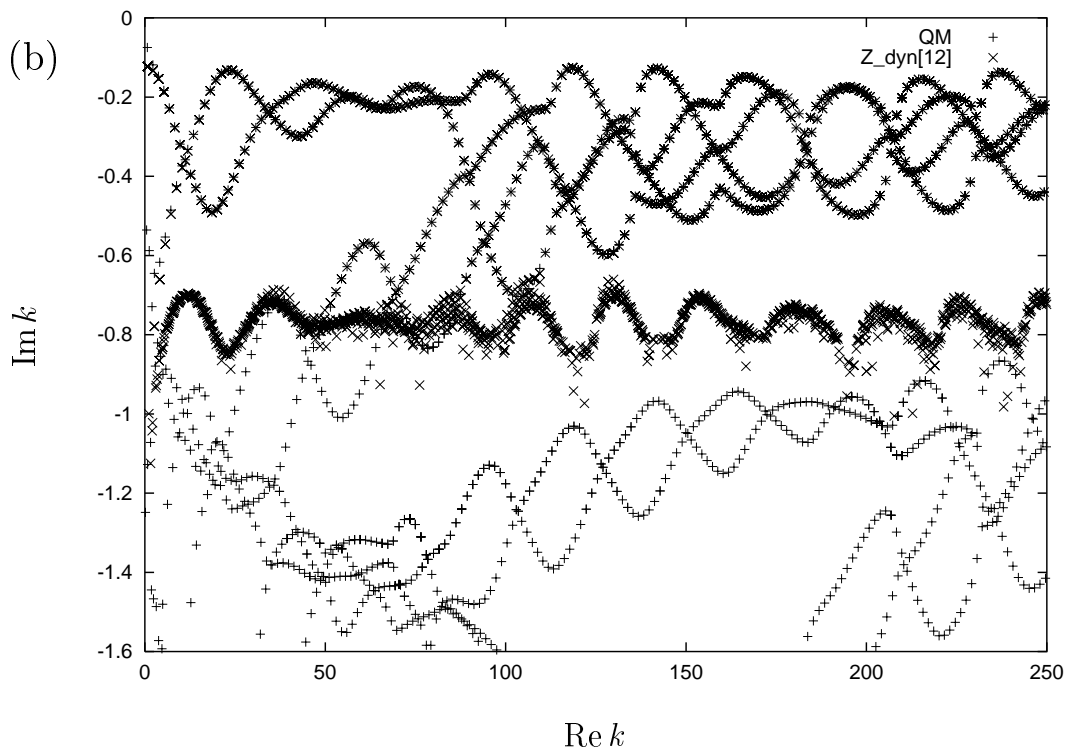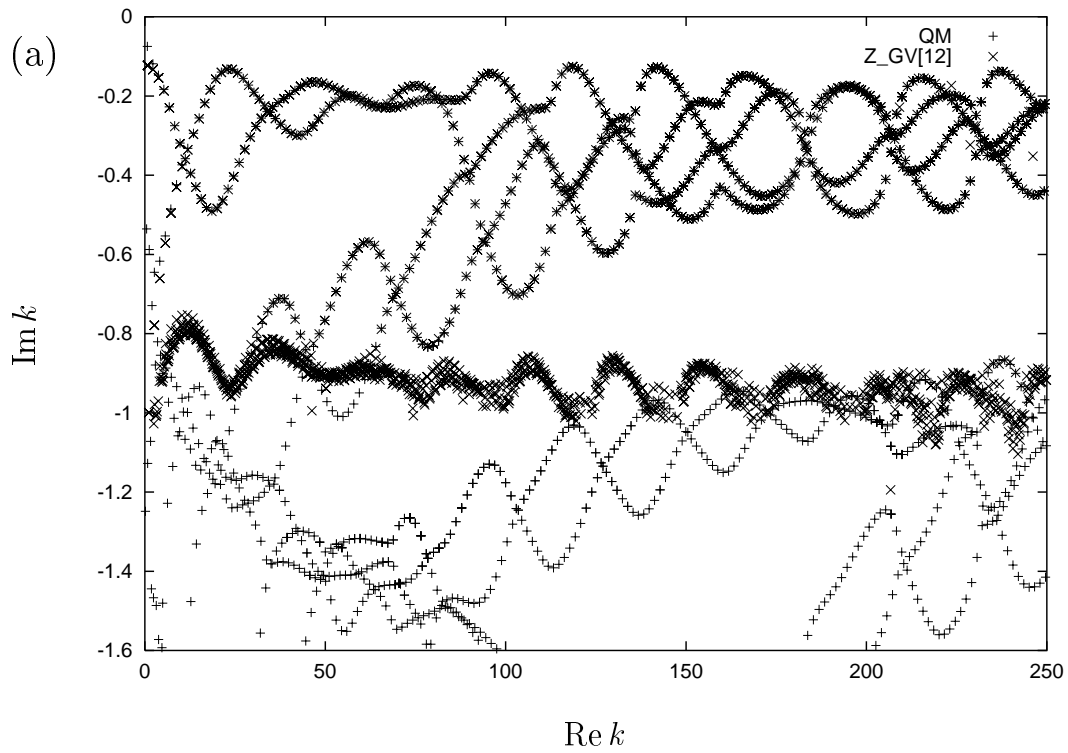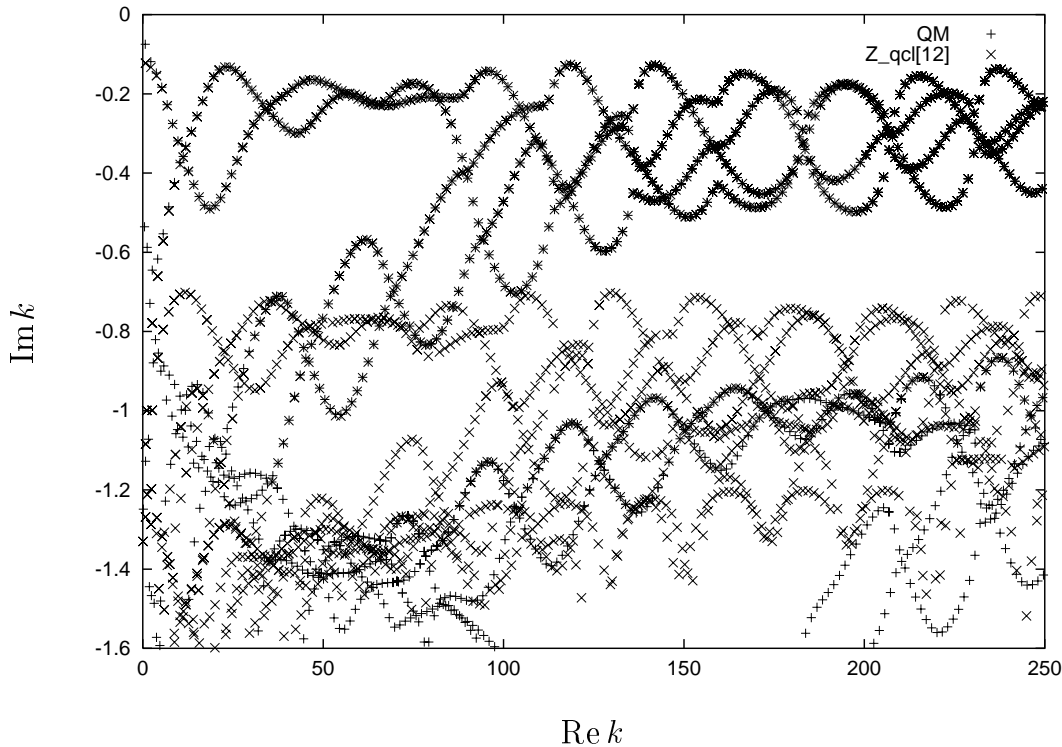
Figure 5.11: *Three-disk system with $d = 6$ (A_1 subspace): Exact quantum resonances ($+$) and semiclassical results ($\times$) from a 12th order cycle expansion of the quasiclassical zeta function (cf. Section 2.4). The figure has been reproduced from Ref. [54].*

$0 \leq \text{Re } k \leq 250$. The exact data are compared with semiclassical results (marked by symbols '$\times$') which have been obtained by 12th order cycle expansions of the Gutzwiller-Voros zeta function, the dynamical zeta function and the quasiclassical zeta function (cf. Section 2.4), respectively. The figures have been taken from Ref. [54].

Close to the real axis, the exact quantum resonances are well reproduced by the semiclassical cycle expansion values. All three zeta functions lead approximately to the same results. The deviations from the exact values are due to the semiclassical nature of the calculations and reflect the fact that Gutzwiller's theory is correct only in lowest order of $\hbar$. Fig. 5.10 illustrates that the cycle expansions of the Gutzwiller-Voros zeta function and the dynamical zeta function converge only for sufficiently small negative imaginary part of the resonances. (For disk separation $d = 6$, the border of convergence of the Gutzwiller-Voros zeta function lies at $\text{Im } k = -0.699\,110$, as was shown by Cvitanović et al. [61].) At the border of convergence, the cycle expansion data contain a large number of extraneous "pseudo-resonances", which originate in the break-down of the cycle expansion. With the help of the quasiclassical zeta function, the resonances with large negative imaginary part are also obtained. But on the other hand, the cycle expansion then yields spurious bands of resonances which have no counterparts in the exact quantum spectrum. Some exact quantum resonances, with very small real parts and imaginary parts $\text{Im } k < -0.5$, have not been reproduced by any of the semiclassical zeta functions. This "diffractive" band of resonances cannot be described by ordinary periodic orbit theory.
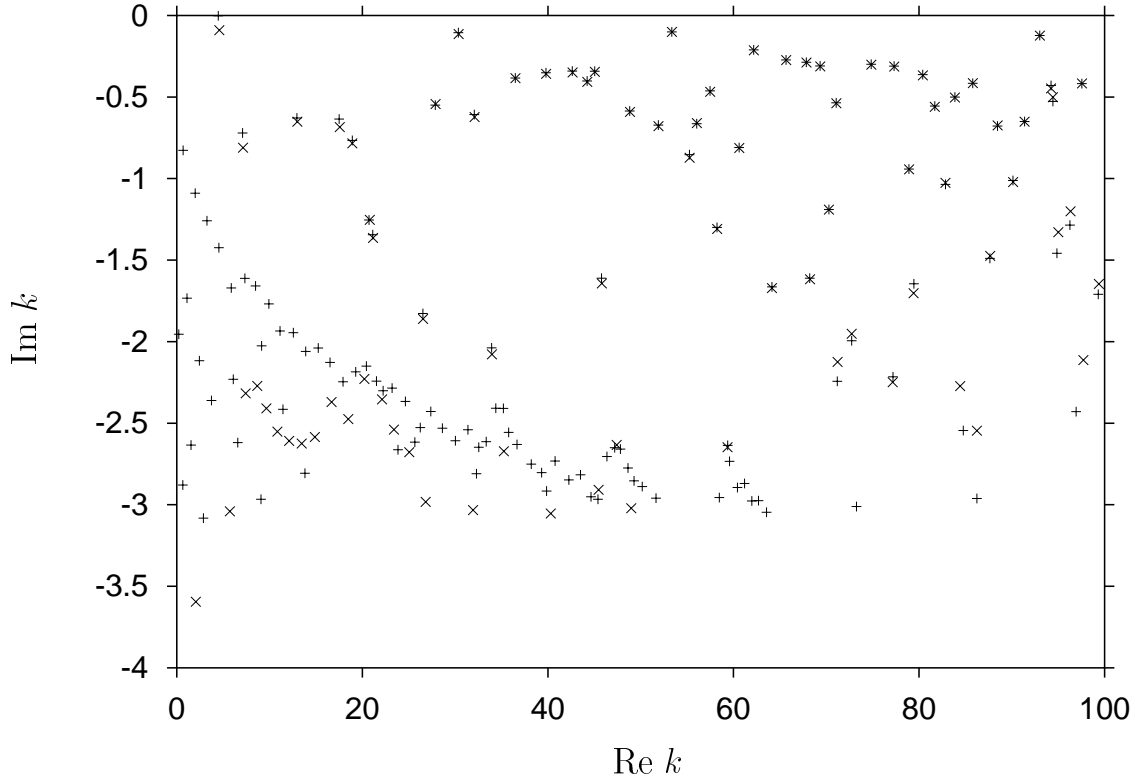
Figure 5.12: *Exact quantum (+) and semiclassical (×) resonances of the three-disk system at disk separation $d = 2.5$ (A_1 subspace). The semiclassical values have been obtained by Wirzba [60] from a 12th order cycle expansion of the Gutzwiller-Voros zeta function.*

In Refs. [62, 63] it was shown that these resonances are associated with "creeping" orbits, and can be obtained by including diffraction terms in Gutzwiller's trace formula.

For the three-disk system with disk separation $d = 2.5$, exact quantum and semiclassical resonances have been calculated by Wirzba [60] in the the region $0 \leq$ Re $k \leq 100$. Figure 5.12 shows the exact quantum resonances (+) and semiclassical results (×) from a 12th order cycle expansion of the Gutzwiller-Voros zeta function. Again, a diffractive band can be seen that is not reproduced by the semiclassical values. Compared to the large disk separation $d = 6$, the mean spacing between the resonances has increased. Note that resonances with much larger negative imaginary parts than in the case $d = 6$ are included in the data.

For the case of touching disks, $d = 2$, exact quantum eigenvalues have been calculated by Tanner et al. [64] and by Scherer [65]. In order to obtain also semiclassical eigenvalues from the trace formula, Tanner et al. combined the cycle expansion method with a functional equation for the spectral determinant. Figure 5.13 shows the results of their calculations, reproduced from [64]. The function plotted is the cycle-expanded semiclassical approximation to the spectral determinant $D(E) = \prod_n (E - E_n)$, where $E = k^2/2$ is the energy, and the E_n are the energy eigenvalues of the system. Only the very shortest orbits were included in the periodic orbit sum. The zeros of the functional determinant
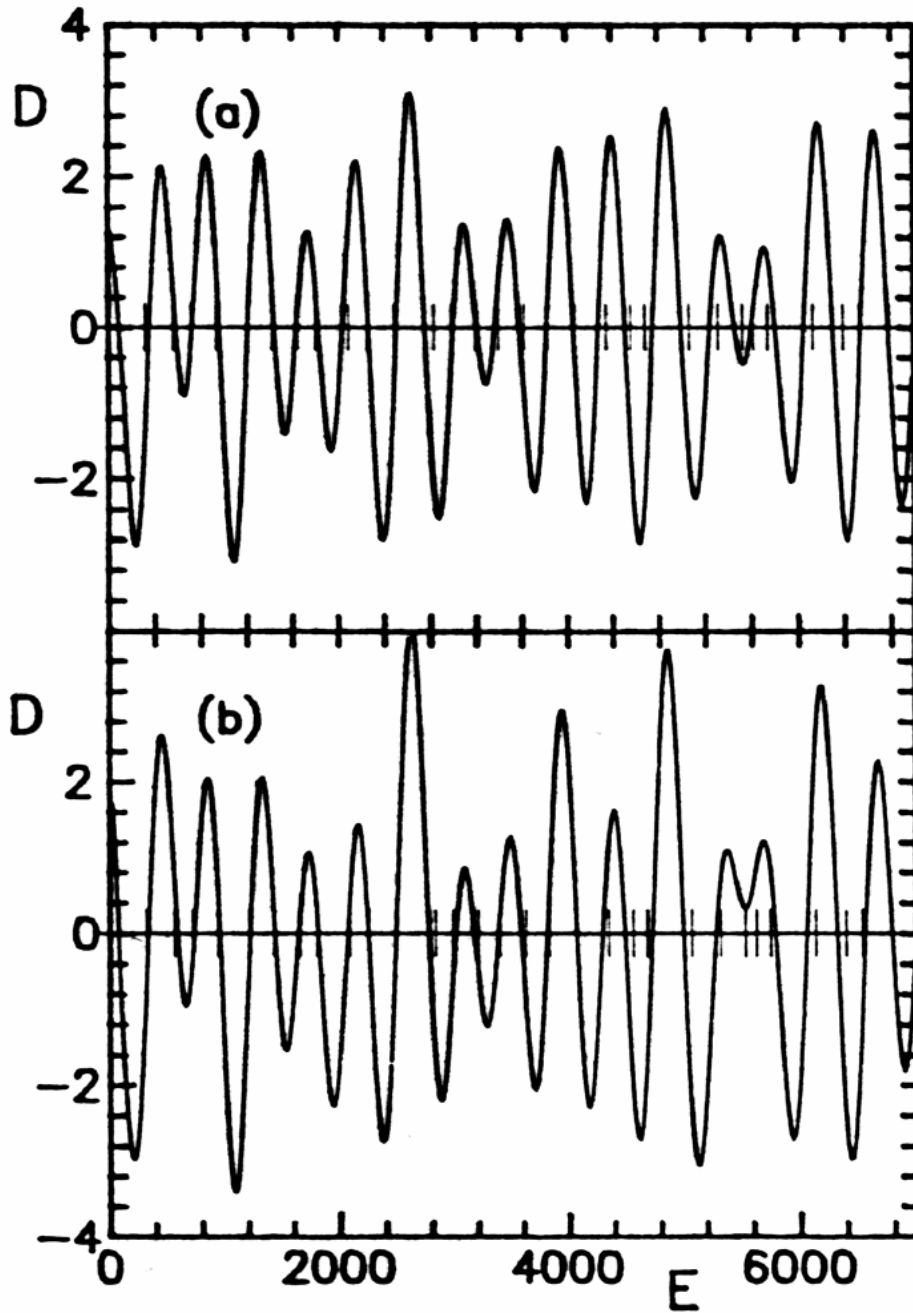
Figure 5.13: *Cycle expanded spectral determinant* $D(E) = \prod_n (E - E_n)$ *of the closed three-disk system (disk separation $d = 2$, A_1 subspace), as a function of $E = k^2/2$. The picture has been taken from Ref. [64]. The zeros of the determinant are the semiclassical approximations to the eigenvalues. In part (a), orbits up to symbol length 2 were included (3 orbits), in (b) orbits up to symbol length 3 (5 orbits). The vertical bars mark the exact quantum eigenvalues.*

are the semiclassical approximations to the eigenvalues. For comparison, the vertical bars mark the exact quantum eigenvalues. Since the system is bound, all eigenvalues are real. For the lowest eigenvalues, the cycle expansion results are in good agreement with the exact quantum values. However, the method fails for higher eigenvalues. Here, only the mean density of states was reproduced. Since the problems with this method arise from the strong pruning of orbits in this system, they are fundamental and cannot be overcome by including more orbits. To the best of my knowledge, no semiclassical method has successfully been applied to obtain higher eigenvalues of this system yet. I will demonstrate that harmonic inversion is able to circumvent the problems of other methods, as it is not restricted to systems with a complete symbolic code or other special properties.

5.2   The open three-disk system: High resolution analysis of quantum spectra

In this section, the harmonic inversion techniques for the analysis of quantum spectra developed in Section 3.2 are applied to the open three-disk scatterer with disk separation $d = 6$. [For disk separations $d = 2.5$ and $d = 2$, not enough quantum data were available in the literature to build a sufficiently long signal.] The analysis of the exact quantum spectrum yields the leading order $\hbar$ contributions to the density of states, which will be compared with the periodic orbit contributions predicted by the Gutzwiller formula. By an analysis of the difference spectrum between exact quantum and semiclassical resonances, first order $\hbar$ corrections to the trace formula are determined. The results will be compared with the correction terms resulting from the theory of Vattay and Rosenqvist discussed in Appendix A.1.

5.2.1   Leading order periodic orbit contributions to the density of states

For the three disk-system, the oscillating part of the semiclassical response function resulting from Gutzwiller's trace formula is given by Eq. (5.5). The corresponding semiclassical density of states reads

$$\rho^{\mathrm{osc}}(w) = \frac{1}{2\pi} \sum_{\mathrm{po}} (-1)^{l_s} \frac{s_{\mathrm{po}}}{r|(\lambda_{\mathrm{po}} - 1)(\frac{1}{\lambda_{\mathrm{po}}} - 1)|^{1/2}} \left(e^{-iws_{\mathrm{po}}} + e^{iws_{\mathrm{po}}}\right), \qquad (5.6)$$

where the scaling parameter w is equal to the wave number k. The exact quantum expression for the density of states is given by Eq. (3.21) with multiplicities $m_k = 1$. Since for the open three-disk system all resonances are complex, the quantum expression does not have to be regularized but can directly be adjusted to Eq. (5.6) by harmonic inversion using the filter-diagonalization method.

For disk separation $d = 6$, I analyzed the four leading bands of the quantum spectrum of the A_1 subspace (see Fig. 5.10), which had been calculated by Wirzba [54, 59, 60]. Note that this set of resonances is of course not complete as the subleading bands with large negative imaginary part are not included. Figure 5.14 shows the resulting quantum mechanical density of states for real values of the wave number k, which is now taken as signal for the harmonic inversion procedure. As for the circle billiard (cf. Section
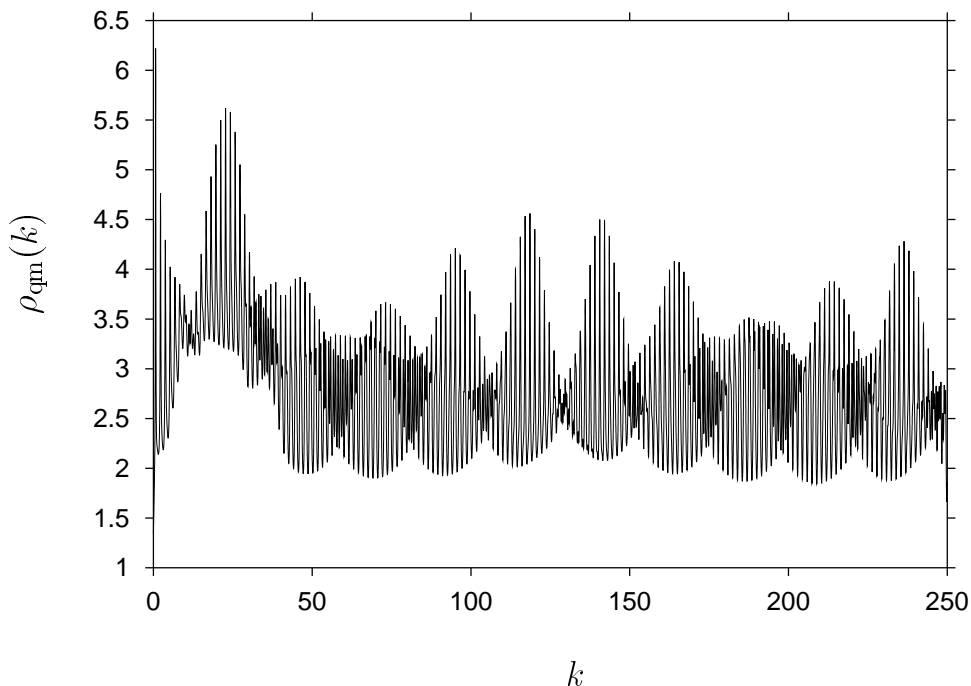
Figure 5.14: *Quantum mechanical density of states of the three-disk system with disk separation $d = 6$ (A_1 subspace) as a function of real values of the wave number k.*

4.2.1), the results of the analysis proved to be more accurate if the lowest part of the signal, determined by the "most quantum" resonances with very low real part, was cut off. I analyzed the spectrum in the range $\mathrm{Re}\, k \in [50, 250]$ to obtain the periodic orbit contributions in three different intervals of the scaled action. The results are presented in Figure 5.15. The solid lines mark the imaginary part of the semiclassical amplitudes,

$$\mathrm{Im}\,\mathcal{A}_{\mathrm{po}}^{(0)} = (-1)^{l_s+1} \frac{s_{\mathrm{po}}}{r|(\lambda_{\mathrm{po}} - 1)(\frac{1}{\lambda_{\mathrm{po}}} - 1)|^{1/2}} \,, \tag{5.7}$$

obtained by classical calculations, versus the scaled action of the symmetry reduced periodic orbits. The crosses show the results from harmonic inversion of the quantum spectrum. Note the different scales of the three plots.

Up to a scaled action of $s = 23$, there is an excellent agreement between the harmonic inversion results and the periodic orbit data from classical calculations. The results clearly confirm the validity of the Gutzwiller trace formula. For larger actions, the results suffer from the fact that the periodic orbits appear in clusters which become larger and more dense for increasing action. This happens because for large disk separations the orbit parameters are mainly determined by the symbol length, see Section 5.1.3. Orbits of the same symbol length therefore form clusters of almost the same action. In the region $s > 23$, some orbits with very similar actions were not resolved. Here, the harmonic inversion procedure yields a mean frequency with the amplitudes of the unresolved orbits added. The resolution may in principle be improved by extending the signal to higher values of the wave number, including further resonances with larger real parts.
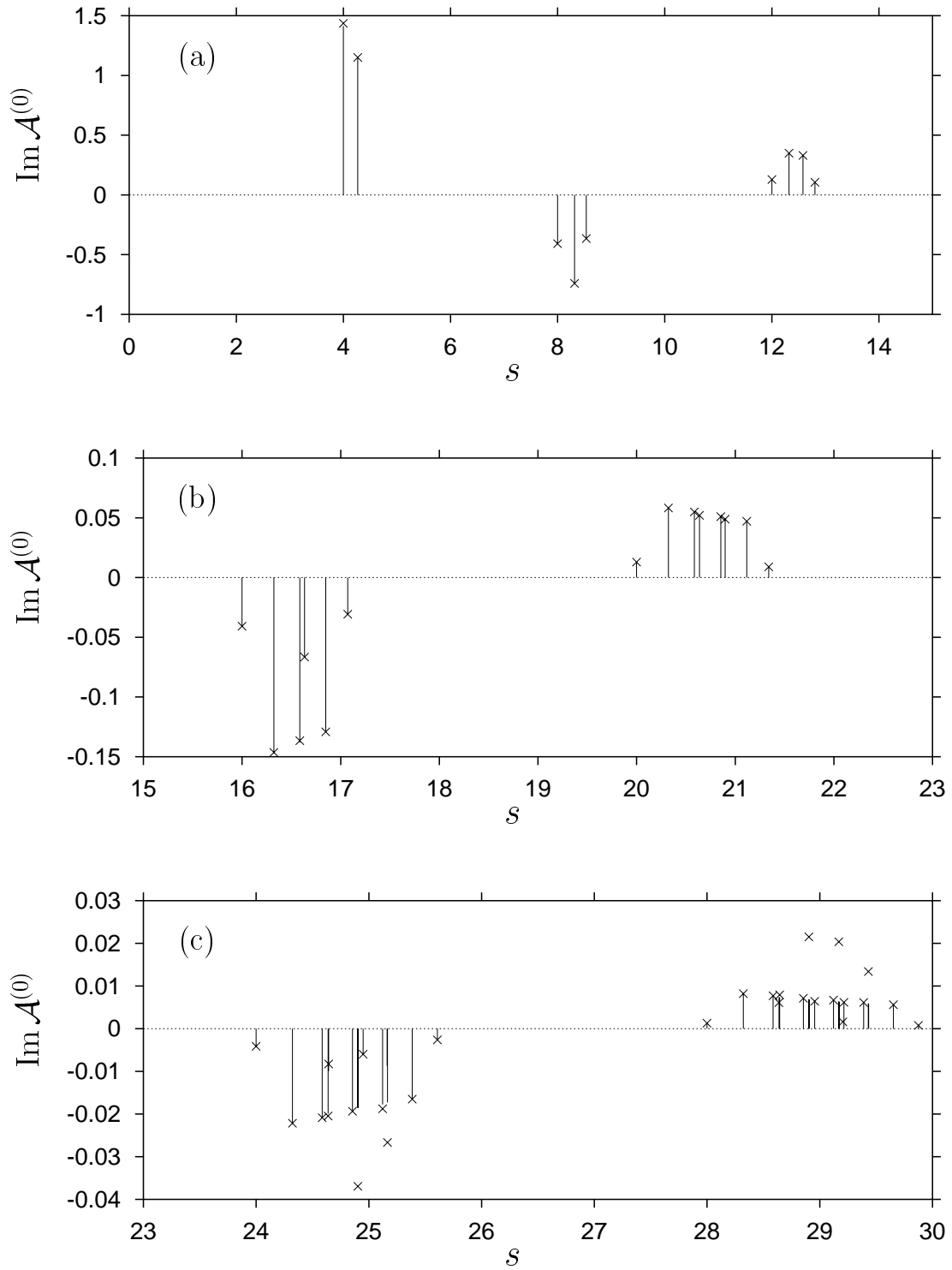
Figure 5.15: *Leading order periodic orbit contributions to the density of states of the three-disk system with disk separation $d = 6$. Solid lines: semiclassical amplitudes versus scaled actions of the symmetry reduced orbits, calculated from classical mechanics. Crosses: results from harmonic inversion of the exact quantum spectrum (A_1 subspace).*

5.2.2 First order $\hbar$ corrections to the trace formula

I will now determine higher order $\hbar$ corrections to the trace formula of the three-disk system with disk separation $d = 6$, using the semiclassical resonances of the A_1 subspace which were calculated by Wirzba [54, 59, 60] (see Section 5.1.4). Following the procedure described in Section 3.2.2, I analyze the difference spectrum between the exact quantum resonances and the semiclassical values from the cycle expansion of the Gutzwiller-Voros zeta function (see Fig. 5.10a) to determine the first order $\hbar$ corrections to the Gutzwiller trace formula. [Since the Gutzwiller-Voros zeta function is directly related to the Gutzwiller trace formula without further approximations (see Section 2.4), the semiclassical resonances resulting from both expressions should be the same.] The signal constructed from the difference spectrum is shown in Figure 5.16. Note that due to the limited radius of convergence of the cycle expansion only resonances with $\operatorname{Im} k \gtrsim -0.8$ could be included in the signal.
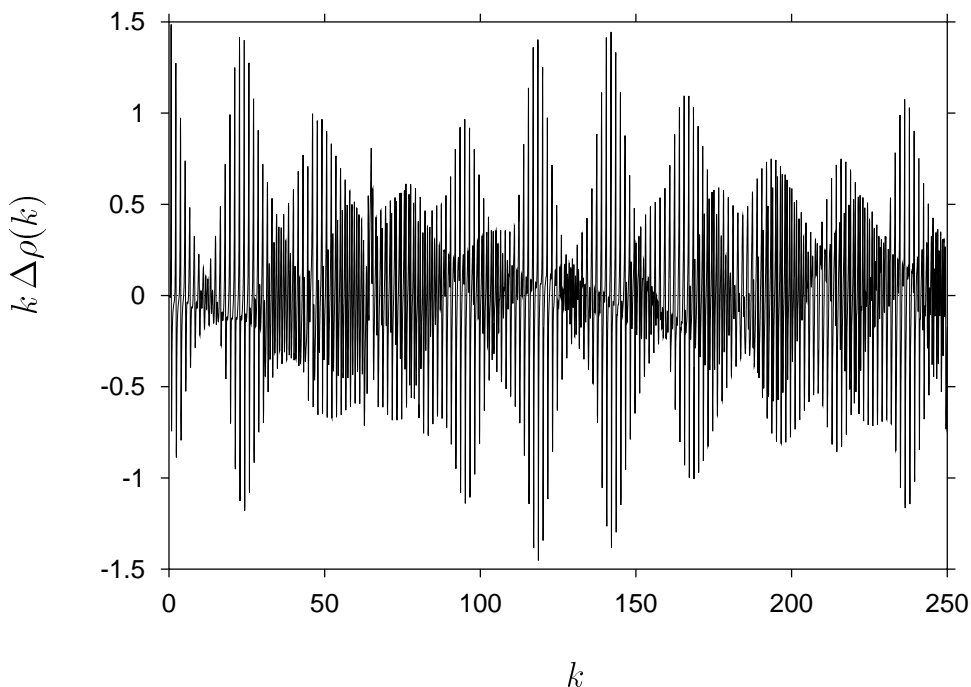
Figure 5.16: *Three-disk system with disk separation $d = 6$: Weighted difference spectrum $k \Delta\rho(k) = k(\rho_{\mathrm{qm}}(k) - \rho_{\mathrm{sc}}(k))$ between the quantum mechanical and the semiclassical density of states (A_1 subspace) as a function of the wave number k.*

For comparison, I calculated the first order amplitudes for each orbit following the method of Vattay and Rosenqvist [20, 21, 42] (see Section 2.3 and Appendix A.1). According to this method, the first order correction to the Gutzwiller trace formula for two-dimensional chaotic billiards is of the form (2.34), with the zeroth order terms $\exp(C_l^{(0)})$ given by Eq. (2.33). Eq. (2.34) can be rewritten in the form

$$g_1(E) = \frac{1}{i\hbar} \sum_{\mathrm{po}} \sum_l \frac{T_{\mathrm{po}}(E)}{r} \exp(C_l^{(0)}) \, \frac{i\hbar}{2} \, C_l^{(1)} e^{\frac{i}{\hbar} S_{\mathrm{po}}(E)} \tag{5.8}$$

with

$$\exp(C_l^{(0)}) = \frac{e^{i\mu_{\mathrm{po}}\pi/2}}{|\lambda_{\mathrm{po}}|^{1/2}\lambda_{\mathrm{po}}^l} \,, \tag{5.9}$$

where the first sum in Eq. (5.8) now runs over *all* periodic orbits, including multiple traversals. The quantity r is the repetition number with respect to the underlying primitive orbit. As for the zeroth order, I use the response function depending on the scaling parameter w, which is here equal to the wave number k. The first order amplitudes as defined in Eq. (3.29) are then given by

$$\mathcal{A}_{\mathrm{po}}^{(1)} = \frac{s_{\mathrm{po}}}{r} \sum_l \exp(C_l^{(0)}) \frac{C_l^{(1)}}{2\hbar k} \tag{5.10}$$

with

$$\exp(C_l^{(0)}) = \frac{(-1)^{l_s}}{|\lambda_{\mathrm{po}}|^{1/2}\lambda_{\mathrm{po}}^l} \tag{5.11}$$

for the three-disk scatterer, where l_s is the symbol length (cf. Section 5.1.2). Since the terms $C_l^{(1)}$ are proportional to the momentum $\hbar k$, as was shown in Ref. [42], the amplitudes are independent of the scaling parameter k. The correction terms $C_l^{(1)}$ have to be determined numerically. I use the code developed by Rosenqvist and Vattay [42, 66] (cf. Appendix A.1). The code requires the flight times between the bounces and the reflection angles as an input. These parameters have to be calculated numerically for each periodic orbit. As the contributions to the amplitude (5.10) for different l are proportional to $|\lambda|^{-l-\frac{1}{2}}$ (see Eq. (5.11)), the sum over l converges fast if the absolute value of the stability eigenvalue λ is large. For most orbits, the leading term $l = 0$ was already sufficient. Only for the very shortest orbits, terms of higher order in l had to be included to ensure convergence of the sum (see Table 5.2).

I calculated the first order corrections for three different intervals of the scaled action. The results are presented in Figure 5.17. The solid lines mark the first order amplitudes calculated from Eqs. (5.10) and (5.11) versus the scaled actions of the symmetry reduced orbits. The crosses show the results from the harmonic inversion of the difference spectrum between quantum and semiclassical cycle expansion values. For the first two action intervals (Figs. 5.17a and 5.17b), the signal was analyzed in the region $\mathrm{Re}\,k \in [100, 250]$; for the third interval (Fig. 5.17c) the range $\mathrm{Re}\,k \in [50, 250]$ was considered.

For most orbits, the harmonic inversion results are in excellent agreement with the amplitudes calculated by the method of Refs. [20, 21, 42], apart from a number of orbits in the region $s > 23$ which again were not resolved. However, there is a distinct discrepancy for the orbit with symbolic code '1' (scaled action $s \approx 4.267949$). The deviation is systematic and appears in the same way if the parameters of the harmonic inversion procedure (such as signal length etc.) are varied. This point still needs further clarification. A possible explanation for the discrepancy is the fact that the set of resonances from which the signal was constructed was not complete, as only resonances near the real axis could be included. However, this does not explain why only one orbit is strongly affected. On the other hand, the error may also lie in the theory of Refs. [20, 21, 42] or in its application to the three-disk system. In fact, the '1' orbit is the orbit with the largest contributions from terms of higher order in l to the sum in (5.10). The contributions from the different l terms and the converged sum over l of the five shortest orbits are compared in Table 5.2.
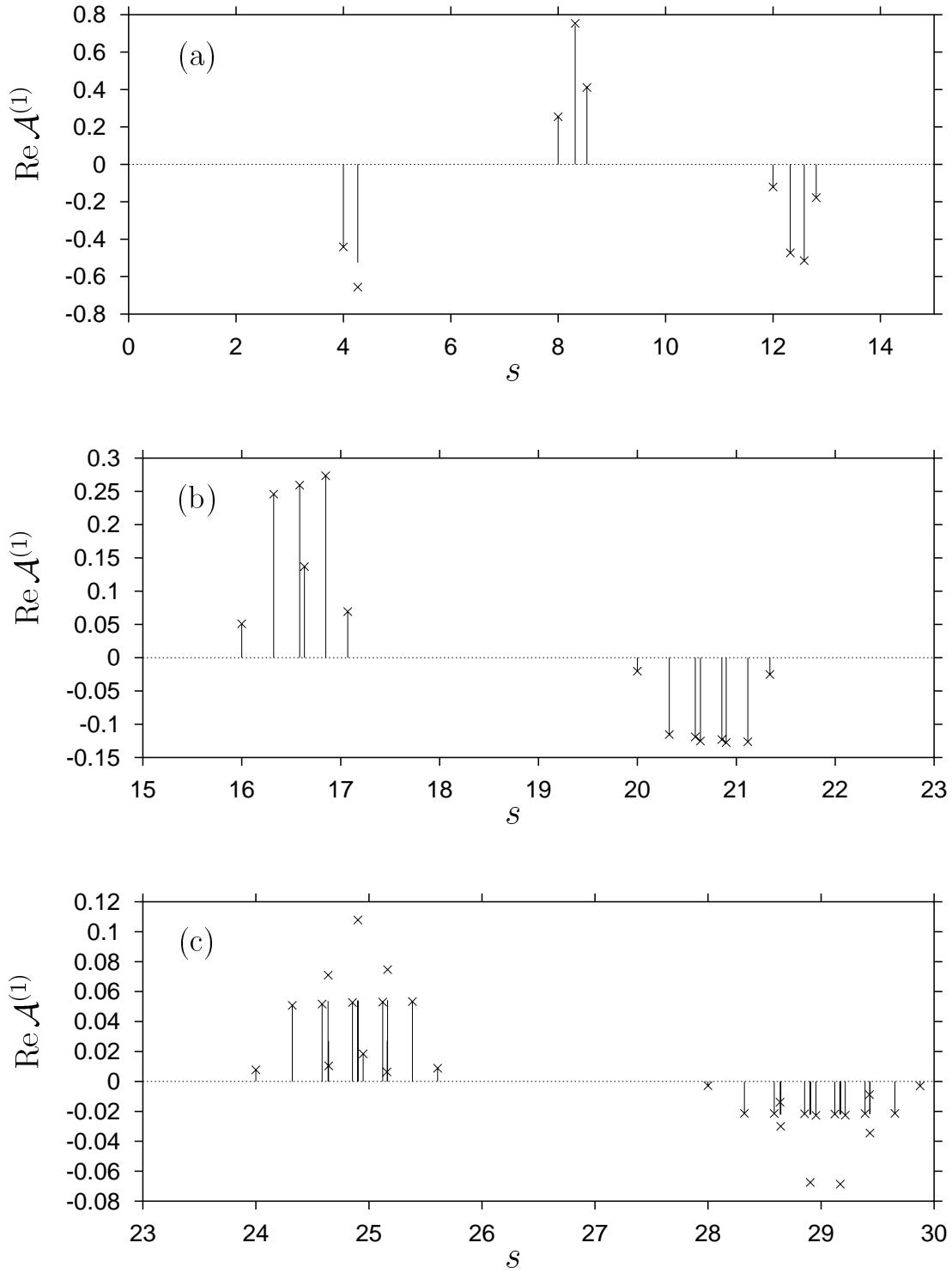
Figure 5.17: *First order ℏ corrections to the trace formula of the three-disk system with disk separation d = 6. Solid lines: first order amplitudes versus scaled actions of the symmetry reduced orbits, determined by classical calculations following the method of Refs. [20, 21, 42]. Crosses: results from harmonic inversion of the difference spectrum between exact quantum resonances and semiclassical cycle expansion values (A_1 subspace).*

Table 5.2: *Correction terms $C_l^{(1)}$ in units of the momentum $\hbar k$ and their contributions $C_l^{(1)}/\lambda^l$ to the first order $\hbar$ amplitude (5.10) for the five shortest periodic orbits of the three-disk system with $d = 6$. The values are compared with the results obtained by harmonic inversion (hi). The orbits are characterized by their symbolic code; their scaled action s and expanding stability eigenvalue λ are also given.*

	l	$C_l^{(1)}$	$\dfrac{C_l^{(1)}}{\lambda^l}$	$\sum\limits_{l=0}^{\infty}\dfrac{C_l^{(1)}}{\lambda^l}$	$\left[\sum\limits_{l=0}^{\infty}\dfrac{C_l^{(1)}}{\lambda^l}\right]_{\text{hi}}$
'0'	0	0.625000	0.625000	0.690360	0.693365
	1	1.125000	0.113648		
$s = 4.000000$	2	-2.750000	-0.028064		
$\lambda = 9.898979$	3	-14.750000	-0.015206		
'1'	0	1.124315	1.124315	0.843867	1.054674
	1	3.661620	-0.311059		
$s = 4.267949$	2	4.383308	0.031633		
$\lambda = -11.77146$	3	1.162291	-0.000713		
$2\times$'0'	0	1.250000	1.250000	1.272357	1.258825
	1	2.250000	0.022962		
$s = 8.000000$	2	-5.500000	-0.000573		
$\lambda = 97.98979$	3	-29.500000	-0.000031		
'01'	0	2.039795	2.039795	1.989582	2.018637
	1	6.278740	-0.050596		
$s = 8.316529$	2	5.881196	0.000382		
$\lambda = -124.0948$	3	-4.066328	0.000002		
$2\times$'1'	0	2.248630	2.248630	2.301937	2.270158
	1	7.323240	0.052850		
$s = 8.535898$	2	8.766615	0.000457		
$\lambda = 138.5672$	3	2.324582	0.000001		

For comparison, the last column of Table 5.2 shows the corresponding values following from the amplitudes of the harmonic inversion results. The '1' orbit exhibits the largest deviation between the $l = 0$ contribution and the converged sum over l, followed by the '0' orbit. For orbits with a symbol length of 2 or longer, the contributions from higher l terms are already so small (due to the large absolute value of the stability eigenvalue λ) that it is impossible to decide whether there is a discrepancy between these terms and the harmonic inversion results. However, the harmonic inversion results for the '0' orbit, which also shows a relatively large contribution from the $l = 1$ term, are in agreement with the theory. Again, it cannot be explained why only the '1' orbit is affected (although in this case the reasons might lie in the special geometrical properties of the '0' orbit).

In summary, it can at least be concluded that the harmonic inversion results confirm the validity of the $l = 0$ approximation to the formula (5.8) for orbits with large stability eigenvalues. On the other hand, the results demonstrate that the theory of higher order $\hbar$ corrections to the Gutzwiller formula still contains unanswered questions, and further investigations are necessary.

5.3 Periodic orbit quantization of the open three-disk system

In this section, the harmonic inversion techniques for periodic orbit quantization discussed in Section 3.3 are applied to the open three-disk system with disk separations $d = 6$ and $d = 2.5$. The results for the semiclassical resonances are compared with the exact quantum resonances and with semiclassical data from cycle expansion. Furthermore, the first order $\hbar$ correction terms to the Gutzwiller formula following from the theory of Vattay and Rosenqvist are used to calculate the first order $\hbar$ corrections to the semiclassical resonances.

5.3.1 Semiclassical resonances of the open three-disk system

The semiclassical response function for the A_1 subspace of the three-disk system is given by Eq. (5.5), where the sum runs over all symmetry reduced periodic orbits. For the periodic orbit quantization of the three-disk system, I use the decimated signal diagonalization method described in Section 3.1.3. A band-limited semiclassical signal is constructed following the procedure outlined in Section 3.3.1. The resulting signal reads

$$C(s) = -i \sum_{\text{po}} (-1)^{l_s} \frac{s_{\text{po}}}{r|(\lambda_{\text{po}} - 1)(\frac{1}{\lambda_{\text{po}}} - 1)|^{1/2}} \frac{\sin[\Delta w(s - s_{\text{po}})]}{\pi(s - s_{\text{po}})} e^{is_{\text{po}}w_0} , \qquad (5.12)$$

with the quantities as defined in Section 5.1.2. The semiclassical signal is adjusted to the corresponding quantum signal, Eq. (3.41), by harmonic inversion.

For disk separation $d = 6$, all symmetry reduced periodic orbits up to symbol length 13 (i. e., 1 377 primitive orbits) were included, which corresponds to a maximum scaled action of $s_{\max} = 56$ (cf. Section 5.1.3). This signal length was sufficient to resolve resonances with a real part up to $\operatorname{Re} k = 250$ and beyond. Figure 5.18 shows the results of the calculation. In order to keep the matrix dimensions in the decimated signal diagonalization small, the frequency range $0 \leq \operatorname{Re} k \leq 250$ was divided into five intervals, each of length 50, which were treated separately. Unconverged frequencies were identified by their small amplitudes. In Figure 5.18 all frequencies with an amplitude $\operatorname{Re} m_k > 0.5$ (cf. Eq. (3.41)) are included.

The harmonic inversion results (marked by crosses) are compared with the four leading bands of exact quantum resonances (marked by circles) in Fig. 5.18a and with the semiclassical values from the cycle expansion of the Gutzwiller-Voros zeta function (circles) in Fig. 5.18b. The exact quantum and cycle expansion values were calculated by Wirzba [60] (cf. Section 5.1.4). The harmonic inversion results are in excellent agreement with the theoretical values. The additional frequencies in the lower right part of the spectrum correspond to resonances of further bands (see Figs. 5.10 and 5.11). It can clearly be seen that, in the regions where the semiclassical error is visible, the harmonic inversion results reproduce the semiclassical values from cycle expansion rather than the exact quantum eigenvalues. However, it has to be emphasized that, with the harmonic inversion method, semiclassical resonances are obtained even in regions of large negative imaginary part, where the cycle expansions of the Gutzwiller-Voros zeta function and the dynamical zeta function do not converge any more (cf. Fig. 5.10). On the other hand, the harmonic inversion method does not possess the disadvantage of producing spurious resonances as is
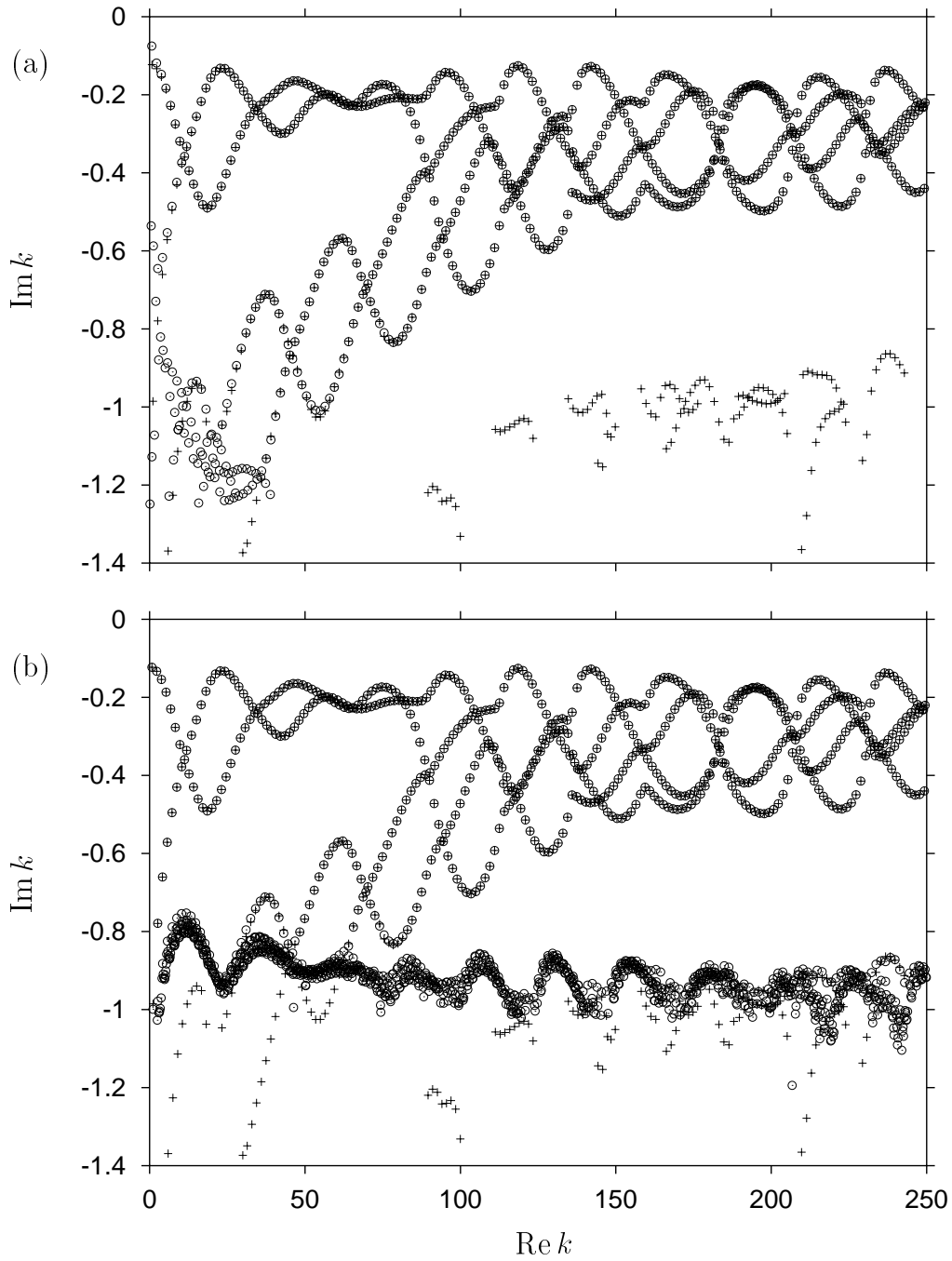
Figure 5.18: *Resonances of the three-disk system with disk separation $d = 6$ (A_1 subspace). The crosses (+) represent the results of the harmonic inversion procedure. These results are compared (a) with the four leading bands of exact quantum resonances (circles) and (b) with the semiclassical data obtained by cycle expansion of the Gutzwiller-Voros zeta function (circles), both taken from Refs. [54, 59, 60].*
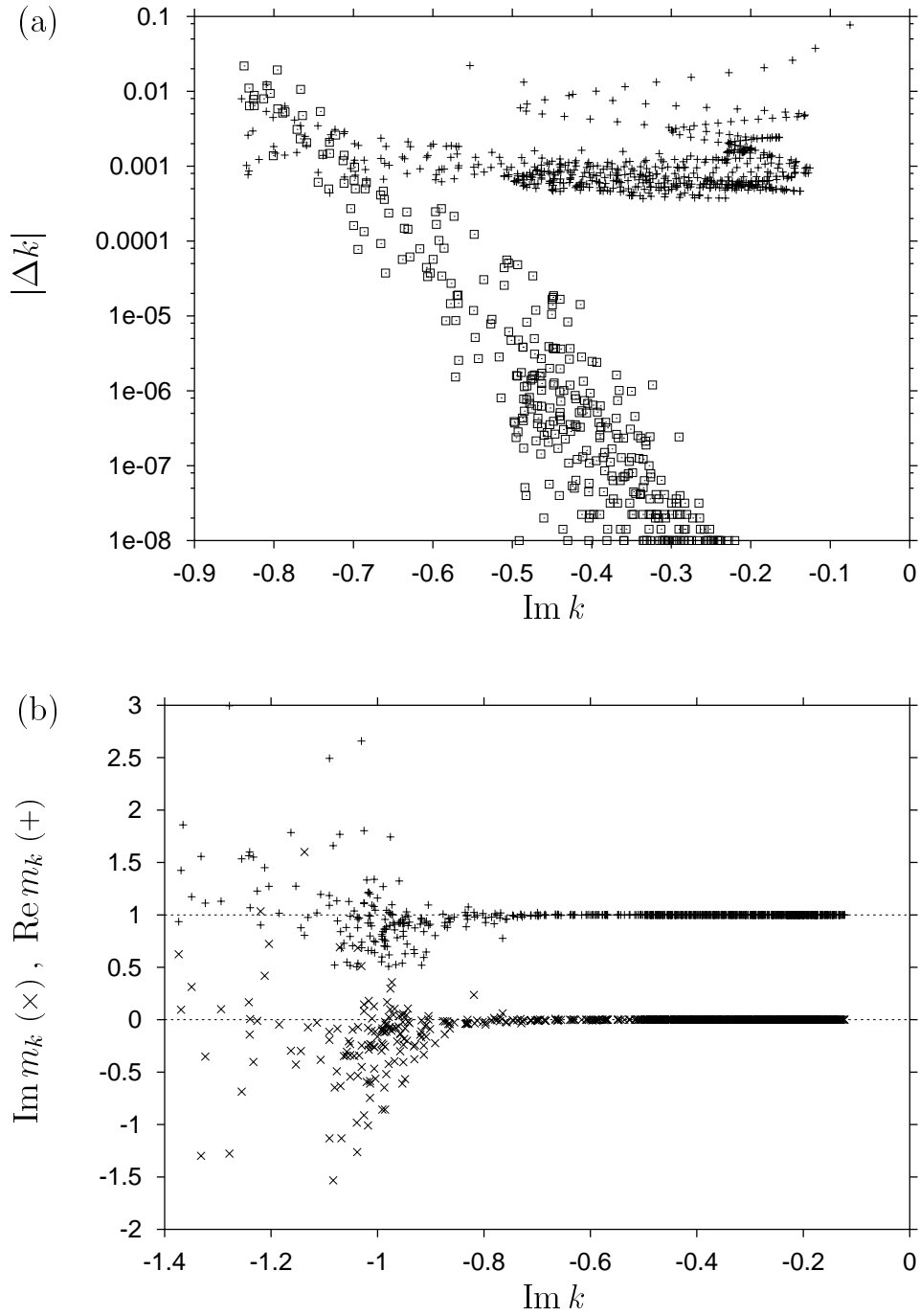
Figure 5.19: *(a) Deviations of the harmonic inversion results from the exact quantum resonances (+) and from the cycle expansion results (□). (b) Real (+) and imaginary (×) part of the multiplicities m_k calculated from the amplitudes of the harmonic inversion results. Only values with $\operatorname{Re} m_k > 0.5$ are included.*

the case with the quasiclassical zeta function (cf. Fig. 5.11). The results for the low-lying resonances are still in good agreement with the exact quantum data.

Figure 5.19a shows the deviations of the harmonic inversion results for the four leading bands from the exact quantum resonances (crosses) and from the cycle expansion results (squares) as a function of the imaginary part of the resonances. Again, it is clearly visible that the cycle expansion results rather than the exact quantum values are reproduced. The accuracy of the results depends on the imaginary part of the resonances. For small negative imaginary part, the deviation of the harmonic inversion results from the cycle expansion values is about four to five orders of magnitude smaller than the semiclassical error, while for imaginary parts $\operatorname{Im} k \lesssim -0.7$ it is of about the same order of magnitude. Part of the deviations might also be due to inaccuracies in the cycle expansion results near the border of convergence. The dependence of the accuracy on the imaginary part of the resonances can also be found for the amplitudes m_k (cf. Eq. (3.41)), which should ideally be exactly equal to 1 (which is the multiplicity of the states). Figure 5.19b shows the real and the imaginary part of the values m_k obtained as a function of $\operatorname{Im} k$. As in Fig. 5.18, only values with $\operatorname{Re} m_k > 0.5$ were included. The condition $m_k = 1$ is well satisfied for $\operatorname{Im} k \gtrsim -0.8$, which implies that the corresponding frequencies are well converged. The dependence of the accuracy on $\operatorname{Im} k$ can be understood by the fact that the negative imaginary part of the resonance causes a damping of the corresponding part of the signal. The contributions to the signal are proportional to $e^{(\operatorname{Im} w_k)s}$, which can be seen from the form of the quantum signal (3.41). For increasing action s, the signal therefore becomes dominated by the resonances near the real axis, and due to the limited numerical accuracy the contributions from deeper resonances are only visible within a shorter "effective" signal length.

In addition to the case $d = 6$, I also considered the relatively small disk separation $d = 2.5$. Here, I calculated the resonances in the range $0 \le \operatorname{Re} k \le 100$. In the signal all periodic orbits up to a scaled action of $s_{\max} = 12$ were included (23 206 primitive orbits). Figure 5.20 compares the harmonic inversion results (marked by crosses) (a) with the exact quantum values and (b) with the results from the cycle expansion of the Gutzwiller-Voros zeta function, both calculated by Wirzba [60] (see Fig. 5.12). For resonances with an imaginary part $\operatorname{Im} k \gtrsim -1.0$, there is again an excellent agreement between the harmonic inversion results and the semiclassical cycle expansion values, apart from two close resonances in the region $\operatorname{Re} k \gtrsim 90$ which were not resolved. A number of resonances with larger negative imaginary part have also been obtained. Figure 5.21a shows the deviation of the harmonic inversion results from the exact quantum values (crosses) and the cycle expansion values (squares), and Figure 5.21b gives the real and the imaginary part of the corresponding amplitudes m_k. Again, it can be seen that the accuracy of the harmonic inversion results depends on the imaginary part of the resonances. In general, the deviations from the cycle expansion values are larger than for disk separation $d = 6$, which is partly due to the fact that the resonances lie deeper in the complex plane. There are two resonances with $\operatorname{Im} k \approx -0.5$ for which the amplitudes show relatively large deviations from the theoretical value $m_k = 1$. These resonances have a large real part, $\operatorname{Re} k > 90$. Probably these values are not well converged because the signal length was not sufficient. The amplitude $m_k \approx 2$ of one of the values suggests that this frequency belongs to two resonances which were not resolved. Especially in the region of large real parts, the results can in principle be further improved by extending the signal to longer orbits. However, due to the proliferation of periodic orbits with growing action,
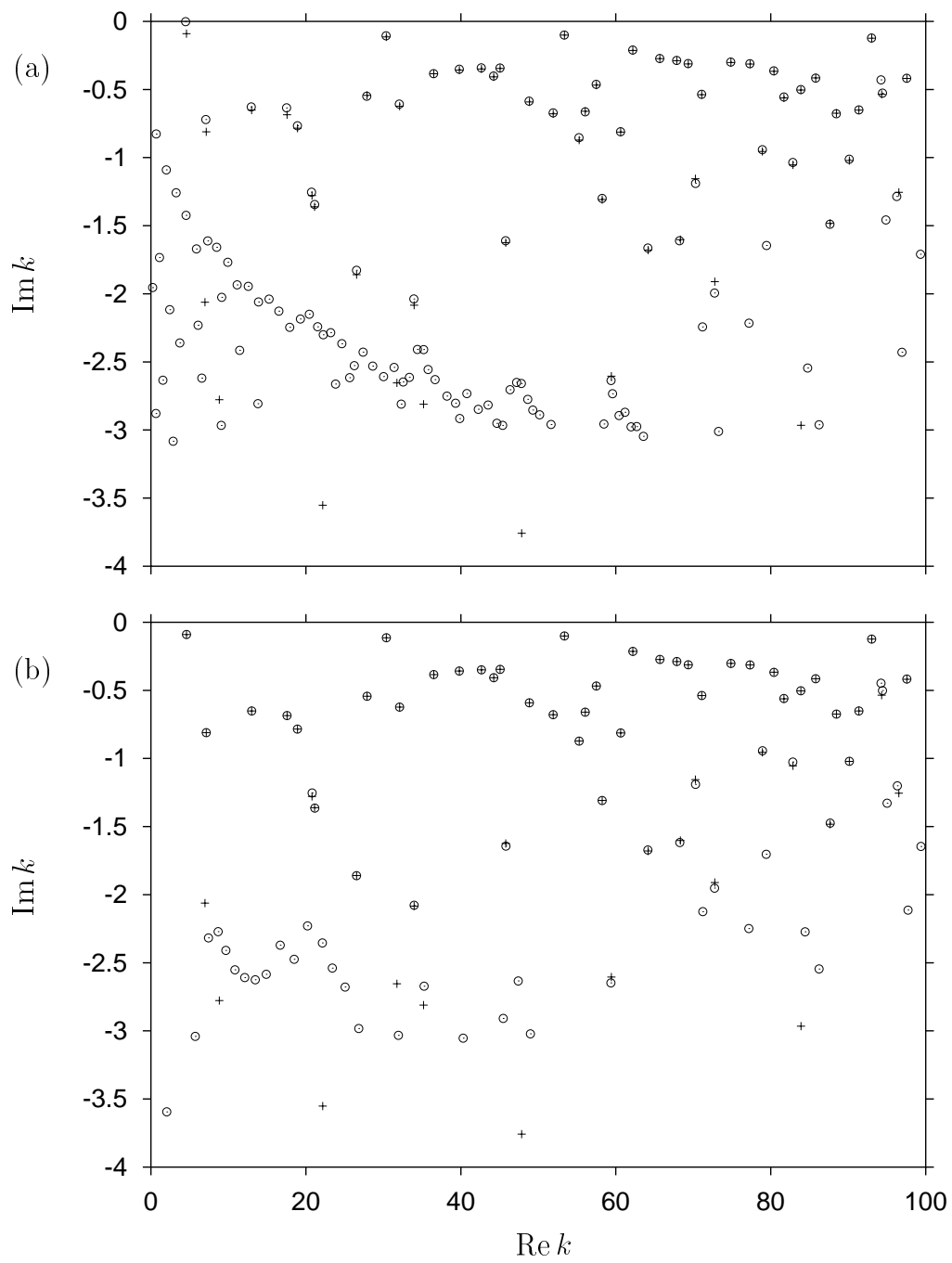
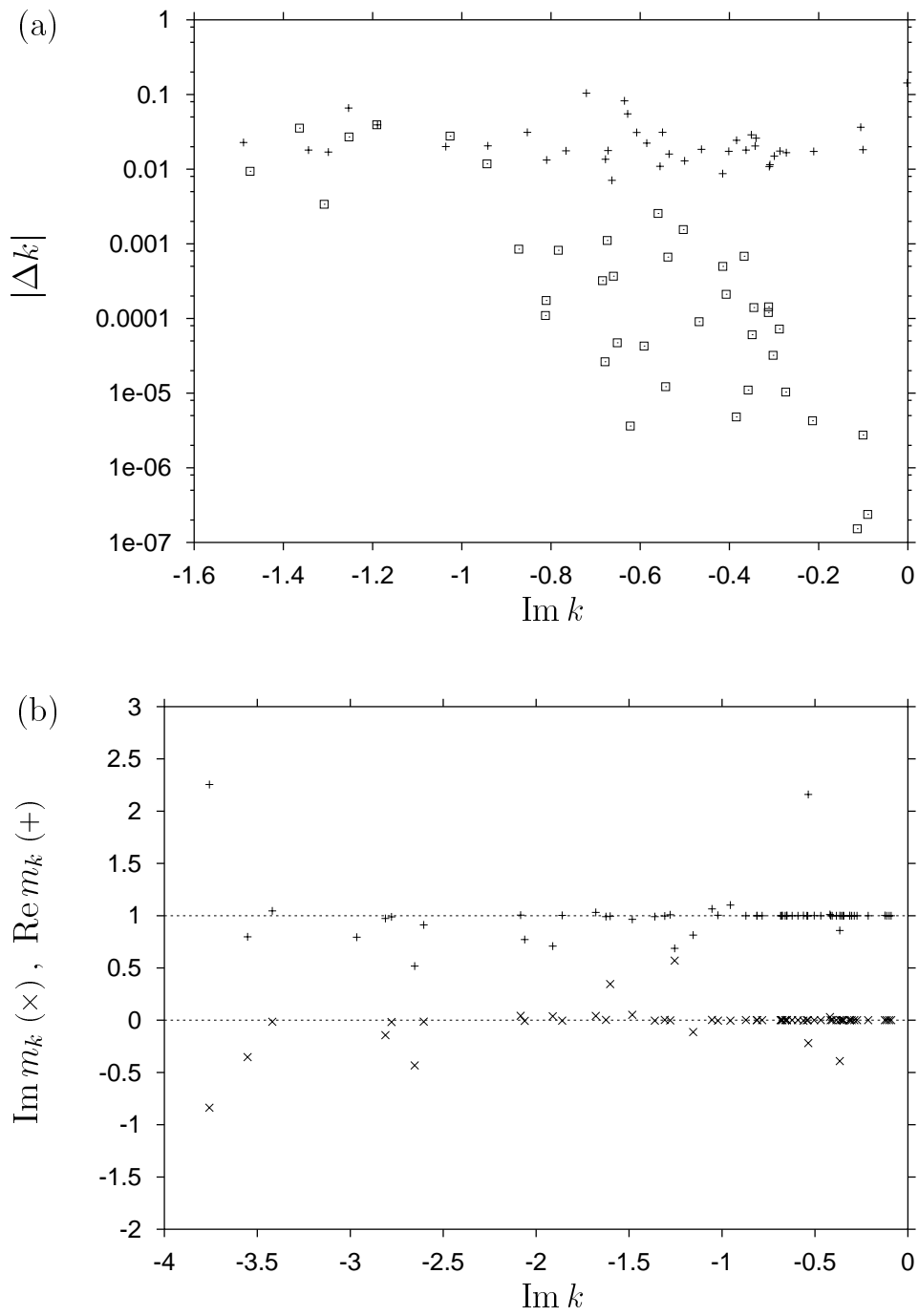Figure 5.20: *As Fig. 5.18, but for disk separation d = 2.5.*

Figure 5.21: *As Fig. 5.19, but for disk separation $d = 2.5$.*

which for $d = 2.5$ is already much more rapid than for $d = 6$, a significant extension of the signal would require a comparatively large numerical effort.

5.3.2 Higher order $\hbar$ corrections

I will now determine the first order $\hbar$ corrections to the semiclassical resonances of the open three-disk scattering system obtained in the previous section, using the techniques developed in Section 3.3.2. According to the theory of Vattay and Rosenqvist [20, 21, 42], the first order $\hbar$ amplitudes of the three-disk system as defined in Eq. (3.44) are given by

$$ \mathcal{A}_{\text{po}}^{(1)} = \frac{s_{\text{po}}}{r} \sum_l \frac{(-1)^{l_s}}{|\lambda_{\text{po}}|^{1/2}\lambda_{\text{po}}^l} \frac{C_l^{(1)}}{2\hbar k} \, , \tag{5.13} $$

as has already been discussed in Section 5.2.2 (see Eqs. (5.10) and (5.11)). The correction terms $C_l^{(1)}$ can be determined numerically with the code developed by Rosenqvist and Vattay [42, 66] (cf. Appendix A.1). Since the contributions to the the amplitude $\mathcal{A}_{\text{po}}^{(1)}$ for different l are proportional to $|\lambda|^{-l-\frac{1}{2}}$, the sum over l can be expected to converge fast if the absolute value of the stability eigenvalue λ is large. For the three-disk system with disk separations $d = 6$ and $d = 2.5$, it could be observed that the leading term $l = 0$ was already sufficient. The inclusion of higher terms in the l-sum does not bring about a qualitative change in the results.

For disk separation $d = 6$, I constructed a band-limited periodic orbit signal of length $s_{\text{max}} = 56$ from the first order amplitudes, which was analyzed by means of decimated signal diagonalization. As for the zeroth order obtained in Section 5.3.1, the frequency range $0 \leq \text{Re}\, k \leq 250$ was divided into five intervals of length 50, which were treated separately. In the first order amplitudes (5.13), only the leading order term $l = 0$ of the sum was included. The results for the first order corrections Δk_1 obtained from the amplitudes of the harmonic inversion results are added to the semiclassical resonances calculated in Section 5.3.1 in order to obtain the first order approximations k_1 to the resonances. Table 5.3 shows part of the results in the regions $\text{Re}\, k \in [0, 20]$ and $\text{Re}\, k \in [150, 155]$ with $\text{Im}\, k \geq -0.69$. The values k_0 are the zeroth order approximations obtained in Section 5.3.1. For comparison, the exact quantum resonances k_{ex} and the semiclassical cycle expansion results k_{ce} (both from Refs. [54, 59, 60]) are also given. Figures 5.22 and 5.23 compare the semiclassical errors of the zeroth (crosses) and first (squares) order approximations as a function of the imaginary and of the real part of the resonances, respectively. [The one-to-one correspondence of the zeroth and first order values plotted is, however, hard to see in the plots.] The deviations in real and imaginary part from the exact quantum values are given separately. In Figure 5.23, only resonances with an imaginary part $\text{Im}\, k \geq -0.5$ were included.

The results show a significant improvement in the accuracy of the real parts of the resonances. For most resonances, the real part of the first order approximation is between two and five orders of magnitude closer to the exact quantum values than the zeroth order approximation. Only for the "most quantum" resonances, with very low real parts, the improvement is rather small. The reason for this lies in the properties of the semiclassical approximation itself; in order to improve these values, second or higher order terms in the $\hbar$ expansion must be considered. On the other hand, the accuracy decreases with increasing negative imaginary part of the resonances. This is probably due to the error of

Table 5.3: *Zeroth (k_0) and first (k_1) order approximations to the resonances of the three-disk system with disk separation $d = 6$ (A_1 subspace), obtained by harmonic inversion of a signal of length $s_{\max} = 56$. For comparison, the semiclassical values from cycle expansion k_{ce} and the exact quantum values k_{ex} are given (both taken from Refs. [54, 59, 60]). Only resonances with $\mathrm{Im}\, k \geq -0.69$ are included.*

Re k_{ce}	Im k_{ce}	Re k_0	Im k_0	Re k_1	Im k_1	Re k_{ex}	Im k_{ex}
0.75831	-0.12282	0.75831	-0.12282	0.61295	-0.14993	0.69800	-0.07501
2.27428	-0.13306	2.27428	-0.13306	2.22417	-0.13960	2.23960	-0.11877
3.78788	-0.15413	3.78788	-0.15413	3.75695	-0.15903	3.76269	-0.14755
5.29607	-0.18679	5.29607	-0.18679	5.27282	-0.19113	5.27567	-0.18322
5.68203	-0.57155	5.68203	-0.57155	5.66706	-0.54992	5.66950	-0.55341
6.79364	-0.22992	6.79364	-0.22992	6.77417	-0.23345	6.77607	-0.22751
7.22422	-0.49541	7.22422	-0.49541	7.21231	-0.48189	7.21527	-0.48562
8.27639	-0.27708	8.27639	-0.27708	8.25953	-0.27932	8.26114	-0.27491
8.77919	-0.43027	8.77919	-0.43027	8.76958	-0.42179	8.77247	-0.42410
9.74763	-0.32082	9.74763	-0.32082	9.73320	-0.32201	9.73451	-0.31881
10.34423	-0.37820	10.34423	-0.37820	10.33588	-0.37289	10.33819	-0.37371
11.21348	-0.35996	11.21348	-0.35996	11.20110	-0.36058	11.20211	-0.35823
11.91345	-0.33573	11.91345	-0.33573	11.90592	-0.33225	11.90760	-0.33223
12.67753	-0.39612	12.67753	-0.39612	12.66681	-0.39642	12.66759	-0.39467
13.48265	-0.29695	13.48265	-0.29695	13.47574	-0.29451	13.47693	-0.29411
14.14241	-0.43006	14.14241	-0.43006	14.13305	-0.43011	14.13370	-0.42883
15.04731	-0.25784	15.04731	-0.25784	15.04086	-0.25605	15.04169	-0.25551
15.61133	-0.46044	15.61133	-0.46044	15.60310	-0.46019	15.60372	-0.45928
16.60256	-0.21887	16.60256	-0.21887	16.59647	-0.21758	16.59706	-0.21700
17.08764	-0.48279	17.08764	-0.48279	17.08035	-0.48214	17.08100	-0.48154
18.14650	-0.18423	18.14650	-0.18423	18.14073	-0.18337	18.14114	-0.18280
18.57319	-0.49141	18.57319	-0.49141	18.56667	-0.49034	18.56736	-0.48994
19.68084	-0.15759	19.68084	-0.15759	19.67538	-0.15710	19.67566	-0.15654
$\vdots$	$\vdots$	$\vdots$	$\vdots$	$\vdots$	$\vdots$	$\vdots$	$\vdots$
150.09512	-0.23623	150.09512	-0.23623	150.09449	-0.23613	150.09450	-0.23613
150.37731	-0.51026	150.37731	-0.51029	150.37657	-0.51023	150.37657	-0.51020
150.76086	-0.40911	150.76086	-0.40911	150.76004	-0.40908	150.76004	-0.40906
151.09908	-0.22292	151.09908	-0.22292	151.09826	-0.22298	151.09826	-0.22297
151.64342	-0.22327	151.64342	-0.22327	151.64279	-0.22321	151.64279	-0.22320
151.90047	-0.51042	151.90046	-0.51046	151.89974	-0.51038	151.89974	-0.51033
152.24814	-0.38924	152.24814	-0.38924	152.24733	-0.38920	152.24733	-0.38919
152.60380	-0.24729	152.60380	-0.24729	152.60298	-0.24735	152.60298	-0.24733
153.19200	-0.21587	153.19200	-0.21587	153.19138	-0.21583	153.19138	-0.21582
153.42259	-0.50494	153.42259	-0.50499	153.42187	-0.50489	153.42188	-0.50483
153.73475	-0.36935	153.73475	-0.36935	153.73395	-0.36932	153.73395	-0.36931
154.11072	-0.27186	154.11072	-0.27186	154.10992	-0.27192	154.10992	-0.27190
154.74201	-0.21392	154.74201	-0.21392	154.74140	-0.21390	154.74140	-0.21389
154.94126	-0.49330	154.94126	-0.49334	154.94054	-0.49323	154.94054	-0.49317
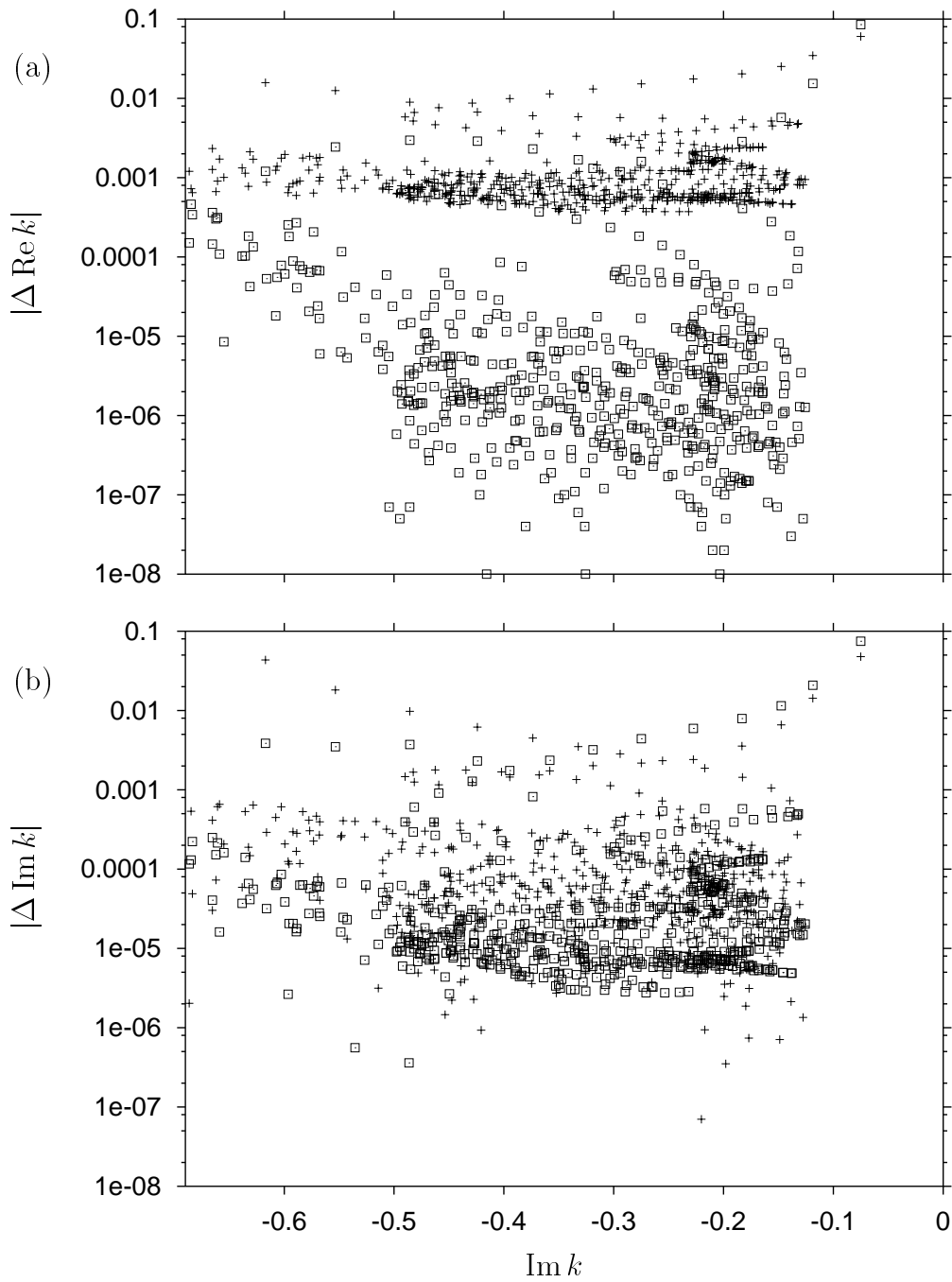
Figure 5.22: *Three-disk system with disk separation $d = 6$: Deviations of the zeroth $(+)$ and first $(\boxdot)$ order $\hbar$ approximations to the resonances, obtained by harmonic inversion, from the exact quantum values (A_1 subspace). (a) Real part, (b) imaginary part of the deviations (absolute values), as a function of the imaginary part of the resonances.*
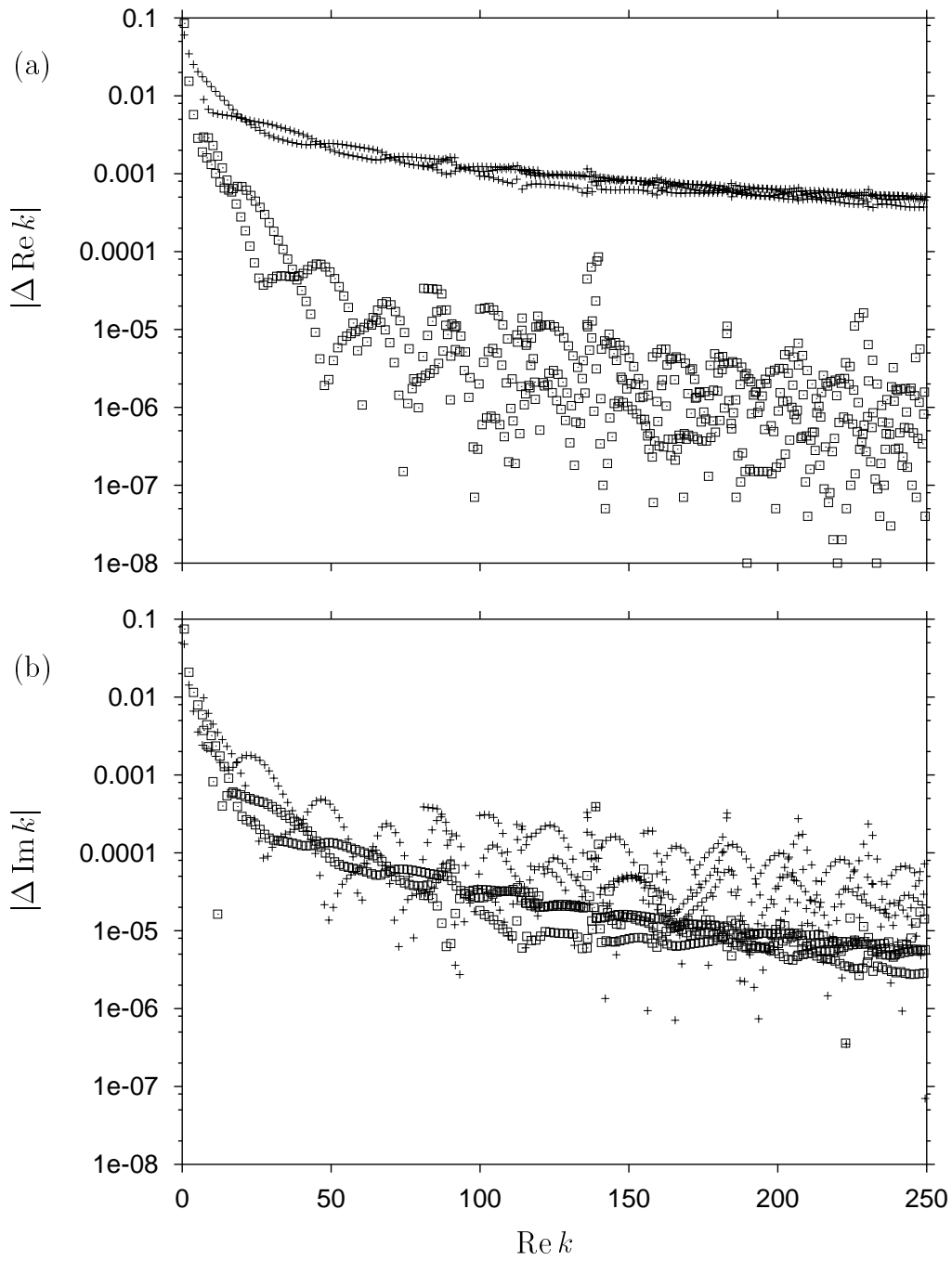
Figure 5.23: *The semiclassical errors of the zeroth (+) and first (⊡) order approximations presented in Fig. 5.22, now plotted as a function of the real part of the resonances. Only resonances with an imaginary part* Im $k \geq -0.5$ *are included.*

Table 5.4: *Zeroth and first order approximations to the resonances of the three-disk system with disk separation $d = 2.5$ (A_1 subspace), obtained from a signal of length $s_{\max} = 12$. The notations are the same as in Table 5.3. The table contains the resonances in the region $1 \le \operatorname{Re} k \le 90$ and $-1.0 \le \operatorname{Im} k \le 0$.*

| $\operatorname{Re} k_{\mathrm{ce}}$	$\operatorname{Im} k_{\mathrm{ce}}$	$\operatorname{Re} k_0$	$\operatorname{Im} k_0$	$\operatorname{Re} k_1$	$\operatorname{Im} k_1$	$\operatorname{Re} k_{\mathrm{ex}}$	$\operatorname{Im} k_{\mathrm{ex}}$
4.58118	-0.08999	4.58118	-0.08999	4.35123	-0.05580	4.46928	-0.00157
7.14412	-0.81073	7.14428	-0.81079	6.90301	-0.66547	7.09171	-0.72079
13.00005	-0.65161	13.00009	-0.65163	12.93645	-0.63795	12.95032	-0.62824
17.56994	-0.68456	17.57004	-0.68486	17.45278	-0.65154	17.50423	-0.63526
18.92665	-0.78369	18.92585	-0.78389	18.93139	-0.72879	18.92545	-0.76629
27.88819	-0.54318	27.88820	-0.54319	27.86253	-0.55690	27.85779	-0.54993
30.38846	-0.11345	30.38846	-0.11345	30.34790	-0.11469	30.35289	-0.10567
32.09670	-0.62237	32.09670	-0.62237	32.05975	-0.61112	32.06937	-0.60774
36.50664	-0.38464	36.50664	-0.38464	36.48222	-0.38774	36.48228	-0.38392
39.81392	-0.35803	39.81392	-0.35801	39.78247	-0.35590	39.78597	-0.35087
42.65565	-0.34928	42.65566	-0.34922	42.62622	-0.34386	42.63124	-0.34036
44.24572	-0.40728	44.24593	-0.40728	44.22724	-0.40137	44.22958	-0.40156
45.06030	-0.34538	45.06035	-0.34525	45.03887	-0.34490	45.04010	-0.34219
48.84178	-0.59135	48.84182	-0.59135	48.81823	-0.58812	48.82031	-0.58534
51.91460	-0.67916	51.91462	-0.67914	51.89581	-0.67282	51.89831	-0.67213
53.37665	-0.10056	53.37665	-0.10056	53.35860	-0.10299	53.35844	-0.10060
55.27905	-0.87225	55.27951	-0.87154	55.24461	-0.85579	55.25449	-0.85300
56.04831	-0.66008	56.04829	-0.65971	56.04603	-0.66240	56.04222	-0.66339
57.48373	-0.46810	57.48381	-0.46814	57.46436	-0.46491	57.46621	-0.46260
60.62041	-0.81265	60.62051	-0.81260	60.60675	-0.81054	60.60752	-0.80981
62.20040	-0.21371	62.20040	-0.21371	62.18253	-0.21311	62.18329	-0.21112
65.68047	-0.27377	65.68047	-0.27378	65.66353	-0.27480	65.66387	-0.27258
67.86884	-0.28819	67.86889	-0.28815	67.85047	-0.28896	67.85151	-0.28656
69.34436	-0.31237	69.34446	-0.31247	69.33251	-0.30929	69.33346	-0.30925
71.08228	-0.53819	71.08294	-0.53828	71.06684	-0.53676	71.06727	-0.53534
74.85527	-0.30225	74.85524	-0.30224	74.83975	-0.30093	74.84053	-0.29941
77.31932	-0.31293	77.31939	-0.31303	77.30827	-0.31116	77.30881	-0.31071
78.92364	-0.94338	78.92015	-0.95466	78.90779	-0.95464	78.90426	-0.94161
80.41738	-0.36702	80.41789	-0.36657	80.39883	-0.36525	80.40022	-0.36289
81.70204	-0.56016	81.69995	-0.56162	81.68874	-0.55515	81.69091	-0.55547
83.87409	-0.50352	83.87557	-0.50399	83.86231	-0.50159	83.86311	-0.50054
85.80010	-0.41476	85.80058	-0.41490	85.79208	-0.41566	85.79189	-0.41529
88.47030	-0.67394	88.46929	-0.67440	88.45699	-0.67931	88.45614	-0.67782
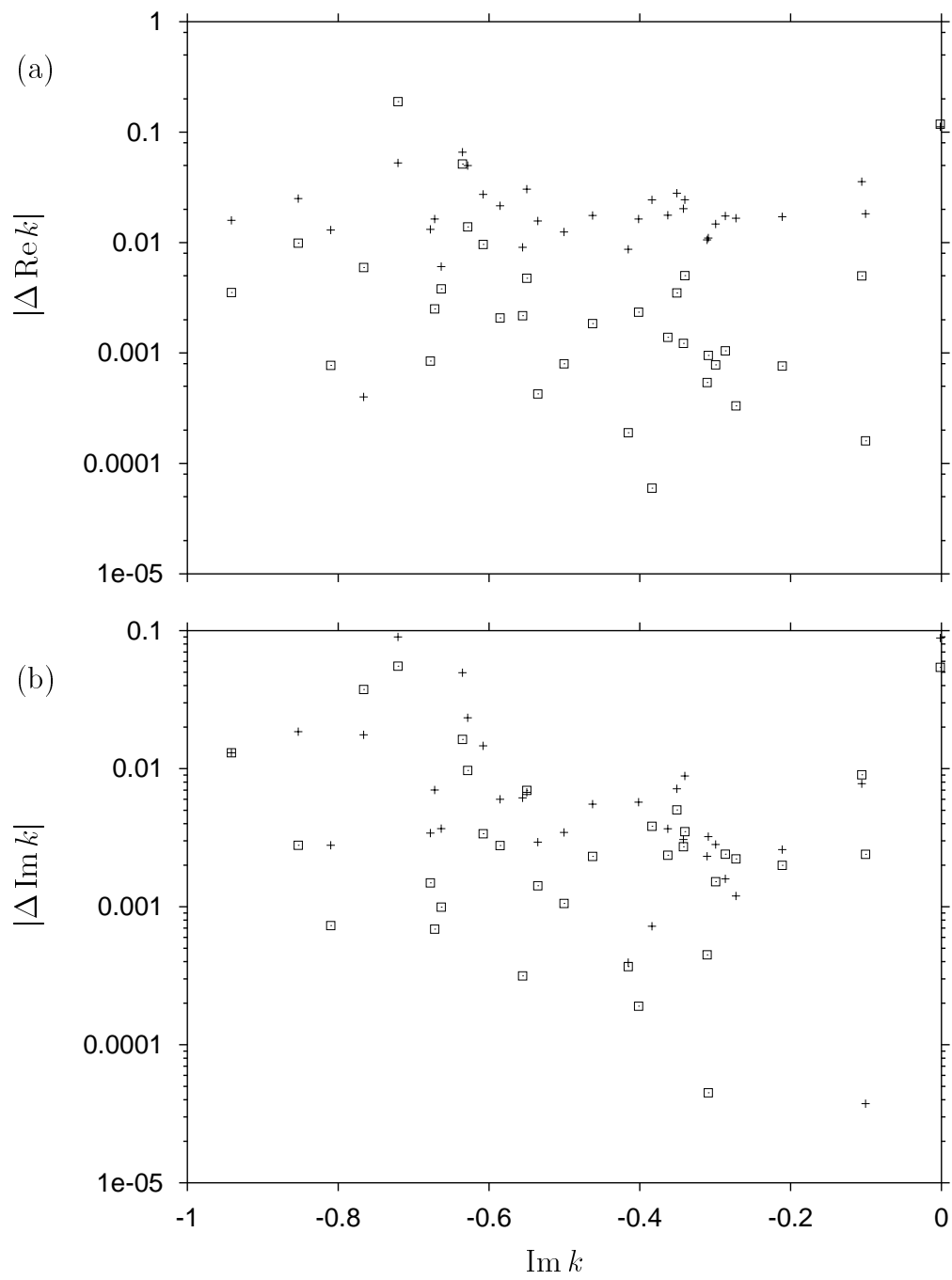
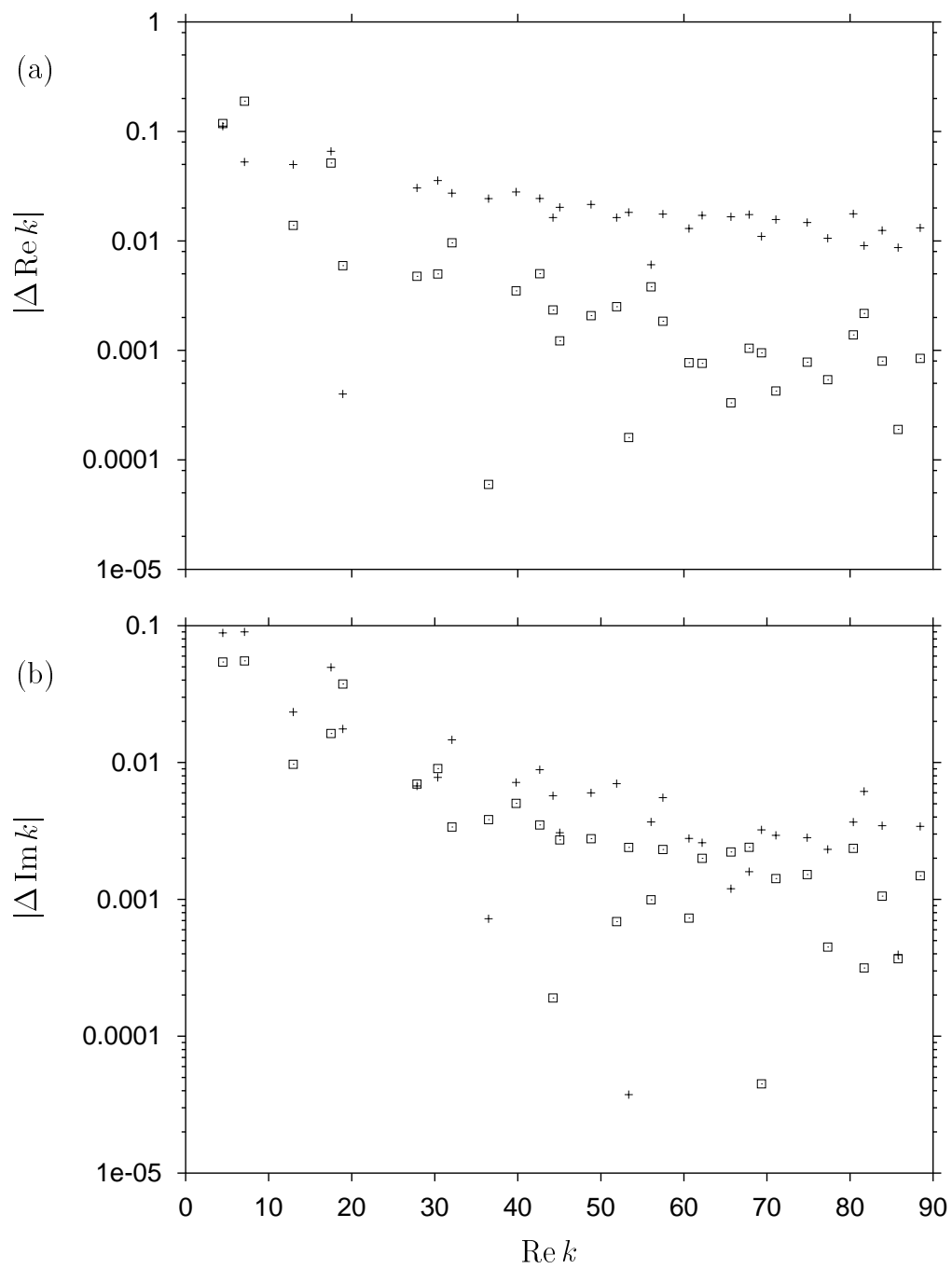Figure 5.24: *As Fig. 5.22, but for disk separation $d = 2.5$.*

Figure 5.25: *As Fig. 5.23, but for disk separation $d = 2.5$. Only resonances with an imaginary part $\operatorname{Im} k \geq -0.82$ are included.*

the harmonic inversion method, and in agreement with the results of Section 5.3.1. It was observed in Section 5.3.1 that the error of the harmonic inversion method becomes of the same order of magnitude as the semiclassical error around $\operatorname{Im} k \approx -0.7$. For resonances with larger negative imaginary part, the accuracy of the zeroth order approximation is therefore not sufficient to expect an improvement by first order corrections.

The accuracy of the imaginary parts of the semiclassical resonances is less significantly improved by the first order corrections than that of the real parts. For some resonances, the zeroth order approximation is even closer to the exact quantum values than the first order approximation. This was also observed by Rosenqvist [42], who calculated first order $\hbar$ corrections to the resonances using the cycle expansion technique. As discussed in Ref. [42], the first order corrections to the periodic orbit sum mainly improve the real part of the resonances, while the imaginary part can be expected to be improved by second order $\hbar$ corrections.

A similar behaviour can be found for disk separation $d = 2.5$. Here, I calculated the first order $\hbar$ corrections to the resonances in the range $0 \leq \operatorname{Re} k \leq 90$ and $-1.0 \leq \operatorname{Im} k \leq 0$ from a band-limited signal of length $s_{\max} = 12$. In the first order amplitudes (5.13), again only the $l = 0$ term was included. Table 5.4 compares the results for the first order approximations to the resonances with the zeroth order approximations, the cycle expansion values, and the exact quantum values. Again, I determined the semiclassical error of the first order approximations to the resonances in comparison to that of the zeroth order order approximation obtained in Section 5.3.1. The results are presented in Figures 5.24 and 5.25. In Figure 5.25, only resonances with $\operatorname{Im} k \geq -0.82$ were included.

Although the general behaviour of the values is similar to the case $d = 6$ discussed above, the improvement of the accuracy achieved by the first order corrections is not as distinct as for $d = 6$. The reason partly lies in the error induced by the harmonic inversion method, which for $d = 2.5$ is already larger in the zeroth order approximation (see Section 5.3.1). The results may in principle be improved by extending the signal to longer orbits. On the other hand, in the part of the spectrum considered, the contributions of second and higher order $\hbar$ corrections may be larger than in the case $d = 6$.

5.4   The closed three-disk system

As discussed in Section 5.1, the three-disk system in the limiting case of touching disks is an especially challenging system for periodic orbit quantization. On the one hand, the number of periodic orbits up to a given scaled action is huge as compared to large disk separations. On the other hand, the system exhibits strong pruning. Common methods for periodic orbit quantization like the cycle expansion method therefore run into serious difficulties, and only the lowest eigenvalues of the system have been reproduced by periodic orbit quantization so far. In this section, I will demonstrate that the harmonic inversion method is not affected by the pruning of orbits and can successfully be used to extract the eigenvalues of the closed three-disk system from the periodic orbit sum. The resolution of the harmonic inversion results will be improved with the help of the cross-correlation technique to also resolve higher eigenvalues. Finally, an alternative method for periodic orbit quantization based on a Padé approximation to the periodic orbit sum will be tested for the closed three-disk system, and the results will be compared with those obtained by harmonic inversion.

5.4.1 Semiclassical eigenvalues of the closed three-disk system by harmonic inversion of a single signal

The periodic orbit quantization of the closed three-disk system by harmonic inversion of a single signal follows exactly the same procedure as for the open three-disk system discussed in Section 5.3.1. As for the open three-disk scatterer, a band-limited semiclassical signal is constructed according to Eq. (5.12), which is then analyzed by decimated signal diagonalization. The scaling parameter w is again equal to the wave number k. For the construction of the signal, I calculated the symmetry reduced periodic orbits of the closed three-disk system up to a maximum scaled action of $s_{max} = 5.0$. As explained in Section 5.1.3, the proliferation of periodic orbits with growing action in this system is so large that one cannot calculate all orbits up to a given action. Following the scheme described in Section 5.1.3, I calculated the orbits channel by channel, always checking for pruning. As cut-off criterion, only orbits with an expanding stability eigenvalue $|\lambda| < 10^8$ and with a maximum number of 12 consecutive symbols '0' in the symbolic code were included. For up to eight symbols '1' in the code, also orbits with a larger absolute value of the stability eigenvalue were added. Altogether, the signal was constructed from about 5×10^6 primitive periodic orbits and their repetitions.
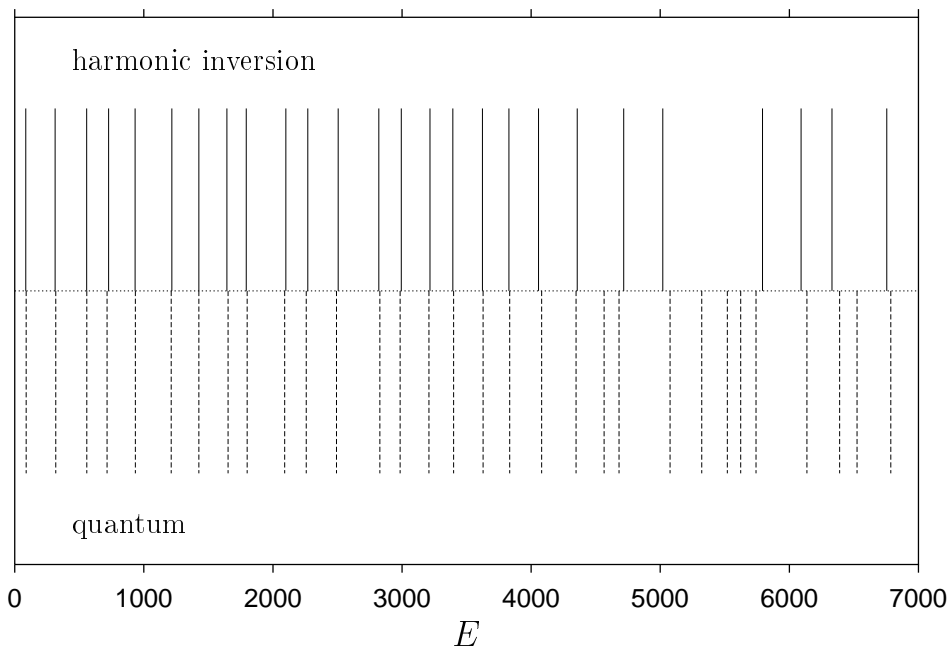
Figure 5.26: *Energy eigenvalues of the closed three-disk system (A_1 subspace). Dashed lines: exact quantum eigenvalues; solid lines: results $E = (\mathrm{Re}\,k)^2/2$ from harmonic inversion of a signal of length $s_{max} = 4.9$.*

I analyzed the signal up to length $s_{max} = 4.9$ to obtain the eigenvalues of the wave number k. Figure 5.26 shows the results obtained by harmonic inversion (solid lines), compared with the exact quantum results (dashed lines). The results are presented in terms of the energy $E = (\mathrm{Re}\,k)^2/2$. The exact quantum eigenvalues were taken from

Figure 5.27: *Amplitudes of the whole set of values $E = (\mathrm{Re}\,k)^2/2$ (all circles) obtained for the energy eigenvalues of the closed three-disk system by harmonic inversio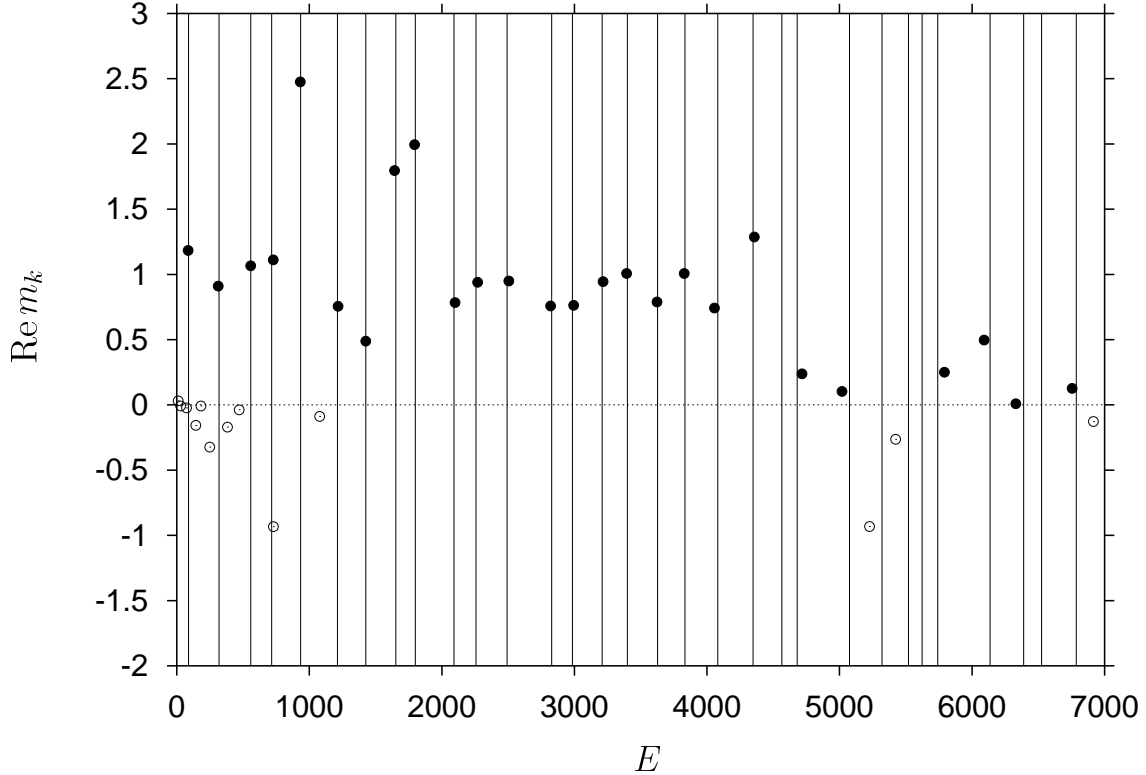n (including also unconverged values). The filled circles mark the values presented in Fig. 5.26. The solid vertical lines indicate the positions of the exact quantum eigenvalues.*

Wirzba [60] and Scherer [65]. Note that while I received exact data of the lowest eight quantum eigenvalues from Wirzba, I had to read off the larger eigenvalues from a diagram in Ref. [65], which may have led to small inaccuracies in the figures presented in this section and in the two following ones. Apart from the values shown in Fig. 5.26, the harmonic inversion of the signal also yielded a number of unconverged frequencies. Converged frequencies were identified by having an imaginary part close to zero (since the eigenvalues of the wave number must be real for bound systems) and an amplitude close to the theoretical value $m_k = 1$. The whole set of frequencies obtained together with the real part of their amplitudes is shown in Figure 5.27. The solid vertical lines mark the positions of the exact quantum eigenvalues. The semiclassical values included in Fig. 5.26 are marked by filled circles in Fig. 5.27.

The harmonic inversion results clearly reproduce the quantum eigenvalues up to $E \approx 4500$. The values are not as well converged as it was the case for the larger disk separations discussed in Section 5.3.1. This can be seen from the amplitudes, which partly show relatively large deviations from the theoretical value $m_k = 1$. However, up to $E \approx 4500$, the eigenvalues can be clearly identified. The signal length was not sufficient to resolve the eigenvalues in the region $E > 4500$, where the density of states with respect to the wave number k becomes too large.

The small deviations of the harmonic inversion results from the exact quantum values
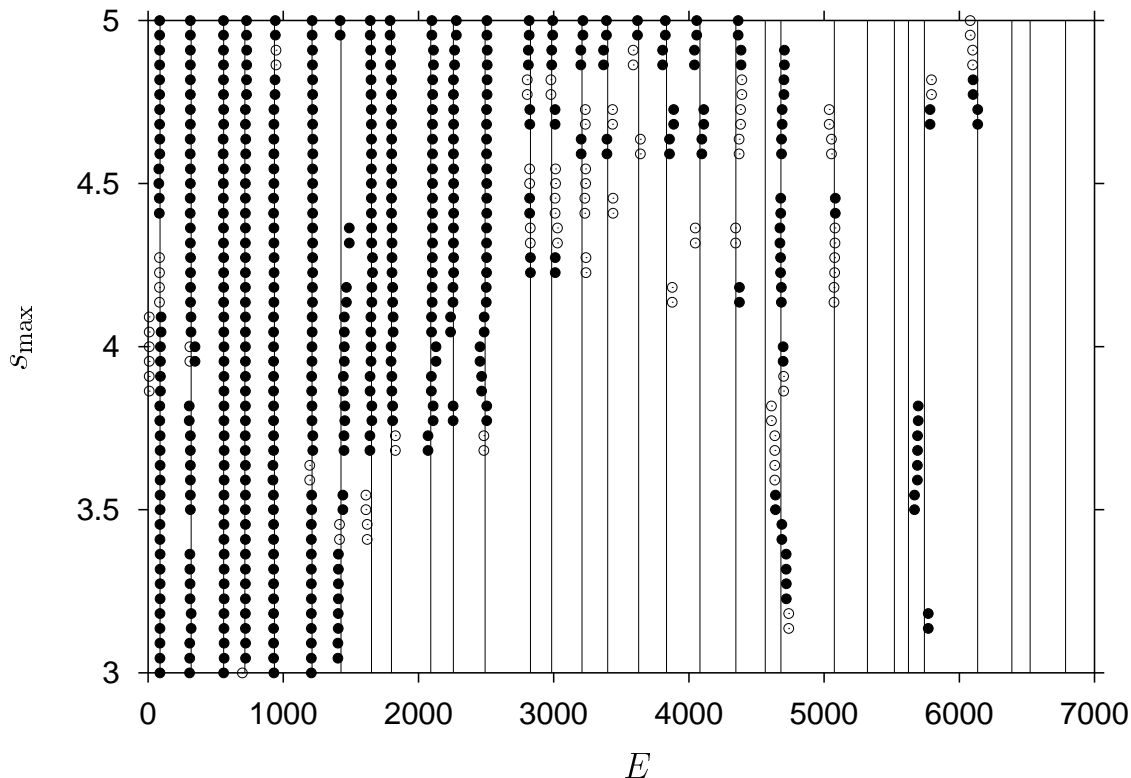
Figure 5.28: *Harmonic inversion results $E = (\mathrm{Re}\,k)^2/2$ for the energy eigenvalues of the closed three-disk system as a function of the signal length $s_{\max}$. Only results with $|\mathrm{Im}\,k| < 1.0$ and amplitudes $\mathrm{Re}\,m_k > 0.2$ are included. The filled circles mark values with $\mathrm{Re}\,m_k > 0.5$. (Solid vertical lines: positions of exact quantum energies.)*

may have different reasons. On the one hand, especially for very small eigenvalues, they will partly be due to the semiclassical error. On the other hand, as explained above, I did not include all orbits in the signal but left out a large number of relatively unstable orbits. Although each of these orbits only gives a negligibly small contribution to the periodic orbit sum, the number of excluded orbits may be so large that their contributions sum up in a way so as to have a visible effect on the density of states. Finally, even in the low part of the spectrum, deviations may arise from the fact that the signal length was very short. The influence of the missing orbits and the relatively short signal length are reflected in the relatively poor convergence of the amplitudes.

In order to test the stability of the results with respect to the signal parameters, and to obtain an estimate of random errors, I performed the same calculation with various sets of different signal parameters. Figure 5.28 shows the harmonic inversion results for the eigenvalues as function of the signal length $s_{\max}$. From all frequencies w_k obtained the values with $|\mathrm{Im}\,w_k| < 1.0$ and with amplitudes $\mathrm{Re}\,m_k > 0.2$ were singled out, respectively. The filled circles mark amplitudes with $\mathrm{Re}\,m_k > 0.5$. It can clearly be seen how the maximum eigenvalue up to which the spectrum can be resolved depends on the signal length. On the other hand, Fig. 5.28 shows that the results for the low eigenvalues are quite stable with respect to variation of the signal length.

Compared with the results obtained by Tanner et al. [64] with the extended cycle

expansion method (see Fig. 5.13 in Section 5.1.4), the analysis of a single signal by harmonic inversion has yielded about the same number of eigenvalues for the closed three-disk system. For the resolution of higher eigenvalues, the signal length was not sufficient. Extending the signal to significantly larger scaled actions is in practice not possible because of the extremely rapid increase of the number of orbits. But it has to be emphasized that, in contrast to the cycle expansion method, which runs into severe problems because of the pruning of orbits in this system, it is at least *in principle* possible to improve the harmonic inversion results by including more orbits. On the other hand, as discussed in Section 3.3.3, the harmonic inversion method offers the possibility to significantly reduce the signal length required for the resolution of eigenvalues by the construction and analysis of cross-correlated periodic orbit sums. In the following section, the cross-correlation technique will be applied to the closed three-disk system in order to improve the resolution of the harmonic inversion results.

5.4.2 Improvement of the resolution by harmonic inversion of cross-correlated periodic orbit sums

In the previous section, the lowest energy eigenvalues of the closed three-disk system were determined by harmonic inversion of a single signal. However, it was impossible to construct a sufficiently long signal for resolving the higher eigenvalues, where the density of states with respect to the wave number k is too large. In this section, I will apply the cross-correlation technique of Section 3.3.3 to the closed three-disk system in order to resolve also higher eigenvalues. As input, I take the same set of periodic orbits as in Section 5.4.1 together with the averages of different classical quantities over the orbits. From the weighted periodic orbits sums (3.51) a cross-correlated set of band-limited signals is constructed, which is analyzed by the decimated signal diagonalization method generalized to cross-correlation functions (cf. Section 3.1).

Figure 5.29 shows the results from the harmonic inversion of a 3×3 signal of length $s_{\max} = 4.8$ (solid lines), which was constructed using the operators $\mathbf{1}$ (unity), r^4 and L^4, where r and L denote the distance from the center of the system and the absolute value of the angular momentum, respectively. The eigenvalues are again presented in terms of the energy $E = (\mathrm{Re}\,k)^2/2$. For comparison, the dashed lines indicate the positions of the exact quantum eigenvalues. The converged eigenvalues of the wave number k have been singled out from the whole set of frequencies obtained by the condition that they should have an imaginary part close to zero and an amplitude close to the theoretical value $m_k = 1$. The amplitudes and the imaginary parts of all frequencies obtained are shown in Figure 5.30 by circles. In particular, the filled circles denote the frequencies included in Fig. 5.29. In Fig. 5.30a, the positions of the exact quantum eigenvalues are marked by the solid vertical lines.

With the cross-correlated signal, one can now clearly identify eigenvalues up to $E \approx 6500$. In addition, the convergence of the lowest eigenvalues is improved as compared to the results from the single signal obtained in Section 5.4.1, as can be seen from the amplitudes. It is not possible to determine to what extent the accuracy of the semiclassical eigenvalues has improved since the results can only be compared with the exact quantum eigenvalues and the size of the semiclassical error is unknown.

Again, I have performed the same calculation for various sets of parameters in the harmonic inversion scheme. Figure 5.31 shows the results from a 3×3 and from a 4×4
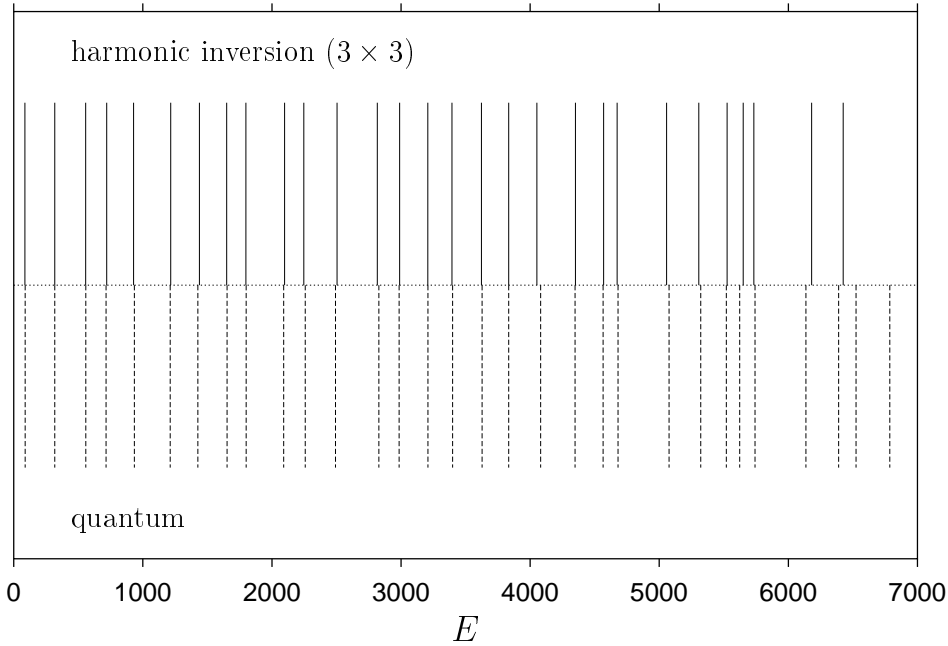
Figure 5.29: *Energy eigenvalues of the closed three-disk system (A_1 subspace). Dashed lines: exact quantum eigenvalues; solid lines: results $E = (\operatorname{Re} k)^2/2$ from harmonic inversion of a 3×3 cross-correlated signal with length $s_{\max} = 4.8$. The operators chosen for the construction of the signal are $\mathbf{1}$ (unity), r^4 and L^4, where r and L are the distance from the center of the system and the absolute value of the angular momentum, respectively.*

signal as functions of the signal length. The 3×3 signal was constructed from the operators $\mathbf{1}$ (unity), r^4 and L^4, and the 4×4 signal contains the operators $\mathbf{1}$, r^2, r^4 and L^4. In both diagrams, only the frequencies with an imaginary part $|\operatorname{Im} k| < 1.0$ and an amplitude $\operatorname{Re} m_k > 0.5$ were included. The filled circles mark values with $|\operatorname{Im} k| < 0.5$. The positions of the exact quantum eigenvalues are again marked by the solid vertical lines.

As with the single signal analyzed in Section 5.4.1, it can be observed that the results for the lowest eigenvalues are very stable with respect to the variation of the signal length as long as the signal is not too short. However, the very lowest frequencies show a tendency to split into two or more, which was a frequent observation if the signal length and the matrix dimensions were chosen too large. The results for the higher eigenvalues depend more sensitively on the signal length as the density of states approaches the limiting resolution that can be achieved with the signal. In this region, the 4×4 signal shows a better resolution than the 3×3 signal.

With the 3×3 signal and the two largest values of the signal length considered, the lowest eigenvalue was not obtained. The reason for this probably lies in inaccuracies at the end of the signal, as the signal length approaches the maximum value $s_{\max} = 5.0$: Every periodic orbit contributes to the band-limited signal mainly in a range of width $\pi/\Delta w$ around its scaled action s_{po}, where Δw is the size of the frequency window (cf. Eq. (3.40)). The main contributions to the signal at a point s therefore come from orbits whose scaled actions lie in a range of width $\pi/\Delta w$ around s. Since only orbits up to a scaled action of

94
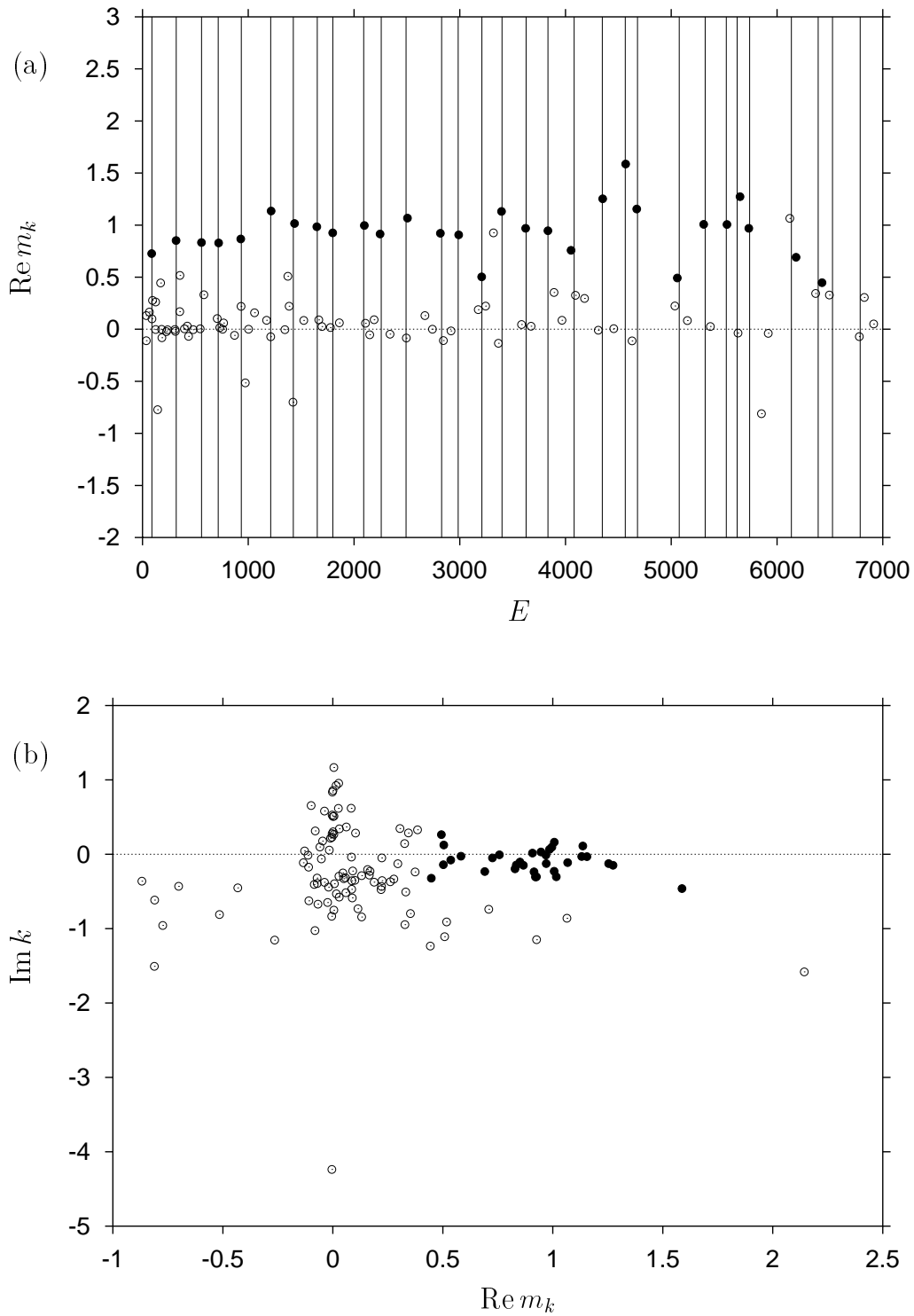
Figure 5.30: *Closed three-disk system: The whole set of frequencies (all circles) resulting from the analysis of the 3×3 signal (see Fig. 5.29). (a) Real part of the amplitudes versus energy $E = (\mathrm{Re}\,k)^2/2$. The solid vertical lines mark the positions of the exact quantum eigenvalues. (b) Imaginary part of the frequencies versus real part of the amplitudes. In both diagrams, the filled circles designate the values included in Fig. 5.29.*
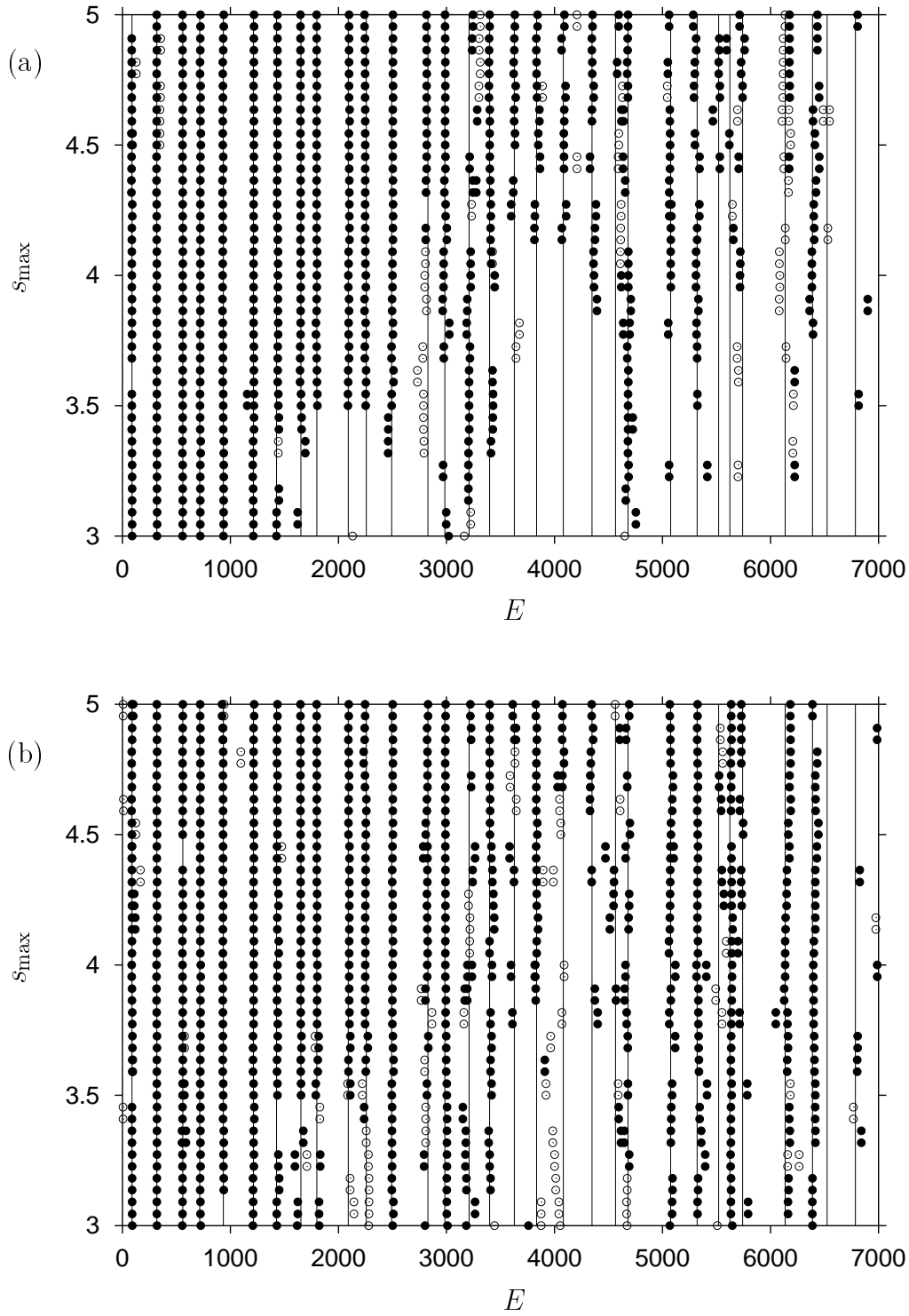
Figure 5.31: *Harmonic inversion results $E = (\operatorname{Re} k)^2/2$ for the energy eigenvalues of the closed three-disk system as a function of the signal length $s_{\max}$, calculated (a) from a 3×3 cross-correlated signal including the operators $\mathbf{1}$ (unity), r^4 and L^4 and (b) from a 4×4 signal including the operators $\mathbf{1}$, r^2, r^4 and L^4 (r: distance from the center of the system, L: absolute values of the angular momentum). Only results with $|\operatorname{Im} k| < 1.0$ and amplitudes $\operatorname{Re} m_k > 0.5$ are included. The filled circles mark values with $|\operatorname{Im} k| < 0.5$. The solid vertical lines indicate the positions of the exact quantum eigenvalues.*

$s_{\mathrm{max}} = 5.0$ were included, a large number of periodic orbit contributions are missing at the very end of the signal if the signal length is close to 5.0.

Some eigenvalues between $E = 3500$ and $E = 5000$ seem to be particularly hard to obtain from the set of orbits used. Possibly these eigenvalues are related to the orbits running very deep into the corners between the disks, which were not included in the signal. I conjecture that the missing orbits as well as the short signal length are again responsible for the deviations especially of the results for higher eigenvalues from the exact quantum values.

In conclusion, with the cross-correlation technique I have succeeded in calculating accurate semiclassical energy eigenvalues of the closed three-disk system up to the region $E \approx 6500$. This would not have been possible with a single signal because, due to the extremely rapid proliferation of periodic orbits with growing action, it is impossible to build a sufficiently long signal. The cross-correlation technique has turned out to be very helpful for improving the resolution in the harmonic inversion results. It is even possible to resolve eigenvalues in the region where the extended cycle expansion method of Ref. [64] only reproduces the mean density of states. To my knowledge, this is the first time that higher eigenvalues of this system have been correctly calculated by periodic orbit theory. In contrast to the method of Ref. [64], which depends on the existence of a complete symbolic code, the harmonic inversion method is not affected by the strong pruning of orbits in this system. As concerns the closed three-disk system, the only restriction for the practical application of the harmonic inversion method lies in the extremely large number of periodic orbits, which is a special feature of this specific system.

5.4.3 Semiclassical eigenvalues of the closed three-disk system by Padé approximation

With the set of periodic orbits of the closed three-disk system up to the action $s_{\mathrm{max}} = 5.0$ at hand, it is possible to also test the quality of an alternative method for periodic orbit quantization which was recently proposed by Main et al. [29]. This method is based on an analytic continuation of the periodic orbit sum by Padé approximation. Like harmonic inversion, the method does not depend on the existence of a symbolic code and is therefore also applicable to systems with pruning. In Ref. [29], the Padé approximation method was successfully applied to the *open* three-disk scatterer. In this section, I will apply the method to the *closed* three-disk system as an alternative to the harmonic inversion procedure. The results will be compared with those obtained by harmonic inversion in the previous sections.

I start by briefly recapitulating the main ideas of the method developed in Ref. [29]. The only requirement of the method is the existence of an integer ordering parameter n_{po} for the classical periodic orbits of the system. A possible ordering parameter is, e. g., the Maslov index (provided not all Maslov indices are equal to zero). The first step is to regroup the terms in the periodic orbit sum

$$g^{\mathrm{osc}}(E) = \sum_{\mathrm{po}} \mathcal{A}_{\mathrm{po}} e^{\frac{i}{\hbar} S_{\mathrm{po}}} \tag{5.14}$$

(cf. Eq. (2.15)) with the help of the ordering parameter. The periodic orbit sum is

rearranged by formally rewriting it as a power series in an auxiliary variable z

$$g(z; E) = \sum_n z^n \left(\sum_{n_{\mathrm{po}}=n} \mathcal{A}_{\mathrm{po}} e^{\frac{i}{\hbar} S_{\mathrm{po}}} \right) =: \sum_n a_n z^n , \qquad (5.15)$$

where the coefficients a_n of the power series depend on the energy E. By setting $z = 1$, the semiclassical response function is regained.

The idea is now to approximate the power series (5.15) by its Padé approximant, which can be calculated from the coefficients a_n. The $[m, n]$ Padé approximant to a function $f(z)$ is defined as the ratio of two polynomials, $P(z)/Q(z)$, where $P(z)$ is of degree n and $Q(z)$ is of degree m in z. If $f(z)$ is given in power series form, the coefficients of the polynomials can be determined from the relation

$$f(z)Q(z) - P(z) = Az^{m+n+1} + Bz^{m+n+2} + \ldots , \qquad Q(0) = 1 \qquad (5.16)$$

(see, e. g., Ref. [67]). For the calculation of the $[m, n]$ approximant, the coefficients of the power series up to order $m + n$ have to be known. For a power series with finite radius of convergence in z, the Padé approximant may provide an approximate analytic continuation into the region where the original power series diverges. The approximation can be expected to converge fast with growing orders m and n.

By replacing the power series (5.15) with its Padé approximant, one obtains an analytic continuation of the semiclassical response function into the region where the eigenvalues or resonances are located. The semiclassical eigenvalues or resonances, which are given by the poles of the response function, are then determined by numerically searching for the zeros of the inverse of the Padé approximant to the periodic orbit sum as a function of the energy E (or, in the case of billiard systems, of the wave number k). For the evaluation of the periodic orbit sum, the Padé approximant to (5.15) is only needed for the value $z = 1$. Following Ref. [29], the approximant is most efficiently calculated by means of the Wynn ϵ-algorithm, using as input the series of partial sums

$$A_n = \sum_{n_{\mathrm{po}} \leq n} \mathcal{A}_{\mathrm{po}} e^{\frac{i}{\hbar} S_{\mathrm{po}}} . \qquad (5.17)$$

For the three-disk system, one suitable ordering parameter is the cycle length (or the Maslov index, which is here equal to twice the cycle length). A second possible parameter, which is a quite natural choice in the case of the closed three-disk system, is the number of symbols '1' in the symbolic code, since it is this quantity which here mainly determines the action of the orbits (cf. Section 5.1.3). I performed calculations with both possible choices of the ordering parameter. As input, I used the same set of periodic orbits as for the harmonic inversion procedure (cf. Sections 5.4.1 and 5.4.2). However, it must be pointed out that this set of orbits is very incomplete with respect to large values of either ordering parameter, since it contains only orbits up to a maximum scaled action $s_{\mathrm{max}} = 5.0$. [The cut-off criteria were chosen according to the needs of the the harmonic inversion procedure, where all orbits up to a maximum action have to be included.]

Figure 5.32 shows the number of primitive orbits in the set as a function of the two ordering parameters. For values of the cycle length up to about 25 and for up to about 10 symbols '1' in the code, an exponential increase of the number of orbits can be observed, which suggests that up to these limits only a small part of the orbits is missing. In
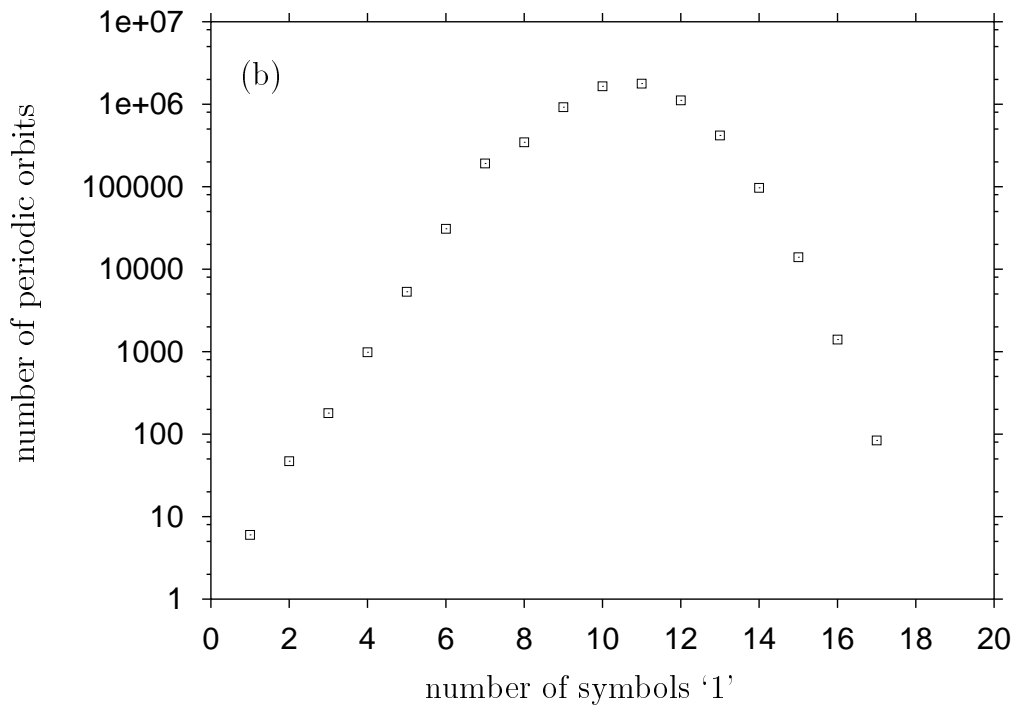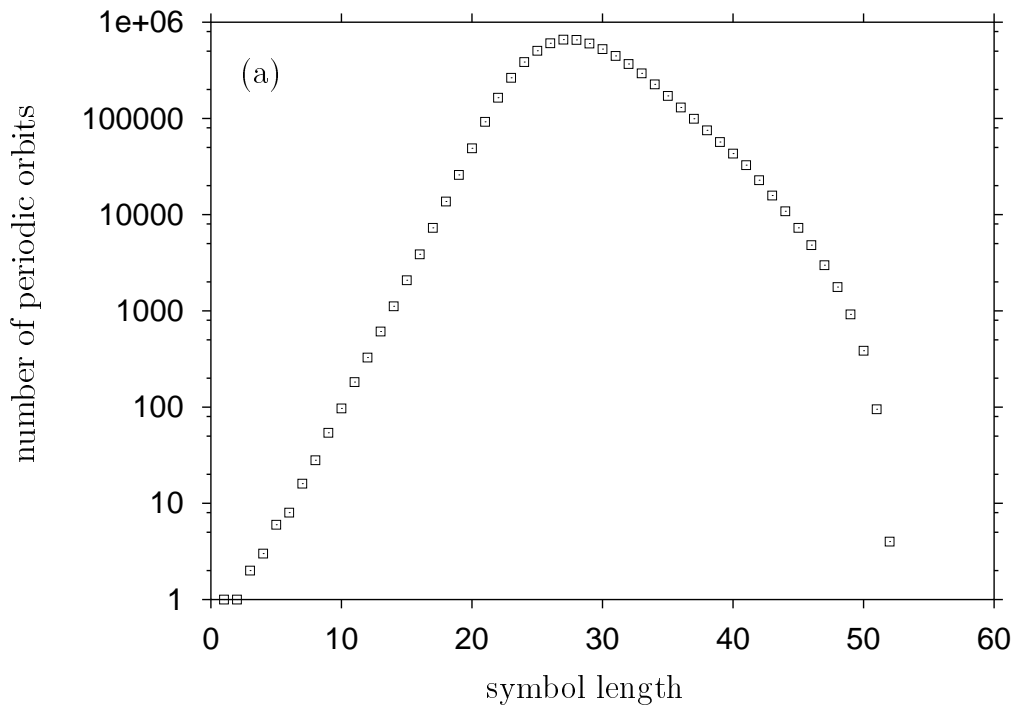
Figure 5.32: *Number of orbits in the set of periodic orbit data used for the closed three-disk system (a) as a function of the symbol length, (b) as a function of the number of symbols '1' in the symbolic code.*

addition to the cut-off at the maximum action, the set of orbits was confined by choosing a maximum absolute value for the expanding stability eigenvalue and a maximum number for consecutive symbols '0' in the code (cf. Section 5.4.1). This will not have much influence as concerns the symbol length as ordering parameter, since the missing orbits will have quite long symbol lengths. On the other hand, with the number of '1's in the code as ordering parameter, the number of missing orbits will be relatively large. [Note the slight discontinuity of the curve in Fig. 5.32b between 7 and 8 symbols '1'. This probably arises from the fact that in the search algorithm the cut-off criterion for the stability eigenvalue was introduced only for orbits with at least 8 symbols '1' in the code.] As discussed in Section 5.4.1, the contribution of each single missing orbit to the periodic orbit sum is very small, but the sum of all missing orbits may have a visible influence.

I calculated the eigenvalues of the wave number k in the closed three-disk system using the orbits up to different maximum values of the respective ordering parameter. From the sequence of partial sums (5.17) determined up to the maximum value $n_{\max}$ of the ordering parameter the $[m, m]$ ($n_{\max} = 2m$) or $[m + 1, m]$ ($n_{\max} = 2m + 1$) approximant was calculated for even or odd $n_{\max}$, respectively. Then the zeros of the inverse of the Padé approximant with respect to the wave number k were determined, which give the approximations to the semiclassical eigenvalues. For the iterative numerical algorithm used for finding the zeros, the Padé approximant has to be calculated repeatedly for different values of k. Figure 5.33 shows the results for the eigenvalues using (a) the symbol length and (b) the number of '1's in the code as ordering parameter. The eigenvalues are given in terms of the energy $E = (\operatorname{Re} k)^2/2$. The solid vertical lines mark the positions of the exact quantum eigenvalues. [As already mentioned in Section 5.4.1, these values may be slightly inaccurate as they were read off from a diagram in Ref. [65].] From the whole set of values obtained for the wave number k, the converged eigenvalues were singled out by the condition that their imaginary part should be close to zero (since the eigenvalues must be real). The size of the imaginary part of the values obtained can be taken as a measure for the accuracy of the results. In Fig. 5.33 only results with $|\operatorname{Im} k| < 0.5$ were included. The filled circles mark results with $|\operatorname{Im} k| < 0.2$.

It can clearly be observed that the number of eigenvalues obtained and the resolution increase with the maximum value of the ordering parameter, i.e., with the number of orbits included. With the symbol length as ordering parameter, the lowest eigenvalue can already be obtained from the orbits up to symbol length 5. Using the orbits up to symbol length 25, the eigenvalues up to $E \approx 4500$ are obtained. This is approximately the same number of eigenvalues that could be resolved with this set of orbits by harmonic inversion of a single signal in Section 5.4.1.

However, the eigenvalues cannot be identified as clearly as was the case with the harmonic inversion method, and the results are not as stable with respect to the variation of the parameters (in this case the maximum of the ordering parameter, i.e., the order of the Padé approximation). There is a number of additional zeros which do not correspond to physical eigenvalues and which seem to appear randomly for different maximum values of the ordering parameter. On the other hand, it has to be noted that here the only criterion for converged eigenvalues was the imaginary part of the values obtained, in contrast to the harmonic inversion procedure, where the eigenvalues were also singled out by the values of their amplitudes. It is conceivable that further criteria could be introduced in order to distinguish between true eigenvalues and spurious values. In the set of results presented in Fig. 5.33, most spurious zeros can be identified by comparing the
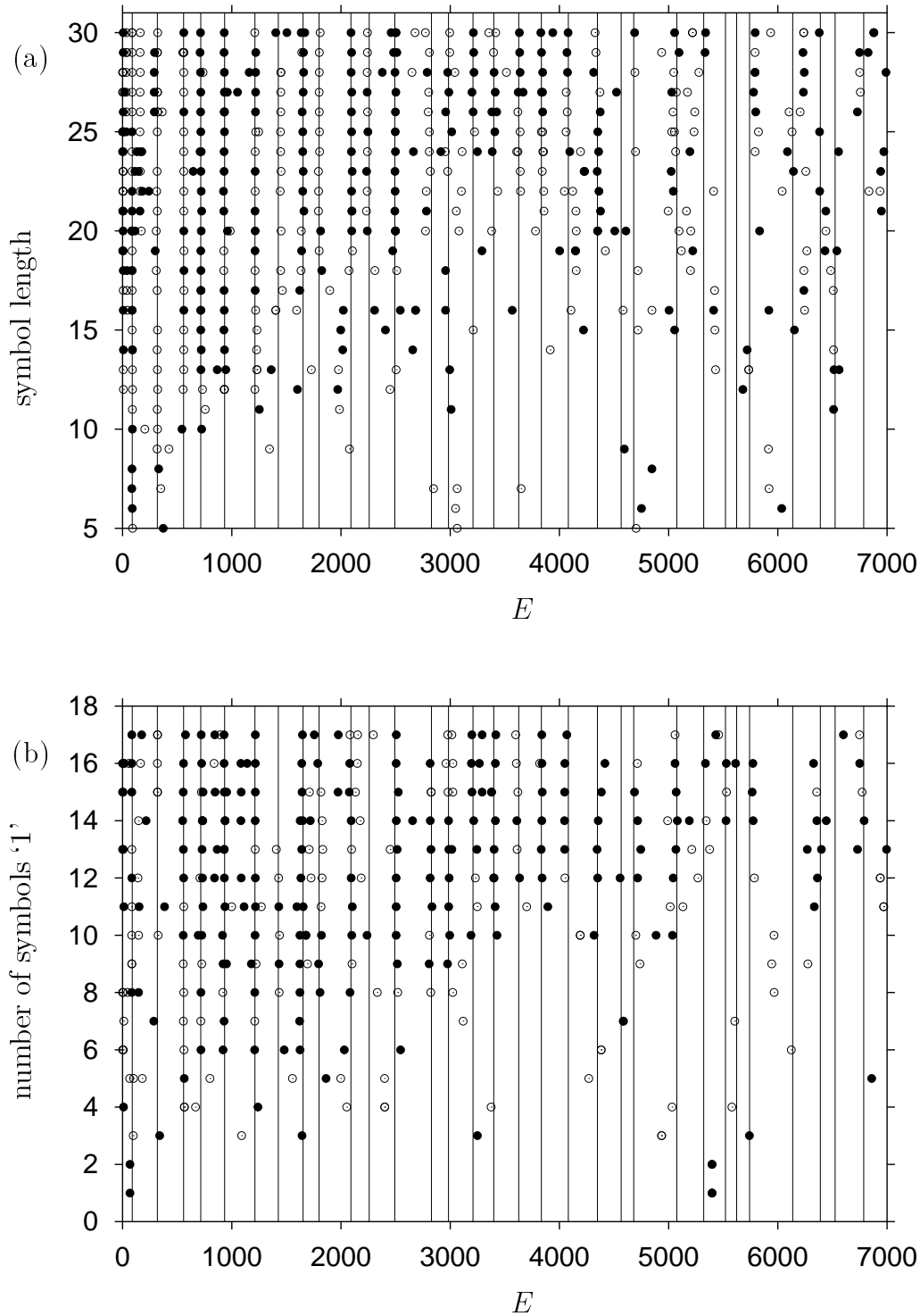
Figure 5.33: *Results for the semiclassical eigenvalues of the closed three-disk system in terms of the energy $E = (\mathrm{Re}\, k)^2/2$, obtained from the Padé approximant to the periodic orbit sum using (a) the symbol length and (b) the number of symbols '1' in the code as ordering parameter. The eigenvalues are given as a function of the maximum value of the ordering parameter up to which the orbits were included (which also determines the order of the Padé approximation, see text). In both diagrams, only results with $|\mathrm{Im}\, k| < 0.5$ were included. Results with $|\mathrm{Im}\, k| < 0.2$ are marked by filled circles. The solid vertical lines designate the positions of the exact quantum eigenvalues.*

101

results of several calculations with different maximum values of the ordering parameter.

A number of spurious zeros is located in the region of very small E. This suggests that the Padé approximation method has convergence problems for small values of the wave number k. These additional zeros disappear for very low values of the ordering parameter, i. e., low order of the Padé approximation.

With the number of symbols '1' as ordering parameter, the Padé approximation method does not yield as good results as with the symbol length. In particular, there are more spurious zeros which do not correspond to physical eigenvalues, and the results are less stable with respect to the maximum value of the ordering parameter. Some eigenvalues cannot be found at all. A possible reason might be that, as discussed above, the set of orbits is much more incomplete with respect to the number of '1's than with respect to the symbol length, since the orbits running very deep into the corner between the disks are missing. Furthermore, with the number of '1's as ordering parameter, I also included values of n_{max} for which already a large number of orbits is missing due to the the cut-off criterion for the action (cf. Fig. 5.32). However, on the whole, the spectrum can be resolved up to the same region of the energy E as with the symbol length as ordering parameter. Note that with $n_{max} = 16$, the three relatively close eigenvalues between $E = 5500$ and $E = 5800$ are resolved, which could not be achieved with the extended cycle expansion method of Ref. [64].

With both possible choices of the ordering parameter, some eigenvalues seem to be particularly hard to obtain from the set of orbits used, as was also the case with the harmonic inversion method. Again one has to conjecture that these eigenvalues are particularly connected to the orbits missing in the set, or they are in a sense more "quantum" than the others and less accessible to semiclassical methods.

In conclusion, the Padé approximation method has been shown as capable of calculating the lowest semiclassical eigenvalues of the closed three-disk system. With the given set of periodic orbits, about the same number of eigenvalues could be resolved as with the harmonic inversion method using a single semiclassical signal. However, the Padé approximation method yields more spurious values, which must be identified by comparing the results for different maximum values of the ordering parameter. This problem may be overcome by introducing an additional criterion for singling out the converged eigenvalues. E. g., it would be possible to additionally calculate the amplitudes (multiplicities), which are automatically obtained in the harmonic inversion scheme, by evaluation of the derivative of the Padé approximant.

Besides the determination of the amplitudes, which, e. g., also allows the calculation of diagonal matrix elements, the essential advantage of the harmonic inversion method lies in the possibility of improving the resolution by the cross-correlation technique, as was demonstrated for the closed three-disk system in Section 5.4.2. Up to now, this technique has no equivalent in the Padé method. Harmonic inversion is therefore clearly superior to the Padé approximation method as concerns the question of how many eigenvalues can be obtained from the same set of periodic orbits.

Chapter 6

Conclusion

Harmonic inversion has been introduced as a powerful tool for the calculation of quantum eigenvalues from periodic orbit sums as well as for the high resolution analysis of quantum spectra in terms of classical periodic orbits. The harmonic inversion technique circumvents the convergence problems of the periodic orbit sum and the uncertainty principle of the usual Fourier analysis, thus yielding results of high resolution and high precision. For the example of the circle billiard and the three-disk scatterer I have demonstrated that the method works equally well for integrable and chaotic systems and does not depend on whether the system is bound or open. The application to the closed three-disk system has demonstrated that, unlike other semiclassical methods, the harmonic inversion scheme is also capable of handling the case of strong pruning. Harmonic inversion has thus been shown to be a universal method, which, in contrast to other high resolution methods, does not depend on special properties of the system such as ergodicity or the existence of a complete symbolic code, and therefore can be applied to a wide range of physical systems. Due to the close formal analogy between the Gutzwiller trace formula for chaotic systems and the Berry-Tabor formula for integrable systems, the same general procedures can be applied for both types of underlying classical dynamics.

With the harmonic inversion method, the contributions of the classical periodic orbits to the trace formula can be calculated from the quantum eigenvalues or resonances with high precision and high resolution, thus verifying the validity of the Gutzwiller and the Berry-Tabor formula, respectively. In addition, the method has been extended in this work to the calculation of higher order $\hbar$ corrections to the trace formulae. By analyzing the difference spectrum between exact and semiclassical eigenvalues, I could determine first order $\hbar$ corrections to the periodic orbit sums of the circle billiard and the open three-disk scatterer. For regular systems, a general theory for the $\hbar$ corrections to the Berry-Tabor formula does not yet exist. By harmonic inversion of the difference spectrum between exact quantum and EBK eigenvalues, I have found strong numerical evidence for the correctness of an expression I propose for the first order $\hbar$ corrections to the Berry-Tabor formula for the circle billiard. The same expression can be derived analytically by using Vattay's and Rosenqvist's method for chaotic systems and introducing some reasonable ad-hoc assumption for the circle billiard. As this is clearly not a strict derivation, it is a rewarding task for the future to develop a general theory for the higher order $\hbar$ corrections to the trace formula for regular systems. In the case of the three-disk scatterer, I have found an overall agreement between the numerical results and the theory of Vattay and Rosenqvist. However, for one particular orbit a distinct discrepancy persisted, which

implies that even in the case of chaotic systems the theory of higher order $\hbar$ corrections still contains unanswered questions.

In addition to calculating semiclassical eigenvalues or resonances from the usual periodic orbit sum, I have demonstrated how further information can be extracted from the parameters of the classical orbits by applying the harmonic inversion technique to different extensions of the trace formula. Using a generalized trace formula including an arbitrary operator, I have shown that the method also allows the calculation of semiclassical diagonal matrix elements from the parameters of the periodic orbits. Furthermore, the harmonic inversion method has been extended in this work to the calculation of higher order $\hbar$ corrections to the semiclassical eigenvalues, which are determined by harmonic inversion of correction terms to the periodic orbit sums. For the case of the circle billiard and the open three-disk scatterer, I found that by including the first order correction the accuracy of the semiclassical eigenvalues compared to the exact quantum eigenvalues could be improved by one or more orders of magnitude.

Although by harmonic inversion the quantum eigenvalues can be calculated from a semiclassical signal of finite length, i.e., from a finite set of periodic orbits, the number of orbits which have to be included may still be large. I have demonstrated that by a generalization of the harmonic inversion method to cross-correlation functions the required signal length may be significantly reduced, even below the Heisenberg time. Because of the rapid proliferation of periodic orbits with growing period, this means that the number of orbits which have to be included may be reduced by about one to several orders of magnitude. This was of particular advantage for the periodic orbit quantization of the closed three-disk system, which exhibits an extremely rapid proliferation of orbits with increasing action. With the help of the cross-correlation technique, it was possible to significantly improve the resolution as compared to a single signal constructed from the same set of orbits. From the cross-correlated signal, energy eigenvalues of the closed three-disk system up to $E \approx 6500$ could be calculated, which to the best of my knowledge has not been achieved with any other semiclassical method yet. The results demonstrate that the harmonic inversion method, unlike other methods, is in fact not affected by the strong pruning of orbits in this system. The only restriction for the practical application lies in the extremely large number of periodic orbits in this specific system.

As an alternative method for periodic orbit quantization, I have applied the Padé approximation method to the closed three-disk system. Using the same set of orbits as for the harmonic inversion procedure, I could resolve about the same number of eigenvalues as with the harmonic inversion of a single semiclassical signal. However, a disadvantage of the Padé method is that the amplitudes are not obtained in a straightforward manner, which would be necessary, e.g., for calculating diagonal matrix elements from the extended periodic orbits sums. Most importantly, the Padé method, at least in its present version, does not provide any equivalent to the cross-correlation technique. Concerning the question of how many eigenvalues can be obtained from a given set of orbits, harmonic inversion is therefore clearly superior to the Padé approximation method.

Appendix A

Calculation of the first order $\hbar$ correction terms to the semiclassical trace formula

As discussed in Section 2.3, the trace formulae for the semiclassical density of states can be extended to include also higher order $\hbar$ corrections. In this appendix, I briefly outline the derivation of the first order $\hbar$ amplitudes $\mathcal{A}_{\mathrm{po}}^{(1)}$ in the extended periodic orbit sum (2.29) for chaotic systems, following the approach of Vattay and Rosenqvist [20, 21, 42], and its specialization to two-dimensional billiards given in Ref. [42]. In Section A.2, I describe how the method can be modified to obtain a first order $\hbar$ correction term for the circle billiard.

A.1 Higher order $\hbar$ corrections for chaotic systems

Vattay and Rosenqvist give a quantum generalization of Gutzwiller's trace formula based on the path integral representation of the quantum propagator. The basic idea of their method is to express the global eigenvalue spectrum in terms of local eigenvalues computed in the neighbourhood of the primitive periodic orbits. The energy domain Green's function $G(q, q', E)$ is related to the spectral determinant $\Delta(E) = \Pi_n(E - E_n)$, with E_n the energy eigenvalues or resonances, by

$$\operatorname{Tr} G(E) = \int dq\, G(q, q, E) = \frac{d}{dE} \ln \Delta(E) \ . \tag{A.1}$$

The trace of the Green's function can be expressed in terms of contributions from primitive periodic orbits

$$\operatorname{Tr} G(E) = \sum_p \operatorname{Tr} G_p(E) \ , \tag{A.2}$$

with the local traces connected to the local spectral determinants by

$$\operatorname{Tr} G_p(E) = \frac{d}{dE} \ln \Delta_p(E) \ . \tag{A.3}$$

The trace of the Green's function can therefore be calculated by solving the local Schrödinger equation around each primitive periodic orbit, which yields the local eigenspectra.

To obtain the local eigenspectra, the ansatz

$$\psi = \Phi e^{iS/\hbar} \tag{A.4}$$

is inserted into the Schrödinger equation, yielding the following differential equations for Φ and S:

$$\partial_t S + \frac{1}{2}(\nabla S)^2 + U = 0 \tag{A.5}$$

$$\partial_t \Phi + \nabla\Phi\nabla S + \frac{1}{2}\Phi\Delta S - \frac{i\hbar}{2}\Delta\Phi = 0 \;, \tag{A.6}$$

where U is the potential entering the Schrödinger equation. The spectral determinant can be calculated from the local eigenvalues of the amplitudes Φ. For arbitrary energy E, the amplitudes Φ_p^l of the local eigenfunctions satisfy the equation

$$\Phi_p^l(t + T_p) = R_p^l(E)\Phi_p^l(t) \;, \tag{A.7}$$

where T_p is the period of the classical orbit. Using Eq. (A.3), the trace formula can be expressed in terms of the eigenvalues $R_p^l(E)$:

$$\mathrm{Tr}\, G(E) = \frac{1}{i\hbar}\sum_p \sum_l \left(T_p(E) - i\hbar\frac{d\ln R_p^l(E)}{dE}\right)\sum_{r=1}^{\infty}(R_p^l(E))^r e^{\frac{i}{\hbar}rS_p(E)} \;, \tag{A.8}$$

where the first sum runs over all primitive periodic orbits. This is the quantum generalization of Gutzwiller's trace formula and holds exactly.

The amplitudes and their eigenvalues are now expanded in powers of $\hbar$:

$$\Phi^l = \sum_{m=0}^{\infty}\left(\frac{i\hbar}{2}\right)^m \Phi^{l(m)} \tag{A.9}$$

$$R^l(E) = \exp\left\{\sum_{m=0}^{\infty}\left(\frac{i\hbar}{2}\right)^m C_l^{(m)}\right\} \tag{A.10}$$

$$\approx \exp(C_l^{(0)})\left(1 + \frac{i\hbar}{2}C_l^{(1)} + \dots\right) \;. \tag{A.11}$$

The terms $C_l^{(0)}$ yield the Gutzwiller trace formula as zeroth order approximation, while the terms with $m > 0$ give $\hbar$ corrections.

To solve Eqs. (A.5) and (A.6) in different orders of $\hbar$, the Schrödinger equation and the functions $\Phi^{l(m)}$ and S are expanded in a multidimensional Taylor expansion around the periodic orbit,

$$S(\mathbf{q}, t) = \sum_{\mathbf{n}}\frac{1}{\mathbf{n}!}s_{\mathbf{n}}(t)(\mathbf{q} - \mathbf{q}_p(t))^{\mathbf{n}} \tag{A.12}$$

$$\Phi^{l(m)}(\mathbf{q}, t) = \sum_{\mathbf{n}}\frac{1}{\mathbf{n}!}\phi_{\mathbf{n}}^{l(m)}(t)(\mathbf{q} - \mathbf{q}_p(t))^{\mathbf{n}} \tag{A.13}$$

(with $\mathbf{n} \equiv (n_1, n_2, \dots)$, $\mathbf{n}! \equiv \prod n_i!$, $\mathbf{q^n} \equiv \prod q_i^{n_i}$), resulting in a set of differential equations for the different orders of the Taylor expansions and different orders in $\hbar$. In one dimension, these equations read explicitly:

$$\dot{s}_n - s_{n+1}\dot{q} + \frac{1}{2}\sum_{k=0}^{n}\frac{n!}{(n-k)!k!}s_{n-k+1}s_{k+1} + u_n = 0 \;, \tag{A.14}$$

106

where u_n are the coefficients of the Taylor expanded potential, and

$$\dot{\phi}_n^{(m+1)} - \phi_{n+1}^{(m+1)}\dot{q} + \sum_{k=0}^{n} \frac{n!}{(n-k)!k!} \left(\phi_{n-k+1}^{(m+1)}s_{k+1} + \frac{1}{2}\phi_{n-k}^{(m+1)}s_{k+2} \right) - \phi_{n+2}^{(m)} = 0 \ . \qquad (A.15)$$

This set of differential equations can be solved iteratively. The l-th eigenfunction is characterized by the condition $\phi_n^{(m)} \equiv 0$ for $n < l$. The different orders of $\hbar$ are connected by the last term in (A.15). Starting from zeroth order $\hbar$ and the lowest nonvanishing order of the Taylor expansion, the functions can be determined order by order. For higher dimensional systems, the coefficient matrices obey similar equations, and the structure of the set of equations remains the same.

For the first order $\hbar$ correction to the Gutzwiller trace formula, one has to calculate the quantities $C_l^{(1)}$. To obtain these quantities, the set of equations (A.15) has to be solved up to the lowest nonvanishing first order $\hbar$ coefficient function $\phi_l^{l(1)}$, respectively. As $\phi_n^{l(m)} \equiv 0$ for $n < l$, this involves solving the equations for s_2, s_3 and s_4, and for the zeroth order $\hbar$ coefficient functions $\phi_l^{l(0)}$, $\phi_{l+1}^{l(0)}$ and $\phi_{l+2}^{l(0)}$. If the initial conditions are set to be $\Phi_l^{l(0)}(0) = 1$ and $\Phi_l^{l(m)}(0) = 0$ for $m > 0$, the correction term $C_l^{(1)}$ is then given by the relation

$$C_l^{(1)} = \frac{\phi_l^{l(1)}(T_p)}{\exp(C_l^{(0)})} \ , \qquad (A.16)$$

which follows from the $\hbar$ expansion of the eigenvalue equation (A.7).

An explicit recipe for the calculation of the first order $\hbar$ correction for two-dimensional chaotic billiards is given in Ref. [42]. For billiards, the potential U in the Schrödinger equation equals zero between two bounces at the hard wall. The functions S and Φ now have to be Taylor expanded in two dimensions,

$$\begin{aligned} S(x,y,t) &= S_0 + S_x\Delta x + S_y\Delta y \\ &+ \frac{1}{2}(S_{x^2}(\Delta x)^2 + 2S_{xy}\Delta x\Delta y + S_{y^2}(\Delta y)^2) \\ &+ \ \ldots \ , \end{aligned} \qquad (A.17)$$

and similarly for Φ. If the coordinate system is chosen in such a way that x is along the periodic orbit and y is perpendicular to the orbit, derivatives with respect to x can be expressed in terms of the derivatives with respect to y using the stationarity conditions

$$S_{x^{n+1}y^m} = \frac{\dot{S}_{x^n y^m}}{S_x} \ , \qquad \phi_{x^{n+1}y^m} = \frac{\dot{\phi}_{x^n y^m}}{S_x} \ . \qquad (A.18)$$

The quantity S_x is equal to the classical momentum of the particle.

For the free motion between the collisions with the wall, the set of differential equations corresponding to (A.14) and (A.15) then reduces to a set of equations involving only derivatives with respect to y. These equations can be solved analytically, with the general solution still containing free parameters. For S_x set equal to 1, the first coefficient functions of the Taylor expanded phase are given by

$$S_{yy}(t) = \frac{1}{t + t_0} \qquad (A.19)$$

$$S_{yyy}(t) = \frac{A}{(t+t_0)^3} \tag{A.20}$$

$$S_{yyyy}(t) = -\frac{3}{(t+t_0)^3} + \frac{B}{(t+t_0)^4} + \frac{3A^2}{(t+t_0)^5} \ , \tag{A.21}$$

where t_0, A and B are free parameters. For given l, the first nonvanishing coefficients of the amplitude read

$$\phi_{y^l}^{(0)}(t) = E\left(\frac{t_0}{t+t_0}\right)^{l+1/2} \tag{A.22}$$

$$\phi_{y^{l+1}}^{(0)}(t) = \frac{E}{(t+t_0)^{l+3/2}}\left[C + (l+1)^2\frac{A}{2}\frac{t_0^{l+1/2}}{(t+t_0)}\right] \tag{A.23}$$

$$\phi_{y^{l+2}}^{(0)}(t) = \frac{E}{(t+t_0)^{l+5/2}}\left\{D + \frac{1}{t+t_0}\left[(l+2)^2\frac{AC}{2} + (l+2)(l+1)(\frac{l}{3}+\frac{1}{2})\frac{B}{2}t_0^{l+1/2}\right]\right.$$
$$\left. + \frac{A^2 t_0^{l+1/2}}{2(t+t_0)^2}\left[\frac{1}{4}(l+2)^2(l+1)^2 + \frac{3}{2}(l+2)(l+1)(\frac{l}{3}+\frac{1}{2})\right]\right\} \ . \tag{A.24}$$

Again, D and E are free parameters.

At the collisions with the hard wall, the phase and amplitude have to obey the bouncing conditions

$$S(x,y,t_{-0}) = S(x,y,t_{+0}) + i\pi \tag{A.25}$$

$$\Phi(x,y,t_{-0}) = \Phi(x,y,t_{+0}) \ , \tag{A.26}$$

from which the bouncing conditions for the coefficients of the Taylor expanded functions S and Φ can be derived. While the general solutions between the bounces are valid for all billiards, the bouncing conditions in their Taylor expanded form depend explicitly on the shape of the hard wall.

An additional condition which the solutions S and Φ have to obey is periodicity along the orbit. With every traversal the phase gains the same constant contributions at the collisions with the wall. The derivatives of the phase are periodic. The amplitude collects the same factor with each traversal, which means that all Taylor coefficients of the amplitude are periodic apart from a constant factor. These conditions together with the bouncing conditions determine the values of the free constants in the general solutions between the collisions.

The solutions can in general be found numerically, by choosing suitable initial conditions and following the evolution of the phase and amplitude functions along the orbit. After several iterations around the orbit, the parameters should converge against their periodic solution. The correction terms $C_l^{(1)}$ are then given by the integral

$$C_l^{(1)} = \int_0^{T_p} \frac{\phi_{y^{l+2}}^{l(0)} + \phi_{y^l x^2}^{l(0)}}{\phi_{y^l}^{l(0)}}dt \ , \tag{A.27}$$

which can be computed explicitly from the solutions found above.

A.2 First order $\hbar$ corrections for the circle billiard

As already explained, the method outlined in the previous section is designed for chaotic systems, as its derivation is based on the assumption that the periodic orbits are isolated. Nevertheless, one obtains reasonable results when applying the method to the circle billiard, taking one periodic orbit from each rational torus and introducing some additional assumptions.

Because of the symmetry of the orbits, it can be assumed that every side of the orbit contributes in the same manner to the $\hbar$ correction term for the whole orbit. This means, if one resets $t = 0$ at the start of each side, the free parameters in the general solutions (A.19) to (A.24) must be the same for each side, apart from the parameter E, which collects the same factor during every collision with the wall. With these assumptions, the differential equations can be solved analytically.

However, it turns out that the bouncing conditions resulting from (A.25) and (A.26) are not sufficient to determine all free parameters, as some of the conditions are automatically fulfilled. One needs additional conditions for the parameters. These can be obtained from the rotational symmetry of the system: Because of this symmetry, it can be assumed that the amplitude of the wave function does not depend on the polar angle φ. The same holds for all derivatives of the amplitude with respect to the radius r. For the zeroth order $\hbar$ amplitudes, expressed in polar coordinates (r, φ), this provides the additional conditions needed:

$$\frac{\partial}{\partial\varphi}\frac{\partial^n \Phi^{l(0)}}{\partial r^n} = 0 \ . \tag{A.28}$$

If one further assumes that the phase separates in polar coordinates,

$$S(r, \varphi) = S_r(r) + S_\varphi(\varphi) \ , \tag{A.29}$$

which implies that all mixed derivatives vanish, it turns out that the bouncing conditions are not needed at all. All parameters can be determined from the symmetry of the system, and the bouncing conditions are automatically fulfilled. I considered only the case $l = 0$, for which I used Eq. (A.29) together with the conditions

$$\frac{\partial}{\partial\varphi}\Phi^{0(0)} = 0 \ , \qquad \frac{\partial}{\partial\varphi}\frac{\partial\Phi^{0(0)}}{\partial r} = 0 \ . \tag{A.30}$$

The final results for the constant parameters in Eqs. (A.19) to (A.24) are

$$t_0 \;=\; -\sin\gamma \tag{A.31}$$
$$A \;=\; -\cos\gamma \tag{A.32}$$
$$B \;=\; 0 \tag{A.33}$$
$$C \;=\; 0 \tag{A.34}$$
$$D \;=\; -\frac{i}{2}\sin^{1/2}\gamma \tag{A.35}$$

with γ as defined in Section 4.1 (see Fig. 4.1). The radius of the billiard was taken to be $R = 1$. Inserting these solutions into (A.27) finally leads to

$$C_0^{(1)} = M_r \left(\frac{1}{3\sin\gamma} - \frac{5}{6\sin^3\gamma} \right) \ , \tag{A.36}$$

where M_r is the number of sides of the orbit.

The first order amplitudes $\mathcal{A}^{(1)}$ are obtained by inserting the $\hbar$ expansion (A.11) into the trace formula (A.8) and comparing the result with the $\hbar$ expansion (2.29). In the units used here (radius $R = 1$ and momentum $\hbar k = 1$), the scaling parameter w is equal to $\hbar$. If one uses only the $l = 0$ contributions and assumes that the terms $\exp(C_0^{(0)})$ are equal to the amplitudes $\mathcal{A}_{\text{po}}^{(0)}$ given by the Berry-Tabor formula, one finally ends up with the expression

$$\mathcal{A}_{\text{po}}^{(1)} = \mathcal{A}_{\text{po}}^{(0)} \frac{i}{2} M_r \left(\frac{1}{3 \sin \gamma} - \frac{5}{6 \sin^3 \gamma} \right) , \tag{A.37}$$

with $\gamma \equiv \pi M_\varphi / M_r$. Using the zeroth order amplitudes from Eq. (4.13), one finally obtains

$$\mathcal{A}_{\text{po}}^{(1)} = \sqrt{w} \sqrt{\pi M_r} \frac{2 \sin^2 \gamma - 5}{6 \sin^{3/2} \gamma} e^{-i(\frac{3}{2} M_r \pi - \frac{\pi}{4})} . \tag{A.38}$$

Although I cannot strictly justify the last step, my analysis of the quantum spectrum in Section 4.2.2 provides strong numerical evidence that Eq. (A.38) is correct. It will be a task for the future to develop a general theory for the $\hbar$ correction terms of integrable systems and thus to provide a rigorous mathematical proof of Eq. (A.38).

Appendix B

Calculation of the stability eigenvalues for the three-disk scatterer

In this section, I briefly describe the algorithm I use to determine the stability eigenvalues of the periodic orbits in the three-disk system.

The monodromy matrix M of a periodic orbit describes how small variations $(\delta p_\perp, \delta q_\perp)$ of momentum and coordinate in the plane perpendicular to the trajectory evolve during one period T of the orbit:

$$\left(\begin{array}{c} \delta p_\perp(T) \\ \delta q_\perp(T) \end{array} \right) = M \cdot \left(\begin{array}{c} \delta p_\perp(0) \\ \delta q_\perp(0) \end{array} \right) . \tag{B.1}$$

In billiard systems, the monodromy matrix of a periodic orbit consisting of n straight lines can be written as a product of $2n$ fundamental matrices M_{R_i} and M_{T_i} describing the reflections at the boundary and the free flights between the reflections,

$$M = M_{R_n} M_{T_n} M_{R_{n-1}} M_{T_{n-1}} \cdots M_{R_1} M_{T_1}. \tag{B.2}$$

The form of the fundamental matrices in two dimensions was derived by Eckhardt et al. in Ref. [53]. If the absolute value of the momentum is taken to be equal to 1, the fundamental matrices are given by

$$M_{T_m} = \left(\begin{array}{cc} 1 & 0 \\ t_m & 1 \end{array} \right) , \qquad M_{R_m} = - \left(\begin{array}{cc} 1 & d_m \\ 0 & 1 \end{array} \right) \tag{B.3}$$

with

$$d_m = \frac{2}{r_m \cos \gamma_m} , \tag{B.4}$$

where t_m is the flight time between the collisions, r_m is the curvature radius at the collision point and γ_m is the incidence angle.

The product (B.2) of the matrices can be evaluated by an algorithm described by Bogomolny [58]. Note that the signs of some terms in Ref. [58] were obviously not correct. I changed the signs according to Ref. [53]. Following Ref. [58], two sequences $K_2^{(\alpha)}$, $K_3^{(\alpha)},\ldots, K_{m+1}^{(\alpha)}$ ($\alpha = 1, 2$) are constructed satisfying the recurrent relationship

$$K_{m+1}^{(\alpha)} = \frac{K_m^{(\alpha)}}{1 + t_m K_m^{(\alpha)}} + d_m . \tag{B.5}$$

The first terms of the sequence are given by

$$K_2^{(1)} = d_1, \quad K_2^{(2)} = \frac{1}{t_1} + d_1 \ . \tag{B.6}$$

For each sequence the following product is constructed:

$$G_n^{(\alpha)} = (-1)^n \prod_{m=2}^{n} \left(1 + t_m K_m^{(\alpha)}\right) \ . \tag{B.7}$$

The elements of the monodromy matrix are then given by

$$\begin{aligned} m_{11} &= t_1 G_n^{(2)} K_{n+1}^{(2)} & m_{12} &= G_n^{(1)} K_{n+1}^{(1)} \\ m_{21} &= t_1 G_n^{(2)} & m_{22} &= G_n^{(1)} \ . \end{aligned} \tag{B.8}$$

The stability eigenvalues follow from the condition

$$\det(M - \lambda \cdot \mathbf{1}) = 0 \tag{B.9}$$

$$\Rightarrow \quad \lambda = \frac{1}{2}\mathrm{Tr}M \pm \sqrt{\frac{1}{4}(\mathrm{Tr}M)^2 - \det M} \ . \tag{B.10}$$

For the three-disk system, the stability eigenvalues of the symmetry reduced periodic orbits are needed. These can be obtained from the stabilities of the corresponding full domain orbits by the following considerations, as was discussed in Ref. [53]: The symmetry reduced orbit corresponds either to the full domain orbit or to a segment of it, mapped into the fundamental domain. The mapping corresponds to additional reflections at the straight boundaries of the fundamental domain (see Fig. 5.1). Since a straight wall has an infinite curvature radius, it follows from Eqs. (B.3) and (B.4) that each such reflection simply changes the sign of the eigenvalues. The symmetry reduced orbit therefore has the same stability eigenvalues as the corresponding segment of the full domain orbit, apart from the sign, which may change by the folding. The correct sign of the eigenvalues can be determined from the symbolic code. As was discussed in Ref. [53], each symbol '0' in the symmetry reduced code corresponds to one collision with a disk and one collision with the straight boundary, while each symbol '1' corresponds to one collision with a disk and two collisions with the straight boundary. Since each collision changes the sign of the monodromy matrix, the overall sign of the eigenvalues is negative for odd number of symbols '1' and positive for even number of symbols '1' in the code.

Bibliography

[1] A. Einstein, Verh. Dtsch. Phys. Ges. **19**, 82 (1917).

[2] L. Brillouin, J. Phys. Radium **7**, 353 (1926).

[3] J. B. Keller, Ann. Phys. (N.Y.) **4**, 180 (1958).

[4] I. C. Percival, Adv. Chem. Phys. **36**, 1 (1977).

[5] M. V. Berry and M. Tabor, Proc. R. Soc. Lond. A **349**, 101 (1976).

[6] M. V. Berry and M. Tabor, J. Phys. A **10**, 371 (1977).

[7] M. C. Gutzwiller, J. Math. Phys. **8**, 1979 (1967).

[8] M. C. Gutzwiller, J. Math. Phys. **12**, 343 (1971).

[9] M. C. Gutzwiller, *Chaos in Classical and Quantum Mechanics*, Springer, New York, 1990.

[10] P. Cvitanović and B. Eckhardt, Phys. Rev. Lett. **63**, 823 (1989).

[11] R. Aurich, C. Matthies, M. Sieber, and F. Steiner, Phys. Rev. Lett. **68**, 1629 (1992).

[12] M. V. Berry and J. P. Keating, J. Phys. A **23**, 4839 (1990).

[13] M. V. Berry and J. P. Keating, Proc. R. Soc. Lond. A **437**, 151 (1992).

[14] J. Main, V. A. Mandelshtam, and H. S. Taylor, Phys. Rev. Lett. **79**, 825 (1997).

[15] J. Main, V. A. Mandelshtam, G. Wunner, and H. S. Taylor, Nonlinearity **11**, 1015 (1998).

[16] J. Main, Phys. Rep. **316**, 233 (1999).

[17] J. Main and G. Wunner, Phys. Rev. Lett. **82**, 3038 (1999).

[18] J. Main and G. Wunner, Phys. Rev. E **60**, 1630 (1999).

[19] S. Hortikar and M. Srednicki, Phys. Rev. E **61**, R2180 (2000).

[20] G. Vattay, chao-dyn/9406005, 1994.

[21] G. Vattay and P. E. Rosenqvist, Phys. Rev. Lett. **76**, 335 (1996).

[22] M. R. Wall and D. Neuhauser, J. Chem. Phys. **102**, 8011 (1995).

[23] V. A. Mandelshtam and H. S. Taylor, Phys. Rev. Lett. **78**, 3274 (1997).

[24] V. A. Mandelshtam and H. S. Taylor, J. Chem. Phys. **107**, 6756 (1997).

[25] J. Main, P. A. Dando, D. Belkić, and H. S. Taylor, J. Phys. A **33**, 1247 (2000).

[26] E. Narevicius, D. Neuhauser, H. J. Korsch, and N. Moiseyev, Chem. Phys. Lett. **276**, 250 (1997).

[27] V. A. Mandelshtam, J. Chem. Phys. **108**, 9999 (1998).

[28] J. Main, V. A. Mandelshtam, and H. S. Taylor, Phys. Rev. Lett. **78**, 4351 (1997).

[29] J. Main, P. A. Dando, D. Belkić, and H. S. Taylor, Europhys. Lett. **48**, 250 (1999).

[30] J. Main, K. Weibert, and G. Wunner, Phys. Rev. E **58**, 4436 (1998).

[31] J. Main, K. Weibert, V. A. Mandelshtam, and G. Wunner, Phys. Rev. E **60**, 1639 (1999).

[32] K. Weibert, J. Main, and G. Wunner, Eur. Phys. J. D **12**, 381 (2000).

[33] M. Brack and R. K. Bhaduri, *Semiclassical Physics*, volume 96 of *Frontiers in Physics*, Addison-Wesley Publishing Company, Inc, 1997.

[34] S. M. Reimann, M. Brack, A. G. Magner, J. Blaschke, and M. V. N. Murthy, Phys. Rev. A **53**, 39 (1996).

[35] D. Ullmo, M. Grinberg, and S. Tomsovic, Phys. Rev. E **54**, 136 (1996).

[36] M. Wilkinson, J. Phys. A **20**, 2415 (1987).

[37] M. Wilkinson, J. Phys. A **21**, 1173 (1988).

[38] B. Eckhardt, S. Fishman, K. Müller, and D. Wintgen, Phys. Rev. A **45**, 3531 (1992).

[39] B. Mehlig, Phys. Rev. E **59**, 390 (1999).

[40] D. Alonso and P. Gaspard, Chaos **3**, 601 (1993).

[41] P. Gaspard and D. Alonso, Phys. Rev. A **47**, R3468 (1993).

[42] P. E. Rosenqvist, PhD thesis, Niels Bohr Institute, Copenhagen, 1994.

[43] A. Voros, J. Phys. A **21**, 685 (1988).

[44] B. Eckhardt and G. Russberg, Phys. Rev. E **47**, 1578 (1993).

[45] P. Cvitanović and G. Vattay, Phys. Rev. Lett. **71**, 4138 (1993).

[46] J. Keating, Chaos **2**, 15 (1992).

[47] M. Sieber and F. Steiner, Phys. Lett. A **144**, 159 (1990).

[48] R. Aurich and F. Steiner, Physica D **39**, 169 (1989).

[49] M. Sieber and F. Steiner, Physica D **44**, 248 (1990).

[50] E. B. Bogomolny, Chaos **2**, 5 (1992).

[51] E. B. Bogomolny, Nonlinearity **5**, 805 (1992).

[52] R. Balian and C. Bloch, Ann. Phys. **69**, 76 (1972).

[53] B. Eckhardt, G. Russberg, P. Cvitanović, P. E. Rosenqvist, and P. Scherer, in *Quantum Chaos*, edited by G. Casati and B. V. Chirikov, page 405, Cambridge University Press, Cambridge, 1995.

[54] A. Wirzba, Phys. Rep. **309**, 1 (1999).

[55] P. Gaspard and S. A. Rice, J. Chem. Phys. **90**, 2225, 2242, 2255 (1989).

[56] K. T. Hansen, Nonlinearity **6**, 753 (1993).

[57] P. Cvitanović and B. Eckhardt, Nonlinearity **6**, 277 (1993).

[58] E. B. Bogomolny, Physica D **31**, 169 (1988).

[59] P. Cvitanović, G. Vattay, and A. Wirzba, in *Classical, Semiclassical and Quantum Dynamics in Atoms*, edited by B. Eckhardt and H. Friedrich, volume 485 of *Lecture Notes in Physics*, page 29, Springer, Berlin, 1997.

[60] A. Wirzba, private communication.

[61] P. Cvitanović, P. E. Rosenqvist, G. Vattay, and H. H. Rugh, Chaos **3**, 619 (1993).

[62] G. Vattay, A. Wirzba, and P. E. Rosenqvist, Phys. Rev. Lett. **73**, 2304 (1994).

[63] P. E. Rosenqvist, G. Vattay, and A. Wirzba, J. Stat. Phys. **83**, 243 (1996).

[64] G. Tanner, P. Scherer, E. B. Bogomolny, B. Eckhardt, and D. Wintgen, Phys. Rev. Lett. **67**, 2410 (1991).

[65] P. Scherer, PhD thesis, Universität Köln, 1991.

[66] G. Vattay, private communication.

[67] G. A. Baker, *The Padé approximant in theoretical physics*, Academic Press, New York, 1970.

Zusammenfassung in deutscher Sprache

Die semiklassische Quantisierung physikalischer Systeme mit Hilfe klassischer Bahnen stellt eines der fundamentalen Probleme der Physik dar. Im Falle integrabler Systeme gibt die Methode der EBK-Torusquantisierung von Einstein, Brillouin und Keller [1, 2, 3] einen direkten Zusammenhang zwischen den quantenmechanischen Eigenzuständen und bestimmten klassischen Bahnen wieder. Die praktische Anwendung der EBK-Quantisierung ist oft problematisch, da sie auf der Kenntnis eines kompletten Satzes von Erhaltungsgrößen beruht, der für viele Systeme schwer zu finden ist. Der größte Nachteil der EBK-Methode liegt jedoch darin, dass sie nur auf reguläre Systeme anwendbar ist und nicht auf Systeme mit chaotischer oder gemischt regulär-chaotischer Dynamik verallgemeinert werden kann.

Im Gegensatz dazu lässt sich die semiklassische *periodic orbit theory* in analoger Form auf reguläre und chaotische Systeme anwenden. Die *Gutzwiller-Spurformel* [7, 9] für klassisch chaotische Systeme und die analoge Formel für integrable Systeme, die *Berry-Tabor-Formel* [5, 6], geben die semiklassische Zustandsdichte wieder als Summe über Beiträge von allen klassischen periodischen Bahnen bzw., im integrablen Fall, von allen rationalen Tori des Systems. Ein fundamentales Problem der *periodic orbit theory* besteht darin, dass die Summen über die periodischen Bahnen meist nicht konvergieren und eine direkte Bestimmung der quantenmechanischen Eigenwerte aus den Spurformeln deshalb nicht möglich ist. In den letzten Jahren wurde eine Reihe von Methoden zur Lösung dieses Problems entwickelt [10, 11, 12, 13]. Die meisten dieser Methoden beruhen allerdings auf speziellen Eigenschaften des Systems und sind deshalb jeweils nur auf bestimmte Klassen von Systemen anwendbar.

Vor kurzem wurde von Main et al. [14, 15, 16] eine Methode zur semiklassischen Quantisierung entwickelt, die auf der *harmonischen Inversion* eines semiklassischen Signals beruht. Diese Methode erlaubt es, die quantenmechanischen Eigenwerte mit Hilfe eines endlichen Satzes von periodischen Bahnen aus der Spurformel zu gewinnen. Umgekehrt lassen sich aus der Analyse der quantenmechanischen Spektren die Beiträge der klassischen Bahnen zur Spurformel mit großer Genauigkeit berechnen. Die Methode setzt keine speziellen Eigenschaften des Systems voraus und ist daher prinzipiell auf alle Klassen von Systemen anwendbar. Wegen der identischen Struktur der Spurformeln für reguläre und chaotische Systeme sind die Prozeduren für beide Arten von Dynamik dieselben. Insbesondere ist die Methode auch für Systeme mit gemischt regulär-chaotischer Dynamik geeignet.

Ziel dieser Arbeit ist es zu zeigen, dass die semiklassische Quantisierung mit Hilfe der harmonischen Inversion tatsächlich eine universelle Methode ist, die sich in gleicher Weise

auf klassisch chaotische und reguläre Systeme anwenden lässt und keine speziellen Forde-
rungen an die Eigenschaften des Systems stellt. Dazu wird die Methode exemplarisch auf
zwei Systeme mit sehr unterschiedlichen Eigenschaften angewendet: auf das Kreisbillard
als Beispiel für ein integrables geschlossenes System und das Drei-Scheiben-Billard mit
verschiedenen Abständen zwischen den Scheiben – im offenen sowie im geschlossenen Fall
– als Beispiel für ein chaotisches System. Das geschlossene Drei-Scheiben-Billard stellt eine
besondere Herausforderung für die semiklassische Quantisierung dar. Während bei hin-
reichend großen Scheibenabständen die periodischen Bahnen des Drei-Scheiben-Systems
durch einen vollständigen symbolischen Code beschrieben werden können, tritt im Grenz-
fall sich berührender Scheiben starkes *pruning* auf (d. h. ein großer Teil der Bahnen wird
unphysikalisch). Diese Eigenschaft führt zum Versagen anderer semiklassischer Methoden
wie der *cycle expansion* [10] beim geschlossenen Drei-Scheiben-Billard.

Neben der Bestimmung von semiklassischen Eigenwerten aus den Spurformeln und
der Analyse von Quantenspektren wird die Methode der harmonischen Inversion in dieser
Arbeit in zweierlei Hinsicht erweitert. Einerseits werden Korrekturterme höherer Ord-
nung in $\hbar$ in die semiklassischen Spurformeln einbezogen, wodurch sich Korrekturen zu
den semiklassischen Eigenwerten berechnen lassen. Die Korrekturterme zu den Spurfor-
meln können umgekehrt durch Analyse des Differenzspektrums zwischen semiklassischen
und exakten quantenmechanischen Eigenwerten gewonnen werden. Andererseits wird in
dieser Arbeit eine Verallgemeinerung der Spurformeln auf semiklassische Matrixelemente
benutzt, um kreuzkorrelierte Signale zu konstruieren. Dadurch kann die für die semi-
klassische Quantisierung benötigte Zahl von Bahnen deutlich reduziert werden, was die
Effizienz der Methode wesentlich erhöht.

Wegen der hohen Aktualität des Forschungsthemas wurde ein Teil der Ergebnisse
dieser Arbeit vorveröffentlicht, siehe Referenzen [30, 31, 32].

In **Kapitel 2** fasse ich zunächst die grundlegenden Ideen der *periodic orbit theory*
zusammen und skizziere kurz die Herleitung der Gutzwiller-Spurformel (2.8) und der
Berry-Tabor-Formel (2.10). Die quantenmechanische Zustandsdichte lässt sich darstel-
len als Imaginärteil der Spur der Greenschen Funktion (*response function*, im weiteren
„Responsfunktion") (2.14), deren Pole die Eigenwerte oder Resonanzen des Systems sind.
Nach der Gutzwiller- bzw. Berry-Tabor-Formel setzt sich die semiklassische Näherung zur
Responsfunktion zusammen aus einem mittleren Anteil und einem oszillatorischen Teil,
der aus einer Summe über Beiträge von allen periodischen Bahnen besteht (siehe (2.15)).
Die Beiträge der einzelnen Bahnen lassen sich aus rein klassischen Rechnungen bestimmen
und haben für reguläre und chaotische Systeme eine ähnliche Struktur.

In dieser Arbeit betrachte ich grundsätzlich skalierende Systeme, bei denen die Form
der periodischen Bahnen unabhängig von einem Skalierungsparameter w ist und ihre
Wirkung S gemäß $S/\hbar = ws$ mit w skaliert. Im Fall von Billardsystemen ist die Wellen-
zahl k eine solche Größe. Für skalierende Systeme führe ich die Zustandsdichte bzw. die
Responsfunktion als Funktion des Skalierungsparameters ein (siehe (2.17)).

Zur Gutzwiller-Formel und zur Berry-Tabor-Formel für die semiklassische Zustands-
dichte existieren verschiedene Erweiterungen, die diagonale Matrixelemente quantenme-
chanischer Operatoren und Korrekturen höherer Ordnung in $\hbar$ einbeziehen. Einerseits
kann eine verallgemeinerte Responsfunktion (2.19) betrachtet werden, bei der die Bei-
träge der einzelnen Zustände mit den entsprechenden Erwartungswerten eines Operators
gewichtet sind. Die semiklassische Näherung zu dieser Funktion erhält man dann dadurch,
dass die Beiträge der periodischen Bahnen bzw. Tori in der Spurformel mit den Mittelwer-

ten der dem Operator entsprechenden klassischen Größe über die Bahn gewichtet werden (siehe (2.20)). Diese Beziehung lässt sich noch weiter verallgemeinern auf das Produkt der Erwartungswerte zweier verschiedener Operatoren (siehe (2.23)) und auf Funktionen von Erwartungswerten (siehe (2.25)). Diese verallgemeinerten Spurformeln werden in dieser Arbeit für die Berechnung diagonaler Matrixelemente und für die Konstruktion von kreuzkorrelierten Signalen benutzt.

Eine zweite Verallgemeinerung der Spurformeln besteht in der Einbeziehung höherer Ordnungen in $\hbar$. Die Gutzwiller- und die Berry-Tabor-Formel sind semiklassische Näherungen, d. h. sie stellen die führenden Terme einer Entwicklung der Zustandsdichte nach Ordnungen von $\hbar$ dar. Ich benutze die Methode von Vattay und Rosenqvist [20, 21, 42], die in Anhang A.1 näher erläutert wird, um Korrekturen erster Ordnung $\hbar$ zu den Spurformeln zu berechnen. Diese Methode ist für chaotische Systeme konzipiert und basiert auf der Lösung der lokalen Schrödinger-Gleichung in der Nähe der periodischen Bahnen. Die so erhaltenen lokalen Eigenwerte gehen in eine quantenmechanisch exakte Verallgemeinerung der Gutzwiller-Spurformel ein. Die Beiträge erster Ordnung $\hbar$ lassen sich mit Hilfe eines rekursiven numerischen Algorithmus aus den Bahnparametern berechnen.

Die Methode von Vattay und Rosenqvist beruht auf der Annahme, dass die periodischen Bahnen isoliert liegen, und kann deshalb nicht direkt auf integrable Systeme übertragen werden. Für integrable Systeme existiert meines Wissens nach noch keine allgemeine Theorie, nach der sich Korrekturen höherer Ordnung in $\hbar$ bestimmen lassen. In Anhang A.2 modifiziere ich die Methode von Vattay und Rosenqvist, um einen Ausdruck für die Korrekturen erster Ordnung $\hbar$ für das Kreisbillard zu erhalten (siehe (A.38)). Dazu führe ich bestimmte zusätzliche Annahmen ein, die auf der speziellen Symmetrie des Systems beruhen, und löse die Gleichungen für die Bestimmung der Korrekturen erster Ordnung analytisch. Meine Vorgehensweise lässt sich nicht in allen Schritten strikt rechtfertigen und ist auch nicht direkt auf andere integrable Systeme übertragbar. Die Aufstellung einer allgemeinen Theorie für die höheren $\hbar$-Korrekturen bei integrablen Systemen bleibt daher eine lohnenswerte Aufgabe für die Zukunft.

Wie bereits erwähnt, besteht das wesentliche Problem der *periodic orbit theory* darin, dass die Spurformeln im allgemeinen nicht konvergieren. In Abschnitt 2.4 fasse ich mehrere Methoden zusammen, die in den letzten Jahren zur Lösung dieses Problems entwickelt wurden. Die *cycle expansion*-Methode von Cvitanović und Eckhardt [10] setzt die Existenz eines symbolischen Codes voraus und basiert auf einer Entwicklung von Zetafunktionen (deren Nullstellen die semiklassischen Eigenwerte sind) anhand des symbolischen Codes. Weitere Methoden wurden u. a. von Berry und Keating [12, 46], Sieber und Steiner [47, 48, 49] und Bogomolny [50, 51] entwickelt. Alle diese Methoden lassen sich im Gegensatz zur harmonischen Inversion nur auf chaotische Systeme anwenden und setzen außerdem spezielle Eigenschaften des Systems voraus.

In **Kapitel 3** stelle ich das Handwerkszeug für die Methode der harmonischen Inversion vor und entwickle die allgemeinen Prozeduren für die verschiedenen Anwendungen der Methode, die in dieser Arbeit untersucht werden sollen. Die harmonische Inversion passt ein zeitabhängiges Signal $C(t)$ an die Form $C(t) = \sum_k d_k e^{-i\omega_k t}$ an, wobei die Frequenzen ω_k und die Amplituden d_k die zu bestimmenden Variationsparameter sind. Im Gegensatz zur gewöhnlichen Fourier-Analyse eines endlichen Signals können die Frequenzen hier beliebig nah beisammen liegen. Die Auflösung, die sich mit der Methode erreichen lässt, hängt direkt mit der Länge des Signals zusammen (siehe (3.2)). Die semiklassischen Signale, die später analysiert werden sollen, enthalten in der Regel unendlich viele Frequenzen.

Eine Methode, die harmonische Inversion in einem endlich großen Frequenzfenster durchzuführen, ist die Filterdiagonalisierung, die von Wall und Neuhauser [22] entwickelt und von Mandelshtam und Taylor [23, 24] weiter verbessert wurde. Dabei wird das Problem der harmonischen Inversion auf ein Eigenwertproblem eines fiktiven Hamilton-Operators zurückgeführt und dieses in einer speziellen Basis gelöst, die dem gewünschten Frequenzfenster angepasst ist. Eine zweite Möglichkeit, die von Main et al. [25] entwickelt wurde, besteht darin, aus dem semiklassischen Signal ein Signal mit eingeschränkter Bandbreite zu konstruieren, was durch Fourier-Transformation und Rücktransformation über ein endliches Frequenzintervall erreicht werden kann. Das Signal lässt sich dann mit verschiedenen numerischen Methoden ohne Filter analysieren. Diese Vorgehensweise hat den Vorteil, dass der Vorgang des Filterns von der tatsächlichen Signalanalyse getrennt wird. Außerdem kann die Zahl der Signalpunkte, die in die Analyse eingehen, so deutlich niedriger gehalten werden, was Ungenauigkeiten aufgrund von Rundungsfehlern verhindern kann.

Eine wichtige Erweiterung beider Methoden besteht in der Konstruktion und Analyse von kreuzkorrelierten Signalen [22, 26, 27]. Statt des einfachen Signals wird hier eine Matrix aus kreuzkorrelierten Signalen aufgebaut, die alle dieselben Frequenzen enthalten. Dieser Satz von Signalen wird im Ganzen analysiert. Wegen des höheren Informationsgehaltes gegenüber dem einfachen Signal kann die Signallänge, die zur Auflösung der Frequenzen nötig ist, auf diese Weise signifikant verringert werden. Umgekehrt lässt sich bei gleicher Signallänge die Auflösung deutlich verbessern.

In **Abschnitt 3.2** diskutiere ich als erste Anwendung der harmonischen Inversion eine generelle Prozedur zur Analyse von Quantenspektren, durch die die Beiträge der periodischen Bahnen zur Zustandsdichte bestimmt werden sollen. Die allgemeine Prozedur, die von Main et al. [28] entwickelt wurde, lässt sich sowohl auf reguläre als auch auf chaotische Systeme anwenden. Aus den quantenmechanischen Eigenwerten bzw. Resonanzen wird die exakte quantenmechanische Zustandsdichte (3.21) als Funktion des Skalierungsparameters berechnet. Diese wird durch harmonische Inversion an die Form der semiklassischen Zustandsdichte (3.22) angepasst. Die Analyse der als Signal aufgefassten quantenmechanischen Zustandsdichte mittels harmonischer Inversion ergibt dann gerade die skalierten Wirkungen der periodischen Bahnen als „Frequenzen", und die erhaltenen Amplituden entsprechen denen der Gutzwiller- bzw. Berry-Tabor-Formel.

Als wichtige Erweiterung wird die oben beschriebene Methode in dieser Arbeit auf die Berechnung von Korrekturen höherer Ordnung in $\hbar$ zu den Spurformeln verallgemeinert. Die $\hbar$-Entwicklung der exakten Responsfunktion lässt sich bei skalierenden Systemen (Skalierungsparameter w) als Entwicklung nach Potenzen von w^{-1} darstellen (siehe (3.29)). Bei der direkten Analyse der exakten Quantenspektren erfüllt nur der führende Term, der der Gutzwiller- bzw. Berry-Tabor-Formel entspricht, den Ansatz (3.1) der harmonischen Inversion mit konstanten Frequenzen und Amplituden. Deshalb ergibt diese Analyse exakt die Beiträge der periodischen Bahnen zu den semiklassischen Spurformeln, ohne Abweichungen durch den semiklassischen Fehler. Sind die exakten Eigenwerte bzw. Resonanzen und die Näherungen $(n-1)$ter Ordnung in $\hbar$ bekannt, so lassen sich die Korrekturterme $n$ter Ordnung durch Analyse des mit w^n gewichteten Differenzspektrums (3.31) zwischen diesen Größen bestimmen. Die Analyse des Differenzspektrums mittels harmonischer Inversion liefert wiederum die Wirkungen der periodischen Bahnen als Frequenzen, während die Amplituden die gewünschten Korrekturterme sind.

Als zweitem Anwendungsgebiet wende ich mich in **Abschnitt 3.3** der semiklassischen

Quantisierung mittels harmonischer Inversion zu. Zunächst stelle ich die Methode zur Berechnung von Eigenwerten aus der Spurformel vor, die von Main et al. [14, 15] entwickelt wurde. Aufgrund der Analogie zwischen der Gutzwiller- und der Berry-Tabor-Formel ist die Prozedur für integrable und chaotische Systeme dieselbe. Aus dem oszillatorischen Anteil der Responsfunktion, der jeweils durch die Spurformel gegeben ist, wird durch Fourier-Transformation ein semiklassisches Signal (3.35) gebildet, das eine Funktion der skalierten Wirkung ist. In das Signal werden alle periodischen Bahnen bis zu einer maximalen Wirkung $s_{\max}$ einbezogen. Die entsprechende exakte quantenmechanische Größe (3.36), die sich durch Fourier-Transformation der exakten Responsfunktion ergibt, ist von der Form $\sum_k d_k e^{-iw_k s}$. Das semiklassische Signal wird nun mittels harmonischer Inversion an diese Form angepasst. Die Analyse liefert als Frequenzen die semiklassischen Eigenwerte w_k des Skalierungsparameters. Aus den berechneten Amplituden lassen sich die Multiplizitäten bestimmen. Mit Hilfe der erweiterten Spurformel (2.20) können auf dieselbe Weise semiklassische diagonale Matrixelemente von quantenmechanischen Operatoren berechnet werden. Dazu werden die Beiträge der Bahnen mit den Mittelwerten der entsprechenden klassischen Größen gewichtet. Die diagonalen Matrixelemente ergeben sich dann aus den Amplituden, die die harmonische Inversion liefert.

Als Erweiterung der Methode zeige ich, wie Korrekturterme höherer Ordnung in $\hbar$ zu den Spurformeln benutzt werden können, um Korrekturen zu den semiklassischen Eigenwerten zu erhalten. Da bei skalierenden Systemen die einzelnen Terme der $\hbar$-Entwicklung der Zustandsdichte proportional zu unterschiedlichen Potenzen des Skalierungsparameters sind, lassen sich die Korrekturterme nicht direkt in das semiklassische Signal einbauen, da das Signal sonst den Ansatz für die harmonische Inversion nicht mehr erfüllen würde. Stattdessen lässt sich aus den Korrekturtermen $n$ter Ordnung jeweils selbst ein Signal (3.50) konstruieren, dessen Analyse durch harmonische Inversion Korrekturen $n$ter Ordnung zu den Eigenwerten oder Resonanzen liefert. Die Korrekturen werden dabei nicht aus den Frequenzen, sondern aus den Amplituden gewonnen (siehe (3.49)).

Als zweite wichtige Erweiterung verallgemeinere ich die Methode der harmonischen Inversion in dieser Arbeit auf die Konstruktion und Analyse von kreuzkorrelierten semiklassischen Signalen. Obwohl die harmonische Inversion es erlaubt, semiklassische Eigenwerte aus einem endlichen Satz von periodischen Bahnen zu bestimmen, kann die Anzahl der benötigten Bahnen immer noch sehr groß sein, da die für die Auflösung der Eigenwerte benötigte Signallänge von der mittleren Zustandsdichte abhängt. Dies ist gerade bei chaotischen Systemen problematisch, weil die periodischen Bahnen dort numerisch bestimmt werden müssen und ihre Anzahl exponentiell mit der Wirkung zunimmt. Um die Anzahl der benötigten Bahnen zu verringern, kann mit Hilfe der auf diagonale Matrixelemente erweiterten Spurformel ein Satz aus kreuzkorrelierten Signalen (3.52) aufgebaut werden. Dieser Satz wird mit Hilfe der auf kreuzkorrelierte Funktionen erweiterten Methode der harmonischen Inversion (siehe Abschnitt 3.1) als Ganzes analysiert. Dadurch kann die zur Auflösung der Eigenwerte erforderliche Signallänge gegenüber dem einfachen Signal erheblich verringert werden.

In **Kapitel 4** wende ich die verschiedenen Methoden, die in Kapitel 3 entwickelt wurden, auf das Kreisbillard als ein Beispiel für ein integrables geschlossenes System an. Im Fall des Kreisbillards lassen sich die Parameter der periodischen Bahnen, die in die Berry-Tabor-Formel eingehen, analytisch bestimmen. Die periodischen Bahnen haben die Form regelmäßiger Polygone (Abb. 4.1) und lassen sich durch ein Paar von ganzen Zahlen parametrisieren. Diese Zahlen bestimmen alle Bahnparameter auf dem entsprechenden ra-

tionalen Torus. Die semiklassische Responsfunktion, die sich aus der Berry-Tabor-Formel ergibt, ist durch (4.13) gegeben. Die exakten quantenmechanischen Eigenwerte des Skalierungsparameters $w = kR$ (k: Wellenzahl, R: Radius des Billards) sind die Nullstellen der Bessel-Funktionen (siehe (4.15)). Die EBK-Eigenwerte des Kreisbillards ergeben sich aus der EBK-Quantisierungsbedingung (4.19). Obwohl generell die semiklassischen Eigenwerte aus EBK-Quantisierung und *periodic orbit theory* nur in niedrigster Ordnung $\hbar$ übereinstimmen, lässt sich für das Kreisbillard zeigen [34], dass dort beide Ansätze in allen Ordnungen $\hbar$ identisch sind, so dass die EBK-Werte hier als Vergleichswerte für die Ergebnisse der harmonischen Inversion herangezogen werden können.

In **Abschnitt 4.2** wende ich die in Abschnitt 3.2 entwickelte Methode zur Analyse von Quantenspektren auf das Kreisbillard an. Neben der reinen Zustandsdichte analysiere ich auch verallgemeinerte Zustandsdichten, bei denen gemäß (2.19) die Beiträge der verschiedenen Eigenzustände mit den Erwartungswerten eines Operators gewichtet sind. Als Operatoren verwende ich hier Funktionen des Drehimpulses L und des Abstandes r vom Kreismittelpunkt. In das Signal werden jeweils die Nullstellen der Bessel-Funktionen zwischen $w_{\min} = 300$ und $w_{\max} = 500$ einbezogen. Das Abschneiden des unteren Endes des Signals bewirkt eine Verbesserung der Ergebnisse. Eine mögliche Erklärung hierfür ist, dass die unteren Eigenwerte in gewissem Sinne nicht „semiklassisch" genug sind. Die Frequenzen und Amplituden, die sich aus der Analyse des Signals mittels harmonischer Inversion ergeben, zeigen eine hervorragende Übereinstimmung mit den Wirkungen der periodischen Bahnen und mit den Amplituden aus der Berry-Tabor-Formel (Abb. 4.3a). Auch die Mittelwerte über die klassischen Größen, die aus der Analyse der gewichteten Zustandsdichten gewonnen wurden (Abb. 4.3b-d), stimmen sehr gut mit den Werten aus klassischen Rechnungen überein. Im untersuchten Bereich liegt ein Häufungspunkt von Bahnen (vgl. Abb. 4.2). Hier wurden nur solche Bahnen aufgelöst, deren Wirkungen sich noch hinreichend unterschieden.

Weiterhin analysiere ich das Differenzspektrum aus semiklassischen und exakt quantenmechanischen Eigenwerten (Abb. 4.4), um Korrekturen erster Ordnung $\hbar$ zur Berry-Tabor-Formel für das Kreisbillard zu bestimmen. Dazu benutze ich die Nullstellen der Bessel-Funktionen und die EBK-Eigenwerte im Bereich $100 < w < 500$. Die durch Analyse des gewichteten Differenzsignals erhaltenen Korrekturterme weisen eine hervorragende Übereinstimmung mit dem Ausdruck (A.38) auf, den ich in Anhang A.2 mit Hilfe der modifizierten Methode von Vattay und Rosenqvist bestimmt habe (Abb. 4.5). Damit ist das analytische Ergebnis (A.38), dessen Herleitung ich nicht strikt rechtfertigen konnte, numerisch bestätigt.

In **Abschnitt 4.3** wende ich mich der semiklassischen Quantisierung des Kreisbillards mittels harmonischer Inversion zu. Zur Bestimmung der semiklassischen Eigenwerte im Bereich $0 < w < 15$ konstruiere ich gemäß Abschnitt 3.3 ein Signal aus den periodischen Bahnen bis zur Länge $s_{\max} = 150$. An den Häufungspunkten von Bahnen bei skalierten Wirkungen von Vielfachen von 2π (vgl. Abb. 4.2) wähle ich eine minimale Seitenlänge als Abbruchkriterium. Die Eigenwerte und Multiplizitäten, die sich aus der harmonischen Inversion des semiklassischen Signals ergeben, werden in Tabelle 4.1 mit den exakten quantenmechanischen Größen und mit den semiklassischen Größen, die aus der EBK-Quantisierungsbedingung folgen, verglichen. Meine Ergebnisse stimmen eindeutig mit den semiklassischen EBK-Werten überein. Die Abweichungen von den EBK-Werten sind deutlich kleiner als der semiklassische Fehler, d. h. die Differenz zwischen quantenmechanisch exakten und semiklassischen Eigenwerten. Zwei Paare von fast entarteten

Eigenwerten wurden nicht aufgelöst. Hier ergab die harmonische Inversion jeweils eine gemittelte Frequenz mit einer Amplitude, die der Summe der beiden einzelnen Amplituden entspricht.

Zusätzlich zur Berechnung von Eigenwerten und Multiplizitäten nutze ich die erweiterten Spurformeln, um semiklassische Erwartungswerte für verschiedene Operatoren zu berechnen (Abb. 4.6). Auch die so erhaltenen Erwartungswerte stimmen hervorragend mit den semiklassischen Werten überein, die sich aus der EBK-Theorie ergeben.

Zu den semiklassischen Eigenwerten berechne ich weiterhin die Korrekturen erster Ordnung $\hbar$ mit Hilfe des Korrekturterms (A.38) zur Spurformel, den ich in Abschnitt 4.2 numerisch bestätigt habe. Die durch harmonische Inversion erhaltenen Korrekturen (Abb. 4.7) werden zu den zuvor bestimmten semiklassischen Eigenwerten addiert. Durch die Korrekturen erster Ordnung verbessert sich die Genauigkeit der semiklassischen Ergebnisse in Bezug auf die exakten quantenmechanischen Werte tatsächlich um eine oder mehrere Größenordnungen (Abb. 4.8). Lediglich die Paare von fast entarteten Eigenwerten wurden wiederum nicht aufgelöst. Die verbleibende Abweichung von den exakten Werten ist auf Korrekturen zweiter oder noch höherer Ordnung in $\hbar$ zurückzuführen.

Schließlich untersuche ich, wie sich durch Anwendung der Kreuzkorrelationstechnik auf das Kreisbillard die Effizienz der Methode verbessern lässt. Dazu wähle ich für die Bestimmung der semiklassischen Eigenwerte zunächst dieselbe Signallänge $s_{\mathrm{max}} = 150$ wie zuvor, konstruiere jetzt aber ein 2×2-Signal, das als Ganzes harmonisch invertiert wird. Es zeigt sich, dass im Gegensatz zu dem zuvor verwendeten einfachen Signal die beiden Paare von fast entarteten Eigenwerten jetzt aufgelöst werden (Tab. 4.2). Mit einem einfachen Signal wäre dazu eine Signallänge von etwa $s_{\mathrm{max}} = 500$ nötig gewesen. Dieser Reduktion der benötigten Signallänge entspricht eine Verringerung der Anzahl von periodischen Bahnen, die für die Auflösung der Eigenwerte berechnet werden müssen, um eine ganze Größenordnung. Als nächstes untersuche ich, wie viele Eigenwerte sich bei konstanter Signallänge, aber verschiedenen Operatoren und Dimensionen der Kreuzkorrelationsmatrix auflösen lassen. (Da die mittlere Zustandsdichte proportional zum Skalierungsparameter wächst, ist beim einfachen Signal die benötigte Signallänge von der Größe der Eigenwerte bestimmt, die aufgelöst werden sollen.) Es zeigt sich, dass der höchste Eigenwert, der aufgelöst werden kann, mit größer werdender Matrixdimension deutlich wächst (Tab. 4.3). Allerdings hängen die Ergebnisse von den verwendeten Operatoren ab. Eine signifikante Verbesserung der Auflösung zeigt sich bei Matrixgrößen bis etwa 5×5; danach lassen sich die Ergebnisse nicht mehr wesentlich verbessern. Während beim einfachen Signal die benötigte Signallänge etwa das Doppelte der Heisenberg-Zeit beträgt, konnte mit einem 5×5-Signal (Abb. 4.9) die benötigte Signallänge deutlich unter die Heisenberg-Zeit reduziert werden.

Beim Kreisbillard kann zusätzlich zu den Mittelwerten von Operatoren auch der Korrekturterm erster Ordnung $\hbar$ in das kreuzkorrelierte Signal mit einbezogen werden. Dadurch erhält man simultan nicht nur die semiklassischen Eigenwerte des Skalierungsparameters und die diagonalen Matrixelemente der verwendeten Operatoren, sondern auch die Korrekturen erster Ordnung zu den semiklassischen Eigenwerten. Als Beispiel beziehe ich die erste Ordnung $\hbar$ in ein 3×3-Signal der Länge $s_{\mathrm{max}} = 150$ ein (Tab. 4.4). Im Gegensatz zur Berechnung der Korrekturen erster Ordnung mit einem einfachen Signal derselben Länge werden jetzt die Paare von fast entarteten Eigenwerten aufgelöst. Um die Korrekturen erster Ordnung zu diesen fast entarteten Werten mit einem einfachen Signal zu berechnen, wäre eine Signallänge von etwa $s_{\mathrm{max}} = 500$ nötig gewesen.

Nach der erfolgreichen Anwendung der verschiedenen Techniken aus Kapitel 3 auf das Kreisbillard betrachte ich in **Kapitel 5** als Beispiel für ein chaotisches System das Drei-Scheiben-Billard mit Scheibenradius $R = 1$ bei verschiedenen Abständen d zwischen den Scheiben. Dieses System, insbesondere der Fall $d = 6$, hat in der Vergangenheit als Modellsystem für verschiedene semiklassische Methoden, insbesondere für die *cycle expansion*-Methode [10, 44, 53, 54], gedient. Die *cycle expansion* lässt sich jedoch nur für hinreichend große Scheibenabstände anwenden. Ich betrachte neben dem relativ großen Abstand $d = 6$ auch den Fall $d = 2.5$, bei dem die *cycle expansion* nur noch langsam konvergiert, und den Fall sich berührender Scheiben ($d = 2$), der wegen des starken *prunings* die Voraussetzungen der *cycle expansion* überhaupt nicht mehr erfüllt.

Die Symmetrie des Drei-Scheiben-Systems erlaubt es, alle Berechnungen auf einen fundamentalen Bereich, der einem Sechstel des Systems entspricht, zu beschränken (Abb. 5.1). Die periodischen Bahnen dieses symmetriereduzierten Systems lassen sich durch einen binären Code beschreiben. Die quantenmechanischen Eigenzustände zerfallen in drei Gruppen unterschiedlicher Symmetrie, die sich aus den symmetriereduzierten periodischen Bahnen gewinnen lassen, indem in der Gutzwiller-Spurformel bestimmte symmetrieabhängige Gewichtungsfaktoren eingeführt werden (Tab. 5.1). In dieser Arbeit betrachte ich grundsätzlich den A_1-Unterraum.

Für die semiklassische Quantisierung mittels harmonischer Inversion müssen alle periodischen Bahnen bis zu einer maximalen skalierten Wirkung berechnet werden. Es zeigt sich, dass die Verteilung der Bahnparameter sich stark mit dem Scheibenabstand d ändert (Abb. 5.4 - 5.6). Im Fall des relativ großen Abstandes $d = 6$ sind die Bahnparameter wie Wirkung und Stabilität im wesentlichen durch die Länge des symbolischen Codes bestimmt. Rücken die Scheiben näher zusammen, so werden alle Bahnen kürzer, und die Zahl der Bahnen bis zu einer vorgegebenen Wirkung steigt rapide an. Die Verteilung der Bahnparameter zeigt ein zunehmend komplizierteres Verhalten. Bei $d = 2.04821419$ setzt *pruning* ein [56], d. h. die ersten Bahnen geraten in die Scheiben und werden dadurch unphysikalisch. Bei meinen Bahnberechnungen wurden zwei unterschiedliche Arten von *pruning* gefunden (Abb. 5.2 u. 5.3), die bei der Bahnsuche berücksichtigt werden müssen. Im Grenzfall sich berührender Scheiben lassen sich die periodischen Bahnen in „Kanäle" einordnen, wobei die Bahnen eines Kanals dieselbe Endsequenz von Symbolen im symbolischen Code, aber eine wachsende Anzahl von führenden Nullen besitzen. Dies entspricht einem immer tieferen Eindringen in die spitzen Bereiche, die von zwei sich berührenden Scheiben gebildet werden (Abb. 5.7 - 5.9). Mit wachsender Anzahl von führenden Nullen im Code ändert sich die Wirkung der Bahnen eines Kanals sehr wenig. Obwohl alle Kanäle bis auf zwei irgendwann abbrechen, weil die Bahnen unphysikalisch werden, ist deshalb die Anzahl der Bahnen bis zu einer vorgegebenen Wirkung enorm groß.

Das unterschiedliche Verhalten der Bahnparameter bei verschiedenen Scheibenabständen erfordert unterschiedliche Strategien bei der numerischen Bahnsuche. Die Suche erfolgt in jedem Fall über den symbolischen Code. Bei größeren Scheibenabständen berechne ich alle Bahnen bis zu einer vorgegebenen Symbollänge. Im Fall $d = 2$ werden die Bahnen Kanal für Kanal berechnet. Wegen der extrem großen Anzahl von periodischen Bahnen müssen für $d = 2$ außerdem zusätzliche Abbruchkriterien eingeführt werden, die die Bahnen mit den größten Beiträgen zur Spurformel herausfiltern.

Für verschiedene Scheibenabstände wurden von Wirzba [54, 59, 60] exakte quantenmechanische Resonanzen berechnet. Außerdem wurden von Wirzba für das offene Drei-Scheiben-Billard semiklassische Resonanzen mit Hilfe der *cycle expansion*-Methode aus

verschiedenen Zetafunktionen bestimmt (Abb. 5.10 - 5.12). Diese Werte benutze ich als Vergleichswerte für die Ergebnisse der harmonischen Inversion. Im Fall des geschlossenen Drei-Scheiben-Billards konnten von Tanner et al. [64] die niedrigsten quantenmechanischen Eigenwerte mit Hilfe einer erweiterten *cycle expansion*-Methode semiklassisch reproduziert werden (Abb. 5.13). Die Methode scheitert jedoch bei höheren Eigenwerten am *pruning* der Bahnen. Mein Ziel ist es zu zeigen, dass sich mit Hilfe der harmonischen Inversion auch höhere Eigenwerte aus der Spurformel bestimmen lassen.

In **Abschnitt 5.2** analysiere ich zunächst das Quantenspektrum des Drei-Scheiben-Billards mit Scheibenabstand $d = 6$. (Für andere Scheibenabstände standen nicht genug quantenmechanische Daten zur Verfügung.) Für $d = 6$ konnten die führenden vier Bänder von Resonanzen bis zur Wellenzahl $\operatorname{Re} k = 250$ (vgl. Abb. 5.10) in die quantenmechanische Zustandsdichte (Abb. 5.14) einbezogen werden. Wie beim Kreisbillard waren die Ergebnisse besser, wenn der unterste Teil des Signals abgeschnitten wurde. Die Analyse des Signals ergibt wiederum eine hervorragende Übereinstimmung der erhaltenen Frequenzen mit den Wirkungen der periodischen Bahnen (Abb. 5.15). Auch die gewonnenen Amplituden entsprechen sehr genau denen der Gutzwiller-Formel. Bei höheren Wirkungen existieren Bahnen mit sehr ähnlichen Wirkungen. Diese wurden zum Teil nicht mehr aufgelöst. Die Analyse liefert hier jeweils eine gemittelte Frequenz mit einer Amplitude, die der Summe der einzelnen Amplituden aus der Gutzwiller-Formel entspricht.

Weiterhin analysiere ich für Scheibenabstand $d = 6$ das gewichtete Differenzspektrum (Abb. 5.16) aus den exakten Resonanzen und den semiklassischen Näherungen für die Resonanzen, die von Wirzba mit Hilfe der *cycle expansion* aus der Gutzwiller-Voros-Zetafunktion berechnet wurden (vgl. Abb. 5.10a). Die so gewonnenen Korrekturen erster Ordnung zur Gutzwiller-Formel vergleiche ich mit den theoretischen Werten, die ich mit Hilfe des numerischen Algorithmus von Vattay und Rosenqvist [42, 66] berechne. Bei den meisten Bahnen stimmen die Ergebnisse der harmonischen Inversion sehr gut mit den theoretischen Werten überein (Abb. 5.17). Im Bereich höherer Wirkungen sind lediglich einige Bahnen wiederum nicht aufgelöst. Auffällig ist dagegen eine deutliche Diskrepanz bei der zweitlängsten Bahn. Hier weicht die Amplitude, die sich mit Hilfe der harmonischen Inversion ergibt, deutlich vom theoretischen Wert ab. Die Abweichung ist systematisch und tritt in derselben Form auf, wenn Parameter der harmonischen Inversion wie Signallänge und Frequenzfenster geändert werden. Eine mögliche Erklärung für diese Diskrepanz ist die Tatsache, dass nur Resonanzen nahe der reellen Achse in das Differenzsignal mit einbezogen werden konnten. Das Signal ist deshalb nicht vollständig. Dies würde jedoch nicht erklären, warum nur bei einer einzigen Bahn deutliche Abweichungen vorhanden sind. Der Grund für die Abweichung könnte andererseits in der Theorie von Vattay und Rosenqvist oder in ihrer Anwendung auf das Drei-Scheiben-Billard liegen. Tatsächlich ist die betroffene Bahn diejenige, bei der in der Summe über das Eigenwertspektrum der lokalen Schrödinger-Gleichung, aus dem die Korrekturen berechnet werden, die höheren Terme den größten Beitrag liefern (Tab. 5.2). Bei den meisten Bahnen spielt nur der führende Eigenwert eine Rolle. Um die genaue Ursache für die Diskrepanz zu finden, müssten umfangreichere Untersuchungen angestellt werden. Meine Ergebnisse zeigen in jedem Fall, dass auch für chaotische Systeme die Theorie höherer $\hbar$-Korrekturen zur Spurformel noch offene Fragen enthält. Für integrable Systeme muss eine solche allgemeine Theorie überhaupt noch erst entwickelt werden.

In **Abschnitt 5.3** wende ich die Methoden zur semiklassischen Quantisierung mittels harmonischer Inversion auf das offene Drei-Scheiben-Billard mit den Scheibenabständen

$d = 6$ und $d = 2.5$ an. Die Werte, die sich aus der Analyse des semiklassischen Signals ergeben, vergleiche ich mit den exakten quantenmechanischen Daten und mit semiklassischen Werten, die mit der *cycle expansion*-Methode berechnet wurden (Abb. 5.18 u. 5.20). Wie beim Kreisbillard reproduzieren meine Ergebnisse auch hier klar erkennbar die semiklassischen und nicht die exakten quantenmechanischen Werte. Die Genauigkeit der Ergebnisse hängt vom Imaginärteil der Resonanzen ab (Abb. 5.19 u. 5.21). Nahe der reellen Achse ist die Abweichung von den Werten aus der *cycle expansion* um mehrerer Größenordnungen kleiner als der semiklassische Fehler. Bei tieferen Resonanzen kommt sie in dieselbe Größenordnung. Dennoch ist hervorzuheben, dass ich mit der harmonischen Inversion auch tiefe Resonanzen erhalte, die jenseits des Konvergenzradius der *cycle expansion* der Gutzwiller-Voros-Zetafunktion (Abb. 5.10a) liegen, ohne jedoch Pseudo-Resonanzen zu erzeugen, wie es bei der *cycle expansion* der quasiklassischen Zetafunktion (Abb. 5.11) der Fall ist. Die Ergebnisse für diese tiefen Resonanzen zeigen immer noch eine gute Übereinstimmung mit den quantenmechanischen Werten.

Für die Scheibenabstände $d = 6$ und $d = 2.5$ berechne ich außerdem Korrekturen erster Ordnung $\hbar$ zu den semiklassischen Eigenwerten. Ich benutze dabei wieder den numerischen Algorithmus von Vattay und Rosenqvist [42, 66], um für die einzelnen periodischen Bahnen die Korrekturterme erster Ordnung $\hbar$ zur Spurformel zu bestimmen, aus denen mittels harmonischer Inversion die Korrekturen zu den Eigenwerten berechnet werden. Die Ergebnisse zeigen, dass durch die Korrekturen erster Ordnung (Abb. 5.22 - 5.25, Tab. 5.3 u. 5.4) vor allem die Realteile der Resonanzen deutlich verbessert werden. Beim Scheibenabstand $d = 6$ liegen die Realteile der Näherungen erster Ordnung größtenteils um zwei bis fünf Größenordnungen näher an den exakten quantenmechanischen Werten als die semiklassische Näherung. Bei $d = 2.5$ sind die Verbesserungen weniger ausgeprägt, aber doch deutlich. Wie auch schon bei den semiklassischen Eigenwerten hängt die Genauigkeit der Ergebnisse außerdem vom Imaginärteil der Resonanzen ab. Die Genauigkeit der Imaginärteile wird nur geringfügig verbessert. Hier sind entscheidende Korrekturen erst in zweiter Ordnung $\hbar$ zu erwarten [42].

In **Abschnitt 5.4** wende ich mich dem Drei-Scheiben-Billard im Grenzfall sich berührender Scheiben zu. Beim geschlossenen Drei-Scheiben-Billard liegt die Schwierigkeit bei der praktischen Anwendung der Methode der harmonischen Inversion für die semiklassische Quantisierung in dem enorm schnellen Anstieg der Zahl der Bahnen mit wachsender Wirkung. Während bei den Abständen $d = 6$ und $d = 2.5$ etwa 10^3 bzw. 10^4 primitive Bahnen gesucht werden mussten, um ein hinreichend langes vollständiges Signal zu konstruieren, liegt die nötige Zahl von Bahnen hier um Größenordnungen höher. Es mussten deshalb zusätzliche Abbruchbedingungen (z. B. für die Stabilität der Bahnen) eingeführt werden, um in jedem Kanal von Bahnen die wichtigsten Bahnen herauszufiltern. In die Konstruktion des semiklassischen Signals wurden schließlich etwa 5×10^6 primitive Bahnen einbezogen. Durch Analyse dieses Signals konnten die untersten 20 quantenmechanischen Eigenwerte reproduziert werden (Abb. 5.26). Dies ist in etwa dieselbe Anzahl Eigenwerte, die Tanner et al. [64] mit der modifizierten *cycle expansion*-Methode erhielten (vgl. Abb. 5.13). Meine Ergebnisse erweisen sich als relativ stabil gegenüber Änderungen der Parameter in der harmonischen Inversion (Abb. 5.28). Für die Auflösung höherer Eigenwerte war die Signallänge nicht ausreichend. Die Ergebnisse sind weniger genau und weniger gut konvergiert als bei den großen Scheibenabständen, was sich an den Amplituden erkennen lässt, die teilweise recht große Abweichungen vom theoretischen Wert 1 aufweisen (Abb. 5.27). Die Gründe hierfür liegen sicherlich in der relativ kurzen Signallänge und

der relativ großen Anzahl fehlender Bahnen, die aufgrund der Abbruchbedingung nicht mit ins Signal einbezogen wurden. Es ist jedoch zu betonen, dass sich meine Ergebnisse zumindest *prinzipiell* verbessern lassen, indem mehr Bahnen ins Signal einbezogen werden. Dies ist nicht der Fall bei der modifizierten *cycle expansion*-Methode von Tanner et al. [64], die wegen des *prunings* auf fundamentale Schwierigkeiten stößt. Ein Teil der Abweichungen ist sicher auch auf den semiklassischen Fehler zurückzuführen, da hier nur exakt quantenmechanische Daten zum Vergleich vorlagen.

Praktisch kann die Signallänge beim geschlossenen Drei-Scheiben-Billard wegen des enorm schnellen Zuwachses an periodischen Bahnen nicht mehr wesentlich verlängert werden. Um dennoch die Auflösung zu verbessern, wende ich auf dieses System die Kreuzkorrelationstechnik an. Dazu verwende ich denselben Satz von periodischen Bahnen wie zuvor, zusätzlich aber die Mittelwerte verschiedener klassischer Größen (z. B. des Drehimpulses) über die Bahnen. Es zeigt sich, dass mit einem 3×3-Signal Energieeigenwerte bis zum Bereich $E \approx 6500$ aufgelöst werden können (Abb. 5.29), während die Analyse des einfachen Signals nur Eigenwerte bis $E \approx 4500$ lieferte. Gegenüber dem einfachen Signal sind außerdem die Ergebnisse für die untersten Eigenwerte besser konvergiert, was an den Amplituden zu erkennen ist (Abb. 5.30a). Zusätzlich zu den konvergierten Eigenwerten ergibt die harmonische Inversion eine größere Anzahl von nicht konvergierten Werten. Diese lassen sich anhand eines relativ großen Imaginärteils der Frequenzen (da die Eigenwerte reell sein müssen) und einer relativ großen Abweichung der Amplitude vom theoretischen Wert 1 idenfizieren (Abb. 5.30b).

Bei Variation der Signallänge erweisen sich die Ergebnisse für die untersten Eigenwerte sowohl bei einem 3×3- als auch bei einem 4×4-Signal als sehr stabil, solange das Signal nicht zu kurz gewählt wird (Abb. 5.31). Allerdings splitten bei zu großer Signallänge die Werte für die ersten Eigenwerte auf. Die Ergebnisse für die höheren Eigenwerte hängen stärker von der Signallänge ab. Einige Eigenwerte scheinen mit dem verwendeten Bahnensatz besonders schwer zu erhalten zu sein. Diese Eigenwerte stehen möglicherweise in besonderem Zusammenhang mit den Bahnen, die bei der Konstruktion des Signals ausgelassen wurden.

Insgesamt hat sich gezeigt, dass die Methode der harmonischen Inversion tatsächlich nicht durch das *pruning* von Bahnen beeinträchtigt wird. Während andere Methoden bei diesem System auf prinzipielle Probleme stoßen, liegt bei der Anwendung der harmonischen Inversion die einzige Schwierigkeit in dem extrem schnellen Anstieg der Anzahl periodischer Bahnen mit wachsender Wirkung in diesem System.

Zusätzlich zur semiklassischen Quantisierung mittels harmonischer Inversion benutze ich den berechneten Bahnensatz für das Drei-Scheiben-Billard, um eine weitere Methode für die Auswertung der Spurformel zu testen, die kürzlich von Main et al. [29] entwickelt wurde. Diese Methode basiert auf einer Padé-Approximation zur semiklassischen Zustandsdichte und setzt als einzige Bedingung an das System die Existenz eines ganzzahligen Ordnungsparameters voraus. Beim geschlossenen Drei-Scheiben-Billard kommen als Ordnungsparameter die Symbollänge (bzw. der Maslov-Index) und die Anzahl der Einsen im symbolischen Code in Frage. Die Summe über die periodischen Bahnen wird anhand des Ordnungsparameters neu geordnet. Aus den Bahnen bis zu einem maximalen Wert des Ordnungsparameters wird die Padé-Näherung zur Summe berechnet. Die semiklassischen Eigenwerte ergeben sich dann als Pole der Padé-Näherung, d. h. als Nullstellen ihres Reziprokwertes (als Funktion der Energie bzw. Wellenzahl).

Für das geschlossene Drei-Scheiben-Billard führe ich Berechnungen für beide mögli-

chen Ordnungsparameter durch. Dabei beziehe ich jeweils Bahnen bis zu verschiedenen Maximalwerten des Ordnungsparameters ein (was verschiedenen Ordnungen der Padé-Approximation entspricht). Es zeigt sich, dass sich mit beiden Ordnungsparametern die Eigenwerte bis etwa $E \approx 4500$ reproduzieren lassen (Abb. 5.33). Dies entspricht derselben Zahl von Eigenwerten, die mit der harmonischen Inversion eines einzelnen Signals bestimmt werden konnten. Die Zahl der erhaltenen Eigenwerte hängt stark vom Maximalwert des Ordnungsparameters, d. h. von der Zahl der berücksichtigten Bahnen ab. Es ist anzumerken, dass der verwendete Bahnensatz bezüglich großer Werte beider möglicher Ordnungsparameter sehr unvollständig wird (Abb. 5.32), was zu einer Verschlechterung der Ergebnisse führt. Das Identifizieren nicht konvergierter Werte ist hier schwieriger als bei den Ergebnissen der harmonischen Inversion. Das einzige Kriterium, das zur Verfügung steht, ist der Imaginärteil der erhaltenen Werte, während bei der harmonischen Inversion auch die Amplituden zur Identifizierung der „echten" Eigenwerte herangezogen werden konnten. Einige zusätzlich auftretende „falsche" Werte lassen sich nur durch Vergleich der Rechnungen mit verschiedenen Maximalwerten des Ordnungsparameters herausfiltern. Wie bei der harmonischen Inversion sind einige bestimmte Eigenwerte mit dem verwendeten Bahnensatz nur sehr schwer zu erhalten. Grundsätzlich sind die Ergebnisse mit der Symbollänge als Ordnungsparameter besser.

Abgesehen von der Schwierigkeit, nicht konvergierte Werte herauszufiltern, konnte mit der Padé-Methode mit dem verwendeten Bahnensatz etwa die gleiche Auflösung erreicht werden wie durch harmonische Inversion eines einzelnen Signals. Aufgrund der Möglichkeit, durch Anwendung der Kreuzkorrelationstechnik die Auflösung deutlich zu verbessern, ist bei diesem System jedoch die harmonische Inversion der Padé-Methode eindeutig überlegen.

Insgesamt haben die Ergebnisse dieser Arbeit bewiesen, dass sich die Methode der harmonischen Inversion auf integrable und chaotische Systeme in gleicher Weise erfolgreich anwenden lässt. Dies gilt sowohl für die Analyse von Quantenspektren als auch für die Prozeduren zur semiklassischen Quantisierung. Die Untersuchungen am geschlossenen Drei-Scheiben-Billard haben gezeigt, dass das Verfahren – im Gegensatz zu anderen semiklassischen Methoden – auch auf Systeme mit starkem *pruning* anwendbar ist. Meines Wissens nach ist dies das erste Mal, dass höhere semiklassische Eigenwerte des geschlossenen Drei-Scheiben-Billards korrekt berechnet werden konnten. Die harmonische Inversion hat sich damit als universelles Verfahren erwiesen, das keine besonderen Eigenschaften des Systems voraussetzt. Die Erweiterung der Methode auf Korrekturen höherer Ordnung in $\hbar$ hat sich sowohl bei der Analyse der Quantenspektren als auch bei der semiklassischen Quantisierung bewährt. Für das Kreisbillard konnte damit der Korrekturterm zur semiklassischen Zustandsdichte numerisch bestätigt werden, den ich durch Modifikation der Methode von Vattay und Rosenqvist gewonnen habe, für dessen Herleitung allerdings noch keine allgemeine Theorie existiert. Die Analyse des Quantenspektrums des offenen Drei-Scheiben-Billards hat gezeigt, dass auch bei chaotischen Systemen die Theorie zu höheren $\hbar$-Korrekturen noch offene Fragen enthält. Als zweite Erweiterung der Methode hat sich die Verallgemeinerung der harmonischen Inversion auf Kreuzkorrelationsfunktionen als sehr erfolgreich erwiesen. Mit diesem Verfahren konnte die zur Auflösung der Eigenwerte benötigte Signallänge und damit die benötigte Anzahl von Bahnen deutlich reduziert werden. Dies bewirkt eine erhebliche Steigerung der Effizienz der Methode insbesondere für Systeme, bei denen die periodischen Bahnen numerisch gesucht werden müssen.

Danksagung

An dieser Stelle möchte ich mich bei allen bedanken, die mich während der Entstehung dieser Arbeit – in physikalischer oder nicht physikalischer Hinsicht – unterstützt haben.

Mein besonderer Dank gilt Prof. Dr. G. Wunner für seine weitreichende Unterstützung, insbesondere für die Schaffung idealer Arbeitsbedingungen „zwischen den Lehrstühlen" und die Gewährung großer Freiräume.

Besonders bedanken möchte ich mich auch bei PD Dr. J. Main für die hervorragende Betreuung, seine Hilfsbereitschaft bei allen Fragen und für die gute Zusammenarbeit.

Außerderm bedanke ich mich bei Dr. A. Wirzba für das Zurverfügungstellen von Daten für das Drei-Scheiben-Billard und bei Dr. G. Vattay für das Übersenden des numerischen Algorithmus für die Bestimmung der $\hbar$-Korrekturen.

Frau G. Buhr danke ich für ihr persönliches Interesse, ihre Anteilnahme und ihre große Hilfsbereitschaft bei allen Problemen.

Weiterhin danke ich allen Mitgliedern des Lehrstuhls für Theoretische Physik I der Uni Bochum und des Lehrstuhls für Theoretische Physik I der Uni Stuttgart für das gute Arbeitsklima und die ständige Hilfsbereitschaft.

Schließlich möchte ich mich bei meinem Freund Karsten Wilmesmeyer bedanken für seine große Geduld und Anteilnahme und dafür, dass er immer für mich da war.

Lebenslauf

Persönliche Daten:

Name:	Kirsten Claudia Weibert
Geburtsdatum:	7. Mai 1972
Geburtsort:	Heide
Eltern:	Claus-Dieter Weibert Ursula Weibert, geb. Tams
Staatsangehörigkeit:	deutsch
Familienstand:	ledig

Schulausbildung:

1978 - 1979	Petri-Grundschule Soest
1979 - 1982	Ostenberg-Grundschule Dortmund
1982 - 1991	Leibniz-Gymnasium Dortmund
	Abitur: Juni 1991

Studium:

ab 1991	Studium der Physik an der Ruhr-Universität Bochum
Oktober 1993	Vordiplom
1994 - 1995	Auslandsaufenthalt an der University of Sussex in Brighton, England
Juni 1997	Diplom

Wissenschaftliche Tätigkeiten/Promotion:

1997-1999	Wissenschaftliche Mitarbeiterin und Doktorandin am Lehrstuhl für Theoretische Physik I der Ruhr-Universität Bochum
seit 2000	Wissenschaftliche Mitarbeiterin und Doktorandin am Institut für Theoretische Physik I der Universität Stuttgart